UNIVERSITY OF CALIFORNIA,
IRVINE

Chromophore Photochemistry and Hydrolysis in Mammalian Opsins
Implications to Visual Physiology

DISSERTATION

submitted in partial satisfaction of the requirements
for the degree of

DOCTOR OF PHILOSOPHY

in Chemistry

by

John Dong-Hoon Hong

Dissertation Committee:
Professor Krzysztof Palczewski, Chair
Professor Gregory Weiss
Professor Chang Liu

2024

DEDICATION

To

my parents, my brothers, and friends

To all mentors who have believed in me and supported me:
Dr. Krzysztof Palczewski
Dr. Michael Oh
Dr. Donny Suh
Dr. Gregory Weiss
Dr. Susan Catalano
Dr. Nicholas Izzo
Dr. Xinyu Liu
Dr. Martin Burke
Dr. Rajesh Aneja
Thomas D Walko III

TABLE OF CONTENTS

LIST OF FIGURES

LIST OF TABLES

ACKNOWLEDGEMENTS

I would like to express my deepest appreciation to my committee chair and research advisor, Professor Krzysztof Palczewski. During my time in the Palczewski lab, I experienced both personal and professional growth. His mentorship and constant motivation have been instrumental to my successes, including earning my NIH F30 award with a score of 13, publishing in multiple journals as first- and co-author, and presenting my findings at multiple national and international conferences. He allowed me to freely explore any question or perform any experiment, giving me the opportunity to learn and grow in my creativity without restriction. He founded the Center for Translational Vision Research, an optimal environment of learning, collaboration, and execution of experimental objectives. Through multi-group lab meetings and seminars, I learned about vision research from a wide range of disciplines, including visual physiology, electrophysiology, organic chemistry, biochemistry, and molecular biology. These seminars routinely featured distinguished and renowned vision researchers from around the world. Research in the Palczewski lab has only further inspired me to pursue a lifelong journey of learning and exploring. I look forward to facilitating the connection between medicine and research, carrying forward the legacy of the Palczewski lab.

I would also like to extend my sincere appreciation to Dr. David Salom, who has been an essential part of my growth in the lab. His expertise on opsin proteins, biochemistry, and structural biology provided me with tremendous assurance and guidance as I navigated experiments and analysis of results. I would like to thank Dr. Elliot Choi for his advice and guidance through my training as an MD-PhD candidate. I also thank Professor Philip Kiser, who I have had the privilege of asking any question or advice on experiments or background knowledge on any topic related to the biochemistry of vision. I am grateful for all the members of the Palczewski lab, who have allowed me to succeed by providing me with their guidance, expertise, and mentorship. Their companionship allowed me to push through challenging moments and celebrate the victories that come along the way.

Many thanks to all the friends who have been with me through the highs and lows. Without you all, I am unsure how I would have made it this far. The emotional, spiritual, and mental support you all provided me will never be forgotten and will always be cherished.

I would like to also thank my committee members, Professors Gregory Weiss and Chang Liu. I am grateful for their technical expertise and their commitment to my growth as a scientist. I appreciate their time and effort in evaluating the work presented in this dissertation and their constructive feedback and guidance.

To all my mentors who believed in me and supported me, I cannot express my gratitude strongly enough. The body of work in this dissertation and the work that is to come are a testament of all your mentorship. You all provide me with a solid foundation and truly allow me to feel what it is like to stand on the shoulders of giants.

Finally, and most importantly, I would like to thank my parents and my older brothers. I am here and the person I am today because of your love and support.

This dissertation and all the work therein would not be possible without the funding from the National Institutes of Health. Financial support was provided by the National Eye Institute Ruth L. Kirschstein National Research Service Award Individual Fellowship (F30) Award 1F30EY03365.

Chapter 1 and portions of chapter 6 are a reprint of the material as it appears in *BioEssays.* 2023 Sep;45(9):e2300068., used with permission from John Wiley & Sons, Inc. The co-author listed in this publication is Krzysztof Palczewski. Link to the article: https://doi.org/10.1002/bies.202300068. PMID: 37454357

Chapters 2 and 3 are a reprint of the material as it appears in *Proceedings of the National Academy of Sciences.* 2022 Nov 8;119(45):e2213911119., used with permission from the National Academy of Sciences. The co-authors listed in this publication are: David Salom, Michał Andrzej Kochman, Adam Kubas, Philip D Kiser, and Krzysztof Palczewski. Link to the article: https://doi.org/10.1073/pnas.2213911119. PMID: 36322748

Chapter 4 and portions of chapter 5 are a reprint of the material as it appears in *Journal of Biological Chemistry*. 2024 Jan 23:105678. The co-authors listed in this publication are: David Salom, Elliot H Choi, Aleksander Tworak, Roman Smidak, Fangyuan Gao, Yasmeen J Solano, Jianye Zhang, Philip D Kiser, and Krzysztof Palczewski. Link to the article: https://doi.org/10.1016/j.jbc.2024.105678. PMID: 38272218

VITA

John Dong-Hoon Hong

EDUCATION

2017 – present	M.D.	Medicine	University of California Irvine
2019 – 2024	Ph.D.	Chemistry	University of California Irvine
2012 – 2016	B.S.	Chemistry	Carnegie Mellon University

HONORS / AWARDS

2023	FASEB Biology and Chemistry of Vision Travel Award
2022	FASEB International Retinoids Conference Travel Award
2013 – 2016	Chemistry Handlos Award for Potential Excellence in Research
2012 – 2016	Carnegie Mellon University Dean's List with High Honors

GRANTS / FUNDING

2022-2026	NIH NEI Ruth L. Kirschstein NRSA F30 Award – score: 13
2015	University of Illinois at Urbana-Champaign Snyder Scholar
2014	Howard Hughes Medical Institute Summer Researcher
2013	Carnegie Mellon University Small Undergraduate Research Grant

RESEARCH EXPERIENCES

Medical Student Research 2023 – present
UC Irvine Department of Ophthalmology – Mentor: Dr. Donny Suh

- Submitted a first-author manuscript to *Clinical Ophthalmology* on the frequency and severity of refractive error and amblyopia in children examined at the UCI EyeMobile clinic.
- Co-author on a manuscript submitted to *JPOS* detailing the ophthalmology referral rates of children examined at the UCI EyeMobile clinic.
- Preparing a manuscript on the biomechanical mechanism of ocular blunt trauma from badminton shuttlecock impact.
- Assisting in obtaining IRB approval for deep learning analyses of pediatric retinal hemorrhages to determine etiologies and for evaluating a pediatric retinal imaging device.

Medical Student Research 2021 – present
UC Irvine Department of Neurosurgery – Mentor: Dr. Michael Oh

- Obtained approval for IRB protocol for a prospective cohort study on second opinions in spine surgery.

- Preparing a manuscript on assessing upper extremity mobility after decompressive spine surgery in patients with degenerative cervical myelopathy, and assisted in the IRB approval for this study.

Graduate Student Research 2019 – present
UC Irvine Department of Chemistry – Mentor: Dr. Krzysztof Palczewski

- Studied the visual cycle kinetics in the rod outer segment using liquid chromatography tandem mass spectrometry (LC-MS/MS) without the need for protein purification. Published a first author manuscript in *PNAS*.
- Investigated the attenuation of rhodopsin bleaching by nanobody chaperones, leading to a co-authorship in a study published in *Nature Communications*.
- Studied the bleaching rate of human cone opsins and retinal g protein receptor (RGR) to elucidate the mechanism of color vision light sensitivity preservation under daylight conditions. Published a first author manuscript in *JBC* and as co-author on a study published in *Cell Reports*.

Graduate Student Research Rotation 2018
University of California Irvine Department of Chemistry – Mentor: Dr. Gregory Weiss

- Worked on developing near-infrared fluorophore tag for visualization of tumor cells for image-guided surgery.
- Synthesized a versatile molecular tag to conjugate proteins with fluorophores, drugs, and other small molecules. Co-authors in the study published in *Bioconjugate Chemistry*.

Research Intern 2016 – 2017
Cognition Therapeutics, Pittsburgh, PA

- Managed biomarker data from animal studies of candidate drug molecule for Alzheimer's Disease.
- Performed MetaCore Pathway Analyses of biomarker data.
- Developed a program in python to merge, sort, and filter MetaCore results for insights into the mechanism of action of the drug candidate.

Undergraduate Student Research 2015 – 2016
University of Pittsburgh Department of Chemistry– Mentor: Dr. Xinyu Liu

- Worked on the chemical synthesis of a psuedotripeptide marine toxin and its derivatives to identify its protein targets and mechanism of action.

Snyder Scholar Summer Research 2015
University of Illinois at Urbana-Champaign – PI: Dr. Martin Burke, MD, PhD

- Completed large-scale synthesis and purification of hinokitiol molecular probe for testing in zebrafish, mice, and rat models of microcytic anemia. Co-authored on the study published in *Science*.

Undergraduate Student Research 2013 – 2015
UPMC Children's Hospital – Mentor: Dr. Rajesh Aneja, MD

- Helped determine the mechanism behind the immunosuppressant effects of Tacrolimus on the secretion of an inflammatory cytokine (HMGB1).
- Investigated attenuation of lipopolysaccharide-induced inflammation by preconditioning with a chemotactic peptide (fMLP).
- Determined levels of circulating mtDNA as a quantitative biomarker of necrosis in cerebrospinal fluid of pediatric traumatic brain injury patients and blood plasma of sepsis/systemic inflammatory response syndrome patients leading to co-authorship in two manuscripts published in *Shock*.

PEER-REVIEWED ARTICLES

Hong JD, Salom D, Choi EH, Tworak A, Smidak R, Gao F, Solano YJ, Zhang J, Kiser PD, Palczewski K. Retinylidene chromophore hydrolysis from mammalian visual and non-visual opsins. *Journal of Biological Chemistry*. 2024 Jan 23:105678. doi: 10.1016/j.jbc.2024.105678. PMID: 38272218

Hong JD, Palczewski K. A short story on how chromophore is hydrolyzed from rhodopsin for recycling. *BioEssays*. 2023 Sep;45(9):e2300068. doi: 10.1002/bies.202300068. PMID: 37454357

Tworak A*, Kolesnikov AV, Hong JD, Choi EH, Luu J, Palczewska G, Dong Z, Lewandowski D, Brooks MJ, Campello L, Swaroop A, Kiser PD, Kefalov VJ, Palczewski K*. Rapid RGR-dependent visual pigment recycling is mediated by the RPE and specialized Muller Glia. *Cell Reports*. 2023 Aug 29;42(8):112982. doi: 10.1016/j.celrep.2023.112982. PMID: 37585292

Wu A*, Salom D*, Hong JD, Tworak A, Watanabe K, Pardon E, Steyaert J, Kandori H, Katayama K, Kiser PD, Palczewski K. Structural basis for the allosteric modulation of rhodopsin by nanobody binding to its extracellular domain. *Nature Communications*. 2023 Aug 25;14(1):5209. doi: 10.1038/s41467-023-40911-9. PMID: 37626045

Hong JD, Salom D, Kochman MA, Kubas A, Kiser PD, Palczewski K. Chromophore hydrolysis and release from photoactivated rhodopsin in native membranes. *PNAS*. 2022 Nov 8;119(45):e2213911119. doi: 10.1073/pnas.2213911119. PMID: 36322748

Choi EH, Gattas S, Brown NJ, Hong JD, Limbo JN, Chan AY, Oh MY. Epidural electrical stimulation for spinal cord injury. *Neural Regeneration Research*. 2021 Dec;16(12):2367-2375. doi: 10.4103/1673-5374.313017. PMID: 33907008

Choi EH, Chan AY, Gong AD, Hsu Z, Chan AK, Limbo JN, Hong JD, Brown NJ, Lien BV, Davies J, Satyadev N, Acharya N, Yang CY, Lee Y, Golshani K, Bhatia NN, Hsu FPK, Oh MY. Comparison of minimally invasive total versus subtotal resection of spinal tumor: A systematic review and meta-analysis. *World Neurosurgery*. 2021 Jul;151:e343-e354. doi: 10.1016/j.wneu.2021.04.045. PMID: 33887496

Richardson MB, Gabriel KN, Garcia JA, Ashby SN, Dyer RP, Kim JK, Lau CJ., Hong JD, Le Tourneau RJ, Sen S, Narel DL, Katz BB, Ziller JW, Majumdar S, Collins PG, and Weiss GA. Pyrocinchonimides Conjugate to Amine Groups on Proteins via Imide Transfer. *Bioconjugate Chemistry*. 2020 May 20;31(5):1449-1462. doi: 10.1021/acs.bioconjchem.0c00143. PMID: 32302483

Grillo AS, SantaMaria AM, Kafina MD, Huston NC, Cioffi AG, Han M, Seo YA, Yien YY, Menon AV, Svoboda DC, Fan J, Nardone C, Hong JD, Anderson JB, Wessling-Resnick M, Kim J, Paw BH, and Burke MD. Restored Iron Transport by a Small Molecule Promotes Gut Absorption and Hemoglobinization. *Science*. 2017 May 12;356(6338):608-616. doi: 10.1126/science.aah3862. PMID: 28495746

Caro VD, Walko III TD, Bola RA, Hong JD, Pang D, Hsue V, Au AK, Halstead ES, Carcillo JA, Clark RSB, and Aneja RK. Plasma Mitochondrial DNA – a Novel DAMP in Pediatric Sepsis. *Shock*. 2016 May;45(5):506-11. doi: 10.1097/SHK.0000000000000539. PMID: 26682947

Walko III TD, Bola RA, Hong JD, Au AK, Bell MJ, Kochanek PM, Clark RSB, and Aneja RK. Cerebrospinal fluid mitochondrial DNA – a novel DAMP in pediatric traumatic brain injury. *Shock*. 2014 Jun;41(6):499-503. doi: 10.1097/SHK.0000000000000160. PMID: 24667615

SUBMITTED / IN-PREPARATION

Hong JD, Choi EH, Suh S, Bui JH, Storch AM, Walker KR, Shahraki K, Yanez C, Torres D, Espinoza J, Molina I*, Suh DW*. UCI EyeMobile Findings for Refractive Error and Amblyopia in 3-to 10-Year-Old Children for the 2022-2023 School Year. *Clinical Ophthalmology* (Submitted)

Choi EH, Hong JD, Suh S, Bui J, Storch A, Walker KR, Espinoza J, Molina I, Suh DW. Exploring pediatric vision care: Insights from five years of referral cases in the UCI Eye Mobile vision screening program. *JPOS* (Accepted)

Zhang A, Hong JD, Kurillo G, Choi EH, Chan V, Hatch MN, Han JJ, Lee YP, Bhatia N, Oh MY. Quantitative assessment of upper extremity mobility using reachable workspace area following decompressive spine surgery for dorsal cervical myelopathy. (In preparation)

Hong JD*, Colmenarez Moreno J*, Choi EH, Suh A, Lam M, Shahraki K, Agrawal R, Gu L, Suh DW. Mechanical Ocular Sequelae from Badminton Shuttlecock Projectile Impact. (In preparation)

Zaw W*, Hong JD*, Choi EH, Suh S, Bui JH, Storch AM, Walker KR, Shahraki K, Yanez C, Torres D, Espinoza J, Molina I*, Suh DW*. UCSD EyeMobile Findings for Refractive Error and Amblyopia in San Marcos. (In preparation)

Choi EH, Colmenarez JA, Hong JD, Gu L, Suh DW. Biomechanical insights into unilateral retinal hemorrhages in shaken baby syndrome. (In preparation)

Choi EH, Hong JD, Espinoza J, Suh DW, Molina I. Trend analysis of refractive errors in school years from 2017 to 2022 from the UCSD Eye Mobile. (In preparation)

ABSTRACT / POSTER PRESENTATIONS

Hong JD, Tworak A, Salom D, Palczewski K. Elucidating the Biochemical Mechanism of Light Sensitivity Preservation During Daytime Vision. *FASEB Biology and Chemistry of Vision Conference 2023*, Tucson, Az.

Tworak A, Kolesnikov AV, Hong JD, Palczewski K. Rapid RGR-dependent visual pigment recycling is mediated by the RPE and specialized Muller glia. *FASEB Biology and Chemistry of Vision Conference 2023*, Tucson, Az.

Hong JD, Tworak A, Salom D, Palczewski K. Elucidating the Biochemical Mechanism of Light Sensitivity Preservation During Daytime Vision. *Gavin Herbert Eye Institute 9th Annual Bench to Bedside Symposium 2023*, Irvine, CA.

Hong JD, Salom D, Palczewski K. Capturing Opsin Photochemistry and Chromophore Hydrolysis. *IOVS Association for Research in Vision and Ophthalmology (ARVO) Annual Meeting 2023*, Vol.64, 8, New Orleans, LA.

Wu A, Salom D, Hong JD, Pardon E, Steyaert J, Kiser PD, Palczewski K. Structure guided GPCR drug development – human single domain antibodies (Nanobody) for Retinitis Pigmentosa. *IOVS Association for Research in Vision and Ophthalmology (ARVO) Annual Meeting 2023*, Vol.64, 8, New Orleans, LA.

Zhang A, Chan V, Hong JD, Hatch MN, Han JJ, Lee YP, Bhatia N, Oh MY. Assessing global upper extremity function before and after decompressive surgery in patients with degenerative cervical myelopathy (DCM). *Congress of Neurological Surgeons Annual Meeting 2022*, San Francisco, CA.

Hong JD, Kiser PD, Palczewski K. Chromophore Hydrolysis and Release from Photoactivated Rhodopsin in Native Membranes and Formation of Retinylidene-Phosphatidylethanolamines. *FASEB International Conference on Retinoids 2022*, Athens, OH.

Hong JD, Placeres A, Tochtrop GP, Palczewski K. Retinylation of Opsins by Retinyl Formate. *IOVS Association for Research in Vision and Ophthalmology (ARVO) Annual Meeting 2021*, Vol.62, 2992.

Nguyen A, Hong JD, Bera K. Evaluating a medical student led nutrition health education workshop for primary care providers at a community clinic. *STFM Conference on Medical Student Education 2020*, Portland, OR.

Hong JD, Richardson M, Weiss G. Synthesis of a Near-IR Fluorophore Linked to a Novel Lysine-Specific Reactive Functionality. *Annual Lake Arrowhead MSTP Conference 2018*, San Bernardino County, CA.

Hong JD, Grillo AS, Burke MD. Iron Transport Restoration by Hinokitiol Ionophore. *Annual Lake Arrowhead MSTP Conference 2017*, San Bernardino County, CA.

Hong JD, Sigindere C, Liu X. Synthesis of Vibrio Modified Tripeptide Marine Toxin. *Meeting of the Minds Annual Meeting 2016*, Pittsburgh, PA

Hong JD, Grillo AS, Burke MD. Large-Scale Synthesis and Purification of C2deOHino. *University Illinois Urbana-Champaign Chemistry Synder Scholar 2015*, Champaign, IL.

Hong JD, Walko TD, Aneja R. Preconditioning with N-formyl-met-leu-phe (fMLP) leads to Lipopolysaccharide (LPS) tolerance. *Meeting of the Minds Annual Meeting 2015*, Pittsburgh, PA.

Hong JD, Walko TD, Aneja R. Microglial Inflammatory Response to Mitochondrial DNA. *Meeting of the Minds Annual Meeting 2014*, Pittsburgh, PA.

ORAL PRESENTATIONS

Capturing Rod Outer Segment Visual Cycle Biochemistry in Native Lipid Membranes. *Annual Lake Arrowhead MSTP Conference 2022*, San Bernardino County, CA.

Capturing Rod Outer Segment Visual Cycle Biochemistry in Native Lipid Membranes. *UC Irvine Chemistry Graduate Symposium 2022*, Irvine, CA.

Capturing Rod Outer Segment Visual Cycle Biochemistry in Native Lipid Membranes. *UC Irvine Gavin Herbert Eye Institute Distinguished Lecture Series 2022 Trainee Presentation* Prelude to Lecture by Dr. Michael Chiang, NIH NEI Director, Irvine, CA

Chromophore Hydrolysis and Release from Photoactivated Rhodopsin in Native Membranes and Formation of Retinylidene-Phosphatidylethanolamines. *FASEB International Conference on Retinoids 2022*, Athens, OH.

VOLUNTEER / EXTRACIRRICULAR ACTIVITIES

Beyond Blindness Volunteer	2023 – present
UC Irvine EyeMobile for Children Vision Screening Program	2023 – present
Orange County Eye Project Clinic (Retina Clinic)	2022 – present
UCI MSTP Distinguished Lecture Series Coordinator	2018 – 2023
UCI MSTP Digital Media Committee Webmaster	2018 – 2022
UCI MSTP Equity Committee	2020 – 2021

LEADERSHIP / TEACHING EXPERIENCE

Carnegie Mellon University Colleges Against Cancer Chapter President	2014 – 2016
Teaching Assistant for Laboratory II: Organic Synthesis and Analysis	2015

ABSTRACT OF THE DISSERTATION

Chromophore Photochemistry and Hydrolysis in Mammalian Opsins

Implications to Visual Physiology

by

John Dong-Hoon Hong

Doctor of Philosophy in Chemistry

University of California, Irvine, 2024

Professor Krzysztof Palczewski, Chair

The two key cycles that are essential to sustain vision are the photocycle of visual opsins and the retinoid or visual cycle. Visual opsins include rhodopsin and cone opsin, which are densely packed in the outer segment of rod and cone photoreceptor cells, respectively. The rhodopsin photocycle was first described by Böll and Kühne in the 1870s, inspiring many major breakthroughs in our understanding of visual physiology. Vision starts when a photon of light isomerizes the 11-*cis*-retinylidene chromophore bound in Schiff base linkage to rhodopsin. The resultant all-*trans*-retinylidene agonist induces a series of conformational changes in photoactivated rhodopsin, leading to the signaling state to elicit phototransduction. Schiff base hydrolysis of the agonist leads to the release of all-*trans*-retinal, which must be recycled into 11-*cis*-retinal by the visual cycle. Apo-opsin binds 11-*cis*-retinal to regenerate rhodopsin pigment for another round of light detection. As such hydrolysis serves as the key step diminishing ongoing phototransduction, as well as bridging both the visual cycle and the photocycle of visual opsins.

Many challenges have been encountered in measuring the rate of this hydrolysis, which has largely been studied indirectly by optical spectroscopy and electrophysiology techniques. Our studies demonstrate the ability to directly measure hydrolysis using a method developed in-house, utilizing liquid chromatography-tandem mass spectroscopy (LC-MS/MS) and a specialized sample preparation involving sodium borohydride in isopropanol ($NaBH_4$/*i*PrOH). $NaBH_4$/*i*PrOH led to simultaneous protein denaturation and reductive trapping of chromophore as a retinyl moiety in secondary amine linkage to opsin. Concurrently, alcohol-induced protein precipitation facilitated fractionation of proteins from lipids to quantitate the amount of agonist remained bound to opsin, measured in the protein fraction, or hydrolyzed as all-*trans*-retinal, measured in the lipid fraction. Subsequent steps of N-retinylidene-phosphatidylethanolamine adduct formation and reduction to all-*trans*-retinol by retinol dehydrogenases were also detected by LC-MS/MS of the lipid fraction. Altogether each successive step of the visual cycle occurring within the rod outer segment was determined for its rate in native membranes, with each successive step an order of magnitude faster than the prior.

Our method was applied to other visual and non-visual opsins, namely cone opsins, retinal G protein-coupled receptor (RGR), and peropsin (RRH). Schiff base hydrolysis of agonist in photoactivated cone opsins was found to be markedly faster than in photoactivated rhodopsin. Reciprocally, RGR displayed *trans*-*cis* photochemistry and subsequent rapid hydrolytic release of 11-*cis*-retinal, followed by immediate re-binding of all-*trans*-retinal. The rapid rate of hydrolysis and regeneration was observed for RGR in microsomal membranes of the retinal pigment epithelium. As such, RGR plays a crucial role in continuously supplying chromophore needed to sustain photopic or color vision under

bright daylight conditions. Though RRH was suspected to function similarly to RGR in the photic production of 11-*cis*-retinal from all-*trans*-retinal, RRH did not exhibit pigment formation with all-*trans*-retinal or any mono-*cis* retinal isomers, leaving uncertain its role in visual physiology.

CHAPTER 1

INTRODUCTION

This chapter is in part derived from the manuscript published in *BioEssays*:
Hong JD, Palczewski K. A short story on how chromophore is hydrolyzed from rhodopsin for recycling. ***BioEssays***. 2023 Sep;45(9):e2300068. doi: 10.1002/bies.202300068. PMID: 37454357

INTRODUCTION

Early discoveries laid the foundation to our current understanding of vision. In 1722, Antonie van Leeuwenhoek using his self-designed single-lensed microscope investigated everything from microbiology to anatomy and became the first to record his observations of a layer of rods and cones in the retina of a frog.[1] In 1782, Francesco Buzzi describes a thin yellow depression lateral to the optic nerve in a dissected human eye of a 35-year old man.[2] This yellow spot was discovered and later named the macula lutea in 1791 by Samuel Thomas von Sömmerring, a prolific neuro-anatomist and physician.[3, 4] He also generated the earliest illustrations of the retina in meticulous detail and color, based on dissected retinas. He was also one of the earliest to describe the connection of the retina to the optic nerve. The macula is now understood to be responsible for our central and color vision, which predominantly dictates our visual experience of the world. The fovea, which is the most central part of the yellow depression of the macula, has the densest packing of cones, responsible for our visual acuity and playing an even larger role in our visual experiences.

In the early 1800s, Jan Evangelista Purkyně, another prolific anatomist and physiologist, recorded some of the earliest observations of the live retina using a concave lens and candle light, before the invention of the ophthalmoscope by Hermann von Helmholtz in 1851.[5] Purkyně's dissertation on the physiology of vision earned him professorship at the University of Wroclaw. He recorded several major findings in his dissertation, including the phenomenon now called the Purkinje shift or effect, where sensitivity to blue light as opposed to red light appears enhanced during dusk or dim light conditions.[6] This is one of the earliest descriptions of rod vs cone light sensitivity.

Meanwhile, a rising star in retinal anatomy, Heinrich Müller discovered the light-sensitive red pigment of rods, later further described by Franz Böll and Wilhelm Kühne and now known as rhodopsin (Rho).[7] He also discovered the neuroglia of the retina, known as Müller cells. The red pigment, also called visual pigment or visual purple, was observed to be purple when highly concentrated.[8] The purple hue is owed to the unique cellular morphology of the rod photoreceptors, possessing an outer segment compartment with tightly stacked membrane discs that are each densely packed with rhodopsin pigment molecules (Figure 1.1).[9] An estimated 10^8 rhodopsin pigment molecules exist per rod photoreceptor cell.[10]

Following Müller's discoveries of the red pigment of rods, Böll and Kühne were the first to document its light-induced color changes, or bleaching, from red to orange, then yellow, and eventually colorless.[8, 11] In the dark, the pigment is gradually restored with a corresponding decrease in the golden yellow oil droplets within neighboring hexagonal epithelial cells called retinal pigment epithelial (RPE) cells.[8, 11] Notably, Kühne was first to prepare a solution of rhodopsin, a membrane protein, using bile salts, which would become crucial to the study of opsins by absorbance or fluorescence spectroscopy.[12] These early findings by Böll and Kühne of the photocycle of the rhodopsin pigment set the stage for over a century of breakthroughs in our understanding of how vision is continuously sustained. Simultaneously, investigations into the biochemistry of opsin proteins laid the groundwork for understanding G-protein coupled receptors, the most pharmacologically targeted family of proteins.

1.1 THE IDENTITY OF THE CHROMOPHORE OF OPSIN

In the 1930s, George Wald discovered vitamin A in abundance in the retina and later showed that the rhodopsin pigment was a complex of opsin with a form of vitamin A called "retinene", now known as retinal.[13, 14] Opsin and retinal was suspected to be in Schiff base linkage, based on the works of Collins, Morton, and Pitts.[15, 16] A Schiff base seemed compelling, given the bathochromic shift in the absorption maximum from the UV range (380 nm of retinal) to the visible range (440nm of N-retinylidene-amine). The additional shift toward 500 nm, the absorption maximum of rhodopsin, was later established to be due to solvatochromatic effects from the interactions of residues within the chromophore-binding pocket with the polyene chain of the bound retinylidene chromophore.[17, 18] Differences in chromophore-binding pocket residue interactions lead to the absorption maximum differences between rhodopsin and cone opsins (Figure 1.2).

Furthermore, just as readily as a Schiff-base can form between retinal and an amine, it can also readily hydrolyze, aligning with observations of rhodopsin pigment bleaching and releasing retinal upon light exposure. The isomeric configuration of the released retinal was known to be all-*trans*-retinal, but the identity of the pigment-forming species was determined to be 11-*cis*-retinal much later in 1956 in the Wald laboratory, much to the surprise of all those involved with its discovery given the high thermodynamic instability of the 11-*cis* configuration.[19]

The covalent Schiff base between rhodopsin and 11-*cis*-retinal was later confirmed by Deric Bownds using borohydride reduction, which converted the retinylidene Schiff base adduct into a nonhydrolyzable retinyl secondary amine linkage.[20] The resultant N-retinyl-opsin reduction product was completely proteolyzed by pronase to determine the site of retinal attachment, shown to be the ε-amino group of a Lys residue.[21] The location of

this Lys residue was heavily pursued by multiple lab groups, systematically determining the entire amino acid sequence of rhodopsin, then using borotritium to reductively trap and radiolabel the retinylidene-adducted Lys residue. The location was eventually determined to be Lys^{296} by Ovchinnikov and Hargrave.[22, 23]

The retinylidene Schiff base of Lys^{296} was later found to be in salt bridge interaction with Glu^{113}, conferring stability to the ground-state rhodopsin pigment.[24-27] After light exposure leading to photoisomerization of the 11-*cis*-retinylidene chromophore to the all-*trans*-retinylidene agonist, the resultant photoactivated rhodopsin (Rho*) undergoes a series of conformational changes to its metarhodopsin II (MII) signaling state. Glu^{113} facilitates the transitions to MII by acting as a proton acceptor in the deprotonation of the all-*trans*-retinylidene Schiff base.[28] Prior to the deprotonation event, Glu^{181} in extracellular loop 2 acts as a partial counterion switch to help relax the Rho* structure to metarhodopsin I (MI).[29, 30] Upon reaching the active MII signaling state, the all-*trans*-retinylidene agonist is hydrolyzed to release all-*trans*-retinal. Regeneration with fresh 11-*cis*-retinal supplied by the visual or retinoid cycle completes the rhodopsin photocycle (Figure 1.3).

Eventually, the crystal structure of chromophore-bound rhodopsin was achieved, representing the first 3-dimensional characterization of a G protein-coupled receptor (GPCR).[31, 32] However, pursuit of the structure of Rho* served as an even greater challenge, given the transient nature of the all-*trans*-retinylidene agonist being susceptible to hydrolysis.[15, 33] Recent methodological advances have allowed the capture of specific Rho* species, including a very early intermediate and potentially the MII signaling state.[34-37]

1.2 PROPERTIES OF PHOTOACTIVATED RHODOPSIN

The visual pigment, appearing purple when concentrated, and red upon dilution, was observed by Kühne and his associates Ewald and Ayres to change to a more persistent "visual yellow" color before eventually becoming colorless, or "visual white", which was later determined to contain free retinal.[8, 13] Further investigations by Lythgoe of rhodopsin kept on ice and exposed to light showed evidence of a "transient orange" form that was not the result of a mixture of visual yellow and unbleached visual red pigments.[38] The orange color was more stable when the rhodopsin preparation was maintained on ice rather than when warmed to 30°C, which led to a pale-yellow color. Upon attempted extraction of retinal, the transient orange and visual yellow forms were found to still contain bound retinal. Furthermore, the visual yellow form was observed to change spectral properties in response to changes in pH; therefore it became more aptly named "indicator yellow."[38] Lythgoe's observations were further followed up by Collins, Morton, and Pitts, who observed analogous pH-dependent spectral changes with a model Schiff base adduct of retinal with a primary amine, mimicking the epsilon amine of a Lys residue.[15, 16] They also reported the hydrolysis of the retinylidene Schiff base occurring fastest at a mildly acidic pH of 5.7, close to its pKa.[15, 16]

Expanding upon Lythgoe's observation of "transient orange," the use of absorbance measurements at very low-temperatures allowed for the capture of each major photo-intermediate of Rho*, prior to the eventual hydrolysis and release of retinal, in the following order: bathorhodopsin (λ_{max} = 543 nm, at < -150°C), lumirhodopsin (λ_{max} = 497 nm, at -140°C to -40°C), MI (λ_{max} = 478 nm, at -35°C to -10°C), and MII (λ_{max} = 380 nm, at -10°C to 0°C).[39] Metarhodopsin III (MIII, λ_{max} = 465 nm) was later identified with its all-*trans*-retinylidene Schiff base in the *syn*-configuration, distinct from the *anti*-configuration

of the previously identified species.[40, 41] This *anti*-to-*syn* conversion has been proposed to occur either through photic or thermal energy.[41, 42] All three metarhodopsin species are in thermal equilibrium, shifting under higher pH conditions counterintuitively towards the protonated states of MI and MIII, and under lower pH conditions towards the deprotonated state of MII.[41] MII, the signaling state of Rho*, exists as the dominant species under physiological pH and has been shown to be the species from which the hydrolysis of the all-*trans*-retinylidene Schiff base largely proceeds (mechanism in Figure 1.4).[34, 35, 43, 44]

1.3 STRUCTURAL WATER NETWORKS OF RHODOPSIN

In 1977, Downer and Englander discovered that an usually vast proportion of rhodopsin, around 70% of amide groups, was interacting with water based on hydrogen-tritium exchange experiments performed on native ROS membrane suspensions; in contrast, this proportion is typically around 20-40% in other proteins.[45] This water network spanning rhodopsin was better characterized later with X-ray crystallographic structures and fourier transform infrared (FTIR) spectroscopy. Water plays an indispensable and integral role within the H-bonding networks of the interhelical spaces of rhodopsin to stabilize structure.[46-48] These structural waters as well as those present within the chromophore binding pocket are essential to the spectral tuning of rhodopsin by solvatochromic interactions with the retinylidene polyene chain[18, 49-55]; additionally, water adjacent to the retinylidene Schiff base influences the pKa of Glu^{113} to shift the proton towards the retinylidene Schiff base along the salt bridge for the bathochromic shift to absorb longer wavelengths of light.[56] Furthermore, this Schiff base in ground-state rhodopsin is protected against hydrolysis by an intradiscal “plug” preventing the entry of

bulk water into the chromophore binding pocket.[57] Therefore, perturbations to the water network and protein structure of rhodopsin lead to instability of ground-state rhodopsin to retain chromophore, leading to retinitis pigmentosa.[58, 59] Similar perturbations in other GPCRs could also affect the stability of their inactive resting state, given the highly conserved nature of structural waters across GPCRs.[60, 61]

Structural waters within rhodopsin not only provide stability but also plasticity to facilitate protein conformational changes upon the photoisomerization of the 11-*cis* chromophore to the all-*trans* agonist.[46, 47, 62, 63] Changes in the water network were observed in the transitions through different photointermediates with the greatest change occurring upon reaching the MII active state. The outward tilting of transmembrane helices 5 and 6 in MII opens a solvent pore on the cytosolic face of rhodopsin, allowing a large influx of bulk water that ultimately hydrolyzes the Schiff base of the all-*trans* agonist for the release of all-*trans*-retinal.[62, 64-70] A significant amount of this bulk water is then displaced upon MII binding of transducin to elicit the phototransduction cascade.[67] The hydrolysis detailed above exhibits stereoselectivity for the all-*trans* configuration, as demonstrated by the lack of hydrolysis of the 11-*cis*-locked retinal analogue that photoisomerizes to an 11,13-*dicis*-agonist that remains bound and thermally reverts to the mono-11-*cis* configuration, re-establishing ground-state rhodopsin.[71]

The water network changes in the photoactivation of rhodopsin are highly conserved across GPCRs.[62, 72, 73] The binding of agonist to the ligand-binding site of GPCRs is analogous to the production of the all-*trans* agonist by photoisomerization. Agonist binding induces concerted protein conformational and water network changes very similar to those observed in rhodopsin. An influx of bulk water occurs in the active state conformation

despite not requiring hydrolysis to release the agonist, given a reversible binding interaction with the ligand-binding site.[72-74] Aberrancies in the water network and protein structure that cause abnormally fast or slow decay of Rho* to apo-opsin and all-*trans*-retinal are implicated in the stability of the active state of other GPCRs and release of their agonist.[59]

1.4 PRIOR QUANTITATIVE APPROACHES TO PHOTOACTIVATED RHODOPSIN DECAY

1.4.1 Absorbance spectral measurements of Rho* decay in native tissue

One of the earliest measurements of the rate at which Rho* decays to retinal and apo-opsin was done by Baumann, using absorbance spectroscopy to study dissected and re-perfused retinal tissue of frogs and humans.[75, 76] He determined the rate constants for decay of MII and MIII, at pH 7.5 and 36°C, to be about k = 0.003 sec^{-1} and k = 0.004 sec^{-1}, respectively, which correspond to half-lives of about 4 min and 3 min, respectively.[76] However, a thorough understanding of the nature of the metarhodopsin species had not been established, especially for MIII, which is now understood to decay much more slowly than MII.[41, 77] Notably, it is not known currently whether MI undergoes hydrolysis to release retinal, and capturing this process is especially challenging given its rapid conversion within milliseconds to the longer-lasting MII form. Furthermore, the broad overlapping nature of the absorption spectra of the ground-state rhodopsin pigment, its photo-intermediates, and free retinal presents challenges to tracking the hydrolysis event, given the difficulty of definitively distinguishing each species in the complex mixture after light exposure.

1.4.2 Tryptophan fluorescence quenching assay of Rho* decay

The problems of absorbance spectroscopy were circumvented through use of fluorescence spectroscopy to study Rho* hydrolysis and release of retinal. The intrinsic fluorescence of the five tryptophan residues of rhodopsin is quenched by bound retinal; therefore, the increase in tryptophan fluorescence emission provides a precise measurement of the overall process of Schiff base hydrolysis and release of retinal from Rho*.[78, 79] The half-life of Rho* decay was found to be on the order of minutes at 20°C, with an activation-energy barrier for the combined events of hydrolysis and retinal release being ~20 kcal/mol.[78] The timescale of Rho* decay (minutes) highlights the importance of rhodopsin kinase and arrestin in halting ongoing phototransduction long after the light stimulus. This role is especially evident in mice lacking rhodopsin kinase or arrestin, where light-induced photoreceptor degeneration occurs very early in life.[80, 81]

Monitoring intrinsic tryptophan fluorescence has provided the most precise way to track Rho* decay; however, it cannot distinguish the two processes of Schiff base hydrolysis and subsequent release of retinal. Furthermore, as typically done to study membrane protein biochemistry, mild detergents were used to solubilize rhodopsin to allow for more precise spectroscopic measurements. The detergents could alter protein properties relative to their native state in the membrane, potentially producing misleading results especially in the case of rhodopsin, which resides in membranes rich in polyunsaturated acyl chains, such as docosahexaenoic acid.[82, 83]

1.4.3 Native MS to capture the first steps of vision

Recent advances have led to the development of mass spectrometry (MS) techniques that can detect whole membrane proteins in their native membranes, along with their complexes with small molecules, lipids, nucleic acids, and other proteins. Using a state-of-the-art native MS system, the Robinson group characterized the very first steps of the visual cycle and phototransduction in rod outer segment (ROS) membranes, avoiding the reductionist approach of studying proteins or complexes in isolation.[84] The hydrolysis of Rho* was tracked in its native environment of natural lipids and proteins, providing the most accurate and precise method to monitor Rho* decay into apo-opsin and retinal. The hydrolysis was found to have a rate constant k'_{hyd} = 3.20 ± 0.17 (x 10^{-3}) sec^{-1} at pH 7.0 and 28°C, corresponding to a half-life of 3.61 ± 0.19 min, in agreement with previous results described above.[84]

Despite its astonishing capabilities in capturing the kinetics of the phototransduction cascade as well as Rho* decay, native MS comes with several limitations. The method is not widely accessible to many laboratories. Furthermore, the method cannot truly discriminate between ground state and Rho*; despite having different isomeric configurations of the retinylidene adduct, both forms have the same molecular weight. Additionally, the method does not allow for non-volatile buffers and salts, including NADPH, which is the required cofactor for reduction of retinal by retinol dehydrogenases (RDHs), which may interact with Rho* and potentially affect the rates of Schiff-base hydrolysis and/or retinal release.[85]

1.5 UNCOVERING THE CLASSICAL VISUAL CYCLE

Following the decay of Rho*, the released all-*trans*-retinal must be recycled into 11-*cis*-retinal to regenerate opsin pigment to sustain vision. In 1949, Wald and Hubbard found that immediately after hydrolytic release from Rho*, all-*trans*-retinal is reduced to all-*trans*-retinol by ROS retinol dehydrogenases (RDHs).[14, 86] The all-*trans*-retinol was later found to be esterified with palmitate or stearate by lecithin retinol acyltransferase (LRAT) in the RPE, and these retinyl esters were determined by George Wald and others to be an important component of the golden oil droplets of the RPE observed by Böll.[14, 87-93] Retinyl esters were later determined to be the substrate of retinoid isomerase (RPE65) to produce the 11-*cis*-retinol for oxidation by RPE-RDHs to the 11-*cis*-retinal chromophore for regeneration of the rhodopsin pigment.[94-97] Together these findings explain the decrease in droplet number and size in the dark with the corresponding regeneration of neuroretina pigmentation. The detailed classical visual cycle can be found in figures 1.4 and 1.5, depicting the series of enzymatic reactions to recycle chromophore for constant regeneration of rhodopsin pigment to sustain vision.

The overall kinetics of the visual cycle was determined indirectly by physiological recordings done on subjects who report the dimmest light observable at different time points to measure the kinetics of dark adaptation. The earliest work done by Selig Hecht demonstrated that full dark adaptation in humans takes arounds 30-40 min with a *k* constant of around 0.016 s^{-1}.[98, 99] Following intense illumination for full cone bleaching, the initial cone dark adaptation kinetics were demonstrated to be more rapid with full dark adaptation by around 10 min with a *k* constant of around 0.7 s^{-1}.[99] Later an alternative light-driven process of 11-*cis*-retinal chromophore generation would be uncovered with retinal g protein receptor (RGR), an opsin with *trans-cis* photochemistry, opposite to the

cis-trans photochemistry of rhodopsin and cone opsins.[100, 101] More about RGR will be detailed in Chapter 4.

1.6 OVERALL OBJECTIVES

The key step that unifies the rhodopsin photocycle and the visual cycle is the Schiff base hydrolysis of the all-*trans*-retinylidene agonist. The hydrolysis supplies all-*trans*-retinal to the visual cycle to replenish 11-*cis*-retinal, while liberating the chromophore binding pocket for entry of fresh 11-*cis*-retinal to regenerate rhodopsin pigment. The main objective of the work presented in this dissertation is to quantitatively measure the rate of hydrolysis of the all-*trans*-retinylidene agonist in Rho* using the direct approach of liquid chromatography-tandem mass spectrometry (LC-MS/MS). This technique is typically available at most institutions and to most laboratories, thereby being more accessible to a wider scientific audience that might seek to use this approach to study their opsin protein of interest. The sample preparation described also uses cheap reagents, with much of the cost coming from sourcing the opsin proteins.

This dissertation will detail our methodology, which has demonstrated incredible versatility in its ability to measure the retinylidene hydrolysis rates of any opsin, and importantly, in their native membrane environments without the need for protein purification. The method was applied to study opsins of the photoreceptors (red, green, and blue cone opsins and rhodopsin) and opsins of the adjacent supporting cells, RPE (RGR and peropsin (RRH)) or Müller glia (RGR). The results demonstrate the differences in rhodopsin vs cone opsin biochemistry, as well as the supportive role of RGR but not RRH in the alternative or photic visual cycle. Serendipitously, this method was adaptable to study

the formation of Schiff base adducts between phosphatidylethanolamines (PEs) and all-*trans*-retinal released from Rho* hydrolysis. The RDH-mediated reduction of all-*trans*-retinal to all-*trans*-retinol could also be studied by $NaBD_4$ as a reducing and isotopic labeling agent. Therefore, the kinetics of each major visual cycle process occurring within ROS could be quantitatively determined by our LC-MS/MS based method without the reductionist approach of isolating or purifying any proteins or constituents.

1.7 Figures

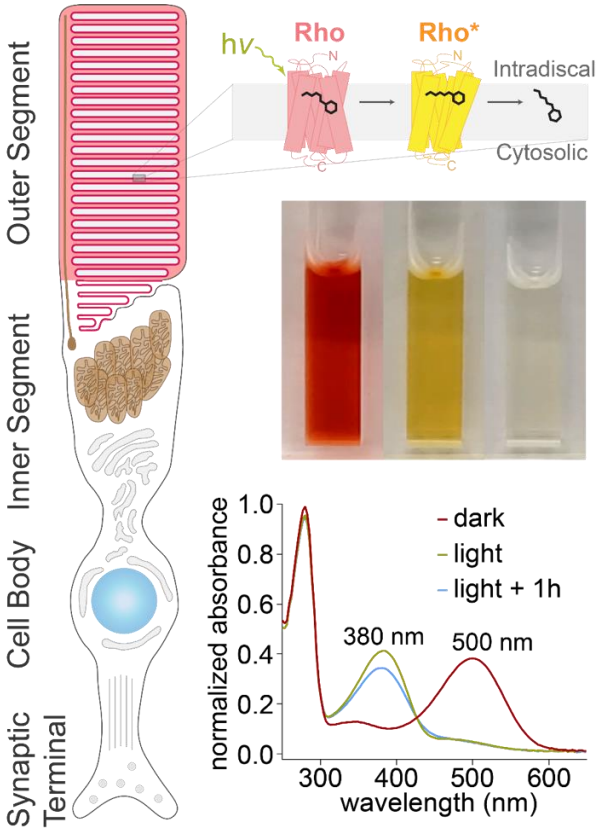

Figure 1.1 Rod photoreceptor with rhodopsin photochemistry. Rhodopsin is abundant and tightly packed in rod outer segment (ROS) discs for high sensitivity to light, needed for optimal capture of photons under dim light conditions. Light induces the characteristic color changes that were observed originally by Böll and Kühne, with gradual bleaching of the red pigment of rhodopsin to the indicator yellow form of Rho*, and eventually to the visual white (or colorless) form of apo-opsin with free retinal [8, 11]. The broad absorbance spectrum with a λ_{max} of 500 nm results in the apparent red color of rhodopsin. The change in absorption maximum to 380 nm from light exposure results in the apparent yellow color of Rho*. The fading of the yellow pigment is due to the Schiff base hydrolysis, releasing all-*trans*-retinal, which has a lower extinction coefficient than the deprotonated retinylidene Schiff base of Rho*.

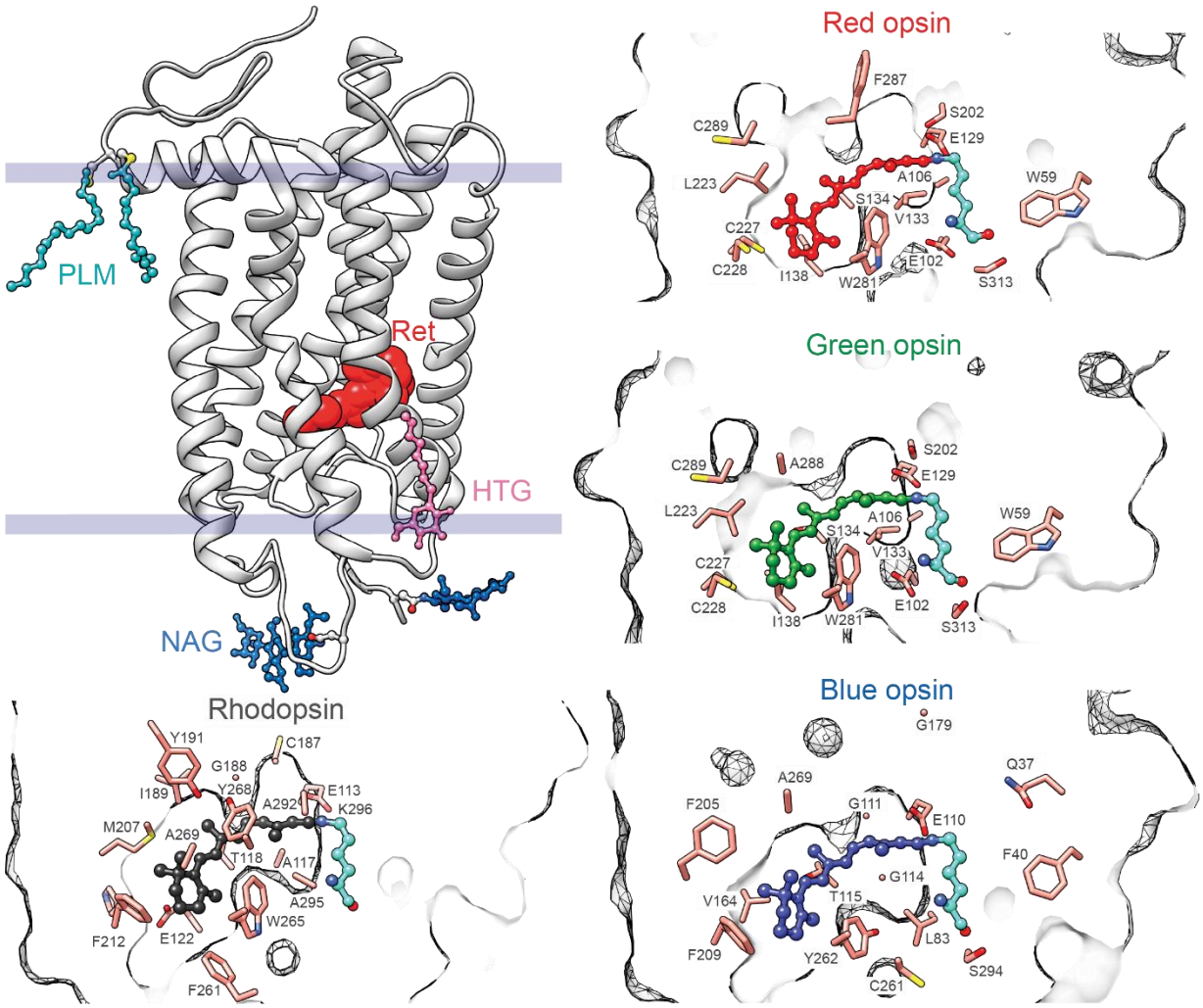

Abbreviations: Ret, retinylidene; PLM, palmitoyl; NAG, N-acetylglucosamine; HTG, Heptyl 1-thio-β-D-glucopyranoside

Figure 1.2 Three dimensional models of rhodopsin and cone opsins. Residues surrounding the chromophore are depicted for rhodopsin and three human cone opsin pigments. The rhodopsin model is based on PDB 1U19, and the homology models of the cone opsin pigments are deposited in the PDB (identifiers 1KPN, 1KPW, and 1KPX for the blue, green, and red cone pigments, respectively) [102]. Each pigment has a characteristic absorbance maximum (λ_{max}): rhodopsin (500 nm), red (560 nm), green (530 nm), blue

(420 nm). The absorbance maximum of the protonated retinylidene Schiff base (λ_{max} = 440 nm) undergoes a bathochromic shift by interaction of the polyene chain with key residues in the chromophore binding pockets of rhodopsin, red opsin, and green opsin; whereas for blue opsin, a hypsochromic shift occurs.

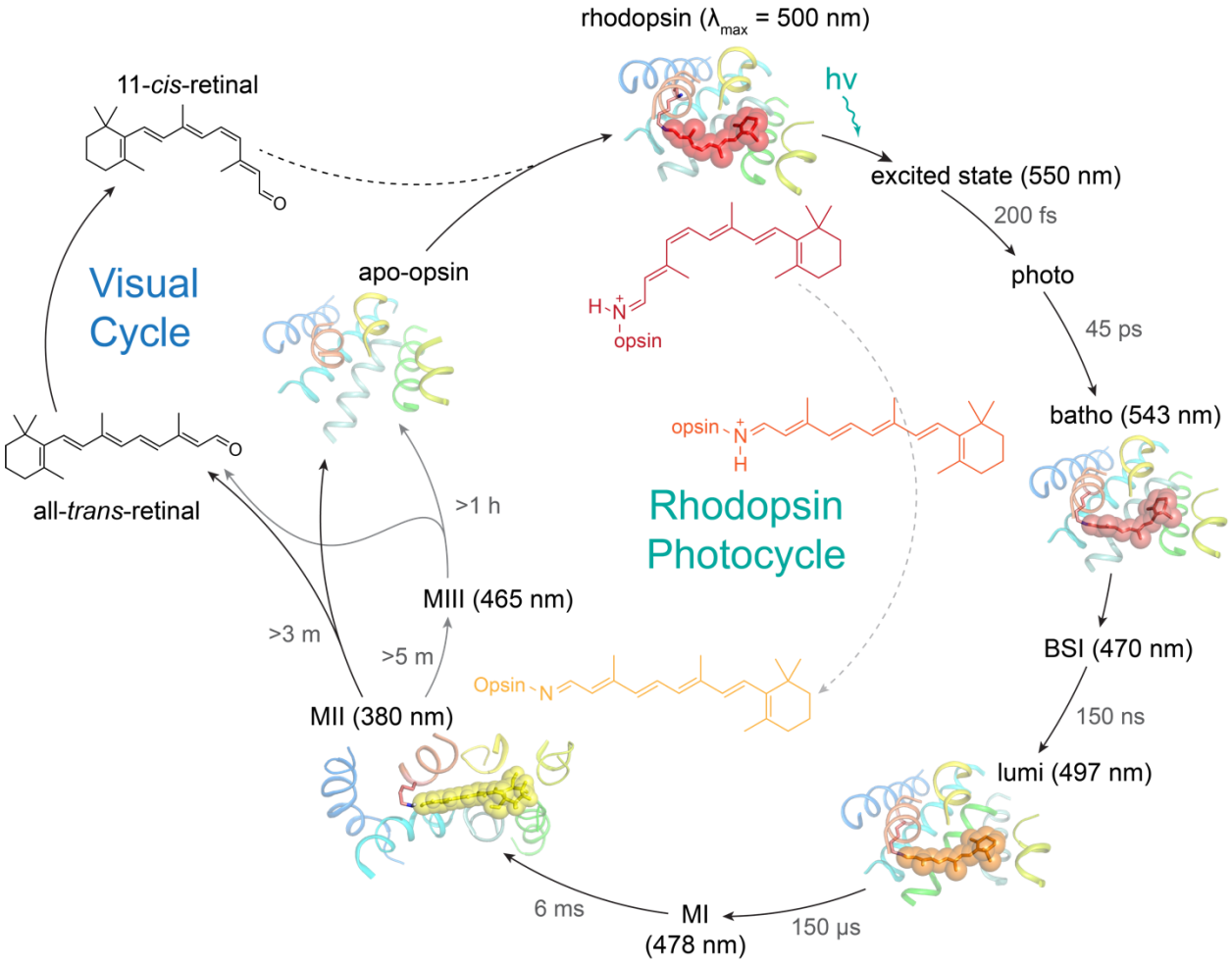

Abbreviations: photo, photo-rhodopsin; batho, batho-rhodopsin; BSI, blue-shifted intermediate; lumi, lumi-rhodopsin; MI, metarhodopsin I; MII, metarhodopsin II; MIII, metarhodopsin III

Figure 1.3 Rhodopsin photocycle. The photocycle is initiated upon photoisomerization of the 11-*cis*-retinylidene chromophore of ground-state rhodopsin to the all-*trans*

configuration. The substantial change in retinylidene ligand structure from the *cis*-to-*trans* configuration induces a series of conformation changes in rhodopsin. Exceedingly transient key photointermediates are formed in the process of relaxing the protein structure to accommodate the all-*trans* agonist in route to the conformation of the MII active signaling state. The subsequent step of hydrolysis is essential not only to the rhodopsin photocycle but also to the visual cycle. Hydrolysis of the retinylidene Schiff base in MII releases all-*trans*-retinal, resulting in apo-opsin that can be regenerated to ground-state rhodopsin by binding fresh 11-*cis*-retinal from the visual cycle. MII can alternatively convert to MIII which possesses the *syn*-configuration of the retinylidene Schiff base, which hydrolyzes significantly slower. PDB IDs used were: bathorhodopsin, 2G87 [103]; lumirhodopsin, 2HPY [104]; MII, 3PXO [34], 3PQR [34], 2I37 [35]; opsin, 3CAP [105]; rhodopsin 1F88 [31]; 1L9H [106].

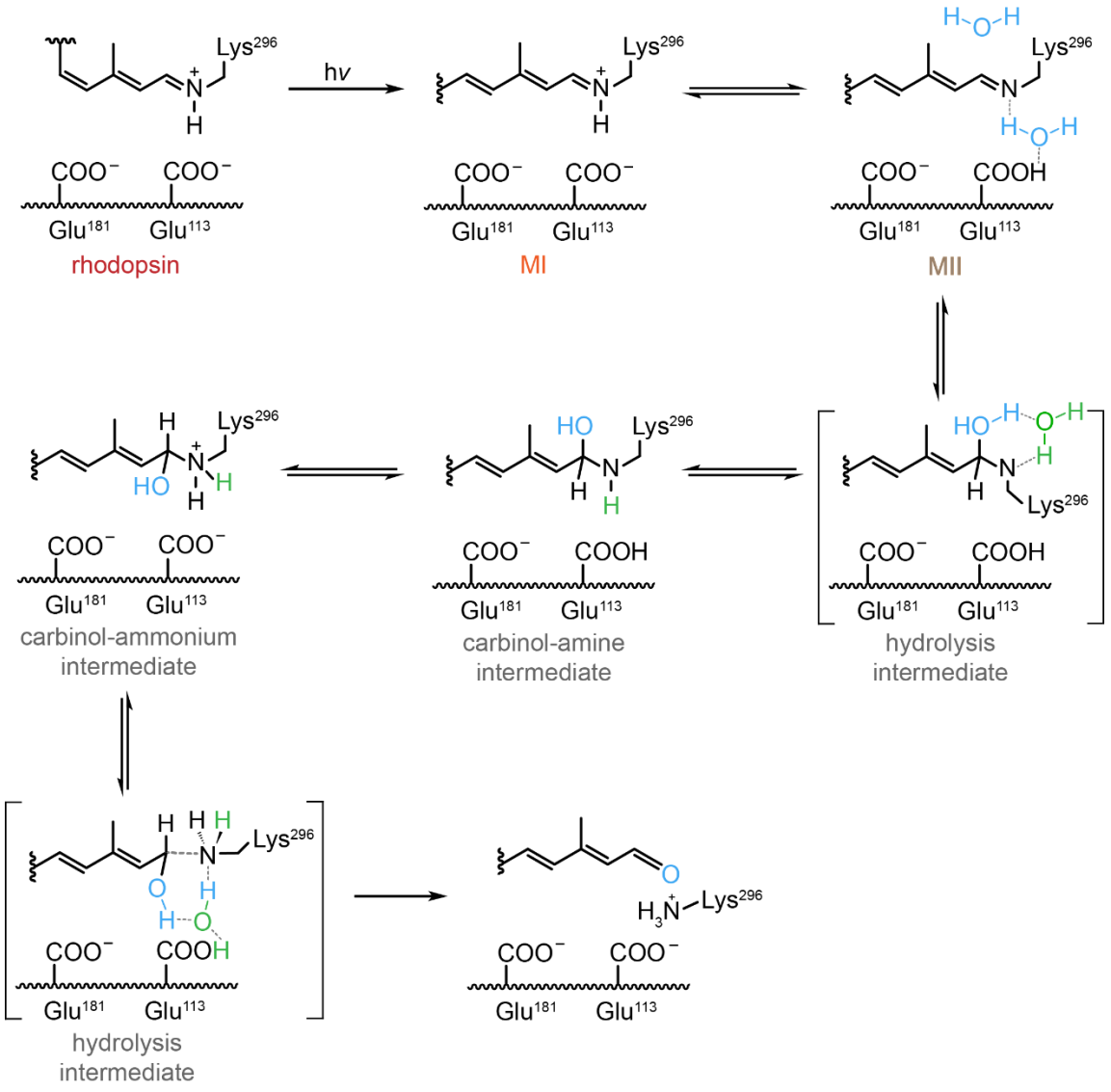

Figure 1.4 Mechanism of the hydrolysis of the all-*trans*-retinylidene agonist of Rho*. The following diagram was adapted from Palczewski 2006 [107] and updated with mechanistic descriptions from Hong, *et al.* 2022.[44] Light exposure of rhodopsin momentarily forms MI, which quickly deprotonates to form MII, the active signaling state for phototransduction. The extensive water network within rhodopsin provides an aqueous environment [68] which can mediate the hydrolysis process through MII.[68, 69] The protic environment provided by water allows for quick transfer of protons as well as H-bonding interactions to help stabilize each intermediate. Nucleophilic attack by water on

C15 of the retinylidene Schiff base forms an intermediate stabilized by H-bonding interactions with water.[69] A series of proton transfers mediated by the protic environment of water produces the carbinol-ammonium intermediate, which is primed for the completion of hydrolysis, with the protonated Lys residue serving as a favorable leaving group. The elimination of the protonated Lys residue leads to formation of the all-*trans*-retinal hydrolysis product. The mechanistic route as well as the protonation states of E113 and E181 shown for MII were based on quantum chemical calculations.[44] The actual protonation state of E181 is unclear, with different conclusions having been reported in previous studies; however, more recent studies have corroborated a deprotonated E181.[29, 30, 108-110] If and how E181 protonation status affects the hydrolysis mechanism requires further experimental investigation to potentially enrich the description above; nevertheless, the presence of E181 in extracellular loop 2 serves to stabilize the Schiff-base-bound chromophore against hydrolysis.[111]

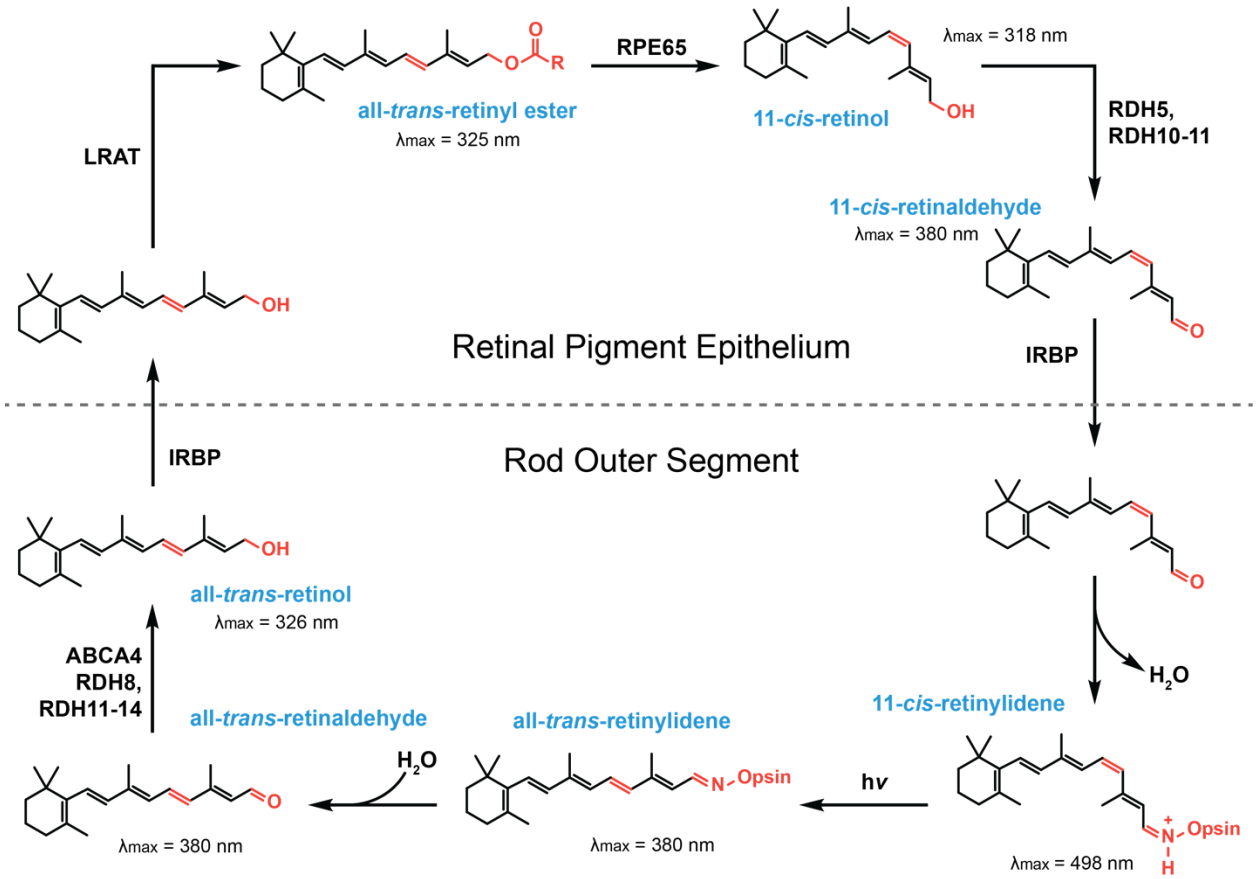

Abbreviations: ABCA4, ATP-binding cassette subfamily A member 4; RDH, retinol dehydrogenase; IRBP, interphotoreceptor retinoid binding protein; LRAT, lecithin retinol acyltransferase; RPE65, retinoid isomerase

Figure 1.5. The retinoid or visual Cycle. Upon light exposure, the 11-*cis*-retinylidene chromophore of Rho is photoisomerized to all-*trans*-retinylidene, generating Rho*. After a series of conformation changes, Rho* reaches its signaling state with deprotonated all-*trans*-retinylidene that is subject to hydrolysis by bulk water for the release of all-*trans*-retinal. This all-*trans*-retinal is released into the intraluminal leaflet of the bilayer of ROS discs and ABCA4 assists with its movement to the cytosolic leaflet for momentary reduction by RDHs to all-*trans*-retinol. IRBP then shuttles all-*trans*-retinol to the RPE for esterification by LRAT. Subsequent processing of all-*trans*-retinyl esters by RPE65

produces 11-*cis*-retinol, which is immediately oxidized by RDHs to 11-*cis*-retinal that can be shuttled to ROS by IRBP for regeneration of Rho pigment.

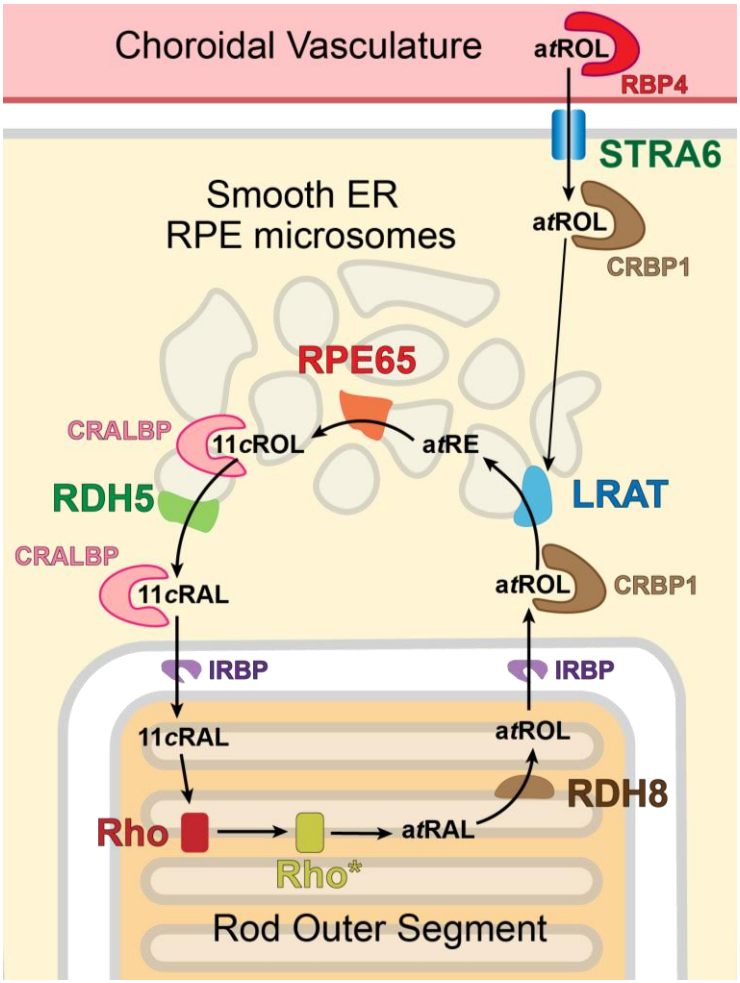

Abbreviations: Rho, rhodopsin; Rho*, photoactivated rhodopsin; a*t*RAL, all-*trans*-retinal; RDH, retinol dehydrogenase; a*t*ROL, all-*trans*-retinol; IRBP, interphotoreceptor retinoid binding protein; CRBP1, cellular retinol-binding protein 1; STRA6, stimulated by retinoic acid 6 or vitamin A receptor; LRAT, lecithin retinol acyltransferase; a. RE, all-*trans*-retinylester; RPE65, retinoid isomerase; 11*c*ROL, 11-*cis*-retinol; 11*c*RAL, 11-*cis*-retinal.

Figure 1.6 The retinoid or visual cycle with subcellular localization of processes. The processes of the ROS include: Rho 11-*cis*-retinylidene chromophore photoisomerization

and consequent photoactivation, hydrolysis of the all-*trans*-retinylidene agonist in Rho* to release a*t*RAL, and immediate reduction by RDHs to produce a*t*ROL. IRBP shuttles a*t*ROL from the ROS to the RPE, where it is bound by CRBP1 and delivered to microsomes for esterification by LRAT and storage as a*t*REs. Another source of a*t*ROL is from the bloodstream, carried in RBP4, and trafficked into the RPE by STRA6. LRAT prompt stores a*t*ROL as esters in microsomes. RPE65 gradually processes the a*t*REs in microsomes into 11*c*ROL, which is promptly oxidized by RDHs into 11*c*RAL. CRALBP binds 11*c*ROL or 11*c*RAL protecting the 11-*cis*-retinoids from thermal isomerization back into the thermodynamically stable all-*trans* configuration. 11*c*RAL is shuttled to the ROS by IRBPs for regeneration of Rho pigment.

CHAPTER 2

Mass spectrometric detection of the site of chromophore attachment

This chapter is in part derived from the manuscript published in *Proceedings of the National Academy of Sciences*:
Hong JD, Salom D, Kochman MA, Kubas A, Kiser PD, Palczewski K. Chromophore hydrolysis and release from photoactivated rhodopsin in native membranes. ***PNAS***. 2022 Nov 8;119(45):e2213911119. doi: 10.1073/pnas.2213911119. PMID: 36322748

2.1 Introduction and Significance

The early comprehensive work of Ovchinnikov and Hargrave demonstrated Lys^{296} as the site of attachment of chromophore in rhodopsin.[22, 23] To achieve this feat, the arduous task of determining the amino acid sequence of rhodopsin was first completed by proteolysis and Edman degradation of peptide fragments. Next, the work by Bownds of reductively trapping the chromophore using borohydride was adapted by using borotritium instead to produce a reduced, radiolabeled retinyl moiety on opsin. The reductive trapping was critical as proteolysis renders the retinylidene adduct labile to hydrolysis by bulk water. Upon determining Lys^{296} as the site of attachment and characterizing the crystal structure of rhodopsin, the chromophore binding pocket and the internal retinylidene Lys residue of other opsins were inferred by homology and determined indirectly by alanine site-directed mutagenesis.[112, 113]

The approach described in this chapter adapts the methods by Bownds with an improved preparation of borohydride and improved enzymes and conditions for proteolysis. The resultant proteolytic products would be analyzed and sequenced by LC-MS/MS to determine the site of attachment. As a proof of concept, the method was performed on a small 11-aa peptide (bovine Rho aa292-302, or bRhoPep) containing Lys^{296} with the N^{ε}-retinyl moiety as such: N^{α}-Ac-AFFA$\mathbf{K^{ret}}$TSAVYN. The N-terminus was acetylated so that only the epsilon amine of Lys^{296} would react to exogenous retinal to form the retinylidene Schiff base that would ultimately be reduced by borohydride to synthesis N^{ε}-retinyl-bRhoPep. Upon proper detection of this retinylated peptide and its proteolyzed products by LC-MS/MS, the method was applied to rhodopsin.

2.2 Results

2.2.1 Proteolysis and LC-MS/MS analysis of Nε-retinyl-bRhoPep

Sodium borohydride ($NaBH_4$) reduction of the Schiff base condensation product of all-*trans*-retinal and bRhoPep generated Nε-all-*trans*-retinyl-bRhoPep (Nε-a*t*-ret-bRhoPep) as shown by Figure 2.1. The LC-MS peak of Nε-a*t*-retinyl-bRhoPep showed the characteristic ultraviolet-visible (UV-Vis) spectrum of the retinyl moiety (λ_{max} = 328 nm), which greatly enhanced the hydrophobicity of the peptide, as reflected in the increased chromatographic retention time from 5 to 31 min (Figure 2.1C-D). MS/MS showed electrospray ionization (ESI)–source fragmentation of the Nε-a*t*-ret-bRhoPep into a retinyl cation and a peptide ion, whose sequence was confirmed by collision-induced dissociation (CID) fragmentation to be that of the bRhoPep (Figure 2.1E-G).

To simulate Nε-retinyl-peptides that would be found from proteolysis of Nε-retinyl-opsin, Nε-a*t*-ret-bRhoPep was proteolyzed with various proteases and the resultant products were analyzed by LC-MS/MS. Digestion with proteinase K yielded four unique Nε-retinyl-peptides, identified by MS/MS to be $K^{ret}TS$, $K^{ret}T$, AK^{ret}, and FAK^{ret}, each with a sequence containing Lys^{296} adducted to the retinyl moiety (Figure 2.2). Complete proteolysis of Nε-a*t*-ret-bRhoPep by pronase at 40 °C yielded one prominent peak and two minor peaks, which were all identified to be Nε-retinyl-Lys (Figure 2.3). Based on the UV-Vis and MS spectra of each synthetic retinyl isomer standard of Nε-retinyl-Lys (Figure 2.4), the most prominent peak was determined to be the all-*trans* isomer, whereas the two minor peaks were determined to be the 9-*cis* and 13-*cis* isomers. These two minor isomers are known to form spontaneously by thermal isomerization of the all-trans isomer.[114] Pronase was found to still be active at 10°C and even completely proteolyzed Nε-retinyl-

opsin while minimizing the thermal isomerization to retain the retinylidene isomeric composition extant in the sample as will be shown in the next section. Serendipitously, N^{ε}-retinyl-Lys standards demonstrate optimal separation between the 11-*cis* and all-*trans* isomers, which are the two physiologically relevant isomers of retinoids for vision. Such a finding seemed fortuitous for using pronase to directly study the photochemistry occurring within opsins.

2.2.2 Proteolysis and LC-MS/MS analysis of N^{ε}-retinyl-opsin

N^{ε}-retinyl-opsin was produced from rhodopsin using a saturated solution of $NaBH_4$ in isopropanol (*i*PrOH). $NaBH_4$/*i*PrOH rapidly denatures rhodopsin while immediately reductively trapping the 11-*cis*-retinylidene adduct. Protein denaturation is crucial since $NaBH_4$ would otherwise be unable to access the internal retinylidene Schiff base that is well protected against even external water. When $NaBH_4$/*i*PrOH is added to ROS, the lipids are solubilized by *i*PrOH, while rhodopsin is denatured and reduced. This allows for the study of rhodopsin in native lipids without the need to purify it. If rhodopsin were purified using detergents (for membrane protein solubilization) and 1D4 immunoaffinity chromatography, $NaBH_4$/*i*PrOH would still be applicable. Detergents and any residual lipids would be solubilized by *i*PrOH while rhodopsin is denatured and reduced.

Following $NaBH_4$/*i*PrOH treatment, the denatured proteins are completely proteolyzed by pronase into a clarified solution that was analyzed by LC-MS/MS. The ROS sample before light exposure had a dominant N^{ε}-11-*cis*-retinyl-Lys peak, whereas after light exposure, a dominant N^{ε}-all-*trans*-retinyl-Lys peak was observed, as confirmed by LC-MS/MS (Figure 2.5). The same was observed for purified rhodopsin (Figure 2.6), serving as

a validation of observations with the ROS sample, which is a complex mixture of not only rhodopsin but other native proteins, including transducin (G_T), phosphodiesterase 6 (PDE6), etc. The N^{ε}-retinyl-Lys peaks were further confirmed to originate from Rho in ROS membranes by LC-MS/MS analysis of the N^{ε}-retinyl-peptides generated from a proteinase K digestion of the ROS-protein precipitate. Proteinase K also clarified the suspension of protein precipitate into a solution of N^{ε}-retinyl-peptides that were identified by LC-MS/MS to be similar to those from the proteinase K digest of N^{ε}-retinyl-bRhoPep (Figure 2.7). The same N^{ε}-retinyl-peptides were observed for proteinase K digestion of $NaBH_4$/*i*PrOH-treated purified rhodopsin (Figure 2.8).

To further validate the reductive trapping of chromophore by $NaBH_4$, sodium borodeuteride ($NaBD_4$) was used in its place. The proteinase K and pronase digests of $NaBD_4$/*i*PrOH-treated ROS or purified Rho resulted in similar N^{ε}-retinyl-peptides and N^{ε}-retinyl-Lys, respectively (Figure 2.9-2.12). By LC-MS/MS, the resultant N^{ε}-retinyl analytes had an increase in mass corresponding to deuteration and source fragmentation producing the C^{15}-D^{1}-retinyl cation at 270 m/z (Figure 2.9-2.12). These results with $NaBD_4$ helps validate the reductive chromophore trapping done by $NaBH_4$, as well as the characteristic source fragmentation of retinyl analytes to yield a retinyl cation and a product peptide or Lys residue for sequencing by CID fragmentation.

2.3 Discussion

Even after the discovery by Ovchinnikov and Hargrave in 1982, determining the site of retinal attachment to opsins remained an arduous and complicated task. The use of borotritium requires special equipment to measure radioactivity and leads to exposure to

radioactivity. The problems also, just to list a few, include: the heterogeneity of the digestion product from the transmembrane segments of opsins, the difficulty in isolating long hydrophobic peptides, the lability of the retinyl polyene chain to degradation by oxidation and even mildly acidic conditions, the decomposition of retinyl peptides by elimination of the retinyl carbocation moiety, the lack of quantitative preservation of the geometric isomers of the retinoids, and no established methodology to comprehensively determine and characterize the identity of retinyl-peptide.

Our results demonstrate that our methods greatly improved upon those of Bownds. Since the 11-*cis*-retinylidene Schiff base of intact ground-state rhodopsin is inaccessible even to water, $NaBH_4$ in *i*PrOH was used to denature rhodopsin for prompt access and reduction of its retinylidene Schiff base. Importantly, the reduction chemistry by $NaBH_4$ was significantly faster than the loss of the retinylidene Schiff base to hydrolysis upon exposure to water with the denaturation of rhodopsin. The reported kinetics of the reduction is exceptionally quick in polar protic solvents such as water (93.0×10^4 $M^{-1}s^{-1}$ at 0 °C), ethanol (97.0×10^4 $M^{-1}s^{-1}$ at 0 °C), and isopropanol (15.1×10^4 $M^{-1}s^{-1}$ at 0 °C).[115, 116] This is approximately 7-8 orders of magnitude faster than the kinetics of Schiff base hydrolysis of the all-*trans*-retinylidene agonist in Rho* ($k = 1.5 \times 10^{-3}$ s^{-1}), as will be covered in the next chapter.

The fast kinetics of reduction by $NaBH_4$ is observable by eye with the immediate chemical bleaching of the red color of ground-state Rho pigment or the pale-yellow color of Rho* in ROS upon addition and mixing of $NaBH_4$/*i*PrOH. Furthermore, by UV-Vis absorbance, the reduction by $NaBH_4$ of retinal occurred faster than the ability to measure another recording after $NaBH_4$ addition. To address whether $NaBH_4$/*i*PrOH quantitatively

reduced all rhodopsin or left some unreduced retinal or Schiff base held up in the denatured protein pellet, Rho and Rho* were each treated with either $NaBH_4$/*i*PrOH or *i*PrOH alone, followed by pronase digestion. Subsequent reverse-phase chromatography showed Rho and Rho* treated with *i*PrOH alone had unreduced retinal, dissociated from the Lys residue likely during the proteolysis (Figure 2.13). However, samples treated with $NaBH_4$/*i*PrOH showed only the reduction and proteolysis product, N^{ε}-retinyl-Lys, with no traceable signals of unreduced retinal (Figure 2.13). Overall, $NaBH_4$/*i*PrOH demonstrated the ability to quickly, reductively trap the chromophore of rhodopsin, and these fast kinetics was valuable in the study of agonist hydrolysis, since studying the kinetics of one process using a process with similar kinetics would be greatly confound the measurements of the process of interest.

Following the quantitative yield of N^{ε}-retinyl-opsin by addition of excess $NaBH_4$/*i*PrOH reagent, our proteolytic conditions and proteases not only digested the denatured protein precipitate of N^{ε}-retinyl-opsin into N^{ε}-retinyl-peptides but also largely preserved the isomeric configuration of the retinyl moiety. This is owed to our proteolytic conditions being slightly basic at a pH of 7.8, while still being within the optimal pH activity range for both proteinase K (pH ~8) and pronase (pH 7-8). Furthermore, the ability of both proteases to still exhibit enough activity at 10 °C to proteolyzes N^{ε}-retinyl-opsin down to small N^{ε}-retinyl-peptides, or even N^{ε}-retinyl-Lys in the case of pronase, was useful in protecting the retinyl moiety against thermal isomerization. The preservation of the isomeric configuration of the retinyl moiety during the pronase proteolysis, as well as the characterization of N^{ε}-retinyl-Lys isomeric standards, allowed for determination of the retinylidene isomer within rhodopsin, whether 11-*cis* or all-*trans.* Therefore, our methods

can be used to capture the photochemistry of rhodopsin (Figure 2.5, 2.6, 2.11, 2.12) and potentially any other opsin protein.

Following proteolysis, the use of LC-MS/MS helped confirm the identities of the N^{ε}-retinyl-peptides and N^{ε}-retinyl-Lys by capturing the full mass of each retinyl analyte, as well as the characteristic UV-Vis spectra of each peak to verify isomeric identity. Furthermore, the N^{ε}-retinyl-analytes had a characteristic partial ESI source fragmentation pattern due to the tendency of the retinyl group to cleave as a retinyl cation, likely due to resonance stabilization of the retinyl cation and the formation of a stable peptide or Lys leaving group upon protonation of the ε-amine by formic acid in the mobile phase. Protonation on other sites of the N^{ε}-retinyl analytes likely led to some preservation for detection of its full mass. With other retinoids, such as retinyl esters or retinol, the retinyl cation is the predominant and only species observed on ESI-MS full scan.[117-120] The partial ESI source fragmentation was favorable in this study, since it serendipitously further validated identity of each N^{ε}-retinyl analyte by showing not only the full mass but also fragments that were consistently the retinyl cation and the product peptide or Lys ion, which can be then identified/sequenced by CID fragmentation.

Given the utility of this method to quantitatively trap the attached retinal and analyze it for its isomeric configuration, the photochemistry of rhodopsin or any opsin can be characterized. Furthermore, the amount of all-*trans*-retinylidene remained bound to Rho* over time can be measured to determine the kinetics of hydrolysis. Overall, our LC-MS/MS technique was applicable to either immunopurifed Rho in detergent micelles or Rho kept in ROS membranes. Therefore, the hydrolysis of agonist from Rho* can be monitored with Rho in its native environment in ROS. This method can be translated to

other opsin proteins, as will be demonstrated in chapters 4-5, to study their photochemistry and the hydrolysis of their photoisomerized retinylidene product (Figure 2.14).

2.4 Materials & Methods

Instrumentation

1100 Series HPLC System (Agilent, Santa Clara, CA); 1260 Infinity HPLC System (Agilent); Dionex Ultimate 3000 UHPLC System (Thermo Fisher Scientific, Waltham, MA); LTQ XL mass spectrometer (Thermo Fisher Scientific); Cary 50 UV-Vis Spectrophotometer (Varian, Palo Alto, CA).

Materials

Chemicals and other materials were purchased as follows: all-*trans*-retinal (Sigma-Aldrich, St. Louis, MO, cat. no. R2500), all-*trans*-retinol (Sigma-Aldrich, cat. no. R7632); bovine rod outer segments (InVision Bioresources, Seattle, WA, cat. no. 98740); 2-[4-(2-hydroxyethyl)piperazin- 1-yl]ethanesulfonic acid (Goldbio, St. Louis, MO, cat. no. H-400-1); 1,3- Bis[tris(hydroxymethyl)methylamino]propane (Sigma-Aldrich, cat. no. B6755); calcium chloride dihydrate (Sigma-Aldrich, cat. no. 223506); n-dodecyl-β-D-maltopyranoside Sol-grade (Anatrace, Maumee, OH, cat. no. D310S); pronase (Sigma-Aldrich, cat. no. PRON-RO); proteinase K solution (Viagen Biotech, cat. no. 501-PK); Amicon Ultra-0.5 Centrifugal Filter (Millipore, Burlington, MA, cat. no. UFC503096); acetonitrile Optima LC/MS grade (Fisher Scientific, Pittsburgh, PA, cat. no. A955); MeOH Optima LC/MS grade (Fisher Scientific, cat. no. A456); iPrOH Optima LC/MS grade (Fisher Scientific, cat. no. A461); formic acid Optima LC/MS grade (Fisher Scientific, cat. no. A117-50); methylene

chloride (HPLC) (Fisher Scientific, cat. no. D143); hexanes (HPLC) (Fisher Scientific, cat. no. H302); ethyl acetate (HPLC) (Fisher Scientific, cat. no. E195); triethylamine (HPLC) (Fisher Scientific, cat. no. O4884); dimethyl sulfoxide (Sigma-Aldrich, cat. no. D2650); N,N-dimethylformamide (Fisher Scientific, cat. no. AC327171000); diethylamine (Sigma-Aldrich, cat. no. 471216); Nα-[(9H-fluoren-9- ylmethoxy)carbonyl]-L-Lys hydrochloride (Fisher Scientific, cat. no. F0586); 1,2-dioleoyl-sn- glycero-3-phosphoethanolamine (Avanti Polar Lipids, Alabaster, Al, cat. no. 850725P); $NaBH_4$ (Alfa Aesar, Haverhill, MA, cat. no. 88983); $NaBD_4$ (Alfa Aesar, cat. no. 35102); Isotemp 3016S Water Bath (Fisher Scientific, cat no. 13-874-28); 85 W 2700 K Hg light bulb (Home Depot, cat. no. EDXR-40-19); Fiber-Coupled 565 nm 9.9 mW (Min) 700 mA LED (Thorlabs, Newton, NJ, cat. no. M565F3); Fiber Patch Cable (Thorlabs, cat. no. M92L01); Compact T-Cube 1200 mA LED Driver with Trigger Mode (Thorlabs, cat. no. LEDD1B); Power Supply Unit with 3.5 mm Jack Connector (Thorlabs, cat. no. KPS201); HPLC columns: BioPureSPN C18 TARGA (nestgrp, Ipswich, MA cat. no. HEM S18R); XBridge C18 (Waters, Milford, MA, 2.1 mm X 100 mm, cat. no. 186003022); Gemini Analytical C18 (Phenomenex, Torrance, CA, 250 x 4.6 mm, cat. no. 00G-4435-E0); Gemini Preparatory C18 (Phenomenex, 250 x 10 mm, cat. no. 00G- 4435-N0); Luna Preparatory Silica (Phenomenex, 250 x 21.2 mm, cat. no. 00G-4091-P0-AX).

Methods

Production of 9-cis-, 11-cis-, and 13-cis-retinal. The method for production of 9-*cis*-retinal, 11-*cis*-retinal, and 13-*cis*-retinal was adapted from Kahremany et al.[121] Thus, all-*trans*-retinal was solubilized in acetonitrile (ACN) at 0.2 M and illuminated with an 85 W Hg light bulb at maximum intensity at a distance of 10 cm for 12 hr at 4 °C. The resultant 9-

cis-, 11-*cis*-, and 13-*cis*-retinal products were purified with a Luna preparatory silica column using 90% hexane and 10% ethyl acetate as the mobile phase at a flow rate of 5 mL/min. The purified products were verified by comparison to standards.

Synthesis of Nε-retinyl-Lys Standards. Nα-Fmoc-L-Lys HCl (15 mg) was dissolved in 0.25 mL dimethylformamide (DMF). Under dim red light in the dark room, 5.25 mg (0.5 eq.) of a retinal isomer (9-*cis*-, 11-*cis*-, 13-*cis*-, or all-*trans*-retinal) in 0.25 mL DMF was added to the DMF solution of Nα-Fmoc-L-Lys. Then 2.6 µL triethylamine (0.5 eq.) was added to the mixture and incubated for 6 hr. Then, about 2 mg of $NaBH_4$ was added, followed by 0.25 mL MeOH. About 3 min later, 0.5 mL diethylamine was added for Fmoc deprotection, and the reaction mixture was incubated for another 30 min. The reaction mixture was concentrated to 0.4 mL under a gentle stream of nitrogen. Then, 0.3 mL 1 M HEPES (pH 7.4) was added slowly to quench excess $NaBH_4$ and to neutralize the reaction mixture. The resultant suspension was centrifuged at 20,000 × *g* for 1 min. The resultant crude product in the supernatant was purified using a Gemini preparatory C18 column and a 30-min gradient of 10% to 40% ACN in water with 0.1% formic acid (FA) at a flow rate of 3 mL/min. Depending on the retinal isomer used (9-*cis*-, 11-*cis*-, 13-*cis*-, or all-*trans*-retinal), the corresponding retinyl isomer of the Nε-retinyl-Lys product was purified and characterized by UV-Vis spectrometry and MS.

Synthesis of Nε-all-*trans*-retinyl-bRhoPep. The peptide of bovine Rho, bRhoPep, encompassing the amino acid sequence 292 to 302 with an N-terminal acetylation modification was produced by Genscript. 4 mg of bRhoPep was dissolved in 200 µL

dimethyl sulfoxide. 2 mg (~2.2 eq.) all-*trans*-retinal was dissolved in 200 µL dimethyl sulfoxide and added to the peptide solution. Approximately 1 µL of triethylamine was added to help deprotonate the ε-amino group of Lys296 of bRhoPep. The reaction was incubated for 12 hr; an excess of $NaBH_4$ (1 mg, ~8.3 eq.) was added to reduce the Schiff base condensate, followed by 400 µL of MeOH. To quench the remaining $NaBH_4$, 200 µL of 1 M ammonium acetate was added slowly. The reaction mixture was concentrated to 400 µL using a stream of nitrogen gas. The concentrated mixture was centrifuged at 20,000 × *g* for 1 min. The product was purified from the supernatant by HPLC using a Gemini analytical C18 column and a mobile phase consisting of water with 0.1% FA (solvent A) and ACN (solvent B). The method consisted of a single 25-min isocratic gradient of 40% solvent B at a flow rate of 1 mL/min. The prominent peak with λ_{max} of 328 nm was collected and the identity of the product was confirmed using LC-MS/MS. The ACN in the purified N$^{\varepsilon}$-a*t*-retinyl-bRhoPep was partially evaporated by a stream of nitrogen, concentrating about 1 mL of N$^{\varepsilon}$-a*t*-retinyl-bRhoPep solution collected directly from the HPLC to 0.5 mL. The concentration of N$^{\varepsilon}$-all-*trans*-retinyl-bRhoPep was measured to be around 50 mM via UV-Vis spectrometry, using the extinction coefficient of all-*trans*-retinol (ε = 52,800 $M^{-1}cm^{-1}$ at λ_{max} = 325 nm).

Pronase Digest of N$^{\varepsilon}$-all-*trans*-retinyl-bRhoPep. 50 µL of 50 mM N$^{\varepsilon}$-all-*trans*-retinyl-bRhoPep was mixed with 100 µL of 1 M BTP pH 7.8 and 100 µL of 1 M $CaCl_2$. The entire mixture was adjusted to 1 mL final volume with nanopure water. Finally, 1 µL of 40 mg/mL pronase was added and the digestion was incubated for 4 hr at 40 °C in the dark. The digest was passed through a BioPureSPN C18 spin column for desalting. The column was washed

with 20% ACN, and proteolysis products were eluted using 50% ACN. The eluted Nε-retinyl-Lys products were separated using a Dionex UHPLC with a XBridge C18 column and a 30 min gradient of 20% to 50% ACN in water with 0.1% FA at a flow rate of 0.3 mL/min. Nε-retinyl-Lys products were detected by UHPLC absorbance readings at 330 nm and identified by MS/MS, using CID fragmentation with the LTQ XL spectrometer.

Proteinase K Digest of Nε-all-*trans*-retinyl-bRhoPep. 50 µL of 50 mM Nε-all-*trans*-retinyl-bRhoPep was mixed with 100 µL of 1 M BTP pH 7.8 and 100 µL of 1 M $CaCl_2$. The entire mixture was adjusted to 1 mL final volume with nanopure water. Finally, 1 µL of 20 mg/mL proteinase K was added and the digestion was incubated for 4 hr at room temperature in the dark. The digest was passed through a BioPureSPN C18 spin column for desalting. The column was washed with 20% ACN, and digest products were eluted using 60% ACN. The eluted Nε-retinyl-peptide products were separated on the Dionex UHPLC with a XBridge C18 column and a 30 min gradient of 20% to 50% ACN in water with 0.1% FA at a flow rate of 0.3 mL/min. Nε-retinyl-peptide products were detected by UHPLC absorbance readings at 330 nm and identified by MS/MS, using CID fragmentation with the LTQ XL spectrometer.

Isolation of bovine ROS membranes. ROS membranes were prepared from fresh bovine retinas (InVision Bioresources) using sucrose gradient isolation as described previously[122], and washed with hypotonic buffer (20 mM HEPES, pH 7.4).

Rho immunopurification from ROS membranes. Rho was immunopurified in a dark room under dim red light, using immobilized 1D4 antibody as previously described (2). ROS membranes were solubilized with DDM in 20 mM HEPES at pH 7.4 with 0.15 M NaCl and incubated with Sepharose beads with immobilized 1D4 antibody for 2 hr. The beads were washed with 10 column volumes of wash buffer A (1 mM DDM in 20 mM HEPES pH 7.4, 0.15 M NaCl) to remove unbound protein as well as solubilized lipids. Rho was then eluted from the beads by adding a 0.5 mM solution of the competing peptide TETSQVAPA (1D4), which was subsequently removed by membrane filtration using a 30 kDa Amicon centrifugal filter. The Rho sample was then concentrated and diluted twice with wash buffer B (0.2 mM DDM, 20 mM HEPES pH 7.4). The final concentration was 2 mg/mL Rho in 20 mM HEPES in roughly 0.5 mM DDM.

Proteinase K Digestion of Rho from ROS Membranes or immunopurified in detergent micelles. In the dark room under dim red light, one part ROS membranes or immunopurified Rho (2 mg/mL or 50 μM Rho) was treated with three parts saturated solution of $NaBH_4$ granules (~100 μM) in cold *i*PrOH for immediate reduction of the retinylidene Schiff base and isolation of Rho by protein precipitation. Cold ethanol (EtOH) can also be used in place of *i*PrOH. After centrifugation at 20,000 × *g* to pellet the protein precipitate, the pellet was washed with cold methanol (MeOH) followed by cold water. The protein pellet was then resuspended in proteinase K buffer (4 M urea, 100 mM bis-tris propane [BTP; pH 7.8], 100 mM $CaCl_2$). Subsequently, proteinase K (20 mg/mL) was added at ~10× the weight of the Rho substrate. Then, the digestion mixture was incubated at room temperature for 24 h, with occasional mixing by brief gentle spinning on a vortex

mixer. The digest was passed through a BioPureSPN C18 spin column for desalting. The column was washed with 20% ACN in water with 0.1% FA, and peptides were eluted using 60% ACN. The eluted N^{ε}-retinyl-peptide products were separated using a Dionex UHPLC with an XBridge C18 column and a 40-min gradient of 20 to 60% ACN in water with 0.1% FA at a flow rate of 0.3 mL/min. N^{ε}-retinyl-peptide products were detected by UHPLC absorbance at 330 nm and identified by MS/MS with CID fragmentation using an LTQ XL spectrometer.

Pronase Digestion of Rho from ROS Membranes. In the dark room under dim red light, one part ROS membranes or immunopurified Rho (2 mg/mL or 50 μM Rho) was treated with three parts saturated solution of $NaBH_4$ granules in cold *i*PrOH (~100 μM) for immediate reduction of the retinylidene Schiff base and isolation of Rho by precipitation. After centrifugation at 20,000 × g to pellet the protein precipitate, the pellet was washed with cold MeOH followed by cold water. The protein pellet was then resuspended in pronase buffer (100 mM BTP [pH 7.8], 100 mM $CaCl_2$). Subsequently, pronase (20 mg/mL in water) was added at ~10× the weight of Rho substrate. Then, the digestion mixture was incubated at 8-10 °C for 24 h with gentle agitation using a shaker. The digest was passed through a BioPureSPN C18 spin column for desalting. The column was washed with 20% can in water, and digest products were eluted using 60% ACN. The eluted N^{ε}-retinyl-Lys products were separated using a Dionex UHPLC with an XBridge C18 column and a 30-min gradient of 20 to 50% ACN in water with 0.1% FA at a flow rate of 0.3 mL/min. N^{ε}-retinyl-Lys products were detected by UHPLC absorbance at 330 nm and identified by MS/MS with CID fragmentation using an LTQ XL spectrometer.

2.5 Figures

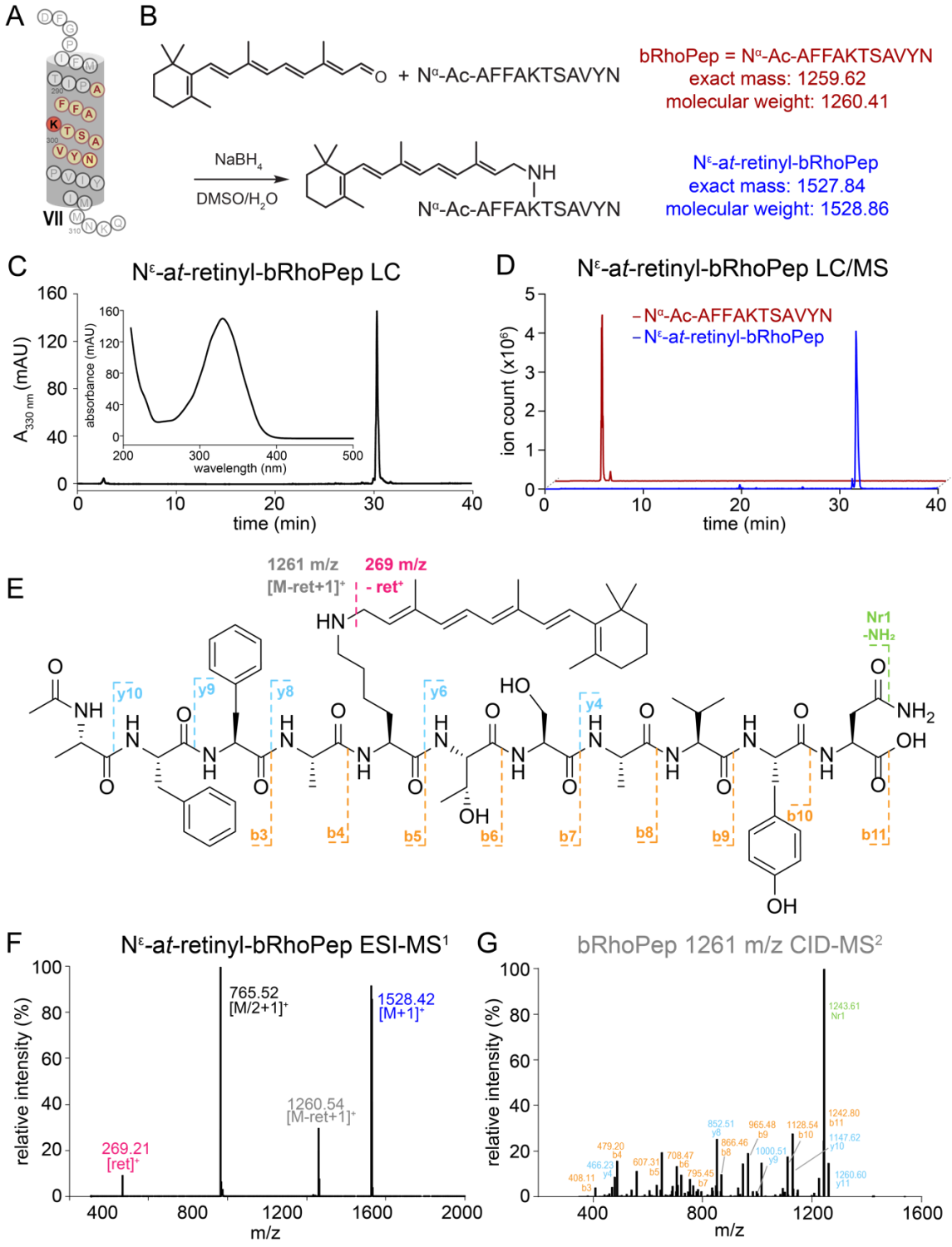

Figure 2.1 Synthesis and characterization of Nε-*at*-ret-bRhoPep. (A) Location of bRhoPep sequence within helix VII of bRho. (B) Synthesis of Nε-*at*-retinyl adducted to

Lys^{296} of the bRhoPep by $NaBH_4$-reduction of the Schiff base between all-*trans*-retinal and bRhoPep. (C) HPLC chromatogram indicating high purity of the synthesized N$^{\varepsilon}$-a*t*-ret-bRhoPep, displaying the characteristic retinyl UV-Vis absorbance spectrum. (D) LC-MS chromatogram showing that the retinyl adduct greatly increased the overall hydrophobicity of the peptide. (E) Diagram of the observed LC-MS/MS ESI source and CID fragmentation patterns of N$^{\varepsilon}$-a*t*-ret-bRhoPep. (F) ESI-MS^1 showed source fragmentation of N$^{\varepsilon}$-a*t*-ret-bRhoPep (1528 m/z) with cleavage at the site of the retinyl adduct, producing a product retinyl cation (269 m/z) and a product peptide ion (1261 m/z). (G) CID fragmentation of the product peptide ion showed the characteristic peptide fragmentation pattern of bRhoPep as diagrammed in (E). mAU, milli absorbance unit

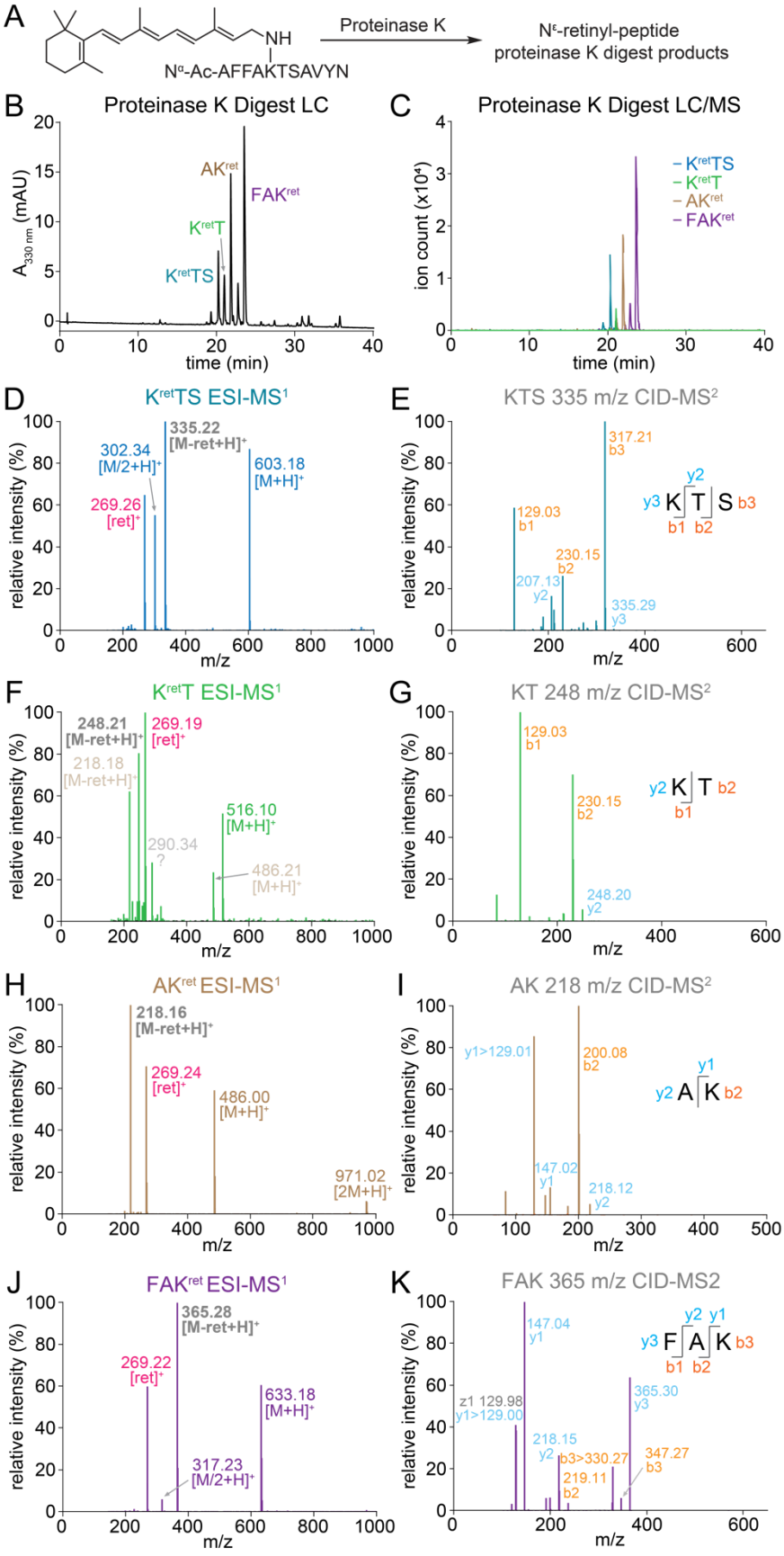
A
Proteinase K
Nε-retinyl-peptide
proteinase K digest products
Nα-Ac-AFFAKTSAVYN
B
Proteinase K Digest LC
AKret
FAKret
KretT
KretTS
A330 nm (mAU)
time (min)
C
Proteinase K Digest LC/MS
KretTS
KretT
AKret
FAKret
ion count (x10⁴)
time (min)
D
KretTS ESI-MS¹
335.22
[M-ret+H]⁺
302.34
[M/2+H]⁺
603.18
[M+H]⁺
269.26
[ret]⁺
relative intensity (%)
m/z
E
KTS 335 m/z CID-MS²
317.21
b3
129.03
b1
230.15
b2
207.13
y2
335.29
y3
y3 K T S b3
b1 b2
y2
relative intensity (%)
m/z
F
KretT ESI-MS¹
248.21
[M-ret+H]⁺
269.19
[ret]⁺
218.18
[M-ret+H]⁺
516.10
[M+H]⁺
290.34
?
486.21
[M+H]⁺
relative intensity (%)
m/z
G
KT 248 m/z CID-MS²
129.03
b1
230.15
b2
248.20
y2
y2 K T b2
b1
relative intensity (%)
m/z
H
AKret ESI-MS¹
218.16
[M-ret+H]⁺
269.24
[ret]⁺
486.00
[M+H]⁺
971.02
[2M+H]⁺
relative intensity (%)
m/z
I
AK 218 m/z CID-MS²
y1>129.01
200.08
b2
147.02
y1
218.12
y2
y2 A K b2
y1
relative intensity (%)
m/z
J
FAKret ESI-MS¹
365.28
[M-ret+H]⁺
269.22
[ret]⁺
633.18
[M+H]⁺
317.23
[M/2+H]⁺
relative intensity (%)
m/z
K
FAK 365 m/z CID-MS2
147.04
y1
z1 129.98
y1>129.00
218.15
y2
b3>330.27
219.11
b2
347.27
b3
365.30
y3
y3 F A K b3
b1 b2
y2 y1
relative intensity (%)
m/z

Figure 2.2 Proteinase K digestion of N$^{\varepsilon}$-a*t*-ret-bRhoPep. (A) Schematic diagram of sample preparation and MS workflow. (B) Chromatogram of N$^{\varepsilon}$-retinyl-peptides displaying UV absorbance at 330 nm. (C) LC-MS chromatogram of various retinyl-peptides that were identified by MS/MS. (D, F, H, J) ESI-MS^1 full scans showed characteristic source fragmentation of the precursor retinyl-peptide analytes to the product retinyl cation (269 m/z) and a product peptide ion. (E, G, I, K) Peptide sequences were determined by CID-MS^2 of each product peptide ion. mAU, milli absorbance unit

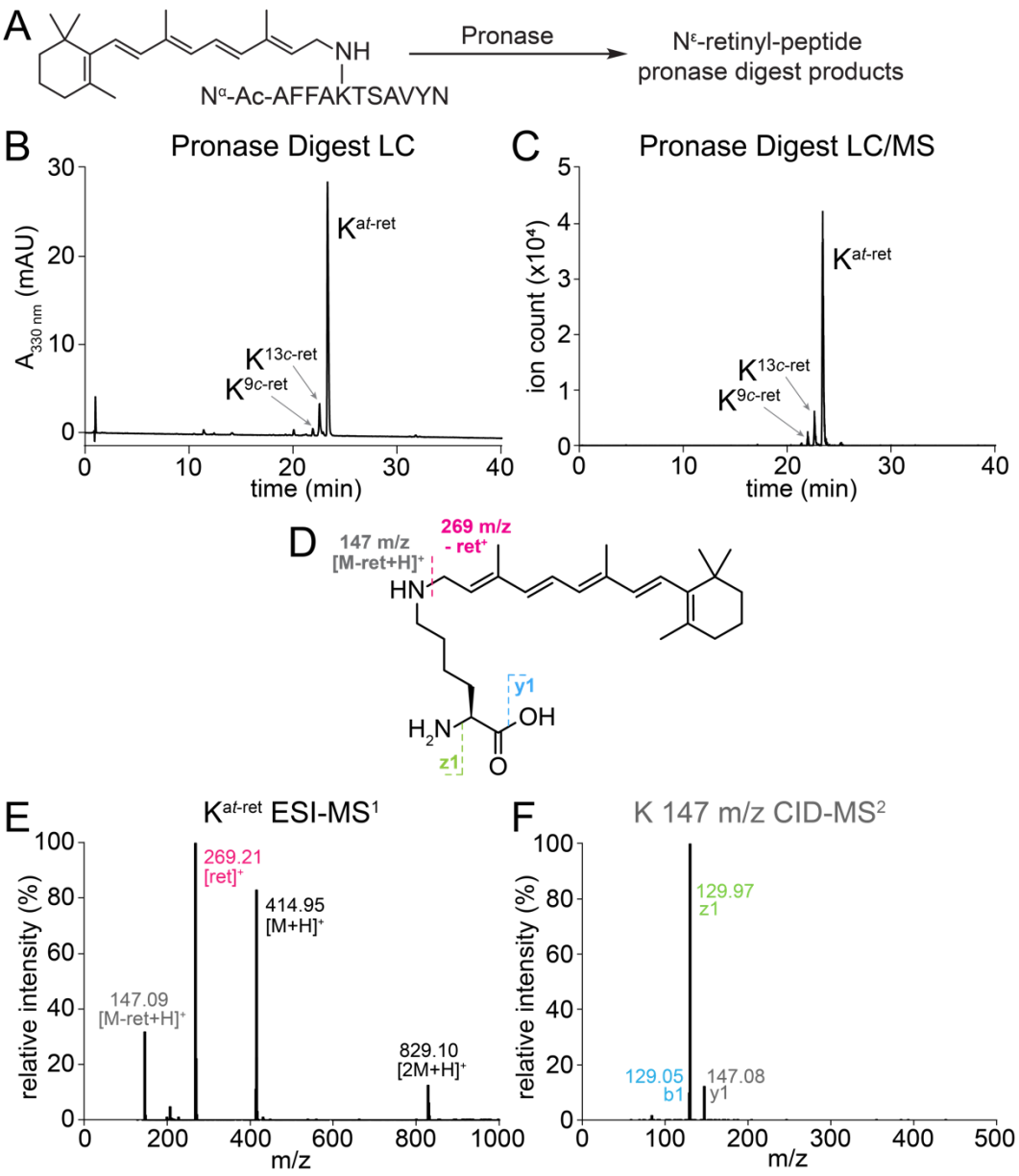

Figure 2.3 Pronase digest of Nε-*at*-ret-RhoPep. (A) Schematic diagram of sample preparation and MS workflow. (B) Chromatogram to detect Nε-a*t*-retinyl-Lys by UV-Vis absorbance at 330 nm. (C) LC-MS chromatogram of Nε-retinyl-Lys digest product that was identified by MS/MS. (D) Diagram of LC-MS/MS fragmentation sites on Nε-retinyl-Lys. (E) ESI-MS^1 showing characteristic source fragmentation of precursor Nε-retinyl-Lys analyte (415 m/z) to a product retinyl cation (269 m/z) and product Lys ion (147 m/z). (F) CID-

MS² of the product Lys ion showed the characteristic fragmentation pattern of Lys. mAU, milli absorbance unit

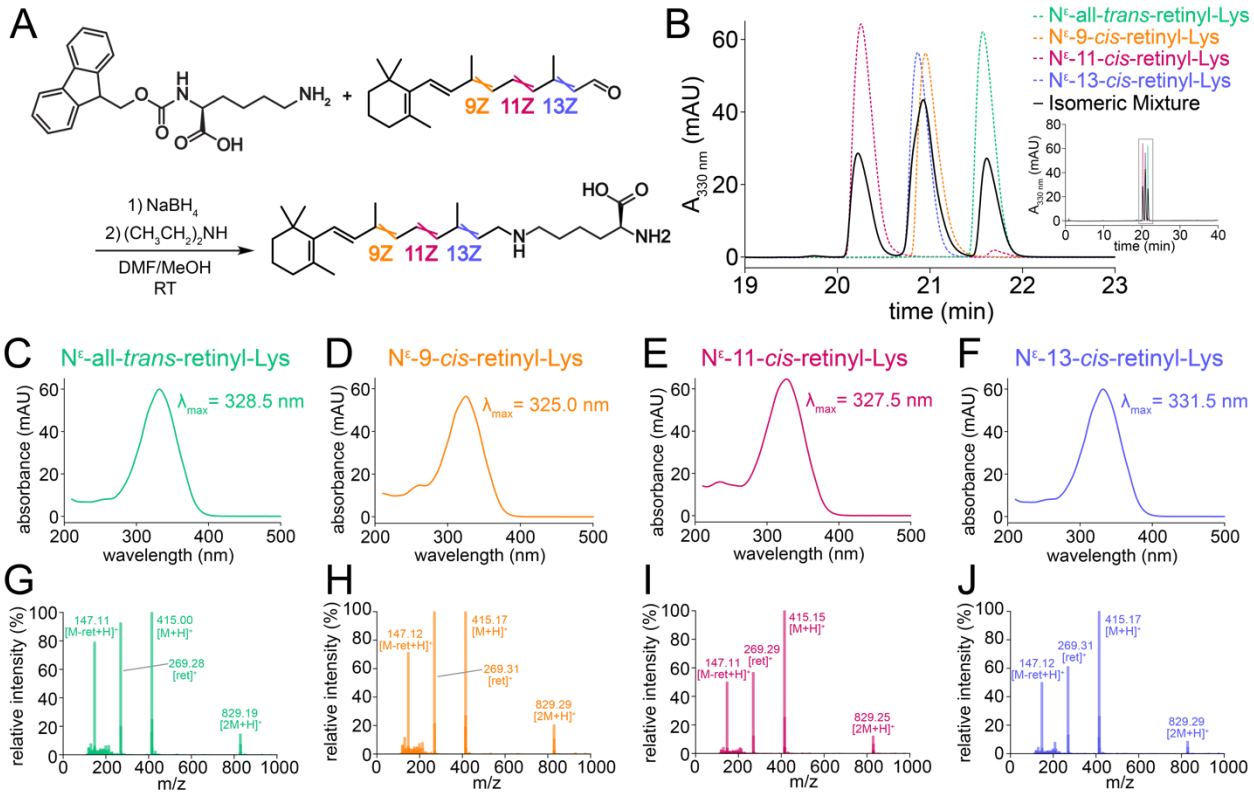

Figure 2.4 Development of a method for synthesis and separation of Nε-retinyl-Lys standards. (A) Nε-retinyl-Lys standards were synthesized by $NaBH_4$-reduction of the Schiff base adducts of the different isomers of retinal with Nα-Fmoc-Lys, followed by Fmoc deprotection using diethylamine. (B) Reverse-phase HPLC traces of each Nε-retinyl-Lys isomer standard displayed separability of the 11-*cis* and all-*trans* isomer standards, demonstrating applicability in studying Rho photochemistry. (C-F) The UV-Vis spectrum of each Nε-retinyl-Lys isomer standard showed unique spectral characteristics, especially the 9-*cis* and 13-*cis* isomers, which were poorly separable by chromatography but were spectrally the most distinct from each other. (G-J) ESI-MS¹ of each isomer demonstrated a

source-fragmentation pattern characteristic of a retinyl moiety, with cleavage of the retinyl cation (269 m/z) from the precursor Nε-retinyl-Lys ion (415 m/z) producing a product Lys ion (147 m/z). mAU, milli absorbance unit

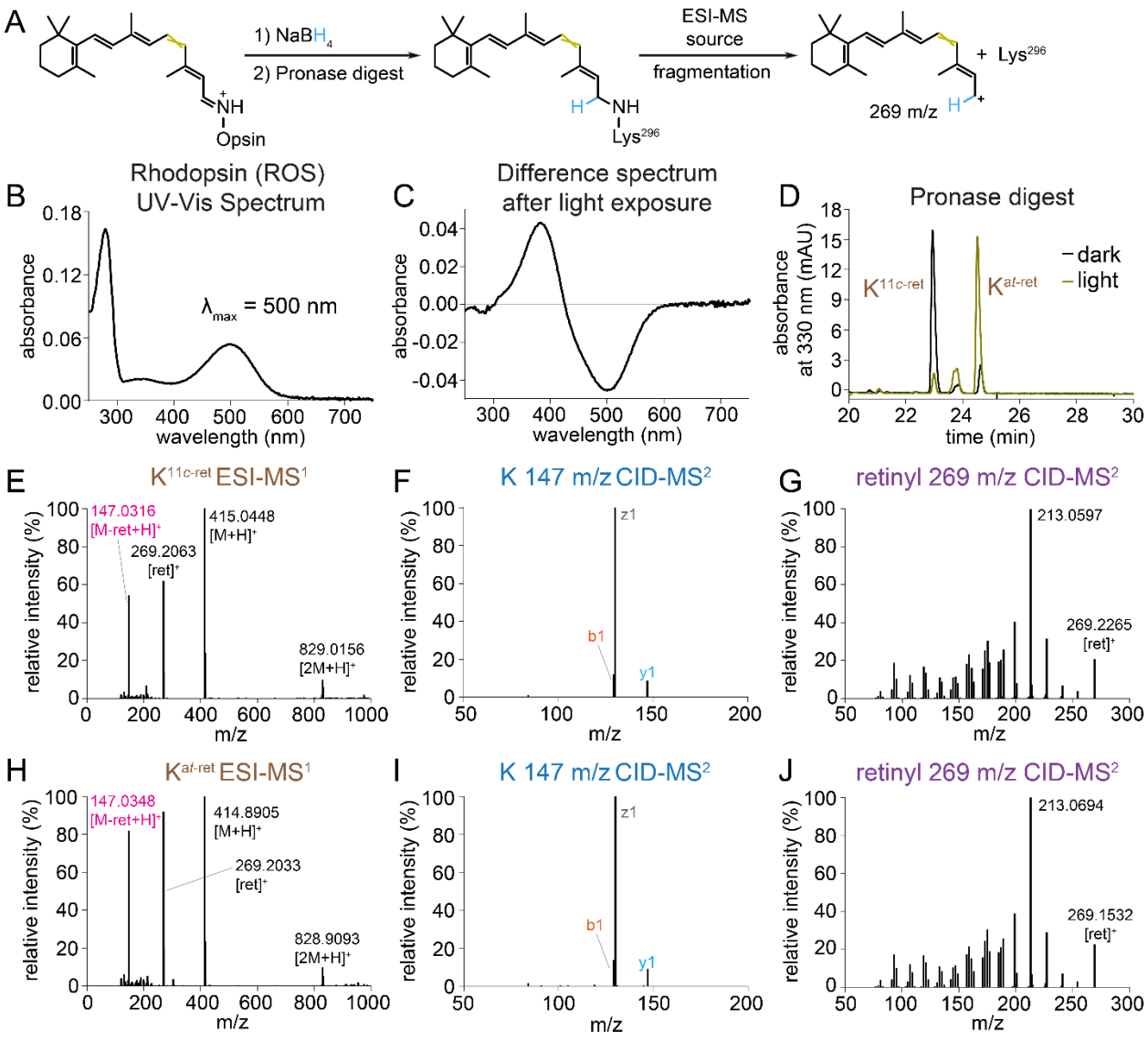

Figure 2.5 LC-MS/MS analyses of pronase digests of Rho and Rho* from native membranes. (A) Schematic diagram of sample preparation and MS workflow. (B) UV-Vis spectrum of Rho from ROS membranes solubilized in DDM. (C) Difference absorbance

spectrum of DDM-solubilized Rho versus Rho* in ROS membranes illuminated with 565-nm fiber light at 625 μW for 10 s at 4°C. (D) Chromatographic separation of N^{ε}-retinyl-Lys peaks from the pronase digests of Rho and Rho* in ROS membranes treated with $NaBH_4$/*i*PrOH. (E, H) ESI-MS^1 spectrum showing characteristic cleavage of retinyl cation (269 m/z) from precursor N^{ε}-retinyl-Lys analyte (415 m/z), producing a product Lys ion (147 m/z). (F, I) CID-MS^2 spectrum of the product Lys ion exhibiting a characteristic fragmentation pattern of Lys. (G, J) CID-MS^2 spectrum of retinyl cation demonstrating a complex fragmentation pattern with a characteristic dominant 213 m/z signal.[123, 124] mAU, milli absorbance unit.

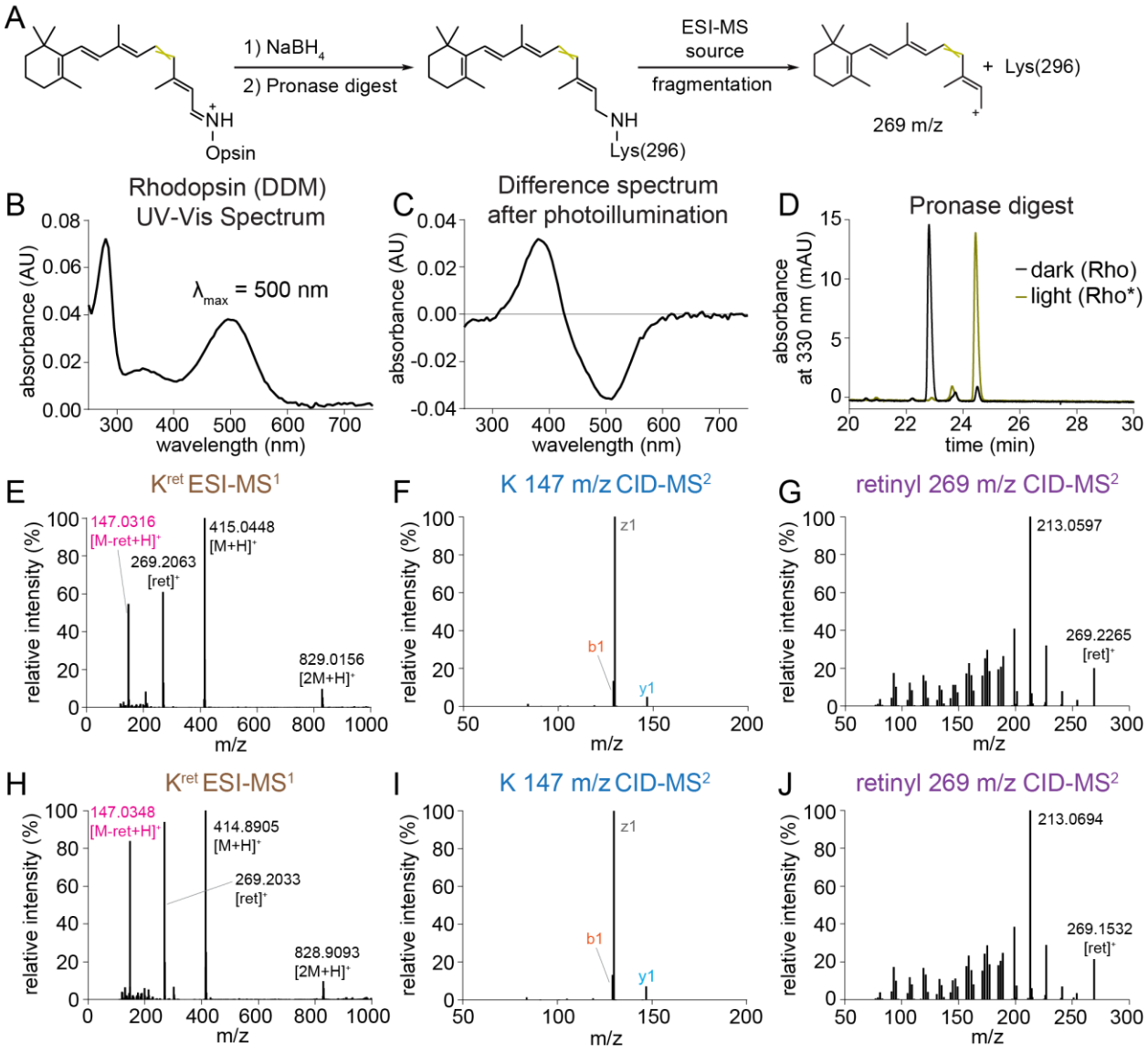

Figure 2.6 LC-MS/MS analyses of pronase digests of Rho and Rho* immunopurified in DDM detergent micelles. (A) Schematic diagram of sample preparation and MS workflow. (B) UV-Vis spectrum of purified Rho in DDM. (C) Difference absorbance spectrum of Rho versus Rho* illuminated with 565-nm fiber light at 625 μW for 10 s at 4°C. (D) Chromatographic separation of N$^{\varepsilon}$-retinyl-Lys peaks from the pronase digests of Rho and Rho* treated with $NaBH_4$/*i*PrOH. (E, H) ESI-MS^1 spectrum showing characteristic cleavage of retinyl cation (269 m/z) from precursor N$^{\varepsilon}$-retinyl-Lys analyte (415 m/z), producing a

product Lys ion (147 m/z). (F, I) CID-MS^2 spectrum of the product Lys ion exhibiting a characteristic fragmentation pattern of Lys. (G, J) CID-MS^2 spectrum of retinyl cation demonstrating a complex fragmentation pattern with a characteristic dominant 213-m/z signal.[123, 124] mAU, milli absorbance unit.

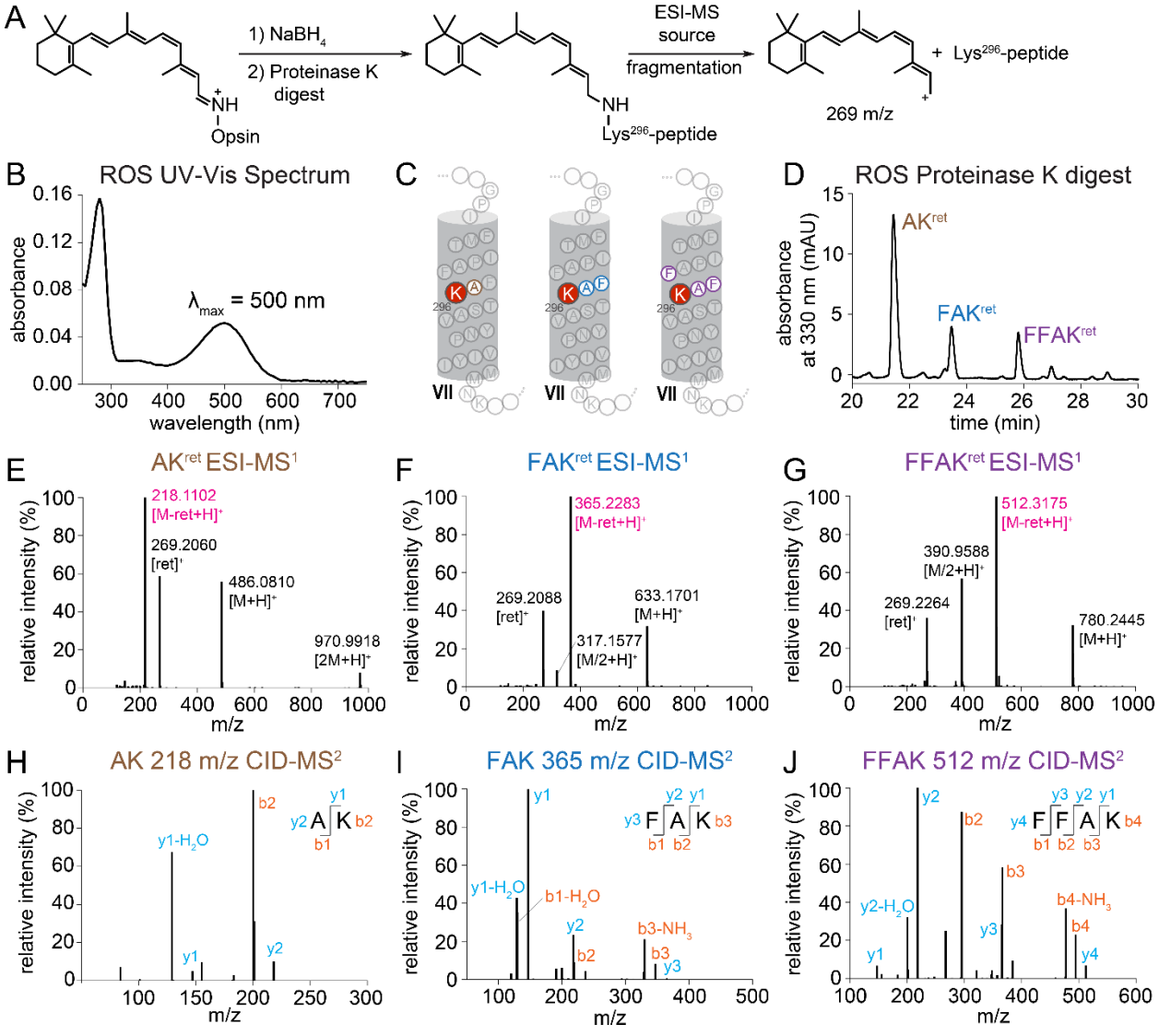

Figure 2.7 LC-MS/MS analysis of proteinase K digest of Rho from native membranes. (A) Schematic diagram of sample preparation and MS workflow. (B) UV-Vis spectrum of Rho from ROS membranes solubilized in DDM. (C) Location of chromophore binding

residue within helix VII of bovine Rho, with labeled N$^{\varepsilon}$-retinyl-peptide fragments detected from the proteinase K digest. (D) Chromatographic separation of N$^{\varepsilon}$-retinyl-peptides from proteinase K digestion of Rho treated with $NaBH_4$/*i*PrOH. (E–G) ESI-MS^1 spectrum showing characteristic cleavage of retinyl cation (269 m/z) from precursor N$^{\varepsilon}$-retinyl-peptide analyte, producing a product peptide ion. (H–J) MS^2 spectrum of CID fragmentation of the product peptide ion for sequence determination. mAU, milli absorbance unit.

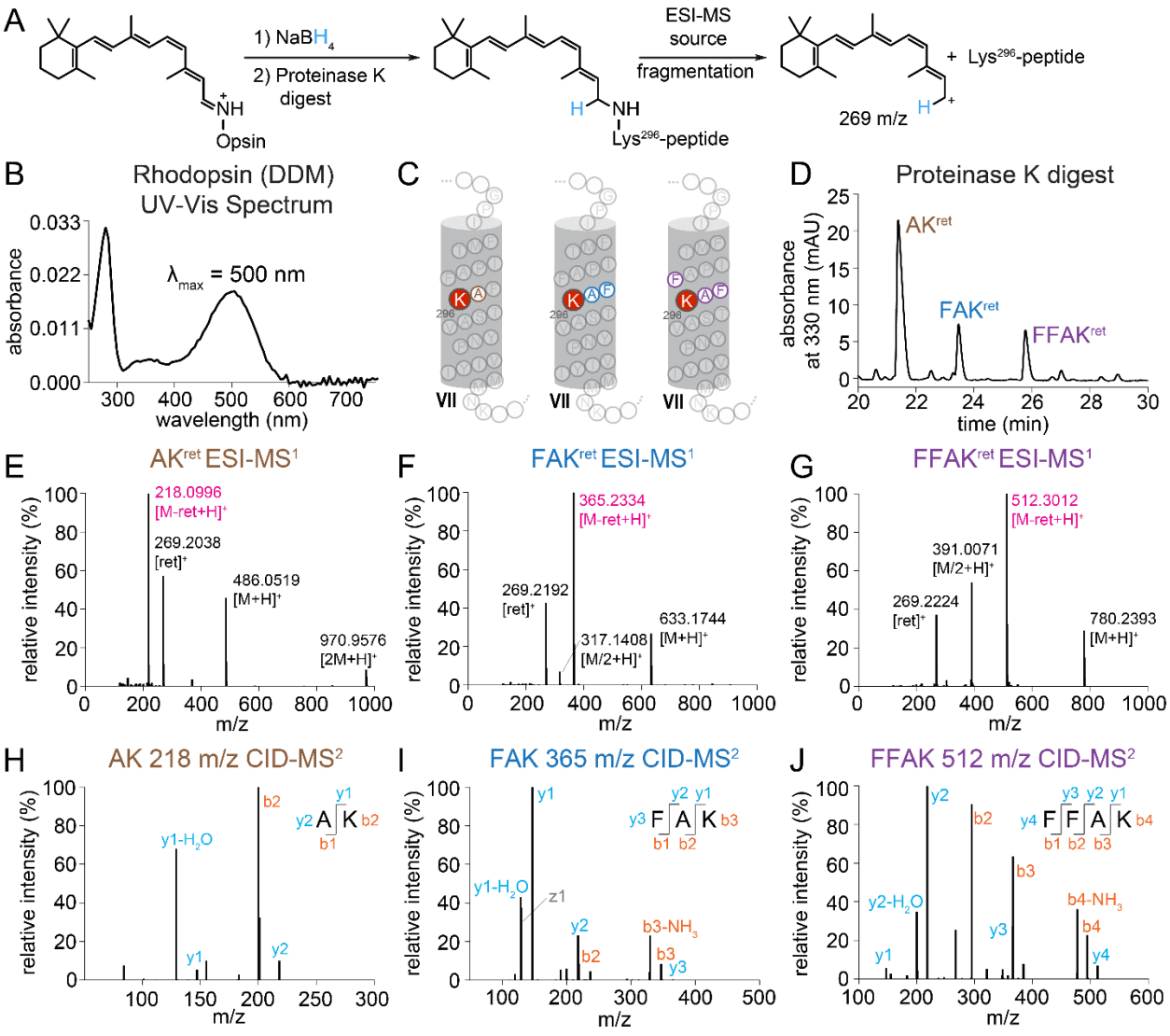

Figure 2.8 LC-MS/MS analysis of proteinase K digests of Rho purified in DDM detergent micelles. (A) Schematic diagram of sample preparation and MS workflow. (B) UV-Vis spectrum of purified Rho in DDM. (C) Location of the chromophore-binding residue within helix VII of bRho, labeled with N^{ε}-retinyl-peptide fragments detected from the proteinase K digest. (D) Chromatographic separation of N^{ε}-retinyl-peptides from proteinase K digestion of purified Rho treated with $NaBH_4$/*i*PrOH. (E-G) ESI-MS^1 spectra showing characteristic cleavage of retinyl cation (269 m/z) from precursor retinyl-peptide analyte, producing a product peptide peak. (H-J) MS^2 spectra of CID fragmentation of the product peptide ion for sequence determination.

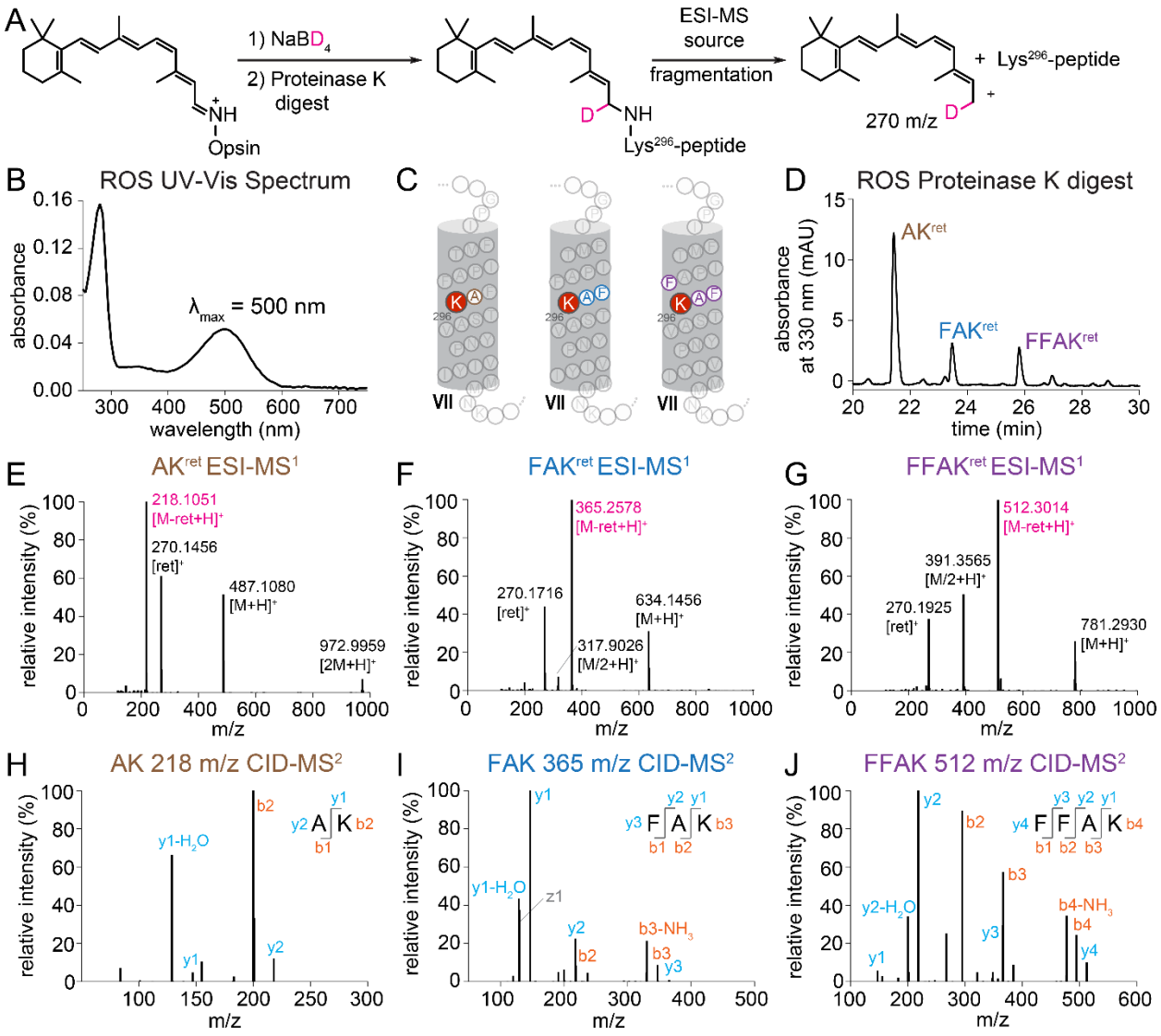

Figure 2.9 LC-MS/MS analysis of the proteinase K digest of NaBD$_4$-treated Rho from native membranes. (A) Schematic diagram of sample preparation and MS workflow. (B) UV-Vis spectrum of Rho from ROS membranes solubilized in DDM. (C) Location of the chromophore-binding residue within helix VII of bRho, labeled with N$^{\varepsilon}$-retinyl-peptide fragments detected from the proteinase K digest. (D) Chromatographic separation of N$^{\varepsilon}$-retinyl-peptide peaks from proteinase K digestion of Rho treated with NaBD$_4$/*i*PrOH. (E-G) ESI-MS^1 spectra showing characteristic cleavage of C^{15}-D^1-retinyl cation (270 m/z) from

precursor C^{15}-D^{1}-retinyl-peptide analyte, producing a product peptide peak. (H-J) MS^2 spectra of CID fragmentation of the product peptide ion for sequence determination.

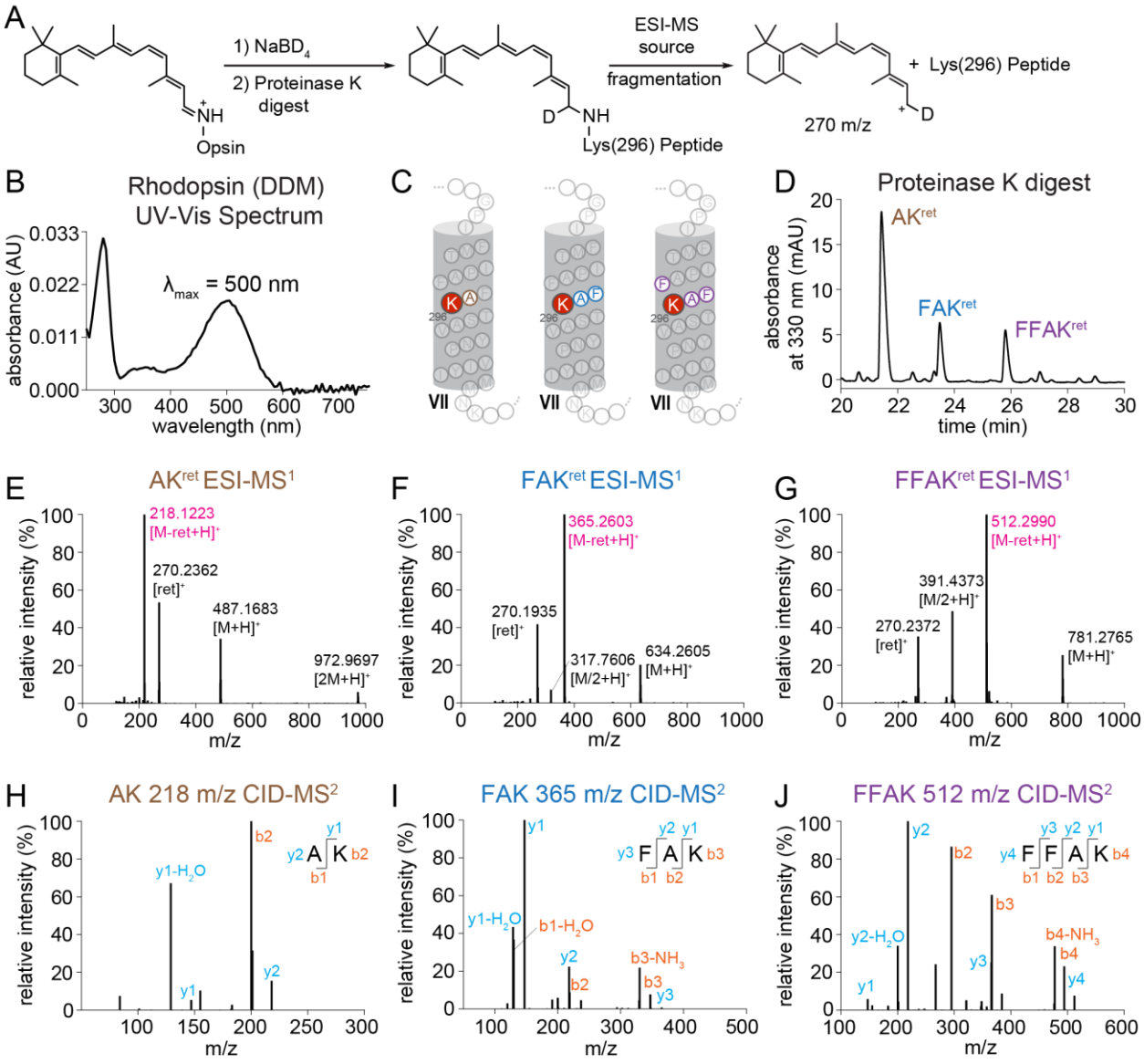

Figure 2.10 LC-MS/MS analysis of the proteinase K digest of $NaBD_4$-treated Rho purified in DDM detergent micelles. (A) Schematic diagram of sample preparation and MS workflow. (B) UV-Vis spectrum of purified Rho in DDM. (C) Location of the chromophore-binding residue within helix VII of bRho, labeled with N^{ε}-retinyl-peptide

fragments detected from the proteinase K digest. (D) Chromatographic separation of N^{ε}-retinyl-peptide peaks from proteinase K digestion of Rho treated with $NaBD_4$/*i*PrOH. (E-G) ESI-MS^1 spectra showing characteristic cleavage of C^{15}-D^1-retinyl cation (270 m/z) from precursor C^{15}-D^1-retinyl-peptide analyte, producing a product peptide peak. (H-J) MS^2 spectra of CID fragmentation of the product peptide ion for sequence determination.

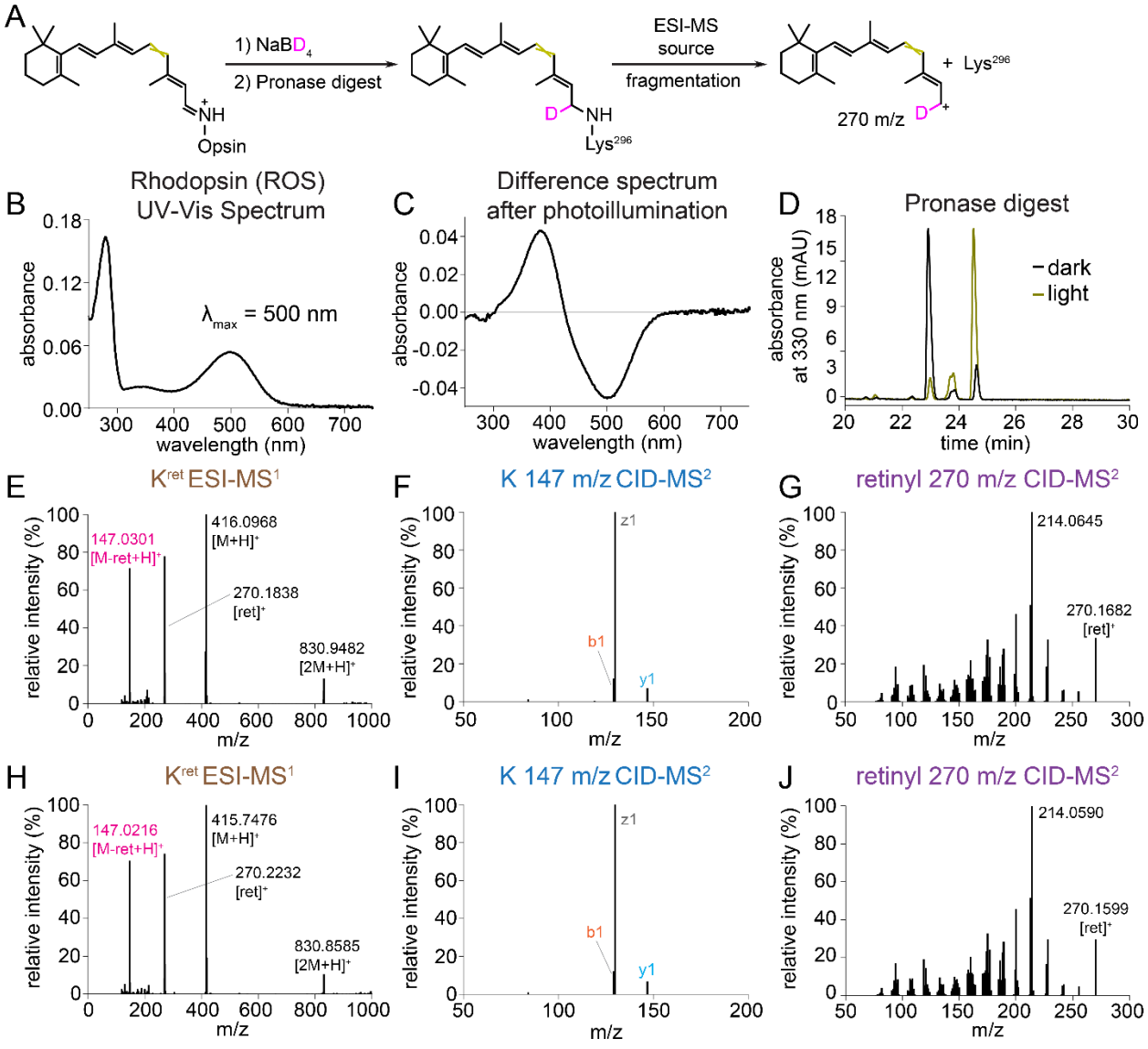

Figure 2.11 LC-MS/MS analyses of pronase digests of $NaBD_4$-treated Rho and Rho* from native membranes. (A) Schematic diagram of sample preparation and LC-MS/MS workflow. (B) UV-Vis spectrum of Rho from ROS membranes solubilized in DDM. (C) Difference absorbance spectrum of DDM-solubilized Rho versus Rho* in ROS membranes illuminated with 565-nm fiber light at 625 μW for 10 s at 4°C. (D) Chromatographic separation of N^{ε}-retinyl-Lys peaks from the pronase digests of Rho and Rho* in ROS membranes treated with $NaBD_4$/*i*PrOH. (E, H) ESI-MS^1 spectrum showing characteristic cleavage of retinyl cation (269 m/z) from precursor N^{ε}-retinyl-Lys analyte (415 m/z), producing a product Lys ion (147 m/z). (F, I) CID-MS^2 spectrum of the product Lys ion exhibiting a characteristic fragmentation pattern of Lys. (G, J) CID-MS^2 spectrum of retinyl cation demonstrating a complex fragmentation pattern with a characteristic dominant 213 m/z signal.[123, 124] mAU, milli absorbance unit.

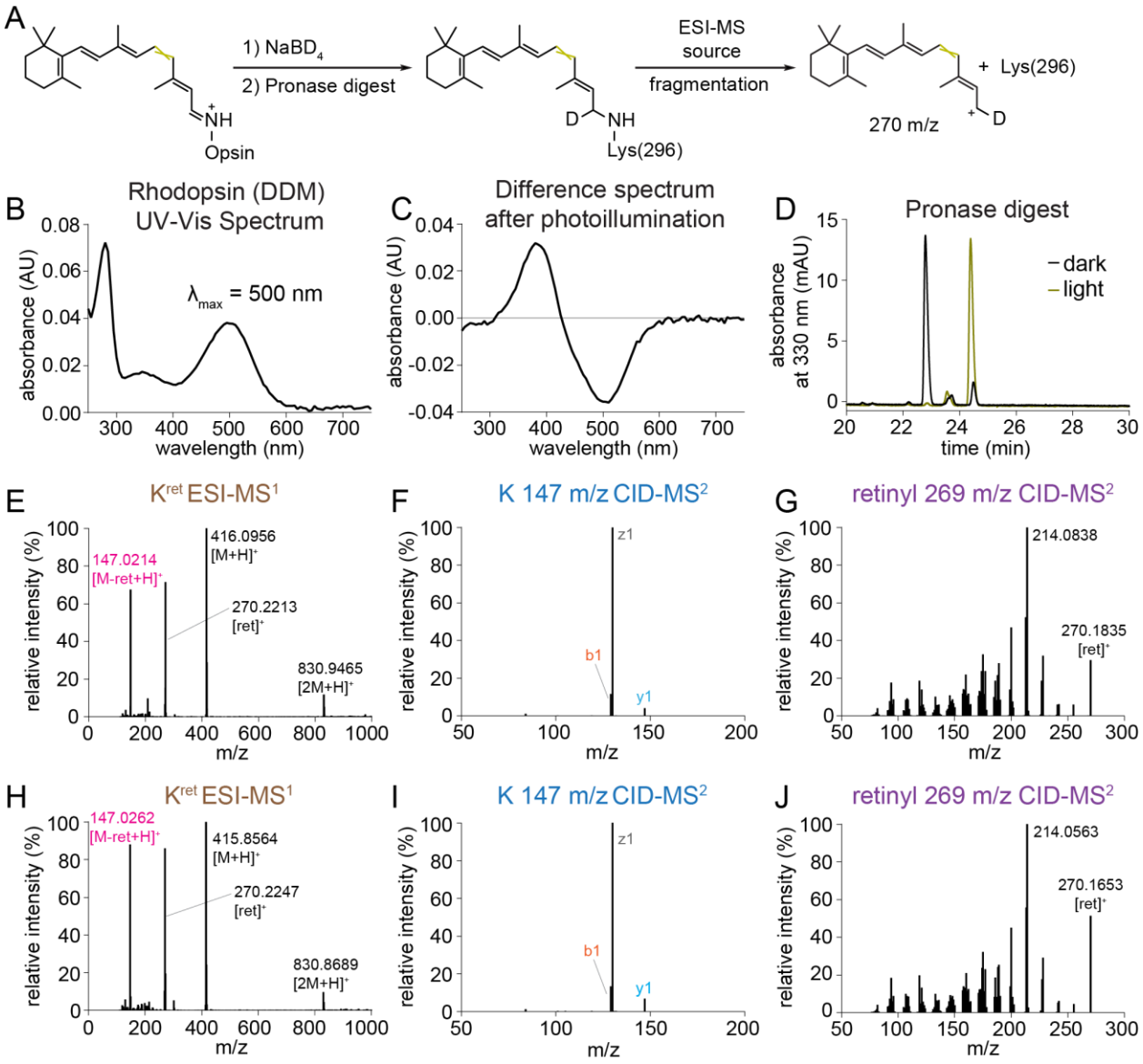

Figure 2.12 LC-MS/MS analyses of pronase digests of NaBD$_4$-treated Rho and Rho* immunopurified in DDM detergent micelles. (A) Schematic diagram of sample preparation and LC-MS/MS workflow. (B) UV-Vis spectrum of purified Rho in DDM. (C) Difference absorbance spectrum of Rho versus Rho* illuminated with 565-nm fiber light at 625 µW for 10 s at 4°C. (D) Chromatographic separation of N$^{\varepsilon}$-retinyl-Lys peaks from the pronase digests of Rho and Rho* treated with NaBD$_4$/*i*PrOH. (E, H) ESI-MS^1 spectrum showing characteristic cleavage of retinyl cation (269 m/z) from precursor N$^{\varepsilon}$-retinyl-Lys

analyte (415 m/z), producing a product Lys ion (147 m/z). (F, I) CID-MS^2 spectrum of the product Lys ion exhibiting a characteristic fragmentation pattern of Lys. (G, J) CID-MS^2 spectrum of retinyl cation demonstrating a complex fragmentation pattern with a characteristic dominant 213 m/z signal.[123, 124] mAU, milli absorbance unit.

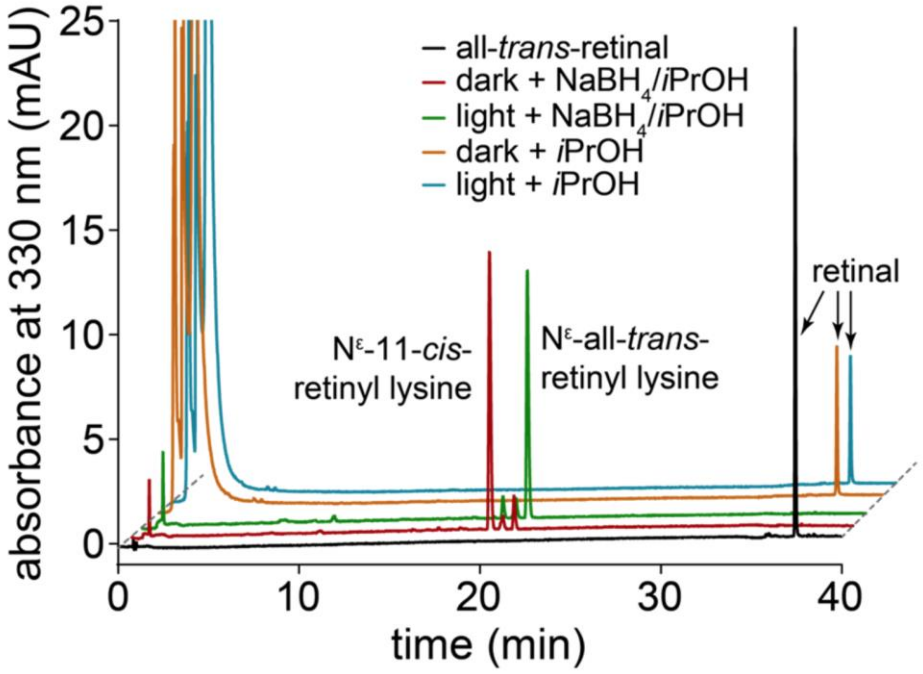

Figure 2.13 Reverse-phase HPLC chromatographic traces of pronase digestion of Rho and Rho* treated with $NaBH_4$/*i*PrOH vs *i*PrOH alone. Rho and Rho* in ROS before and after light exposure was treated with *i*PrOH alone, leading to the detection of retinal from the pronase-digested denatured protein precipitate. With $NaBH_4$/*i*PrOH treatment, only N^{ε}-retinyl-Lys was detected, without detection of any retinal from retinylidene Schiff base left unreduced.

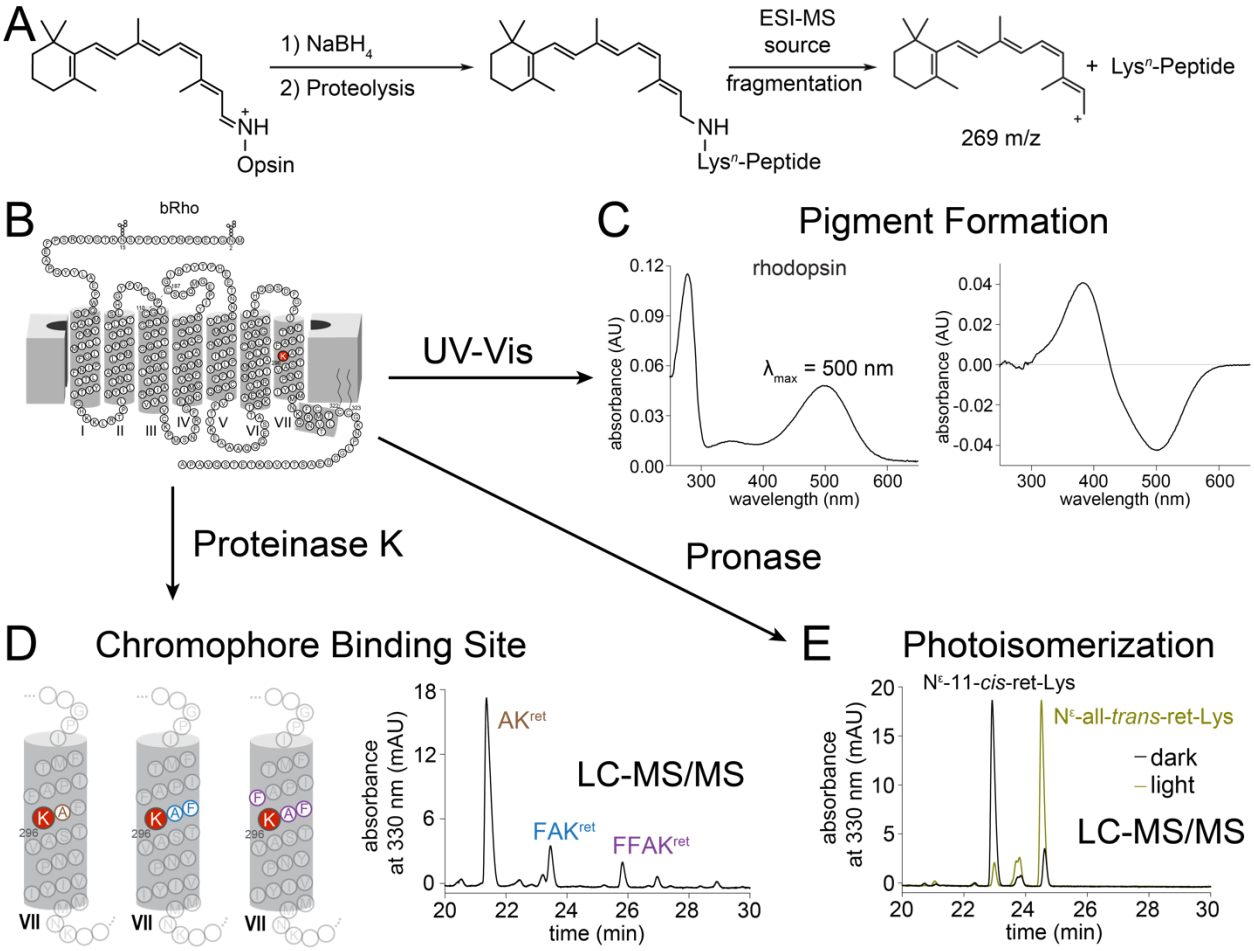

Figure 2.14 Schematic diagram of the protocol for determining retinylidene-opsin pigment chromophore binding site and photoisomerization reaction. (A) Overall scheme of sample preparation for MS analysis. (B) Opsins are mapped to determine presence of an internal Lys residue for retinylidene Schiff base attachment within the putative chromophore binding pocket. (C) The formation of retinylidene-opsin pigment, as well as the shift in the absorption maximum following exposure to light, is characterized by UV-Vis spectrophotometry. (D) Retinylidene-opsin pigments are treated with $NaBH_4$/*i*PrOH for the reductive trapping of chromophore. After proteolysis by proteinase K, LC-MS/MS analyses can detect resultant N^{ε}-retinyl-peptides, which undergoes ESI source fragmentation to a retinyl cation and product peptide ion. The peptide ion can be then

sequenced by CID fragmentation. (E) The photoisomerization of the chromophore is documented by LC-MS/MS analysis of the pronase digest of the pre- and post-illuminated opsin pigment treated with $NaBH_4$. Analyses at various time points after illumination can be performed to monitor hydrolysis kinetics of the chromophore photoproduct.

CHAPTER 3

Determination of the kinetics of rod outer segment visual cycle processes in native membranes

This chapter is in part derived from the manuscript published in *Proceedings of the National Academy of Sciences*:
Hong JD, Salom D, Kochman MA, Kubas A, Kiser PD, Palczewski K. Chromophore hydrolysis and release from photoactivated rhodopsin in native membranes. ***PNAS***. 2022 Nov 8;119(45):e2213911119. doi: 10.1073/pnas.2213911119. PMID: 36322748

3.1 Introduction and Significance

The key step that bridges the rhodopsin photocycle and the visual cycle is the Schiff base hydrolysis of the all-*trans*-retinylidene agonist. The hydrolysis provides the visual cycle with all-*trans*-retinal to recycle into 11-*cis*-retinal, while also liberating the chromophore binding pocket for entry of fresh 11-*cis*-retinal to regenerate rhodopsin pigment. Prior measurements of this hydrolysis were largely done using either absorbance or fluorescence spectroscopy, which requires detergents to solubilize rhodopsin. Detergents could potentially alter protein structure and dynamics, thereby compromising the biochemistry that would occur in native membranes. The detergent effects could be dramatic in the case of rhodopsin, which resides in membranes rich in polyunsaturated acyl chains, such as docosahexaenoic acid.[82, 83] Polyunsaturated lipids confer greatly enhanced lipid membrane fluidity, which is particularly important for membrane protein dynamics.[125-127]

The method described in chapter 2 using $NaBH_4$/*i*PrOH allowed for the detection of chromophore status within Rho or Rho* in native membranes. The use of *i*PrOH solubilize the lipids while precipitating protein. The alcohol-solubilized lipids should contain the released all-*trans*-retinal from the hydrolysis of all-*trans*-retinylidene agonist in Rho*. By measuring the amount of all-*trans*-retinylidene still bound to Rho* and the all-*trans*-retinal released at different timepoints, a detailed analysis of the kinetics of the hydrolysis can be determined.

Notably, the released all-*trans*-retinal is reported to form Schiff base condensates or adducts with phosphatidylethanolamines (PEs) of ROS membranes, producing N-retinylidene-PEs (N-ret-PEs).[128-131] The detergents used in the study of hydrolysis of all-

trans-retinylidene agonist in Rho* compromises the membrane integrity and the phospholipid composition around Rho, thereby complicating the study of subsequent N-ret-PE formation. Whether N-ret-PE formation has any influence on preceding step of all-*trans* agonist hydrolysis from Rho* has yet to be investigated. Furthermore, N-ret-PEs have documented important roles as the substrate for ABCA4, which flips N-ret-PEs from the intraluminal to the cytosolic leaflet to facilitate RDH-mediated reduction of retinal, which is in equilibrium of being bound and unbound to PE.[128, 130, 132] As such, a consideration of N-ret-PE formation and clearance is critical for understanding the pathophysiology of ABCA4-associated retinal diseases, such as Stargardt disease-1.[131, 133]

Excess released all-*trans*-retinal, beyond the available reductive capacity of the rods due to intense light exposure, leads to accumulation of N-ret-PEs that serve as the starting point for the formation of autofluorescent bisretinoids upon a second Schiff base condensation event with another all-*trans*-retinal.[133-135] Bisretinoids are thought to be a biomarker of age-related macular degeneration (AMD) and to contribute to photo-oxidative damage to the neuroretina and RPE.[136-139] Though bisretinoids have been observed in fundus autofluorescence imaging of mice and humans[134, 135, 137, 140, 141], N-ret-PEs have not been definitively shown to be present in the retina. Prior methods suggest the presence of N-ret-PEs in the organic-aqueous extraction of lipids from retina.[133] However, the N-ret-PEs could be an artifact of the extraction method itself, whereby Schiff base condensation between the released all-*trans*-retinal and PEs could have occurred during the extraction with chloroform/methanol spiked with HCl, which is known to catalyze Schiff base formation.[82, 133, 142]

Our method, which both momentarily solubilizes lipids and immediately reduces retinylidene Schiff bases, should be able to capture any N-ret-PEs that have formed. Addition of $NaBH_4$/*i*PrOH at different time points should even allow for measurements on the kinetics of N-ret-PE formation, as will be demonstrated by our results. As illustrated by Figure 3.1, the entire sequential process, from chromophore photoisomerization to agonist hydrolysis and N-ret-PE formation, can be monitored using $NaBH_4$/*i*PrOH to reductively trap the chromophore at different stages of its progression through these initial steps of the visual cycle in the rod outer segment.

Notably, 11-*cis*-retinal enters and all-*trans*-retinal exits the opsin protein through different sites.[85] The entry site does not bind all-*trans*-retinal and is highly selective for 11-*cis*-retinal. The exit site solely allows all-*trans*-retinal to leave without reentry.[85] Released all-*trans*-retinal is subsequently reduced to all-*trans*-retinol catalyzed by NADPH-dependent RDHs.[143] Whether RDHs interact with Rho* to directly obtain all-*trans*-retinal then influences Rho* hydrolysis of all-*trans* agonist has yet to be understood. The kinetics of RDH activity, particularly in native membranes, has not yet previously been quantitatively measured.

By substituting $NaBH_4$ with $NaBD_4$, our method was hypothesized to capture RDH activity in native membranes by analyzing the all-*trans*-retinol, which would possess at C-15 either a hydrogen from the hydride of the NADPH cofactor of RDHs or a deuterium from the deuteride of $NaBD_4$. Any all-*trans*-retinal unreduced by RDHs would therein be reduced by $NaBD_4$ and be found as deuterated all-*trans*-retinol. Therefore, isotopic labeling can be leveraged to monitor RDH reduction kinetics (Figure 3.2). The following results will demonstrate the ability to track chromophore from its photoisomerization in Rho, to its

hydrolysis as agonist from Rho*, then its formation of PE-adducts with lipid membrane, and finally its reduction to all-*trans*-retinol, all in native membranes. Therefore, the entire processes of the visual cycle occurring within ROS would be captured using our method, without the need for the reductionist approach of studying purified proteins or constituents of ROS.

3.2 Results

3.2.1 Separation and Identification of N-ret-PEs.

Given that treatment of ROS with $NaBH_4$/*i*PrOH also solubilizes lipids, the alcohol-solubilized lipid fraction was isolated from the protein precipitate by centrifugation. Since $NaBH_4$ rapidly reduces any retinylidene Schiff bases, the elusive N-ret-PEs were expected to be trapped as N-retinyl-PEs, which can be identified by LC-MS/MS. Indeed, 16 minutes after light exposure to ROS, some of the released all-*trans*-retinal had formed Schiff base adducts with various PE species, known to be abundant in ROS (Figure 3.3). The acyl chains in sn-1 and sn-2 positions of N-ret-PE were determined by LC-MS/MS (Figure 3.4). These species had saturated acyl chains, namely palmitate (16:0) or stearate (18:0), in the sn-1 position.[82, 144] Importantly, these species had polyunsaturated acyl chains, namely docosahexaenoic acid (DHA, 22:6), docosapentaenoic acid (DPA, 22:5), and docosatetraenoic acid (DTA, 22:4), in the sn-2 position, with DHA being most abundant, followed by DPA, then DTA.[82] The characteristic six N-retinyl-PE species, containing the combination of sn-1 and sn-2 acyl chains listed above, were again observed in the same ratios upon addition of exogenous all-*trans*-retinal to ROS unexposed to light (Figure 3.3D).

3.2.2 Kinetics of Rho* Hydrolysis and Subsequent N-ret-PE Formation.

Our trapping procedure enabled a detailed kinetic analysis of each step as it occurred in the native phospholipid bilayer (Figures 3.1 and 3.5A). $NaBH_4$/*i*PrOH was added to ROS at different time points after illumination to trap the remaining all-*trans*-retinylidene in Rho*, the liberated all-*trans*-retinal, and the subsequently formed N-ret-PEs. Snapshots of the progressive Rho* hydrolysis of all-*trans*-retinylidene Schiff base are captured by the decrease in N^{ε}-all-*trans*-retinyl-Lys signal over time (Figure 3.5B). There is a reciprocal increase in signal of all-*trans*-retinol and N-retinyl-PEs, which are the $NaBH_4$ reduction productions of the released all-*trans*-retinal and subsequent formed N-ret-PEs (Figure 3.5C). The rate of hydrolysis followed pseudo first-order decay kinetics and increased with temperature (Figure 3.5D).

The released all-*trans*-retinal reacted reversibly with PE, reaching a steady state of around 40% all-*trans*-retinal bound to PE as N-ret-PE (Figure 3.5E). The kinetics of this N-ret-PE formation also followed pseudo first-order kinetics and became faster with increasing temperature; however, the steady-state level of N-ret-PE decreased with temperature (Figure 3.5E). The amount of released all-*trans*-retinal unbound to PE showed an inverse relationship with the amount of N-ret-PEs (Figure 3.5F).

From the temperature dependence of the Rho* hydrolysis reaction, an Arrhenius plot (Figure 3.5G) was generated, yielding an activation energy (E_A) of 17.7 ± 2.4 kcal/mol. The rate of Rho* hydrolysis was also measured in n-dodecyl-β-D-maltoside (DDM) micelles to mimic conditions of mild detergent solutions that are typically used for spectrophotometric measurements of Rho. The rate of hydrolysis in DDM was found to be ~50% slower than that in the ROS membranes (Figure 3.5H).

3.2.3 pH Dependency of Rho* Hydrolysis and N-ret-PE Formation.

As mentioned prior, the protonation state of the retinylidene Schiff base of Rho* behaves inversely to changes in the external protic environment of Rho*.[145] This behavior was observed by UV-Vis spectroscopy, showing that higher pH shifts the metarhodopsin equilibrium from MII, the deprotonated state, toward protonated states, namely MI and MIII (Figure 3.6A). Schiff base hydrolysis of Rho* occurred to a greater magnitude at lower pH, where MII is favored (Figure 3.6B). However, lower pH appeared to slow down the overall rate of N-ret-PE formation with also lower amounts of N-ret-PE and higher amounts of free all-*trans*-retinal unadducted to PE (Figure 3.6C-D).

To isolate the reaction between all-*trans*-retinal and PE to obtain the rate of N-ret-PE formation independently, exogenous all-*trans*-retinal was added to ROS membranes and tracked by addition of $NaBH_4$/*i*PrOH at different time points. The representative chromatograms of the Schiff base condensation reaction of all-*trans*-retinal with PE over time showed a decline in all-*trans*-retinal starting material with the formation of N-ret-PEs (Figure 3.6E). The rate of N-ret-PE formation exhibited pH dependency, with a greater proportion of all-*trans*-retinal forming N-ret-PEs and a faster reaction as pH increased (Figure 3.6F). In summary, Rho* hydrolysis of all-*trans*-retinylidene Schiff base was faster at lower pH, which favors MII, whereas N-ret-PE formation was slower at lower pH.

3.2.4 Computational Analysis of Rho* Hydrolysis of all-*trans*-retinylidene Schiff base.

In collaboration with Dr. Adam Kubas at the Polish Academy of Sciences, the mechanistic basis for the pH dependency of Rho* hydrolysis was explored by

computationally modeling the energy landscapes of each intermediate step of all-*trans*-retinylidene hydrolysis for each metarhodopsin species (Figure 3.7). The influence of Glu^{113} and Glu^{181} on the energy levels of each metarhodopsin species was examined and of subsequent intermediates of hydrolysis, considering the following factors: the spatial location of these Glu residues within the chromophore binding pocket, their influence on the spectral characteristics of the retinylidene chromophore, and their role in forming the water and H-bonding network that surrounds the chromophore and spans throughout Rho.[46, 106]

Upon photoactivation to MII, Glu^{113} and Glu^{181} shift from their position in Rho, translocating so that both surround and interact with the all-*trans*-retinylidene Schiff base.[29, 146] The protonation states of Glu^{113} and Glu^{181} could vary with external pH, leading to presence of either a negatively charged or neutral carboxyl residue near the all-*trans*-retinylidene Schiff base, which can take either a *syn*- or *anti*-configuration. The configuration of the protonated retinylidene Schiff base is 15-*anti* for MI and 15-*syn* for MIII.[40, 41] The exact stereoisomerism of the deprotonated Schiff base of MII is unclear, but it could loosely adopt either a 15-*anti* or 15-*syn* configuration.[40, 41] For either protonated or deprotonated states of the Schiff base, the *anti*-configuration is dominant over the *syn*, since the *anti*-*syn* interconversion requires addition light or thermal energy.[40, 41]

Quantum chemical calculation to map the energetic landscape of hydrolysis were performed, considering both the Schiff base protonation state and its *anti* vs *syn* configurations, as well as the protonation states of Glu^{113} and Glu^{181}. Our calculations were performed on a hydrogen-saturated cluster model of the Rho active site derived from the

current highest-resolution structure of a metarhodopsin species to date, 3PQR, proposed to correspond to MII, with a deprotonated Schiff base in the *anti*-configuration (Figure 3.8).

For protonated Schiff base, our initial calculations showed a preference for Glu^{113} and Glu^{181} in their deprotonated states. Furthermore, the *syn*-configuration of the protonated Schiff base was found to be 3.3 kcal/mol lower in energy (more stable) than the anti-configuration. This aligns with the understanding of the greater thermodynamic stability of MIII than MI, especially given the exceedingly transient nature of MI. The nucleophilic attack of the Schiff base by water, producing an oxonium intermediate, is exothermic for protonated Schiff base in the *anti*-configuration but endothermic for *syn*-configuration (Figure 3.7B). The protonate transfer between the oxonium and nitrogen facilitated by the polar protic environment of the pocket is exothermic, but the final C-N bond cleavage is considerably endothermic such that the final products (Figure 3.7B, Id) were 2.0 kcal/mol higher in energy than reactants (Figure 3.7B, Ia). Therefore, the hydrolysis of protonated all-*trans*-retinylidene Schiff base was found to be an overall endothermic process (Figure 3.7B).

In contrast, hydrolysis of either the *anti*- or *syn*-isomers of the deprotonated Schiff base was overall exothermic (Figure 3.7C). Under low pH conditions favoring the deprotonated Schiff base, our calculated showed a preference for Glu^{181} in its deprotonated state and Glu^{113} in its protonated state. The deprotonated Schiff base in its *anti*-configuration was significantly lower in energy than the *syn*-configuration by 4.4 kcal/mol.

Nucleophilic attack by water of either the *anti*- or *syn*-isomers of deprotonated retinylidene Schiff base was considerably exothermic, as well as the proceeding proton transfer from Glu^{113} to the nitrogen of the Lys296-carbinolamine intermediate, likely via

water or the H-bonding network of the pocket (Figure 3.7C, IIb, IIc). At low pH, Glu^{113} becomes re-protonated (Figure 3.7C, IId). The re-protonation of Glu113, followed by the C-N bond cleavage, are both endothermic; however, the overall energy change in the process is exothermic by ~8.0 kcal/mol (Figure 3.7C, IIe). Assuming linear relationships between the effective activation barriers and the overall change in energy, external pH definitively influences the protonation patterns of internal Glu^{113} and Glu^{181} carboxyl moieties and the retinylidene Schiff base to the ε-amine of Lys^{296}. These protonation patterns have a decisive effect on the resultant energetics of the Schiff base hydrolysis for different metarhodopsin species.

3.2.5 Reduction of all-*trans*-retinal in Native Membranes.

In the visual cycle, all-*trans*-retinal is reduced to all-*trans*-retinol by RDHs.[143] Our method, using $NaBD_4$ in place of $NaBH_4$, allowed us to track this step of the visual cycle in ROS, thereby studying the fate of all-*trans*-retinal after its hydrolytic release from Rho* in the presence of the essential dinucleotide cofactor NADPH (Figures 3.2 & 3.9A). The extent of Rho* hydrolysis to release all-*trans*-retinal was similar in the presence or absence of NADPH ($NADP^+$ was used as a control), suggesting that RDH activity in reducing all-*trans*-retinal does not influence the biochemistry of Rho* hydrolysis (Figure 3.9B). RDH activity was observed only in the presence of NADPH with the reduction of nearly all released all-*trans*-retinal to all-*trans*-retinol with negligible amounts of N-retinyl-PEs at both 8- and 16-min post-illumination (Figure 3.9C).

To determine whether N-ret-PEs play a role in transferring its all-*trans*-retinal to RDHs, NADPH was added to ROS, containing N-ret-PEs in steady state with the exogenously

added all-*trans*-retinal at pH 7.4. The all-*trans*-retinal adducted to PE as N-ret-PEs appeared to be initial unaffected by the addition of NADPH, indicating N-ret-PEs as not a direct source of substrate for RDHs (Figure 3.9D-E). The presence of NADPH did not accelerate the dissociation of N-ret-PEs as would have been observed if N-ret-PEs played an indispensable role in all-*trans*-retinal-substrate delivery to RDHs (Figure 3.9D-E). Within the first 4 min, N-ret-PE levels were reduced to a small extent, but nearly 25% of free all-*trans*-retinal was reduced by the RDHs (Figure 3.9E). Therefore, the RDHs exhibited their activity on free all-*trans*-retinal in native membranes rather than on PE-bound all-*trans*-retinal. By 32 min, the RDH-mediated reduction of all-*trans*-retinal had been gone to completion, with the equilibrium of free all-*trans*-retinal and N-ret-PE continually providing free all-*trans*-retinal for reduction, thereby eventually depleting levels of N-ret-PEs (Figure 3.9E).

3.3 Discussion

A critical step in the visual cycle is the release of the spent chromophore, all-*trans*-retinal, which is ultimately transformed back to 11*c*RAL. The steps immediately following retinal photoisomerization (i.e., hydrolytic release of all-*trans*-retinal, formation of N-ret-PE, and reduction of all-*trans*-retinal to all-*trans*-retinol) have only been subjected to preliminary investigation due lack of instrumentation and/or methodology to measure each reaction as they occur in the complex mixture of molecules and processes within native membranes. These challenges were largely overcome through our sample preparation using $NaBH_4$/*i*PrOH to fractionate lipids and proteins, allowing for subsequent LC-MS/MS for the lipid contents and the proteolyzed protein contents. Analysis of retinyl

species in the protein fraction allowed the detection of all-*trans*-retinal still bound to Rho* as all-*trans*-retinylidene Schiff base. Analysis of retinyl species in the lipid fraction allowed the tracking of free all-*trans*-retinal from Rho* Schiff base hydrolysis, as well as its subsequent adducts with PE. By substituting $NaBH_4$ with $NaBD_4$, RDH reduction all-*trans*-retinal to all-*trans*-retinol was also tracked in the lipid soluble fraction. Therefore, all visual cycle processes occurring within the rod outer segment were measured using readily accessible and cheap reagents, and using LC-MS/MS, which is typically accessible at many institutions and to laboratories through core facilities.

By measuring the retinyl signal in the protein fraction and lipid fraction at various time points, the overall rate of Rho* hydrolysis was determined. The rate of hydrolysis was faster with Rho* in ROS membranes than in DDM detergent micelles, demonstrating how the nature of the lipid environment can alter molecular dynamics (Figure 3.5H). Our calculated E_A of 17.7 kcal/mol for Rho* hydrolysis in ROS membranes at pH 7.4 is close to early measurements performed by photocalorimetry, which produced values of 22.1 kcal/mol at pH 8.0 and 11.7 kcal/mol at pH 5.4 for Rho* in ROS membranes.[147] The lower E_A of hydrolysis at pH 5.4 also aligned with the results of our Rho* hydrolysis experiments with ROS, which showed hydrolysis occurring to a greater extent at lower pH, thereby supporting the longstanding notion that hydrolysis proceeds via the MII signaling state of Rho. Our computational results further support the favorability of hydrolysis proceeding via the deprotonated Schiff base of MII over the protonated Schiff base of MI or MIII. Our computational studies demonstrated the importance of Glu^{113} and Glu^{181} residues and their protonation states on the energetic landscape of the reaction, with the hydrolysis process being exothermic at lower pH.

The formation of N-ret-PE also displayed pH dependency, with faster rates and higher steady states as pH increased, likely due to a greater proportion of PE with its amine deprotonated and available for Schiff base formation with free all-*trans*-retinal. Therefore, pH changes had opposite effects on the rate of Rho* hydrolysis versus the rate of N-ret-PE formation; at lower pH, there was more Rho* hydrolysis but less N-ret-PE formation. Furthermore, the overall rate of N-ret-PE formation from released all-*trans*-retinal was slower than the rate of Rho* hydrolysis at low pH (k_{hyd} = 0.001537 s^{-1} vs. k_{NretPE} = 0.001062 s^{-1}). Prior to our examination of the kinetics of N-ret-PE formation, we hypothesized that PE could potentially play a role in facilitating the hydrolysis of all-*trans*-retinylidene of Rho* by serving as a proximal acceptor of the released all-*trans*-retinal. However, based on our pH studies of the Rho* hydrolysis and the N-ret-PE condensation reaction, the rate of hydrolysis did not appear to be influenced by the subsequent formation of N-ret-PE with the all-*trans*-retinal from Rho* hydrolysis. Instead, the hydrolysis of the all-*trans*-retinylidene agonist relied mainly on the protein dynamics of Rho, reflecting the dependency of the hydrolysis kinetics on pH-driven changes in the metarhodopsin equilibrium.

At physiological pH, the rate of N-ret-PE formation was an order of magnitude faster than the rate of Rho* hydrolysis (k_{hyd} = 0.001479 s^{-1} vs. k_{NretPE} = 0.01819 s^{-1}). Furthermore, N-ret-PE formation is a reversible reaction and reached a steady state mole fraction of 0.4, meaning that close to half the all-*trans*-retinal forms adducts with PE. The significant proportion of N-ret-PE adducts, along with the fast rate of reaction, demonstrates the high potential for the eventual formation of phototoxic bisretinoids that are abundant with Stargardt disease and age-related macular degeneration.[133, 138, 141] Although bisretinoids

were not observed under the conditions and timescale of our studies of Rho* hydrolysis, their formation could be facilitated by any number of factors, including delayed reduction (e.g., by intense illumination and depletion of NADPH), attenuated phagocytosis, and genetic alterations of pertinent visual cycle proteins and enzymes.[148, 149] Longer durations of light exposure and incubation periods with released all-*trans*-retinal or accelerated supply of 11-*cis*-retinal that is constitutively supplied by the retinal pigment epithelium could also lead to bisretinoid formation.[150] However, N-ret-PE formation was recently shown to not always lead to a pathologic outcome but could very well serve as a nonclassical means of chromophore regeneration via production of 9-*cis*- or 11-*cis*-retinal through N-ret-PE photoisomerization.[151]

Another physiological role that was hypothesized for N-ret-PEs was as a shuttle for all-*trans*-retinal delivery to RDHs at the membrane periphery. However, RDHs were found to exhibit activity selectively on free all-*trans*-retinal, with little effect on the proportion of all-*trans*-retinal sequestered as N-ret-PE adducts upon addition of NADPH. N-ret-PE levels began gradually declining as the equilibrium of all-*trans*-retinal bound and unbound to PE was shifted towards free all-*trans*-retinal, with its reduction to all-*trans*-retinol. If NADPH were present before light exposure to generate Rho*, the all-*trans*-retinal released by Rho* hydrolysis was immediately reduced by RDHs, with near complete attenuation of N-ret-PE formation. This observation is supported by the rate of RDH reduction being measured at yet another magnitude faster, $k_{red} = 0.169\ s^{-1}$, than the rate of N-ret-PE formation. Such an observation highlights the significance of RDHs in the clearance of reactive all-*trans*-retinal, as well as prevention of the formation and accumulation of N-ret-PEs after light exposure. However, if intracellular NADPH were eventually depleted, then all-*trans*-retinal and PE-

adducts can accumulate. NADPH is likely to quickly deplete upon intense light exposure, which with 10^8 rhodopsin molecules per rod would lead to a massive dose of released all-*trans*-retinal. The reductive capacity of photoreceptor cells would be quickly overwhelmed, contributing to oxidative stress and cell death.[152]

Our results demonstrated the capability of using $NaBD_4$ to monitor redox biochemical reactions involving functional groups, such as aldehydes or ketones, that are susceptible to borohydride/deuteride chemistry. Either the oxidation of alcohols to aldehydes or ketones, or the reduction of aldehydes or ketones to alcohols can be studied, since $NaBD_4$ would reduce aldehydes or ketones for their mass spectrometric quantification as the deuterium-labeled alcohol product. Therefore, this method can be broadly applicable in the study of such redox processes and can be done so not only for cytosolic but also membrane-bound dehydrogenases like RDHs. This provides the opportunity to analyze the redox biochemistry of lipids, such as vitamin A in the context of our study.

In a prior collaboration studying the first steps of vision with the Robinson group, native MS remarkable capture both phototransduction and visual cycle processes simultaneously, directly in crude ROS without the need for purification of any protein or constituents. [84] However, native MS showed a couple of deficiencies that were resolved by our method. Namely, native MS has limited tolerance for salts, such as NADH and NADPH, which leads to technical challenges when studying redox biochemistry. The method described by our study offers yet another advantage over native MS, which is its ability to resolve the isomeric composition of the retinylidene adduct of opsins in a sample exposed to light. While native MS can be used to observe the hydrolysis of the retinylidene Schiff

base, it cannot be used in the study of photochemistry, since Rho and Rho* have the same overall mass.

Overall, the method described by our study demonstrated its ability to monitor in sequence: the photochemistry of Rho, the Schiff base hydrolysis of agonist from Rho*, the formation of adducts between released all-*trans*-retinal and PE, and the RDH-mediated reduction of all-*trans*-retinal to all-*trans*-retinol. Our study using our methodology showed that each process of the visual cycle within ROS occurs in series, one order of magnitude faster than the prior step in the following order: Rho* hydrolysis, N-ret-PE formation, and RDH reduction. Our results are consistent with hydrolysis being rate limiting, such that soon after all-*trans*-retinal is released, it is immediately reduced, or forms adducts with PE when NADPH is depleted. Importantly, these processes were studied without the need for the reductionist approach of studying a purified protein or any component in isolation from its native environment. Furthermore, the method requires cheap, readily accessible reagents, as well as instrumentation that is typically available at many institutions and laboratories; therefore, showing promise in its broad application in other labs.

In the following chapters, our method will be applied to study the photochemistry of other opsin relevant to the physiology of vision, namely cone opsins, RGR, and RRH. The hydrolysis of their photo-isomerized chromophore will also be analyzed to better understand the turnover of chromophore by cone opsins relative to rhodopsin, as well as the potential rate of chromophore recycling performed by RGR or RRH to maintain these visual opsin pigments to sustain vision under daylight conditions.

3.4 Materials & Methods

Instrumentation

1100 Series HPLC System (Agilent, Santa Clara, CA); 1260 Infinity HPLC System (Agilent); Dionex Ultimate 3000 UHPLC System (Thermo Fisher Scientific, Waltham, MA); LTQ XL mass spectrometer (Thermo Fisher Scientific); Cary 50 UV-Vis Spectrophotometer (Varian, Palo Alto, CA).

Materials

Chemicals and other materials were purchased as follows: all-*trans*-retinal (Sigma-Aldrich, St. Louis, MO, cat. no. R2500), all-*trans*-retinol (Sigma-Aldrich, cat. no. R7632); bovine rod outer segments (InVision Bioresources, Seattle, WA, cat. no. 98740); 2-[4-(2-hydroxyethyl)piperazin- 1-yl]ethanesulfonic acid (Goldbio, St. Louis, MO, cat. no. H-400-1); 1,3- Bis[tris(hydroxymethyl)methylamino]propane (Sigma-Aldrich, cat. no. B6755); calcium chloride dihydrate (Sigma-Aldrich, cat. no. 223506); n-dodecyl-β-D-maltopyranoside Sol-grade (Anatrace, Maumee, OH, cat. no. D310S); pronase (Sigma-Aldrich, cat. no. PRON-RO); proteinase K solution (Viagen Biotech, cat. no. 501-PK); Amicon Ultra-0.5 Centrifugal Filter (Millipore, Burlington, MA, cat. no. UFC503096); acetonitrile Optima LC/MS grade (Fisher Scientific, Pittsburgh, PA, cat. no. A955); MeOH Optima LC/MS grade (Fisher Scientific, cat. no. A456); iPrOH Optima LC/MS grade (Fisher Scientific, cat. no. A461); formic acid Optima LC/MS grade (Fisher Scientific, cat. no. A117-50); methylene chloride (HPLC) (Fisher Scientific, cat. no. D143); hexanes (HPLC) (Fisher Scientific, cat. no. H302); ethyl acetate (HPLC) (Fisher Scientific, cat. no. E195); triethylamine (HPLC) (Fisher Scientific, cat. no. O4884); dimethyl sulfoxide (Sigma-Aldrich, cat. no. D2650); N,N-dimethylformamide (Fisher Scientific, cat. no. AC327171000); diethylamine (Sigma-

Aldrich, cat. no. 471216); Nα-[(9H-fluoren-9- ylmethoxy)carbonyl]-L-Lys hydrochloride (Fisher Scientific, cat. no. F0586); 1,2-dioleoyl-sn- glycero-3-phosphoethanolamine (Avanti Polar Lipids, Alabaster, Al, cat. no. 850725P); $NaBH_4$ (Alfa Aesar, Haverhill, MA, cat. no. 88983); $NaBD_4$ (Alfa Aesar, cat. no. 35102); Isotemp 3016S Water Bath (Fisher Scientific, cat no. 13-874-28); 85 W 2700 K Hg light bulb (Home Depot, cat. no. EDXR-40-19); Fiber-Coupled 565 nm 9.9 mW (Min) 700 mA LED (Thorlabs, Newton, NJ, cat. no. M565F3); Fiber Patch Cable (Thorlabs, cat. no. M92L01); Compact T-Cube 1200 mA LED Driver with Trigger Mode (Thorlabs, cat. no. LEDD1B); Power Supply Unit with 3.5 mm Jack Connector (Thorlabs, cat. no. KPS201); HPLC columns: BioPureSPN C18 TARGA (nestgrp, Ipswich, MA cat. no. HEM S18R); XBridge C18 (Waters, Milford, MA, 2.1 mm X 100 mm, cat. no. 186003022); Gemini Analytical C18 (Phenomenex, Torrance, CA, 250 x 4.6 mm, cat. no. 00G-4435-E0); Gemini Preparatory C18 (Phenomenex, 250 x 10 mm, cat. no. 00G- 4435-N0); Luna Preparatory Silica (Phenomenex, 250 x 21.2 mm, cat. no. 00G-4091-P0-AX).

Methods

Synthesis of N-retinyl-dioleoylphosphatidylethanolamine standard.

Dioleoylphosphatidylethanolamine (DOPE, 100 mg) was dissolved in 4 mL of 4:1 methylene chloride/MeOH. Under dim red light in a dark room, 50 mg of all-trans-retinal (1.3 eq.) dissolved in 1 mL of methylene chloride was added to the solution of DOPE. Subsequently, 18.7 µL of triethylamine (1 eq.) was added, and the reaction mixture was left to incubate in the dark room overnight. The reaction mixture was concentrated to 0.5 mL under a gentle stream of nitrogen. 200 µL DMF and 200 µL MeOH were added, the mixture was re-concentrated to ~0.4 mL, and then centrifuged at 20,000 × g for 1 min. The

supernatant was chromatographed using a Gemini preparatory C18 column and a mobile phase consisting of water with 0.1% FA (solvent A) and MeOH with 0.1% FA (solvent B). The conditions were as follows: a 10-min gradient of 95% to 100% solvent B, followed by a 20-min isocratic gradient of 100% solvent B at a flow rate of 3 mL/min. The only peak with a λ_{max} of 450 nm, characteristic of N-retinylidene-DOPE, was collected into a vial on ice containing 3 mg of $NaBH_4$. Any excess $NaBH_4$ was quenched by 10 μL additions of 1 M ammonium acetate until no further bubbling was observed. The resultant reduced product was concentrated to 0.2 mL under a gentle stream of nitrogen and chromatographed using the same HPLC conditions to purify the dominant peak at 330 nm, which was confirmed to be N-retinyl-DOPE by MS/MS, using CID fragmentation.

Kinetic studies of N-ret-PE formation. In the dark room under dim red light, ROS membranes (2 mg/mL or 50 μM Rho) were prepared as a suspension in 20 mM HEPES-buffered solution at pH 5.6, 7.4, or 8.3. The reaction between all-*trans*-retinal and ROS lipids was initiated upon addition of 2.5 molar equivalents of all-*trans*-retinal relative to the amount of Rho within the ROS. The reaction was performed in an isothermal water bath set to 20 °C. To 1 part ROS membranes, 3 parts saturated solution of $NaBH_4$ granules (about 100 μM) in cold *i*PrOH was added at different time-points after the addition of all-*trans*-retinal. Lipids solubilized by the *i*PrOH were analyzed by analytical reverse-phase HPLC, as described above. The molar quantity of free all-*trans*-retinal (reduced to all-*trans*-retinol) was determined from a standard curve generated with all-*trans*-retinol standard. The molar quantity of N-ret-PE products (reduced to N-retinyl-PE) was determined from a standard curve generated with synthetic N-retinyl-DOPE. The rate of formation of N-ret-PE

was determined by plotting the mole fraction of N-ret-PEs over the total molar amount of free and PE-bound all-*trans*-retinal at each time-point.

Kinetic studies of N-ret-PE formation following Rho* hydrolysis. A suspension of ROS (2 mg/mL or 50 μM Rho) in 20 mM HEPES (pH 7.4) buffered solution was illuminated with 565 nm fiber light for 10 sec at an intensity of 625 μW. The illuminated ROS membranes were incubated in the dark in an isothermal water bath at various temperatures (15, 20, 25, 31, and 37 °C). To 1 part ROS membranes, 3 parts saturated solution of $NaBH_4$ granules (about 100 μM) in cold *i*PrOH was added at different time-points to halt any further Rho* hydrolysis and any further SB condensation reaction between all-*trans*-retinal and PE. Lipids solubilized by the *i*PrOH were analyzed by analytical reverse-phase HPLC to determine the kinetics of N-ret-PE formation as described above. The kinetics of N-ret-PE formation was determined also as described above. The rate of the formation of N-ret-PE was determined by plotting the mole fraction of N-ret-PEs over the total molar amount of free and PE-bound all-*trans*-retinal produced from Rho* hydrolysis at each time-point.

Kinetic studies of Rho* hydrolysis. Aliquots of the same ROS samples treated with $NaBH_4$ in *i*PrOH (described above for tracking N-ret-PEs formed from all-*trans*-retinal released from hydrolyzed Rho*) were used to obtain the protein precipitate, which was digested with pronase to produce N^{ε}-retinyl-Lys as described in methods of Chapter 2. The resultant N^{ε}-retinyl-Lys products were analyzed chromatographically using an Agilent 1260 Infinity HPLC system with a XBridge C18 column and an 18-min gradient of 30% to 39% ACN in water with 0.1% FA at a flow rate of 0.3 mL/min. N^{ε}-retinyl-Lys products were detected by

HPLC absorbance at 330 nm and identities were confirmed by MS/MS as described above. The molar quantity of each isomer of N$^{\varepsilon}$-retinyl-Lys (9-*cis*, 11-*cis*, 13-*cis*, and *all-trans*) was determined based on a standard curve generated using synthetically produced N$^{\varepsilon}$-retinyl-Lys isomers. The mole fraction of opsin-bound retinal (measured as moles of N$^{\varepsilon}$-retinyl-Lys) over the total retinal content (measured as the sum of the moles of N$^{\varepsilon}$-retinyl-Lys and the moles of all-*trans*-retinal produced from Rho* hydrolysis, determined above when analyzing N-ret-PE formation kinetics) was plotted for each time-point, generating a curve which was consistent with pseudo first order decay kinetics. An Arrhenius plot (-ln(k) vs T; equation $k = \mathrm{Ae}^{-\mathrm{E_A/RT}}$; linearized equation $\ln(k) = -\frac{E_A}{RT} + \ln(\mathrm{A})$) was generated based on hydrolysis rate constants (k) determined at each temperature(15, 20, 25, 31, and 37 °C) to yield the $\mathrm{E_A}$ based on the slope of the Arrhenius curve ($m = -\mathrm{E_A/R}$ or $\mathrm{E}_A = -m\mathrm{R}$, where $m =$ slope and $R =$ gas constant).

pH studies of Rho* hydrolysis and subsequent N-ret-PE formation. The same kinetic studies of both reactions as described above were repeated at 20 °C, using buffers adjusted to pH 5.6 and pH 8.3, to obtain rate constants at each pH value.

Rho immunopurification from ROS membranes. Rho was immunopurified in a dark room under dim red light, using immobilized 1D4 antibody as previously described [153]. ROS membranes were solubilized with DDM in 20 mM HEPES at pH 7.4 with 0.15 M NaCl and incubated with Sepharose beads with immobilized 1D4 antibody for 2 hr. The beads were washed with 10 column volumes of wash buffer A (1 mM DDM in 20 mM HEPES pH 7.4, 0.15 M NaCl) to remove unbound protein as well as solubilized lipids. Rho was then eluted

from the beads by adding a 0.5 mM solution of the competing peptide TETSQVAPA (1D4), which was subsequently removed by membrane filtration using a 30 kDa Amicon centrifugal filter. The Rho sample was then concentrated and diluted twice with wash buffer B (0.2 mM DDM, 20 mM HEPES pH 7.4). The final concentration was 2 mg/mL Rho in 20 mM HEPES in roughly 0.5 mM DDM.

Kinetic studies of hydrolysis of detergent-solubilized Rho* and subsequent formation of N-ret-PE. Using immunoaffinity-purified Rho depleted of lipid content and solubilized in DDM detergent, kinetic studies of Rho* hydrolysis and N-ret-PE formation analogous to those described above were conducted at pH 7.4 and 20 °C to obtain rate constants. The rates for detergent-solubilized Rho were compared to those for Rho in ROS membranes.

Quantum chemical calculations. Calculations were performed on a cluster model of the Rho active site that was extracted from the X-ray crystal structure (PDB accession code: 3PQR) [34]. This structure is interpreted to correspond to the MII state. We note that the active site pocket of Rho remains unchanged among various structures reported for all-*trans* Rho. We included all residues within 6 Å of all-*trans*-retinal (Figure 3.8). The free valences were saturated with hydrogen atoms. The active site was filled with an additional eight water molecules that saturate H-donors/acceptors, including Glu residues and the N^{ε} atom of the all-*trans*-retinylidene Schiff base. The size of such a model (ca. 550 atoms) is too large to carry out full quantum chemical (QM) optimizations, so we decided to carry out two-level hybrid QM1-QM2 calculations, where QM1 and QM2 denote high-level and low-

level QM methods, respectively. Accordingly, the positions of the carbonyl carbon atoms of the residues that comprise the active site pocket were frozen. We refer here to Figure 3.8 for the list of QM residues and indices of the fixed atoms. The calculations were carried out within the density functional theory approach (DFT), with the recently developed robust r2SCAN functional and def2-TZVP basis set as the QM1 method and the tight-binding DFT method GFN2-xTB as the QM2 economic method [154-156]. The cluster's environment was simulated with the analytical linearized Poisson-Boltzmann (ALPB) model [157]. Protonation energy **IIc** → **IId** was estimated as the change in energy in the following reaction: **IIc** + $(H_3O^+)(H_2O)_3$ → **IId** + $(H_2O)_4$. Numerical partial Hessian calculations were performed at the QM1 atoms to obtain estimates of the zero-point energies (ZPE) and confirm the nature of the located states. The final values reported throughout the manuscript are ZPE-inclusive. All calculations were performed with the ORCA 5.0.2 program coupled to Grimme's standalone xtb 6.4 code [158, 159]. XYZ coordinates of all structures reported can be accessed free of charge via RepOD repository: https://doi.org/10.18150/9HP0S1

Monitoring all-*trans*-retinal reduction by RDHs using LC-MS. The visual cycle occurring in the outer segment starting from the hydrolytic release of all-*trans*-retinal from Rho* to the formation of N-ret-PEs and ultimate reduction of all-*trans*-retinal by RDHs can be tracked with the use of $NaBD_4$ (Figure 3.2). Treatment of 1 part ROS membranes (2 mg/mL or 50 μM Rho) with 3 parts saturated $NaBD_4$ in cold ethanol (EtOH) effects essentially the same outcomes as with $NaBH_4$ (described above), reducing Rho*-hydrolyzed, Rho*-bound and PE-bound all-*trans*-retinal; however, in this case each species is labeled with a deuterium as shown in Figure 3.2. All-*trans*-retinal reduced by NADPH produces all-*trans*-

retinol, whereas all-*trans*-retinal reduced by $NaBD_4$ produces C^{15}-D^1- all-*trans*-retinol. All-*trans*-retinol and C^{15}-D^1-all-*trans*-retinol can be distinguished by MS and detected by tracking their ESI source-fragmentation retinyl cation products with m/z ratios of 269 and 270, respectively. The percentage of 269 m/z signal intensity was calculated relative to the total signal intensity from the 269 and 270 m/z peaks in each sample and normalized to the natural-abundance percentage of 269 m/z signal in in the C^{15}-D^1-all-*trans*-retinol standards, representing no reduction of all-*trans*-retinal by NADPH and RDHs; or to the natural-abundance percentage of 269 m/z signal in the all-*trans*-retinol standards, representing if reduction of all-*trans*-retinal had gone to completion. Thus, the normalized percentage of 269 m/z signal in a sample indicates the amount of free all-*trans*-retinal reduced by NADPH and RDHs. Any N-ret-PEs observed in ROS membranes were treated as all-*trans*-retinal unreduced by RDHs. RDH activity was thereby captured by tracking both the proportion of all-*trans*-retinal bound as N-ret-PE and the percent of free all-*trans*-retinal reduced by RDHs with NADPH.

In the dark room under dim red light, ROS membranes (2 mg/mL or 50 μM Rho) were prepared in 20 mM HEPES at pH 7.4 with 250 μM dinucleotide, either NADP or NADPH; or 250 μM NaCl, control. Then membranes were illuminated with a 565 nm fiber light at 625 μW for 10 sec followed by incubation at 20 °C. To 1 part ROS membranes, 3 parts saturated solution of $NaBD_4$ in cold EtOH was added at 0, 8, and 16 min after illumination. The extent of Rho* hydrolysis yielding all-*trans*-retinal and the proportion of released all-*trans*-retinal bound to PE were determined as described previously. The extent of subsequent all-*trans*-retinal reduction by RDHs was determined also as described above.

To track RDH activity in the presence of pre-formed N-ret-PE, ROS membranes (2 mg/mL or 50 μM Rho) were prepared in 20 mM HEPES at pH 7.4 and spiked with 4 molar equivalents of all-*trans*-retinal relative to the amount of Rho. After 16 min incubation with all-*trans*-retinal, NADPH was added in excess for a final concentration of 500 μM and mixed by gentle vortex agitation. The reduction was tracked by adding 3 parts saturated solution of $NaBD_4$ in cold EtOH to 1 part ROS membranes at various time-points up to 32 min after addition of NADPH. The extent of all-*trans*-retinal reduced by RDHs was determined also as described above by measuring the proportion of PE-bound all-*trans*-retinal and the proportion of free all-*trans*-retinal reduced by RDHs, as indicated by the percentage of 269 m/z signal.

3.5 Figures

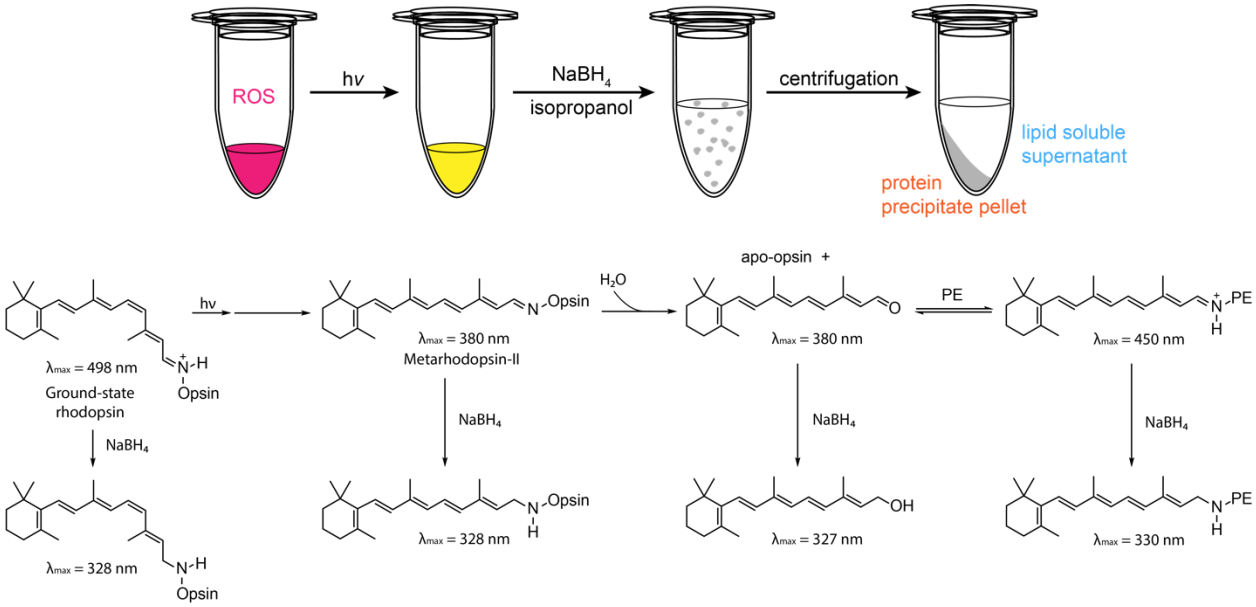

Figure 3.1 Strategy to monitor N-ret-PE formation following hydrolytic release of all-*trans*-retinal from Rho*. The addition of $NaBH_4$/*i*PrOH reduces retinal and its Schiff base to halt Schiff base hydrolysis and condensation chemistry to capture the amounts of each species, whether ground-state Rho, Rho*-MII, all-*trans*-retinal from Rho* hydrolysis, or N-ret-PE. N^{ε}-retinyl-opsin, produced by $NaBH_4$ reduction of either Rho or Rho*, resides in the protein pellet, which can be proteolyzed by pronase and analyzed by LC-MS/MS. The amount of Rho or Rho* can be determined by intensity of their N^{ε}-retinyl-Lys signal. The amount of all-*trans*-retinal or N-ret-PE can be determined by LC-MS/MS analysis *via* quantification of their $NaBH_4$ reduction products, all-*trans*-retinol or N-retinyl-PE, respectively. Therefore, all stages of the chromophore can be tracked from its residence within Rho to the formation adducts with PE.

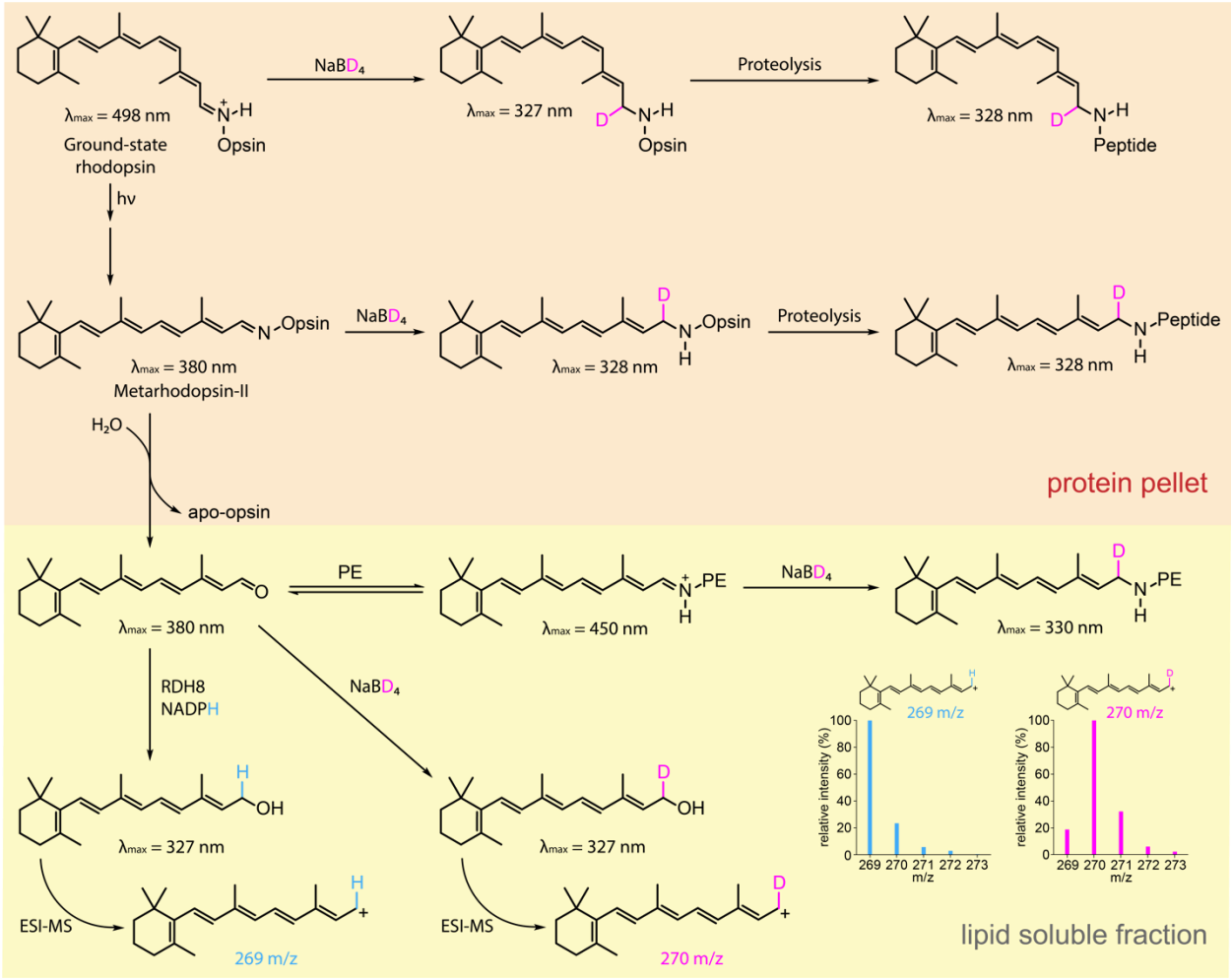

Figure 3.2 Strategy using $NaBD_4$ to monitor NADPH reduction by RDHs after Rho photoactivation. $NaBD_4$ mimics $NaBH_4$ in reducing Rho*-bound, PE-bound, and free all-*trans*-retinal, with the only difference being the labeling all species with a deuterium. Reduction of all-*trans*-retinal by NADPH and RDHs prior to $NaBD_4$ addition would produce non-deuterated all-*trans*-retinol. The all-*trans*-retinol and C^{15}-D^1-all-*trans*-retinol can be detected by their ESI source-fragmentation retinyl-cation products. The ratio of all-*trans*-retinol to C^{15}-D^1-all-*trans*-retinol can be tracked, as well as the N-C^{15}-D^1-retinyl-PEs, to assess RDH activity on all-*trans*-retinal produced from Rho* hydrolysis. Following LC-MS/MS analysis of the lipid-soluble fraction as described, Rho* hydrolysis kinetics could

also be tracked by proteolysis and LC-MS/MS analysis of the protein pellet as described previously.

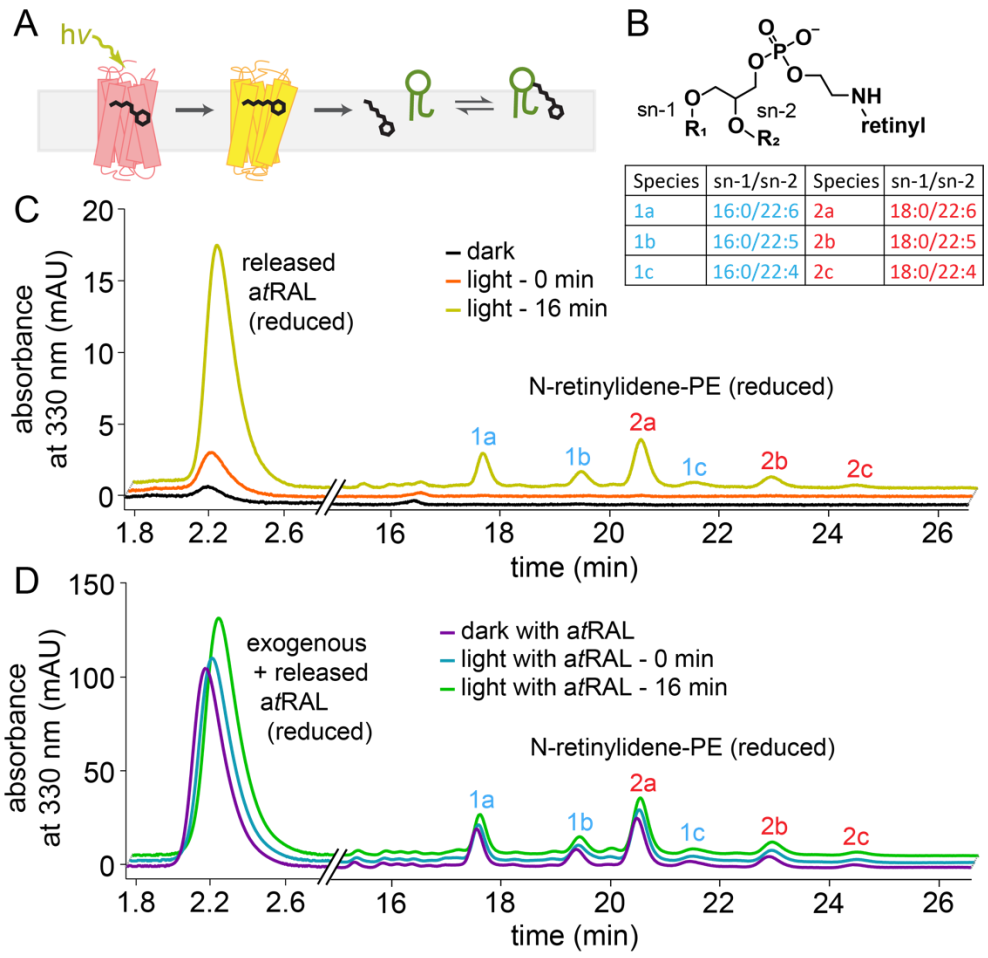

Species	sn-1/sn-2	Species	sn-1/sn-2
1a	16:0/22:6	2a	18:0/22:6
1b	16:0/22:5	2b	18:0/22:5
1c	16:0/22:4	2c	18:0/22:4

Figure 3.3 Formation of N-ret-PE in native membranes after light exposure. (A) Diagram of N-ret-PE formation after illumination of ROS membranes. (B) Chemical structure of N-ret-PE, with a table of major species found in the ROS membranes. (C) Chromatogram of all-*trans*-retinal released and resultant N-ret-PE in ROS at 0 and 16 min after illumination for 10 s with 565 nm fiber light at 625 µW. (D) Analogous experiment to that in panel C, but with exogenous all-*trans*-retinal added to the ROS membrane suspension prior to illumination. mAU, milli absorbance unit.

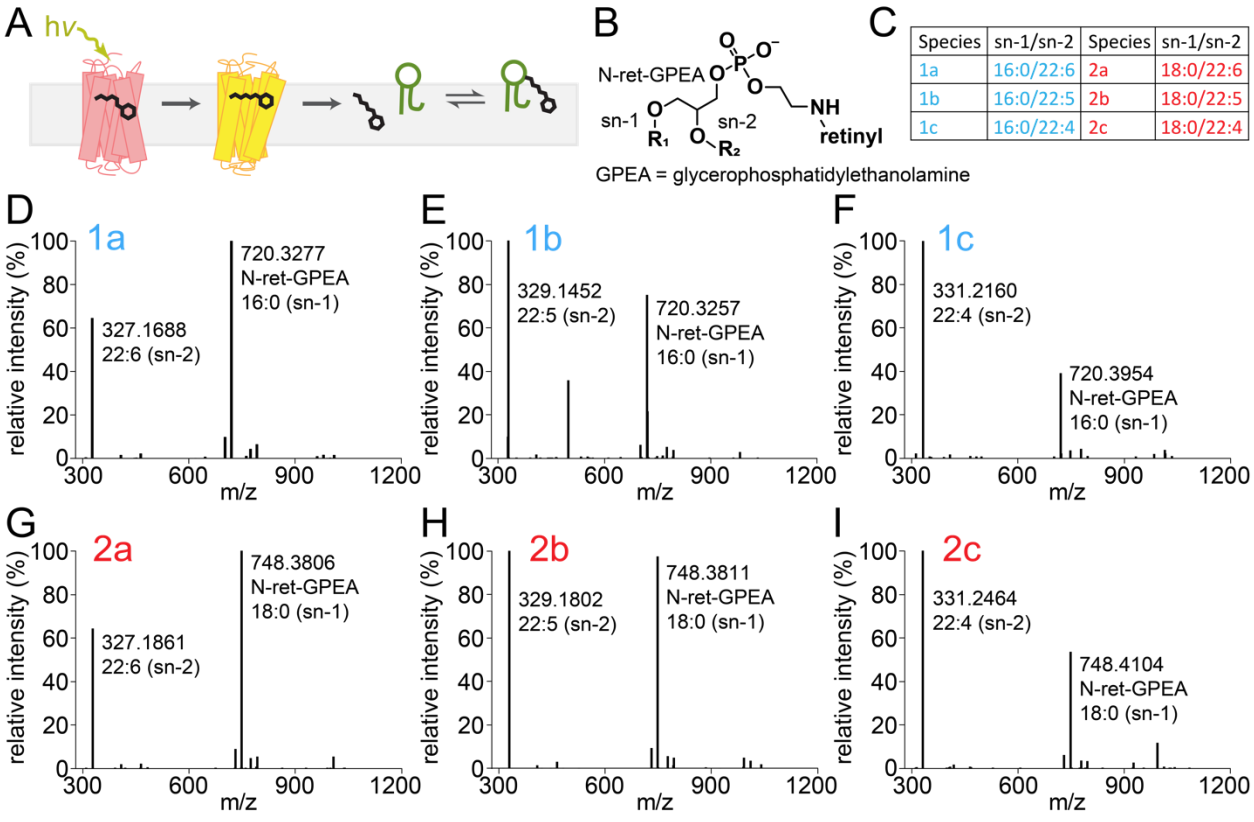

Species	sn-1/sn-2	Species	sn-1/sn-2
1a	16:0/22:6	2a	18:0/22:6
1b	16:0/22:5	2b	18:0/22:5
1c	16:0/22:4	2c	18:0/22:4

Figure 3.4 CID-MS^2 identification of N-ret-PE species. (A) Diagram of N-ret-PE formation after illumination of ROS membranes. (B) Chemical structure of N-ret-PEs. (C) Table of major N-ret-PE species found in the ROS membranes. (D-I) CID-MS^2 spectrum of each N-ret-PE with cleavage at the sn-2 position of the polyunsaturated acyl chain, using normalized collision energy of 35 eV.

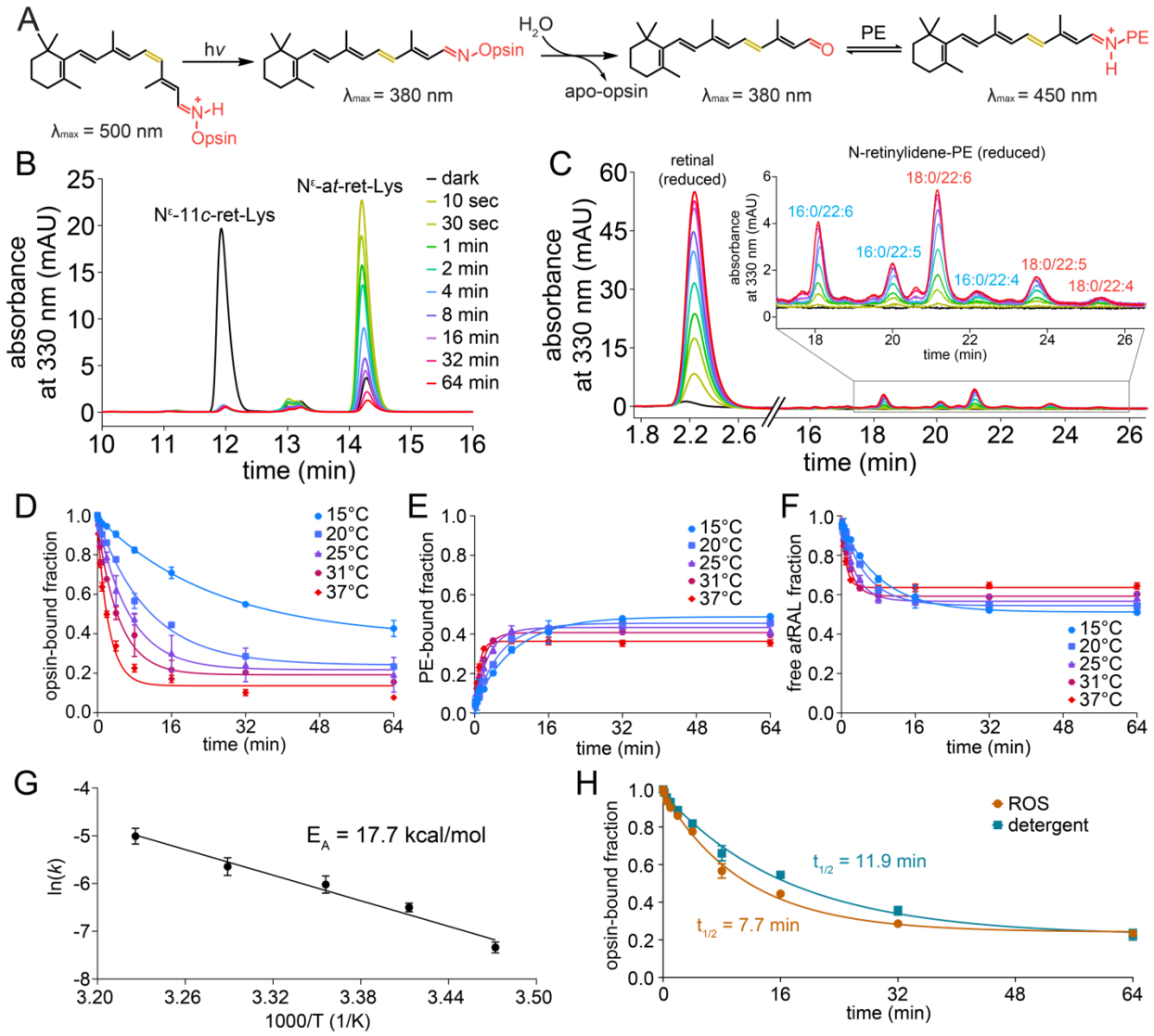

Figure 3.5 Temperature dependence of Rho* hydrolysis and subsequent N-ret-PE formation. (A) Scheme of hydrolysis reaction following light exposure. (B) Chromatograms of pronase digests of Rho* protein pellets obtained from ROS membranes treated with $NaBH_4$/*i*PrOH after brief light exposure (565 nm fiber light at 625 µW for 10 s) and subsequent incubation in the dark for different periods of time at 37 °C. (C) Chromatograms of the *i*PrOH-solubilized lipid fractions from the corresponding samples from panel B for detection of $NaBH_4$-reduced free and PE-bound all-*trans*-retinal from Rho* hydrolysis at 37°C. (D) Rho* hydrolysis exhibited pseudo first-order decay kinetics at

various temperatures. (E) The formation of N-ret-PEs at different temperatures from all-*trans*-retinal produced by Rho* hydrolysis followed pseudo first-order kinetics. (F) The proportion of the all-*trans*-retinal from Rho* hydrolysis that was unbound to PE tracked inversely to the proportion that formed PE adducts. (G) The Arrhenius plot of hydrolysis rate constants at different temperatures yielded an E_A of 17.7 kcal/mol. (H) Rho* hydrolysis was faster in ROS membranes than in DDM detergent micelles at 20 °C. mAU, milli absorbance unit.

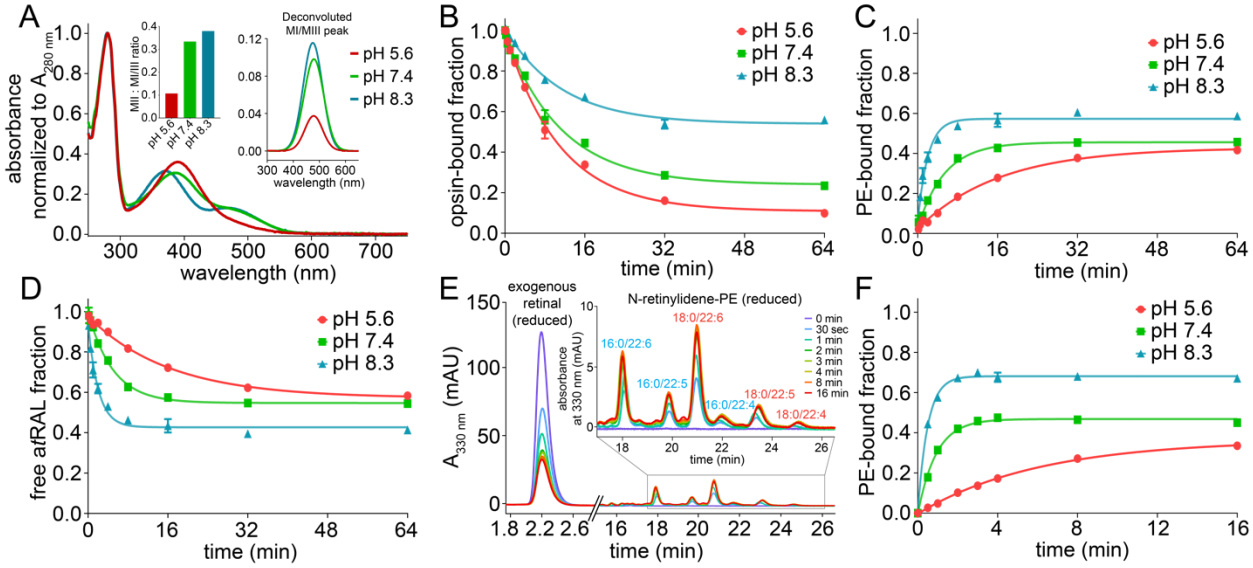

Figure 3.6 pH-dependent Rho* hydrolysis and N-ret-PE formation in native membranes. (A) UV-Vis spectrum of Rho after illumination with a 565 nm fiber light at 625 µW for 10 s and incubation for 12 h at 4 °C. Spectral analysis and deconvolution of the protonated retinylidene Schiff base absorbance peak demonstrated inverse pH dependency, with a greater proportion of protonated Schiff base (MI/III) appearing with increasing pH. (B) Rho* Schiff base hydrolysis at 20 °C occurred to the greatest extent at lower pH in which the MI-MII equilibrium shifts toward MII. (C) The rate of N-ret-PE

formation at 20°C also exhibited pH dependency and was fastest at high pH. (D) The proportion of released all-*trans*-retinal that did not form PE adducts tracked inversely to the proportion that formed PE adducts. (E) Chromatographic traces of N-ret-PE formation over time at pH 8.3 and 20°C, after addition of exogenous all-*trans*-retinal to ROS membranes. (F) The mole fraction of N-ret-PE formed at 20°C from exogenous all-*trans*-retinal over time exhibited pseudo first-order kinetics, with faster rates and higher steady state levels as pH increased. mAU, milli absorbance unit.

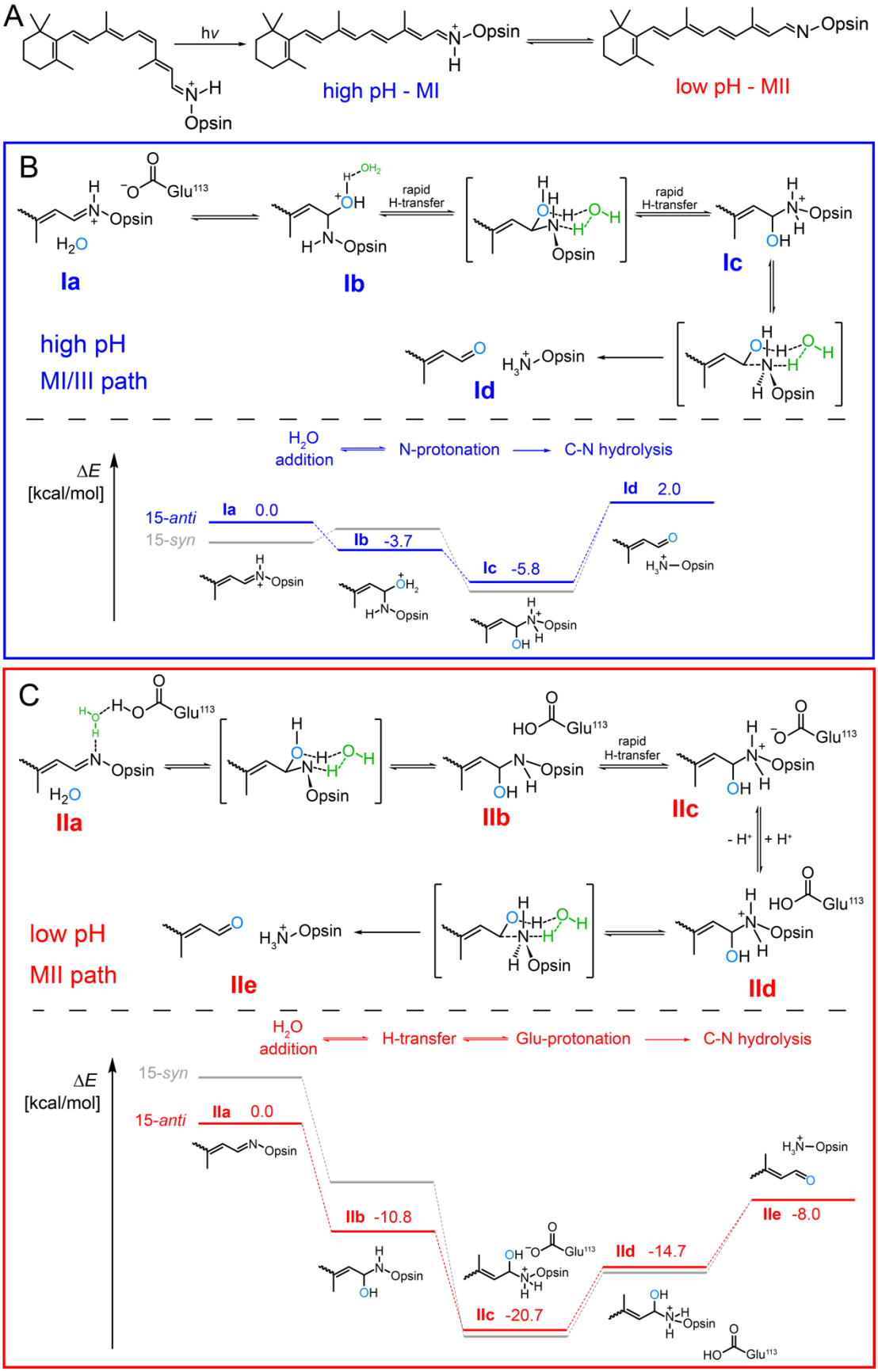
A
hν
Opsin
high pH - MI
low pH - MII
B
Glu113
Opsin
H2O
Ia
Ib
rapid
H-transfer
rapid
H-transfer
Ic
high pH
MI/III path
Id
H3N
Opsin
H2O
addition
N-protonation
C-N hydrolysis
ΔE
[kcal/mol]
15-anti
15-syn
Ia 0.0
Ib -3.7
Ic -5.8
Id 2.0
C
IIa
IIb
IIc
rapid
H-transfer
- H+
+ H+
low pH
MII path
IIe
IId
H2O
addition
H-transfer
Glu-protonation
C-N hydrolysis
ΔE
[kcal/mol]
15-syn
15-anti
IIa 0.0
IIb -10.8
IIc -20.7
IId -14.7
IIe -8.0

Figure 3.7 Energy landscape of the hydrolysis of all-*trans*-retinylidene Schiff base of different metarhodopsin species. (A) Rho photoisomerization to Rho*, which is in pH-dependent equilibrium of metarhodopsin states. (B and C) Highlighted in blue is panel B (high pH, MI/III path) and in red is panel C (low pH, MII path). The energy landscapes were computationally determined for both paths in the hydrolysis of either 15-*anti* or 15-*syn* configurations of protonated (MI/MIII path) or deprotonated (MII path) all-*trans*-retinylidene Schiff base. The numbers reported are relative energies with respect to the initial states Ia or IIa. Energy levels for the 15-*syn* configuration are shown in gray for reference.

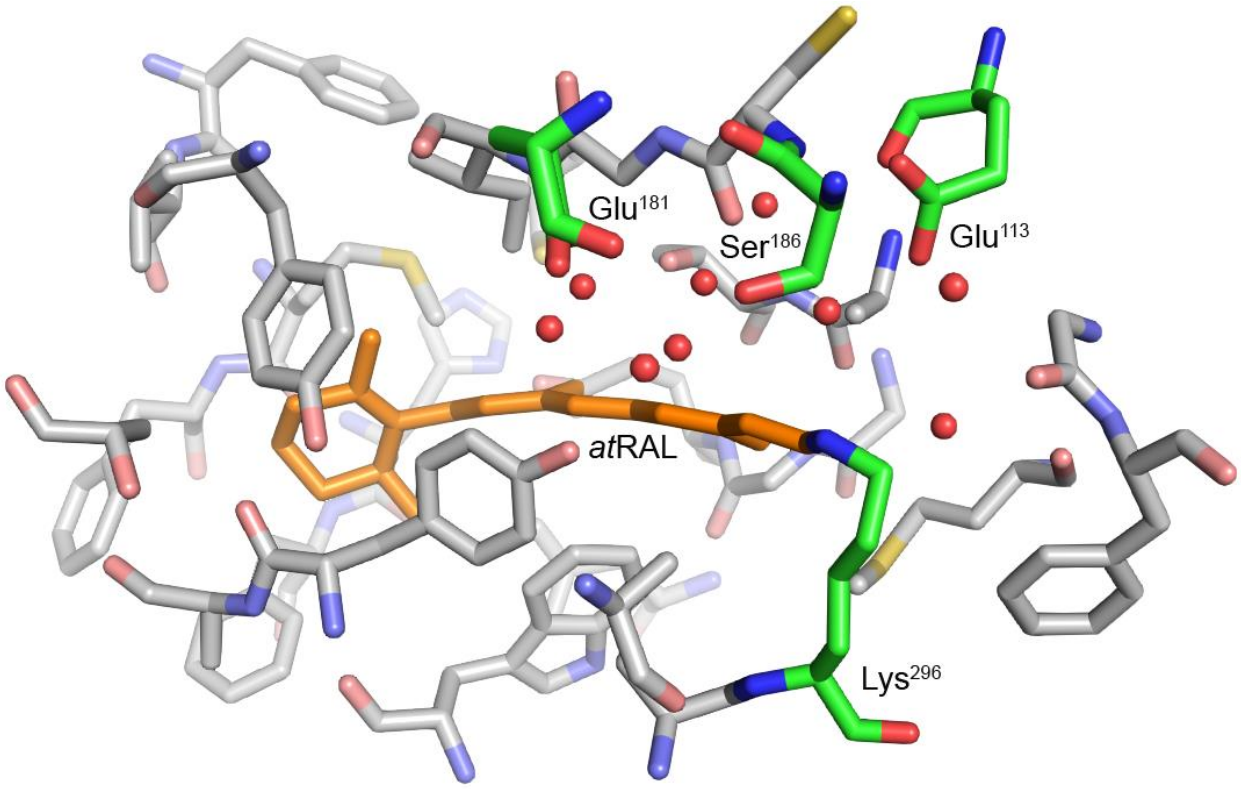

Figure 3.8 Molecular model used in quantum mechanical calculations. IIa structure and hydrogen atoms were omitted for clarity. Carbon atoms of the high-level QM1 region

are highlighted in orange (all-*trans*-retinal) and green (Glu^{113}, Glu^{181}, Ser^{186}, Lys^{296}). The region contains additionally nine water molecules (shown in red). Active site pocket (QM2) region includes the following residues: Met^{86}, Gly^{90}, Phe^{91}, Ala^{117}, Thr^{118}, Gly^{120}, Gly^{121}, Glu^{122}, Leu^{125}, Cys^{167}, Cys^{187}, Gly^{188}, Ile^{189}, Tyr^{191}, Phe^{203}, Val^{204}, Met^{207}, Phe^{208}, His^{211}, Phe^{212}, Trp^{265}, Tyr^{268}, Ala^{269}, Ala^{272}, Ala^{292}, Ala^{295}. The following atoms were kept frozen in the final H-saturated cluster: 3, 12, 21, 27, 193, 205, 217, 228, 235, 233, 264, 144, 149, 254, 181, 164, 173, 275, 168, 156, 316, 197, 129, 133, 121, 125, 239, 184, 289, 301, 306.

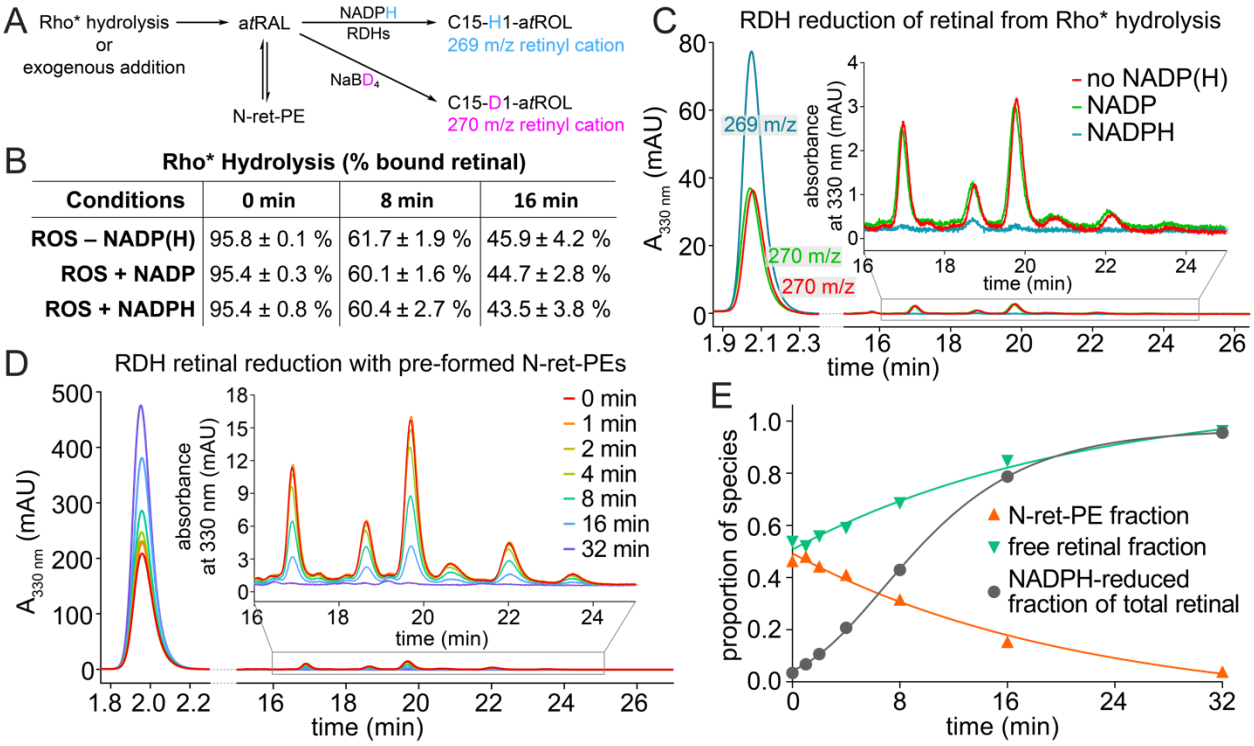

Figure 3.9 Reduction of all-*trans*-retinal by RDHs in native membranes. (A) Simplified diagram from Figure 3.2 depicting $NaBD_4$-based monitoring of RDH activity by tracking NADPH-reduced vs. $NaBD_4$-reduced retinal. (B) In ROS membranes, Rho* hydrolysis at pH 7.4 and 20 °C is unaffected by addition of dinucleotides, NADP or NADPH. (C) At 16 min of

Rho* hydrolysis, the released all-*trans*-retinal was reduced by RDHs in the presence of NADPH, substantially attenuating the formation of N-ret-PEs. (D) In the presence of both free all-*trans*-retinal and N-ret-PEs in equilibrium at pH 7.4 and 20 °C following addition of exogenous all-*trans*-retinal to ROS, RDH activity was initiated upon addition of NADPH. The NADPH-reduced all-*trans*-retinal and $NaBD_4$-reduced free and PE-bound all-*trans*-retinal were monitored over time by LC-MS. (E) In samples corresponding to those of panel D, the fraction of NADPH-reduced all-*trans*-retinal followed sigmoidal growth kinetics, with the concurrent reduction of the initially available free all-*trans*-retinal and the all-*trans*-retinal gradually supplied from the equilibrium with N-ret-PE, as demonstrated by the gradual decline of N-ret-PEs over time. mAU, milli absorbance unit

CHAPTER 4

Characterization of retinylidene photochemistry and hydrolysis in visual and non-visual opsins by LC-MS/MS

This chapter is derived from the manuscript published in *Journal of Biological Chemistry*:
Hong JD, Salom D, Choi EH, Tworak A, Smidak R, Gao F, Solano YJ, Zhang J, Kiser PD, Palczewski K. Retinylidene chromophore hydrolysis from mammalian visual and non-visual opsins. ***Journal of Biological Chemistry***. 2024 Jan 23:105678. doi: 10.1016/j.jbc.2024.105678. PMID: 38272218

The photochemistry and hydrolysis kinetics of the retinylidene adduct of RGR was derived from contributions as co-author of manuscript published in *Cell Reports*:
Tworak A*, Kolesnikov AV, **Hong JD**, Choi EH, Luu J, Palczewska G, Dong Z, Lewandowski D, Brooks MJ, Campello L, Swaroop A, Kiser PD, Kefalov VJ, Palczewski K*. Rapid RGR-dependent visual pigment recycling is mediated by the RPE and specialized Muller Glia. ***Cell Reports***. 2023 Aug 29;42(8):112982. doi: 10.1016/j.celrep.2023.112982. PMID: 37585292

4.1 Introduction and Significance

Vision begins with the photochemistry of the opsin-chromophore pigment complexes that reside in the photoreceptor outer segments. Incident light induces photoisomerization of the adducted 11-*cis*-retinylidene chromophore to produce the all-*trans*-retinylidene agonist. Photoproduction of the agonist immediately leads to conformational changes in opsin, which converts to its photoactivated signaling state and initiates the phototransduction cascade.[39, 160] The subsequent hydrolysis of the Schiff-base-bound all-*trans* agonist leads to its release from opsin as all-*trans*-retinal.[88] This bleachable property of these pigments is characteristic of Rho and cone opsins responsible for vertebrate vision. The process of photoisomerization and hydrolysis (bleaching) supplies all-*trans*-retinal to the visual cycle to be recycled to 11-*cis*-retinal to maintain the photocycle of the opsins.[161] Notably, cone opsins have been understood to bleach significantly faster than Rho, based on indirect spectroscopic and electrophysiological measurements.[80, 162, 163] However, there has yet to be any direct measurements of the bleaching rate of cone pigments, as has been done recently for Rho.[44, 84] Their faster bleaching rate suggests a faster photocycle and consumption of 11-*cis*-retinal.

11-*cis*-retinal is recycled from all-*trans*-retinal either by a light-dependent process through retinal G protein-coupled receptor (RGR) or by the light-independent classical visual cycle.[99, 112] The rate of 11-*cis*-retinal production of the classical visual cycle is demonstrably slow with full dark adaptation requiring up to 40 min in humans and 2-4 h in mice.[99, 164-166] Under bright daylight conditions stimulating photopic or color vision, the classical visual cycle alone would likely be inadequate to meet the demands for 11-*cis*-retinal by cone opsin to sustain vision. This demand is understood to be supported by RGR,

engaging in *trans*-*cis* photochemistry to directly convert all-*trans*-retinal into 11-*cis*-retinal. As such, the very conditions that bleach cone opsins would also support their regeneration *via* RGR. However, RGR is also understood to be a bistable opsin, therefore engaging in persistent photoisomerization alternating between the all-*trans*-retinylidene adduct and its 11-*cis* configuration without hydrolysis to release 11-*cis*-retinal.[167] As a bistable opsin, RGR would be unable to participate in the production of 11-*cis*-retinal for visual pigment regeneration. However, the photochemistry of RGR and its apparent bistability were observed with recombinant RGR reconstituted and purified in detergent micelles. As shown by our prior study, detergents greatly impair hydrolysis[44]; therefore, RGR should be studied in its native environment in its specialized subcellular compartment of microsomes within RPE cells.

Notably, the photoisomerization of the 11-*cis*- to all-*trans*-retinylidene is far more common among vertebrate opsins as compared to the *trans*-*cis* isomerization exhibited by RGR. Like RGR, vertebrate RRH also resides in the RPE, specifically in the apical surface.[168] RRH was also reported to be potentially capable of the *trans*-*cis* isomerization; however, its pigment formation and isomerization has yet to be characterized, since most studies have focused on an invertebrate homolog.[169, 170] Given the presence of an internal Lys residue within the putative chromophore binding pocket of vertebrate RRH, such as bovine RRH (bRRH), there remains a strong possibility of its ability to form pigment and engage in the purported *trans*-*cis* photochemistry.

Previously, photoisomerization of the 11-*cis*-retinylidene chromophore of Rho to the all-*trans*-retinylidene agonist was captured in membrane preparations of ROS and in detergent micelle using liquid chromatography with tandem mass spectrometry (LC-

MS/MS).[44] The same analytical procedure tracked the hydrolytic release of the Schiff-base-bound agonist from Rho in either milieu. Sample preparation using $NaBH_4$ in isopropanol ($NaBH_4$/*i*PrOH) facilitated the reductive trapping of the opsin-bound chromophore and isolation of the opsin protein *via* precipitation; then, proteolysis and LC-MS/MS analysis identified and quantified the products, as illustrated schematically in Figure 2.14. The photoisomerization reaction of any opsin that forms pigment, as well as the hydrolytic release of the Schiff-base-bound photoproduct of the chromophore, can be studied *via* this technique.

Our current study aimed to directly measure the relative bleaching rate of cone opsins compared to Rho, utilizing our LC-MS/MS based methods. Here, these same approaches are applied to bovine RGR (bRGR) to definitively characterize the *trans*-*cis* photochemistry occurring at the internal Lys of its putative chromophore binding pocket, as well as the potential hydrolytic release of 11-*cis*-retinal. Furthermore, bRRH was investigated for whether it behaves similarly to bRGR.

4.2 Results

4.2.1 Proteolysis of borohydride-reduced visual pigments and LC-MS/MS analysis of resultant N^{ε}-retinyl-peptides

The principal visual pigments, namely rhodopsin and the cone opsins, were obtained from bovine ROS (bROS) and from recombinant expression, respectively. Pigment formation with each visual opsin was confirmed by UV-Vis absorbance spectroscopy, showing each opsin with the expected absorbance spectrum and absorption maximum (Figure 4.1A-D). Each opsin also exhibited the expected absorbance spectral change upon

light exposure with the shift in absorption maximum to 380 nm (Figure 4.2E-H), given that both the meta-II signaling state and the hydrolytically released all-*trans*-retinal has an absorption maximum at 380 nm. Following treatment with $NaBH_4$/*i*PrOH, each opsin was proteolyzed by proteinase K to produce N^{ε}-retinyl-peptides. Subsequent LC-MS/MS analyses confirmed the location of the chromophore bound to the expected internal Lys-residue within the chromophore-binding pocket of the respective opsins (Figure 4.1I-L, and Appendix A, Figures S1-S5).

The procedure was repeated using $NaBD_4$ in place of $NaBH_4$, which verified the reductive trapping of the chromophore-Schiff base-attachment by deuterium labeling of the C^{15} position of the resultant retinyl group, consequently in secondary amine linkage to opsin (Appendix A, Figures S1-S5). Use of $NaBD_4$ for reductive trapping of chromophore and LC-MS/MS analysis of the proteolysis products also later confirmed the characteristic fragmentation pattern of retinyl-peptides into a product retinyl cation and a product free peptide ion, which can be sequenced by CID fragmentation. For $NaBH_4$, the retinyl cation had an expected m/z of 269, while the $NaBD_4$ treatment resulted in a retinyl cation with an expected m/z of 270.

The use of pronase in place of proteinase K allowed for complete proteolysis and detection of relevant isomers (11-*cis* or all-*trans*) of N^{ε}-retinyl-Lys. For pigments treated with $NaBH_4$ or $NaBD_4$ in the dark, the resultant N^{ε}-retinyl-Lys was predominantly in the 11-*cis* configuration; however, upon brief illumination of pigments, the 11-*cis* peak decreased with emergence of a dominant all-*trans* peak (Figure 4.2A-D, and Appendix A, Figures S6-S10). Although UV-Vis spectroscopy also detected this *cis*-*trans* photochemistry with the shift in absorbance spectrum of each pigment to the spectrum of the photoactivated state

(λ_{max} = 380 nm), subsequent Schiff-base hydrolysis of the all-*trans* agonist cannot be properly resolved due to the overlapping spectrums of photoactivated opsin and all-*trans*-retinal, each with λ_{max} = 380 nm. Since LC-MS/MS of the pronase proteolysis detects presence of retinylidene adduct as N^{ε}-retinyl-Lys, the extent of Schiff-base hydrolysis of the all-*trans* agonist in photoactivated cone opsins and rhodopsin can be compared. During the brief illumination of cone opsins, most of the N^{ε}-all-*trans*-retinyl-Lys peak had already disappeared, with only 3-5% bound agonist remaining in photoactivated cone opsins, in contrast to the 95% remaining in photoactivated rhodopsin at 20°C (Figure 4.2).

4.2.2 Proteolysis and LC-MS/MS analysis of bRGR photoisomerization reaction and production of 11-*cis*-retinal

The photic recycling of all-*trans*-retinal to 11-*cis*-retinal is facilitated by bRGR in two steps: photoisomerization of the all-*trans*-retinylidene adduct to the 11-*cis* adduct, which then must be hydrolyzed to release 11-*cis*-retinal for regeneration of visual opsin pigments (Figure 4.3A). For a better understanding of purified bRGR, a mammalian cell line was establishing in HEK293S GnTI^{-} with stable expression of bRGR C-terminally tagged with 1D4 peptide for eventual immunopurification (Appendix A, Figure S11). The recombinantly produced bRGR adducted with all-*trans*-retinal was immunopurified in LMNG micelles for measurement of the bRGR. UV-Vis absorbance spectrum (Figure 4.3B, and Appendix A, Figures S12-S13). The site of chromophore attachment to Lys^{256} in bRGR was verified by $NaBH_4/D_4$ treatment followed by proteolysis by proteinase K and LC-MS/MS analyses (Appendix A, Figure S12). Following brief illumination, changes in the UV-Vis absorbance spectrum were found to be minor (Figure 4.3B-C) and were unable to clearly depict that

photoisomerization of the all-*trans*-retinylidene adduct to the 11-*cis*-configuration had occurred. The photoisomerization reaction of bRGR was captured by LC-MS/MS of the pronase digestion of bRGR before and after light exposure, treated with $NaBH_4/D_4$ (Appendix A, Figure S13).

In parallel to the photoisomerization detailed for the recombinant bRGR, the photoisomerization reaction of native bRGR in isolated bRPE microsomal membranes was also investigated. Microsomal bRGR reconstituted with slight excess of all-*trans*-retinal was analyzed by LC-MS/MS after $NaBH_4$ treatment and proteinase K digestion. The resultant N^{ε}-retinyl-peptides were determined to be from bRGR with Lys^{256} as the site of chromophore attachment. The *trans-cis* photoisomerization reaction of bRGR within the complex environment of bRPE microsomes was validated by LC-MS/MS analysis of the proteinase K (Figure 4.3D) and pronase digests (Figure 4.3E), before and after exposure of the all-*trans*-retinal-treated microsomes to light. The hydrolytic production of 11-*cis*-retinal by bRGR in native membranes was demonstrably rapid (Figure 4.3D-G) with a half-life of around 7.7 sec, nearly 60 times faster than the hydrolytic release of all-*trans*-retinal by Rho* in ROS membranes. Our LC-MS/MS based assay for bRGR* hydrolysis in RPE microsomal membrane demonstrated similar findings with a half-life of around 7.5 sec in the first ever demonstration of bRGR monostability in the study by Tworak et.al.[171] However, this hydrolysis rate was dramatically slowed by nearly six-fold for bRGR depleted of cell membrane lipids *via* immunopurification in detergent micelles (Figure 4.3 G-I), as performed in previous studies of bRGR biochemistry.[167] Notably, as 11-*cis*-retinal was rapidly hydrolytically released, the resultant apo-bRGR also quickly formed pigment with available all-*trans*-retinal (Figure 4.3E-I). Overall, our findings highlights the rapid photic

processing of all-*trans*-retinal to 11-*cis*-retinal performed by bRGR, demonstrating its important physiological role in the light-driven alternative visual cycle that supplements the light-independent classical visual cycle.

4.2.3 Thermostability study of bRho and bRGR

Prior studies on the thermostability of bRho in detergent micelles showed thermal isomerization and release of chromophore at 60 °C.[172-174] However, our results demonstrated that bRho pigment was still very stable at 60 °C if retained in native membranes (Figure 4.4A). The melting temperature (T_m) of bRho was 67 °C in bROS membranes as compared to 56 °C in detergent micelles depleted of membrane lipids (Figure 4.4A). Similar findings of higher thermostability in native membranes was observed for bRGR pigment. The T_m of bRGR pigment was 66 °C in bRPE microsomal membranes as compared to 62 °C in detergent micelles depleted of membrane lipids (Figure 4.4B). Altogether, these results indicate a common effect of lipids in stabilizing visual-associated opsins, and highlight the importance of studying membrane proteins in their native lipid environments rather than solubilized and purified in detergent micelles as is typically done.

4.2.4 Mammalian RRH is a non-pigment forming opsin

Prior work with invertebrate RRH suggested a role similar to RGR in the photic production of 11-*cis*-retinal from all-*trans*-retinal.[169, 170] Therefore, this potential analogous role was explored with mammalian RRH, testing bRRH in the same manner as for bRGR (above). As shown in **Table 4.1**, prior single-cell RNA-sequencing data for human, mouse,

and bovine RPE cells revealed a similar pattern of expressions of visual cycle elements.[112, 175-177] The expression of bRRH appears to be significantly lower than other elements in the RPE, except for mouse RPE where the expression of RRH is significantly higher compared to human or bovine RPE, aligning with prior studies investigating the presence of mouse RRH in the RPE apical surface.[168, 178]

Given the low abundance of bRRH from native bRPE sources (Table 4.1), a mammalian cell line was established in HEK293S GnTI$^-$ with stable expression of bRRH (Appendix A, Figure S16). GFP was localized to the cytoplasm, whereas ID4 tagged bRRH was present in the plasma membranes. Membrane isolates of bRRH were treated with different retinal isomers and subsequently immunopurified in LMNG detergent for facile UV/Vis spectroscopic detection of any potential bRRH pigments. However, the absorbance spectra of bRRH treated with each retinal isomer showed negligible difference from that of bRRH treated with vehicle (Figure 4.5A), suggesting a lack of pigment formation. Subsequent $NaBH_4$/*i*PrOH treatment and proteolysis by either proteinase K or pronase was performed for LC-MS/MS detection of any N^{ε}-retinyl-peptides or N^{ε}-retinyl-Lys, respectively, to capture any binding that was not detected by UV-Vis spectral measurements. However, LC-MS/MS analysis revealed no N^{ε}-retinyl-peptides or N^{ε}-retinyl-Lys, further supporting the lack of pigment formation with retinal in bRRH (Figure 4.5B).

The same LC-MS/MS analyses were performed for bRRH kept in membrane isolates, unperturbed by the addition of LMNG detergent and depletion of membrane lipids. Membrane isolates of HEK293S GnTI$^-$ with and without stable expression of bRRH were treated with different isomers of retinal. LC-MS/MS analyses displayed non-specific binding with negligible levels of N^{ε}-retinyl-peptides or N^{ε}-retinyl-Lys near baseline levels

from membrane isolates of HEK293S cells either with or without bRRH expression (Figure 4.5C-D). Thus far, no studies have conclusively demonstrated pigment formation with mammalian RRH. Based on our results, its role in the photoconversion of retinal in vertebrate systems remains unclear.

For a better understanding of bRRH, a comparative structural study was performed by overlaying the predicted AlphaFold structure of bRRH with the crystal structures of bRho, its photoactivated state, and apo-opsin (Figure 4.6). From the structural alignment with bRho and its photoactivated state, bRRH appears to have a binding pocket with sufficient space to fit either 11-*cis*-retinal or all-*trans*-retinal. Given that the 3D model was calculated using bRRH devoid of ligand, the same structural alignments were performed for apo-opsin, which resulted in a better fitting for all-*trans*-retinal than for 11-*cis*-retinal (Figure 4.6).

The observation that bRRH has ample space to bind retinoids, an internal Lys residue (K284) within the putative chromophore-binding domain and an available counterion (D169) for a protonated Schiff base contrasts with our results showing lack of pigment formation with any of retinal isomers. One possible explanation would involve the presence of bulk water that could participate in the destabilization and hydrolysis of any retinylidene Schiff base that could form within bRRH, similarly to the role of bulk water in Rho* [46, 69]. To explore this possibility, the binding pocket of bRRH was compared to that of invertebrate (*Hasarius adansoni*) RRH (HaRRH), known to form stable pigment with bistable retinylidene photochemistry. The comparison demonstrated that a wider binding pocket of bRRH that is more accessible to bulk water as compared to HaRRH, whose binding is closed off from the external environment (Figure 4.7).

Overall, given the findings from the comparative structural study and our LC-MS/MS analysis of proteolyzed bRRH treated with various isomers of retinal, the role of RRH in retinylidene photoisomerization in vertebrate systems remains largely unclear. These negative results of RRH contrast with the positive identification of Schiff base formation in the case of bRGR and the three cone opsins. Since the experiments for the four heterologously expressed opsins (cone opsins and RGR) were done in similar conditions, the existence of a systematic artifact of our methodology for the case of bRRH appeared unlikely.

4.3 Discussion

Hydrolysis of all-*trans* agonist from photoactivated rhodopsin and cone opsins bridges two crucial cycles that are responsible for continuous vision: the classical visual cycle and the opsin photocycle. The chromophore release has been thoroughly studied with rhodopsin but not nearly as rigorously explored in cone opsins, which are crucial for our daylight vision. Cone opsins are underexplored for several reasons, including the lack of adequate and available mammalian sources rich in cone opsins and difficulties with heterologous expression.[179, 180] All-*trans* agonist hydrolysis from photoactivated cone opsin has largely been investigated indirectly using UV-Vis or fluorescence spectroscopy and electrophysiology.[80, 162, 163]

As shown by the current study, our LC-MS/MS-based method of direct monitoring of the retinylidene covalent linkage allowed the characterization of agonist hydrolysis in photoactivated cone opsins.Our findings that photoactivated cone opsins hydrolyze their agonist much more rapidly than photoactivated rhodopsin aligns with previous spectral

and electrophysiological findings. The much quicker release of all-*trans*-retinal indicates a faster photocycle or rates of hydrolysis and regeneration for cone opsins than for rhodopsin. Indeed, in prior biochemical experiments using absorbance spectroscopy, the decay of photoactivated cone pigment takes seconds, whereas minutes for rhodopsin.[181] In electrophysiological studies by Hecht, full cone dark adaptation occurs around 10 times faster than full rod dark adaptation, requiring over 30 min.[99] Furthermore, rods saturate under dim light conditions, while cones can continue to be responsive under very bright light conditions, suggesting an alternative rapid supply of 11-*cis*-retinal to cones mediated by light.[182-184] This alternative pathway of chromophore production by light was recently shown to be facilitated by RGR.[171]

RGR in native RPE microsomal membranes demonstrated rapid photic processing all-*trans*-retinal into 11-*cis*-retinal. Following the photoconversion of the all-*trans*-retinylidene adduct, the 11-*cis* product is quickly hydrolyzed and all-*trans*-retinal is subsequently taken up promptly from the milieu. As such, under constant daylight illumination of the retina, RGR can plausibly serve to rapidly turnover all-*trans*-retinal to meet the demands for 11-*cis*-retinal by the cones. This role of RGR has recently been elucidated *in vivo* by co-authored electrophysiological study, investigating cone function with a mouse model designed to conditionally activate RGR expression.[171] These observations overall indicate RGR to be a monostable non-visual opsin with *trans*-*cis* photoisomerization activity. Recent studies have suggested the bistability of RGR [167], which is a plausible interpretation under the conditions used (RGR in detergent micelles). Considering our findings that the hydrolysis of the 11-*cis*-retinylidene adduct is much slower in RGR immunopurified in detergent micelles as compared to native microsomal

membranes, the delayed hydrolysis rate in detergent would allow time for another photoisomerization event, thereby conferring an apparent bistable nature.

The effect of detergent micelles to delay hydrolysis of the photoisomerized retinylidene products in opsin proteins was previously observed for photoactivated rhodopsin.[44] The hydrolysis of rhodopsin and RGR photoproducts in detergent as compared to native membranes was slowed to around half [44] and to under a sixth, respectively. Given that detergent micelles are commonly used to study membrane proteins; our results highlight an important observation about the artifactual effects detergents have on membrane protein biochemistry. These effects are further emphasized by our findings that detergents decreased the thermostability of both rhodopsin and RGR as compared to native membranes.

Like RGR, RRH resides in the RPE, but in the apical membrane surface of the RPE as opposed to microsomes. This location would be ideal for the capture of all-*trans*-retinal from photoreceptor outer segments, if it exhibited pigment formation and *trans*-*cis* photoisomerization activity similar to RGR. However, such activity by RRH has only been confirmed for invertebrate homologs.[169, 170] Instead, our study showed that bRRH, unlike bRGR, was unable to form pigment with all-*trans*-retinal, or any of the three major mono-cis isomers of retinal (9-*cis*, 11-*cis*, or 13-*cis*), despite possessing an internal Lys residue within the putative chromophore-binding domain. Our result is consistent with previous studies that have shown the lack of a robust phenotype in RRH knockout mice.[185] Furthermore, our analysis of single-cell RNA sequencing data showed very low expression levels of RRH, which was corroborated by proteomics data showing very low RRH protein levels, relative to other proteins from the RPE.

One study reported RRH expression in ocular tissue during early development of human and mouse eyes, with expression prior to rhodopsin, cone opsins, and RGR [178]. However, given the lack of a significant phenotype in RRH knockout mice, the exact role of RRH either in development or in the visual cycle remains unclear. Another study has suggested a potential role for RRH in trafficking retinoids to the RPE from photoreceptors in mice, perhaps even guiding visual cycle directionality [185]. However, the lack of expression within other vertebrates, like humans and cows, to the extent found in mice, and significantly lower relative expression as compared to other retinoid carrier proteins, such as cellular retinaldehydes-binding protein 1 (CRALBP) and interphotoreceptor retinoid-binding protein (IRBP), could suggest an alternative role to retinoid trafficking. Furthermore, RRH also lacks the NPXXY motif implicated for G-protein signaling.

For a better understanding of bRRH, the predicted AlphaFold structure of bRRH was compared against that of HaRRH, and the crystal structures of bRho, its photoactivated state, and apo-opsin. The comparison with the crystal structures of bRho, bRho*, and apo-opsin revealed that bRRH had ample space in its putative chromophore binding pocket to bind either 11-*cis*-retinal or all-*trans*-retinal in Schiff base interaction with its internal Lys residue (Figure 4.6). However, the wide cavity of this binding site was found to be connected to multiple open channels, where bulk water can enter, thereby rendering any retinylidene Schiff base labile to hydrolysis. By contrast, the chromophore binding pocket of HaRRH was much tighter and closed off from the external environment, preventing entry of bulk water (Figure 4.7).

In summary, our study provides direct measurements of hydrolysis of agonist from photoactivated cone opsins, confirming the quick photocycle of cone opsins and

documenting the large demand for 11-*cis*-retinal and the hefty production of all-*trans*-retinal to be cleared and recycled by RGR and/or the classical visual cycle providing a consistent supply of chromophore under constant illumination to support to sustain photopic vision. Upon probing RGR biochemistry, the N-terminus and the lipid environment surrounding the transmembrane helices appeared to strongly influence hydrolytic production of 11-*cis*-retinal following *trans-cis* photoisomerization. Our study also highlights the importance of studying membrane proteins in their native membrane environments, especially when investigating biochemical rates or activity. Lastly, our study demonstrated the lack of RRH pigment formation for subsequent photoisomerization activity, as well as highly variable expression in the mammalian RPE, leaving an unanswered question on the role of RRH in the eye.

4.4 Materials & Methods

Instrumentation

HPLC System (Agilent 1100 Series, Santa Clara, CA); 1260 Infinity HPLC System (Agilent); Dionex Ultimate 3000 UHPLC System (Thermo Fisher Scientific, Waltham, MA); LTQ XL mass spectrometer (Thermo Fisher Scientific); Cary 50 UV-Vis Spectrophotometer (Varian, Palo Alto, CA); Isotemp 3016S Water Bath (Fisher Scientific, cat no. 13-874-28); Fiber-coupled 565-nm 9.9-mW (Min) 700-mA LED (Thorlabs, Newton, NJ, cat. no. M565F3); Fiber-coupled 530-nm 6.8-mW (Min) 1000-mA LED (Thorlabs, cat. no. M530F2); Fiber-coupled 455-nm 17-mW (Min) 1000-mA LED (Thorlabs, cat.no. M455F3); Fiber Patch Cable (Thorlabs, cat. no. M92L01); Compact T-Cube 1200-mA LED Driver with Trigger Mode

(Thorlabs, cat. no. LEDD1B); Power Supply Unit with 3.5-mm Jack Connector (Thorlabs, cat. no. KPS201).

Materials

Chemicals and other materials were purchased as follows: all-*trans*-retinal (Sigma-Aldrich, St. Louis, MO, cat. no. R2500), all-*trans*-retinol (Sigma-Aldrich, cat. no. R7632); bROS (InVision Bioresources, Seattle, WA, cat. no. 98740); 2-[4-(2-hydroxyethyl)piperazin-1-yl]ethanesulfonic acid (Goldbio, St. Louis, MO, cat. no. H-400-1); 1,3-bis[tris(hydroxymethyl)methylamino]propane (Sigma-Aldrich, cat. no. B6755); calcium chloride dihydrate (Sigma-Aldrich, cat. no. 223506); n-dodecyl-β-D-maltopyranoside sol-grade (Anatrace, Maumee, OH, cat. no. D310S); lauryl maltose neopentyl glycol (Anatrace, Maumee, OH, cat. No. NG310); (3-((3-cholamidopropyl) dimethylammonio)-1-propanesulfonate) CHAPS detergent Anagrade (Anatrace, OH, cat. no. C316); pronase (Sigma-Aldrich, cat. no. PRON-RO); proteinase K solution (Viagen Biotech, cat. no. 501-PK); Amicon Ultra-0.5 Centrifugal Filter (Millipore, Burlington, MA, cat. no. UFC503096); ACN Optima LC/MS grade (Fisher Scientific, Pittsburgh, PA, cat. no. A955); methanol Optima LC/MS grade (Fisher Scientific, cat. no. A456); isopropanol Optima LC/MS grade (Fisher Scientific, cat. no. A461); FA Optima LC/MS grade (Fisher Scientific, cat. no. A117-50); methylene chloride (HPLC grade) (Fisher Scientific, cat. no. D143); hexanes (HPLC grade) (Fisher Scientific, cat. no. H302); ethyl acetate (HPLC) (Fisher Scientific, cat. no. E195); triethylamine (HPLC) (Fisher Scientific, cat. no. O4884); dimethyl sulfoxide (Sigma-Aldrich, cat. no. D2650); N,N-dimethylformamide (Fisher Scientific, cat. no. AC327171000); diethylamine (Sigma-Aldrich, cat. no. 471216); N^{α}-[(9H-fluoren-9-ylmethoxy)carbonyl]-L-

Lys hydrochloride (Fisher Scientific, cat. no. F0586); 1,2-dioleoyl-sn-glycero-3-phosphoethanolamine (Avanti Polar Lipids, Alabaster, Al, cat. no. 850725P); $NaBH_4$ (Alfa Aesar, Haverhill, MA, cat. no. 88983); $NaBD_4$ (Alfa Aesar, cat. no. 35102; 85 W 2700 K Hg light bulb (Home Depot, cat. no. EDXR-40-19); BioPureSPN C18 TARGA (nestgrp, Ipswich, MA cat. no. HEM S18R); XBridge C18 (Waters, Milford, MA, 2.1 mm X 100 mm, cat. no. 186003022); Gemini Analytical C18 (Phenomenex, Torrance, CA, 250 x 4.6 mm, cat. no. 00G-4435-E0); Gemini Preparatory C18 (Phenomenex, 250 x 10 mm, cat. no. 00G-4435-N0); Luna Preparatory Silica (Phenomenex, 250 x 21.2 mm, cat. no. 00G-4091-P0-AX).

Methods

Production of 9-*cis*-, 11-*cis*-, and 13-*cis*-retinal and the corresponding retinol isomers. The method for production of 9-*cis*-retinal, 11-*cis*-retinal, and 13-*cis*-retinal was adapted from Kahremany *et al.*[121] Thus, all-*trans*-retinal was solubilized in ACN at 0.2 M and illuminated with an 85-W mercury light bulb at maximum intensity at a distance of 10 cm for 12 hr at 4 °C. The resultant 9-*cis*-, 11-*cis*-, and 13-*cis*-retinal products were purified with a Luna preparatory silica column using 90% hexane and 10% ethyl acetate as the mobile phase at a flow rate of 5 mL/min. The purified products were verified by comparison to standards, using HPLC and UV-Vis absorbance spectroscopy. Each retinal isomer was reduced with excess $NaBH_4$ in methanol to produce the corresponding retinol isomer. The methanol solvent was evaporated by a flow of nitrogen, and the corresponding retinol product was isolated from the crude oil by organic-aqueous extraction using 1:1 hexane/water. The hexane layer was dried with anhydrous magnesium sulfate. The crude product was purified with a Luna preparatory silica column, using 90% hexane and 10%

ethyl acetate as the mobile phase at a flow rate of 5 mL/min. The purified products were verified by comparison to standards, using HPLC and UV-Vis absorbance spectroscopy.

Isolation of bROS membranes. bROS membranes were prepared from fresh bovine retinas (InVision Bioresources) using sucrose gradient isolation as described previously [122], and washed with hypotonic buffer (20 mM HEPES, pH 7.4).

Expression of red-cone opsin. The red-cone opsin (OPSR) construct consisted of human long-wavelength-sensitive opsin 1 (UNIPROT ID P04000) in which the C-terminus was truncated after Lys352 and tagged with 1D4 peptide, and residues Gln253-Lys254 from the third intracellular loop were replaced by a modified T4 lysozyme (UNIPROT ID P00720, with M1 and its three C-terminal residues truncated, and mutations C54T and C97A). The OPSR construct was expressed in-house in Sf9 insect cells as described previously.[179, 186] The OPSR construct was cloned into the pFastBac HT vector from a Bac-to-Bac Vector Kit (Thermo Scientific, Waltham, MA) with their N-terminal His tags removed. DH10Bac *E. coli* was transformed using the resultant recombinant plasmid to produce bacmid, and isolated by mini-prep following the Invitrogen protocol for the Bac-to-Bac Baculovirus Expression System (Carlsbad, CA). Sf9 insect cells were transfected during log-phase growth with 1 μg of bacmid DNA. The supernatant was harvested after 5 days. 1.5 mL of P1 virus was added to 40 mL of cells at a density of 1.5×10^6 cells/mL. After 4 days, the culture was centrifuged at 2,500 × g for 5 min to harvest the P2 virus. P2 virus (2 mL) was added to 800 mL of Sf9 cells at a density of 2×10^6 cells/mL to obtain P3 virus. Large-scale expression of OPSR was started with Sf9 cells at 3.5×10^6 cells/mL of culture. Sf9 cells were subsequently infected

with P3-stage virus at a 1:100 volume ratio in 3-liter flasks with shaking at 135 rpm in a 27.5 °C incubator for 2 days. Then cells were collected 48 hr post-infection. Cell pellets were frozen and stored at -80 °C.

Expression of green-cone opsin. The green-cone opsin (OPSG) construct consisted of the human medium-wavelength-sensitive opsin 1 (UNIPROT ID P04001) in which the C-terminus was truncated after residue Lys^{352}, and 1D4-tagged. Expression of OPSG in insect Tni cells was conducted by Expression Systems LLC (Davis, California, US). Cell cultures were seeded at 1×10^6 cells/mL in ESF 921 medium, and cultured overnight. The following day the culture was infected with baculovirus at a MOI of 10:1. The culture was harvested 72 hr post infection. Cells were pelleted by centrifugation and frozen at -80 °C.

Expression blue-cone opsin. The blue-cone opsin (OPSB) construct consisted of human short-wavelength-sensitive opsin 1 (UNIPROT ID P03999) in which the C-terminus was truncated at residue Lys^{334}, and replaced with the 1D4 tag. The OPSB construct was expressed in-house in Sf9 insect cells, as described above for OPSR.

Generation of HEK293S GnTI$^-$ cell line stably expressing bRGR. A HEK293S GnTI$^-$ cell line stably expressing bRGR (UNIPROT ID P47803) was established using a previously published method [187]. Retroviral expression vectors were generated by introducing EcoRI and NotI restriction sites at the ends of the bRGR coding sequence by PCR with the following primers: forward, 5'-CGGGAATTCATGGCAGAGTCTGG-3; reverse: 5'-CGAATGCGGCCGCTTAGGCAGGCGCCACTTGG-3'. Subsequently, the bRGR cDNA was

inserted into a pMX-IP retroviral vector, generously provided by Dr. T. Kitamura from the University of Tokyo [188].

An internal ribosomal entry site (IRES) and a puromycin selection gene were placed downstream of the bRGR coding region, enabling puromycin-based selection. HEK293S GnTI$^-$ cells were transduced with retrovirus, which was harvested from Phoenix-AMPHO cells transfected with the pMXs-IP vector carrying the bRGR sequence. Following three days of selection with puromycin, the transduced cells were maintained with FreeStyle 293 expression medium (Thermo Fisher Scientific; 12338018) containing 3% v/v heat-inactivated fetal bovine serum (Thermo Fisher Scientific; A3840001), 1% v/v Penicillin/Streptomycin mix (Thermo Fisher; 151401122). Suspension cells were maintained at 37 °C under an atmosphere of air adjusted to 8% CO_2.

Generation of HEK293S GnTI$^-$ cell line stably expressing bRRH. A HEK293S GnTI$^-$ cell line stably expressing bRRH (UNIPROT ID F1MR98) was established by transduction of GnTI- HEK293S cells with retrovirus obtained from Phoenix-Ampho cells, transfected with either pMXs-bRRH-WT-IRES-GFP, according to a previously published protocol [189]. Transduced cells were sorted by a FACSAria Fusion cell sorter (BD Biosciences) to selectively collect transduced GFP+ cells. WT bRRH with a C-terminal 1D4 tags and flanking EcoRI and NotI restriction sites were synthesized and cloned into pcDNA3.1+ by GenScript. The vectors were then digested with EcoRI and NotI and cloned into the MCS of pMXs-IRES-GFP (a gift from T. Kitamura at the University of Tokyo [188]). The downstream sequence of the internal ribosomal entry site (IRES) and GFP allows co-expression of bRRH and GFP, thereby enabling cell sorting by flow cytometry. Cells were cloned by limited

dilution and the expression of RRH was determined by 1D4 immunoblotting. Clones were then adapted to FreeStyle 293 expression medium (Thermo Fisher Scientific; 12338018) containing 3% v/v heat-inactivated fetal bovine serum (Thermo Fisher Scientific; A3840001), 1% v/v Penicillin/Streptomycin mix (Thermo Fisher; 151401122). Suspension cells were maintained at 37 °C under an atmosphere of air adjusted to 8% CO_2.

Immunopurification of retinylidene-opsin pigments. Frozen cell pellets were thawed and homogenized in hypotonic buffer (20 mM HEPES, pH 7.0, containing 1 mM $MgCl_2$, benzonase nuclease, Roche protease inhibitor cocktail) with a Dounce homogenizer. Membranes were isolated by centrifugation at 50,000 x g for 1 hr, then homogenized further in the same hypotonic buffer. The resultant membranes were then washed twice in hypertonic buffer (50 mM HEPES, pH 7.0, 1 M NaCl, 1 mM $MgCl_2$, benzonase nuclease, Roche protease inhibitor cocktail). The washed membranes were resuspended in hypertonic buffer, and incubated for 2 hr with retinal. 11-*cis*-retinal was used for cone opsins, and all-*trans*-retinal was used for bRGR. All four retinal isomers were tested for binding to bRRH, as a native chromophore has not been identified. All four retinal were prepared at 20 mM concentration in dimethylformamide for addition to membranes. After incubation, membranes were solubilized in a buffered-detergent solution (final concentration: 10 mM Lauryl Maltose Neopentyl Glycol (LMNG), 20 mM HEPES, pH 7.4, 0.25 M NaCl). For bRho, bROS membranes, isolated as described above, were solubilized similarly. Each retinylidene-opsin pigment was immunopurified in a dark room under dim red light, using immobilized 1D4 antibody as previously described [153, 190, 191]. Solubilized membranes were incubated for 2 hr with Sepharose beads with immobilized 1D4 antibody.

The beads were washed with 10 column volumes of wash buffer (0.2 mM LMNG in 20 mM HEPES, pH 7.4 containing 0.15 M NaCl) to remove unbound protein as well as solubilized lipids. The retinylidene-opsin pigment was then eluted using a 0.5 mg/mL solution of the competing peptide TETSQVAPA (1D4) in wash buffer. Using an Amicon 30-kDa MWCO centrifugal filter, retinylidene-opsin pigments were concentrated to at least 1 mg/mL while removing 1D4 peptide with two passes of wash buffer B (0.1 mM LMNG, 20 mM HEPES, pH 7.4, 0.14 M NaCl).

Isolation of bRPE microsomes. The preparation of bRPE microsomes was done as previously described [192]. RPE cells were collected from bovine eye cups by gentle brushing, then lysed using a Dounce homogenizer. bRPE microsomes were isolated from the homogenate by differential centrifugation at 20,000 × *g* for 20 min at 4 °C, yielding a supernatant fraction containing microsomes that were pelleted by subsequent centrifugation at 150,000 × *g* for 1 hr at 4 °C. The microsomal pellet was resuspended in 10 mM HEPES buffer, pH 7.4, at a protein concentration of about 5 mg/mL containing about 0.2 mg/mL bRGR regenerated with all-*trans*-retinal.

Proteinase K and pronase digestion of opsin pigments. Opsin pigments were prepared in a dark room under dim red light, at 1-2 mg/mL in 10 mM HEPES, pH 7.4, containing 140 mM NaCl. One volume of opsin pigment solution was treated with two to three volumes of saturated $NaBH_4$ or $NaBD_4$ in ice cold *i*PrOH for immediate reduction of the retinylidene Schiff base, and isolation of reduced opsin pigment by *i*PrOH protein precipitation (cold EtOH can be used in place of *i*PrOH). The suspension of protein precipitate was diluted with

3 parts cold MeOH and 1 part 50 mM HEPES buffer, pH 7.4, to facilitate quenching of unreacted $NaBH_4$ or $NaBD_4$. After centrifugation at 20,000 × *g*, the protein pellet was washed again with cold MeOH, followed by cold water. The protein pellet was resuspended in either proteinase K buffer (100 mM BTP, pH 7.8, 100 mM $CaCl_2$, 4 M urea) or pronase buffer (100 mM BTP, pH 7.8, containing 100 mM $CaCl_2$, 0.5% w/v CHAPS). Then, proteinase K or pronase were added at approximately 10 times the weight of the opsin substrate. The proteinase K digestion mixture was incubated at room temperature while the pronase digestion mixture was incubated at 6-10 °C. Both digestions proceeded for 24 hr with gentle agitation using a shaker. Each digest was passed through a BioPureSPN C18 spin column for desalting. The column was washed with 20% ACN in water with 0.1% FA, and peptides were eluted using 50% ACN. The eluted N^{ε}-retinyl-peptide or N^{ε}-retinyl-Lys products were separated using a Dionex UHPLC with a XBridge C18 column and a 40 min gradient of 20% to 60% ACN in water with 0.1% FA at a flow rate of 0.3 mL/min. The N^{ε}-retinyl products were detected by HPLC absorbance measurements at 330 nm and identified by LC-MS/MS with collision-induced dissociation (CID) fragmentation, using an LTQ XL mass spectrometer.

Kinetic analysis of Schiff-base hydrolysis of opsin pigment photoproducts. Each opsin pigment in 10 mM HEPES, pH 7.4, containing 140 mM NaCl was illuminated for 10 sec with a fiber-coupled monochromatic LED at an intensity of 125 μW at wavelengths indicated as follows: 505 nm for rhodopsin, 565 nm for red opsin, 530 nm for green opsin, 455 nm for blue opsin, 530 nm for bRGR. After light exposure, $NaBH_4$/*i*PrOH was added at different timepoints to track the hydrolysis of the photoisomerized retinylidene Schiff base of each

opsin protein. The protein precipitate was digested with pronase as described above, producing N^{ε}-retinyl-Lys to determine the amount of remaining opsin-bound retinal. The supernatant was analyzed to quantify the hydrolytically released retinal as follows: all-*trans*-retinol, the $NaBH_4$-reduction product of all-*trans*-retinal, was separated and quantified by high-performance liquid chromatography (HPLC) using the Agilent 1260 Infinity HPLC system with an XBridge C18 column with a gradient in water with 0.1% FA of 95% to 100% of MeOH with 0.1% FA for 10 min at a flow rate of 0.3 mL/min. In the study of cone opsins, the Schiff-base hydrolysis of the photoproducts was studied at different temperatures (0°C and 20°C), given the rapid rate of hydrolysis during the 10 sec illumination period. The resultant extents of hydrolysis were compared to those of rhodopsin under the same conditions. In the study of bRGR, a different HPLC method was used to separate the 11-*cis*-retinol product of $NaBH_4$-reduction from all-*trans*-retinol, because all-*trans*-retinal had been added in slight excess to initially regenerate the bRGR pigment. Using the same HPLC system and column, the procedure entailed a gradient in water with 0.1% FA of 80% to 100% MeOH with 0.1% FA for 15 min at a flow rate of 0.3 mL/min. From the pronase digest, the resultant N^{ε}-retinyl-Lys products were analyzed chromatographically using the same HPLC system and column, but a faster method was used with an 18-min gradient of 30% to 39% ACN in water with 0.1% FA at a flow rate of 0.3 mL/min. The detection of N^{ε}-retinyl-Lys products by HPLC absorbance detection at 330 nm and LC-MS/MS were done as described above. Isomeric identities were confirmed by UV-Vis absorbance spectra collected during chromatography. The molar quantity of each isomer of N^{ε}-retinyl-Lys (9-*cis*, 11-*cis*, 13-*cis*, and *all-trans*) was determined based on a standard curve generated using synthetically produced N^{ε}-retinyl-Lys isomers, as

described previously.[44] The mole fraction of opsin-bound retinal (measured as moles of N^{ε}-retinyl-Lys) over the total retinal content (measured as the sum of the moles of N^{ε}-retinyl-Lys and the moles of retinal produced from hydrolysis of retinylidene Schiff base) was plotted for each time-point, generating a curve consistent with pseudo first-order decay kinetics.

Thermostability studies of bRho and bRGR. All aliquots of bROS, bRPE microsomes, immunopurified bRho, and immunopurified bRGR were prepared in 20 mM HEPES, pH 7.4, containing 140 mM NaCl. Each were incubated for 10 min at various temperatures (20°C, 37°C, 50°C, 60°C, 70°C, 80°C, and 90°C), followed by addition of $NaBH_4$/*i*PrOH for chromophore trapping. The amount of chromophore bound to opsin at each temperature was determined by the signal intensity of Nε-retinyl-Lys after proteolysis by pronase as described above. The signal intensities at each temperature were normalized to that of 20°C, generating a sigmoidal plot of thermostability to determine the melting temperature for each opsin either in native membranes or in detergent micelles depleted of lipids.

Assessment of bRRH ability to form retinylidene-opsin pigment. The immunopurification of bRRH was performed as described above, testing each isomer of retinal (9-*cis*, 11-*cis*, 13-*cis*, and all-*trans*) and vehicle control (dimethylformamide). The immunopurified bRRH was prepared in 20 mM HEPES, pH 7.4, containing 140 mM NaCl. $NaBH_4$/*i*PrOH was added to trap any bound chromophore for subsequent LC-MS/MS analysis of any N^{ε}-retinyl-peptides or N^{ε}-retinyl-Lys by proteolysis with proteinase K or pronase, respectively, as described above.

Concurrently, HEK293S GnTI$^-$ with and without stable expression of bRRH was cultured in suspension and harvested. Both samples were homogenized in hypotonic buffer (20 mM HEPES, pH 7.0, containing 1 mM $MgCl_2$, benzonase nuclease, Roche protease inhibitor cocktail) with a Dounce homogenizer. Membranes were isolated by centrifugation at 50,000 x g for 1 hr, then homogenized further in the same hypotonic buffer. The resultant membranes were then washed twice in hypertonic buffer (50 mM HEPES, pH 7.0, 1 M NaCl, 1 mM $MgCl_2$, benzonase nuclease, Roche protease inhibitor cocktail).
Membranes from HEK293S GnTI$^-$ with and without stable expression of bRRH were each washed three times in 20 mM HEPES, pH 7.4, containing 140 mM NaCl, for final preparation of membranes in this buffered condition at a concentration of 1.5 mg/mL total protein. Membranes from the HEK293S stably expressing bRRH was determined to have 3.5 ug bRRH per mg of protein. The membranes from each cell line were treated with each isomer of retinal (9-*cis*, 11-*cis*, 13-*cis*, and all-*trans*) or vehicle control (dimethylformamide). Retinal was incubated for at least 2 h, followed by addition of $NaBH_4$/*i*PrOH for LC-MS/MS analysis of any N^{ε}-retinyl-peptides or N^{ε}-retinyl-Lys by proteolysis with proteinase K or pronase, respectively, as described above.

Structural comparative analysis of the putative chromophore binding pocket of bRRH. In order to compare the hypothetical retinal binding pocket of peropsin to that of rhodopsin, the AlphaFold [193, 194] 3D model of bRRH (UNIPROT ID F1MR98) and the crystal structures of metarhodopsin II (PDB ID 3PXO) and apo-rhodopsin (PDB ID 3CAP) were superimposed in Pymol Molecular Graphic System (v1.2, Schrödinger) to the crystal structure of ground state rhodopsin (PDB ID 7ZBC). In addition, the binding pockets of

AlphaFold models for bRRH and jumping spider's (*Hasarius adansoni*) RRH (HaRRH, UNIPROT ID E1CFG1) were compared side-by-side on Pymol.

Proteomic analysis of bRPE cells. Bovine RPE cells were resuspended in different proteolysis buffers to assess whether buffer conditions alter proteolytic selectivity and resultant distribution of peptides. The three buffers tested were: UA buffer (8.0 M Urea, 0.1 M Tris-HCl, pH 8.3), SDS buffer 1 (0.1 % SDS, 0.1 M Tris-HCl pH 8.3), and SDS buffer 2 (4.0 % SDS, 0.1 M Tris-HCl, pH 8.3). Protease inhibitor cocktail (Bimake #14001) was added to each buffer before use. The respective suspensions were sonicated on ice for 4 min, followed by centrifugation at 12,000 × *g* for 10 min at 4 °C. The supernatants were collected and digested by the filter-aided sample preparation (FASP) method. Briefly, the supernatant was transferred into a spin filter column (30-kDa cutoff). Proteins were reduced with 10 mM DTT for 1 hr at 56 °C, and alkylated with 20 mM iodoacetic acid for 30 min at room temperature in the dark. Next, the buffer was diluted and exchanged with 50 mM NH_4HCO_3 by washing the membrane three times. Free trypsin was added into the protein solution at a trypsin to protein ratio of 1:50 and incubated for 4 hr at 37 °C. Next, the digestion mixture was mixed at a 1:1 ratio (v:v) with buffer containing 20 mM $CaCl_2$ and 200 mM Tris-HCl, pH 8.3). Free chymotrypsin was then added to the digestion mixture at a chymotrypsin to protein ratio of 1:50 and incubated overnight at room temperature. After centrifugation at 12,000 × *g*, the proteolysis products were recovered in the supernatant. The supernatant was vacuum-dried and then adjusted to 200 µL with 0.5% acetic acid. The peptide mixtures were then subjected to C18 solid-phase extraction (The Nest Group, Inc.) for desalting.

Mass spectrometric data acquisition. Proteomics data were acquired *via* LC-MS/MS using an UltiMate 3000 UHPLC (Thermo Fisher Scientific), coupled in-line with an Orbitrap Fusion Lumos mass spectrometer (Thermo Fisher Scientific) with an ESI nanospray source. Mobile phase A was composed of 0.1% FA in water, and mobile phase B was comprised of 0.1% FA in ACN. The total flow rate was 300 nL min^{-1}, and peptides were separated over an 89-min gradient from 1% to 22% buffer B (total run time 120 min per sample) on an Acclaim PepMap RSLC column (50cm x 75 µm). Survey (MS) scans were acquired in Orbitrap (FT) with automated gain control (AGC) target 8E5, maximum injection time 50 msec, and dynamic exclusion of 30 sec across the scan range of 375-1800 m/z. MS/MS spectra were acquired in data-dependent acquisition mode with an inclusion list of predicted m/z values for the peptides of bRRH, at top speed for 3 sec per cycle (**Table 1**); the AGC target was set to 4E5 with maximum injection time of 35 msec. Ions were subjected to stepped-energy higher-energy collision dissociation (seHCD) fragmentation at a normalized collision energy (NCE) of 30%.

Table 1. Mass (m) and *to* charge (z) ratio for analyzed peptides.

Peptide Sequence	**m/z**
NNLGNSSDC(carbamidomethyl)K	554.738
SQTEHNIVAAY	616.799
LITAGVISILSNIIVLGIF	978.611
TPTNAIIINLAVTDIGVSSIGYPMSAASDLHGSW	1736.377
GMASIGLLTVVAVDR	751.424
LTIC(carbamidomethyl)HPDAGR	570.285
ISMILGAW	445.744
ALMPIIGW	450.754
APDPTGATC(carbamidomethyl)TINW	702.317
TMMVVAINF	513.262

IVPLTVMF	460.270
HVTQSIK	406.735
HHGTNNC(carbamidomethyl)TEY	616.7415
SDQVDVTK	446.225
MSVIMILMF	542.784
IPPSMAIIAPLF	635.367
C(carbamidomethyl)QTTQAMPVTSVLPMDVPQNPLTSGK	1400.688

Label-free quantification analysis. The raw LC-MS/MS data files were analyzed using MaxQuant (version 1.5.2.8), with the spectra searched against the Uniprot mouse database (updated on May 21st, 2018). For identification of the peptides, the mass tolerances were 20 ppm for initial precursor ions, and 0.5 Da for fragment ions. Two missed cleavages in tryptic digests were allowed. Cysteine residues were set as static modifications. Oxidation of methionine was set as the variable modification. Filtering for the peptide identification was set at a 1% false discovery rate (FDR).

4.5 Tables and Figures

Table 4.1 Single cell RNA sequencing and proteomics of various visual cycle components in the RPE.[a]

Gene	Human RPE	Mouse RPE	Bovine RPE	Bovine RPE (lysis buffer 1)[b,c]	Bovine RPE (lysis buffer 2)[b,d]	Bovine RPE (lysis buffer 3)[c,e]
	scRNAseq[a]			Proteomics[a]		
RRH	0.6	4.2	0.3	0.19	0.0	0.039
CRALBP (RLBP1)	34.5	24.8	74.0	3.0	4.7	0.84
IRBP (RBP3)	5.3	2.1	0.9	4.2	4.2	4.0
RGR	25.1	111.8	49.9	4.1	7.0	1.8
LRAT	4.5	7.8	11.9	0.43	2.6	0.0
RPE65	114.4	42.1	61.3	5.6	22.4	4.2
RDH5	2.2	53.6	8.1	2.0	12.1	1.4
RDH10	6.7	14.6	0.3	0.15	0.27	0.0

Abbreviations: RRH, peropsin; CRALBP, cellular retinaldehyde-binding protein; RLBP, retinaldehyde-binding protein; IRBP, interphotoreceptor retinoid-binding protein; RBP, retinol binding protein; RGR, retinal G protein-coupled receptor; LRAT, lecithin retinol acyltransferase; RPE65, retinoid isomerase; RDH, retinol dehydrogenase.

[a]The scRNAseq were generated in previous studies.[112, 175-177] Proteomic data are obtained in this work as described in the Supplemental Method section. For scRNAseq, the data represent the relative average expression values calculated for the RPE cell clusters using the average expression function of Seurat;; for proteomics, the data are expressed in intensity-based absolute quantification (iBAQ) units

[b]iBAQ values were determined by the sum of ion intensities (x10^7) of peptides matching a specific protein divided by the theoretical number of observable tryptic peptides

[c]Buffer:10 mM Tris/HCl, pH 8.3, containing 0.1% SDS.

[d]Buffer:10 mM Tris/HCl, pH 8.3, containing 4% SDS.

[e]Buffer:10 mM Tris/HCl, pH 8.3, containing 8 M urea.

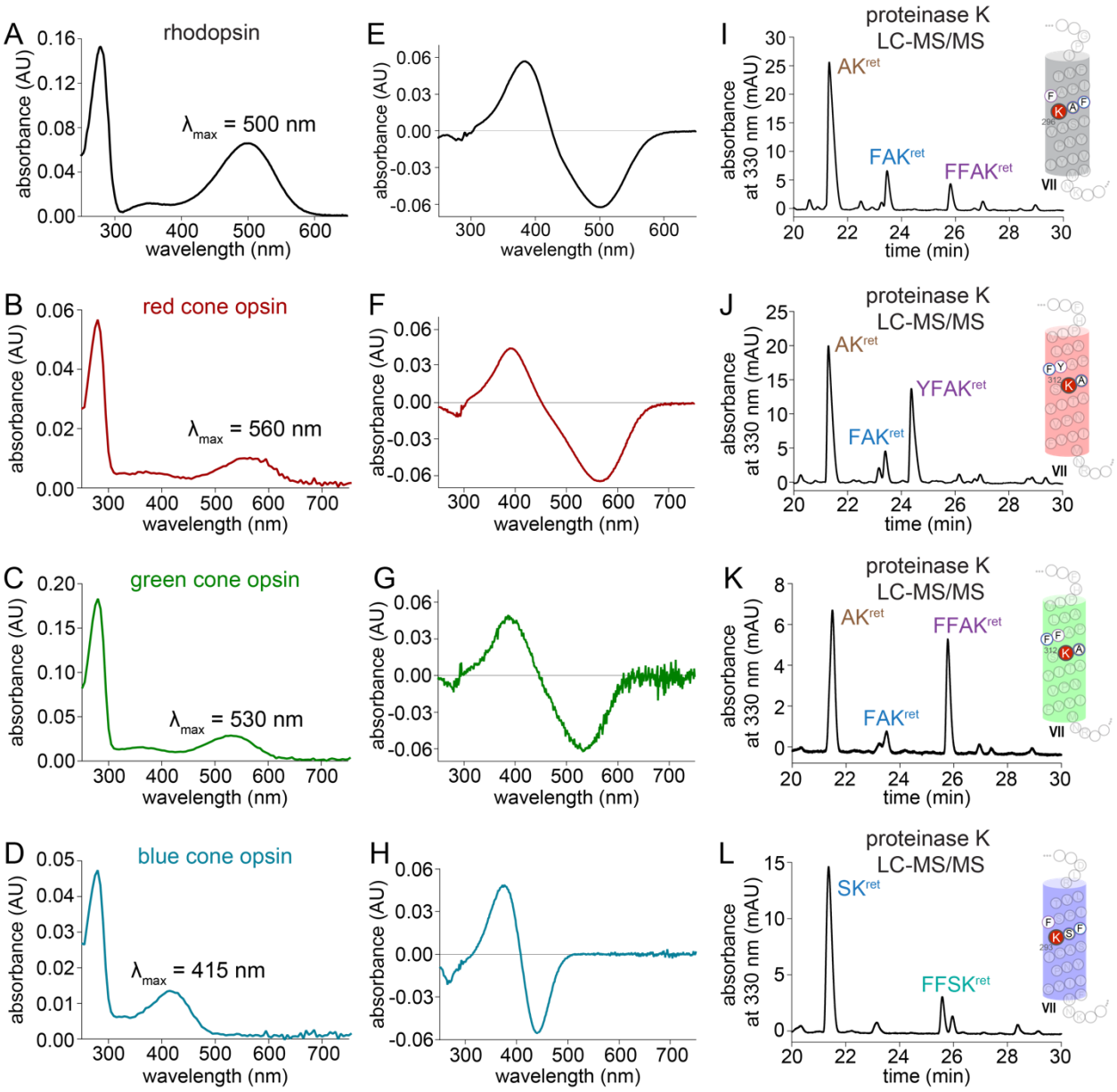

Figure 4.1 Spectral characterization and chromophore binding site identification of visual pigments. (A-D) UV-Vis spectrum of purified bRho (panel A), hRed-cone opsin (panel B), hGreen-cone opsin (panel C), and hBlue-cone opsin (panel D) in LMNG. (E-H) Characteristic difference spectra after illumination of purified bRho (panel E), hRed (panel F), hGreen (panel G), and hBlue (panel H) in LMNG. (I-L) Chromatographic separation and MS/MS identification of N^{ε}-retinyl-peptides from the proteinase K digest of $NaBH_4$/*i*PrOH-treated purified bRho (panel I), hRed (panel J), hGreen (panel K), and hBlue (panel L). Location of the chromophore-binding residue within helix VII is identified by the corresponding labeled N^{ε}-retinyl-peptide fragments detected from the proteinase K digest of each opsin-chromophore preparation. Detailed LC-MS/MS analyses are shown in Appendix A, Figures S1-S5.

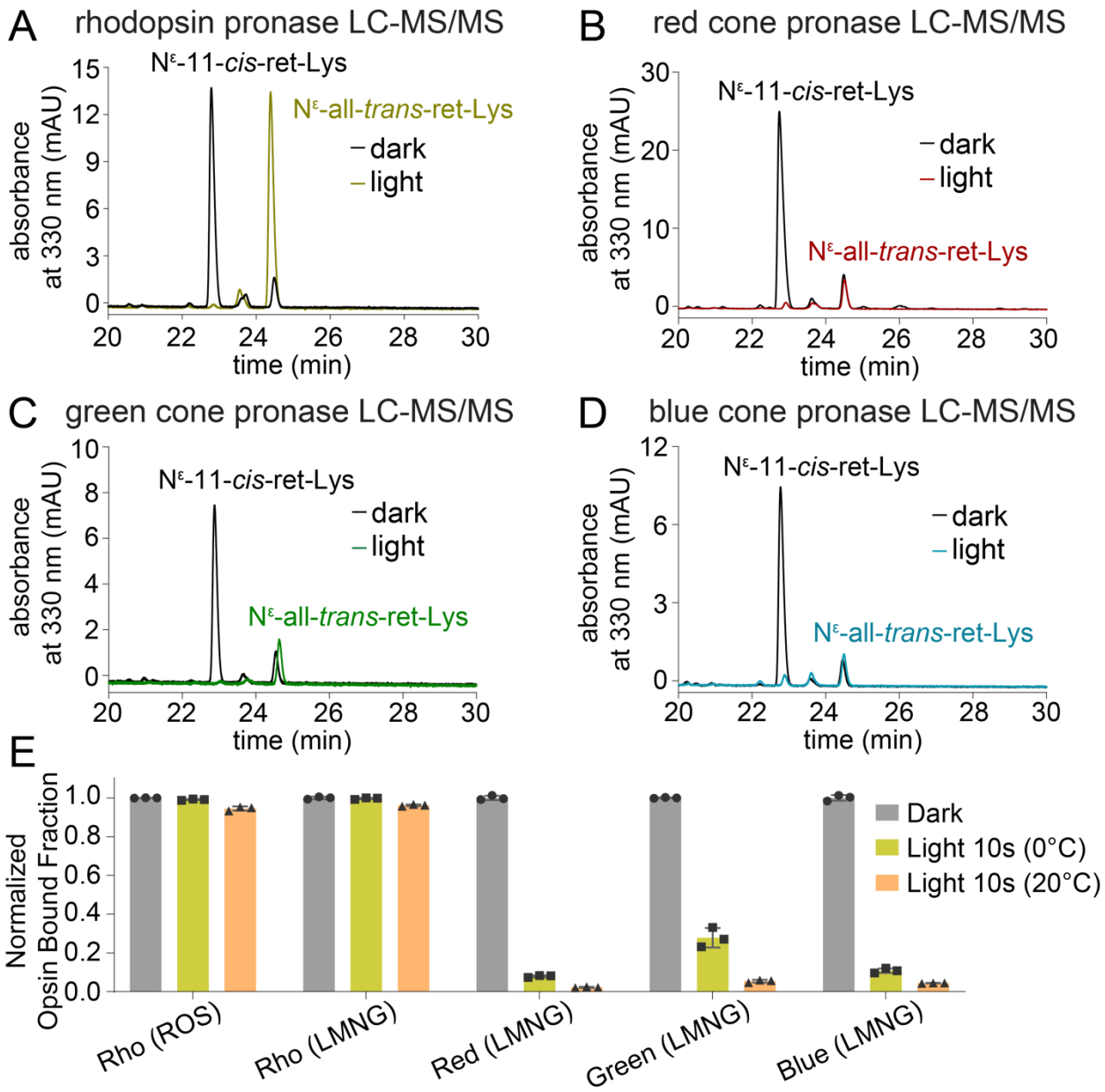

Figure 4.2 Characterization of visual pigment photoisomerization reaction and subsequent hydrolysis of all-*trans* agonist. (A-D) Chromatographic separation of Nε-retinyl-Lys products from pronase digests of photoactivated and ground-state bRho (panel A), hRed-cone opsin (panel B), hGreen-cone opsin (panel C), and hBlue-cone opsin (panel D), each treated with $NaBH_4$/*i*PrOH. Chromatograms in panels A-D reflect the chromophore photoisomerization observed at 0 °C. Detailed LC-MS/MS analyses are shown in Appendix

A, Figures S6-S10. (E) Comparison of the extents of hydrolysis of the all-*trans*-retinylidene agonists, demonstrating much faster hydrolysis of the agonist in photoactivated cones opsins than in photoactivated rhodopsin. Each bar represents the mean from three replicates, represented as data points, and the error bars represent the standard deviation.

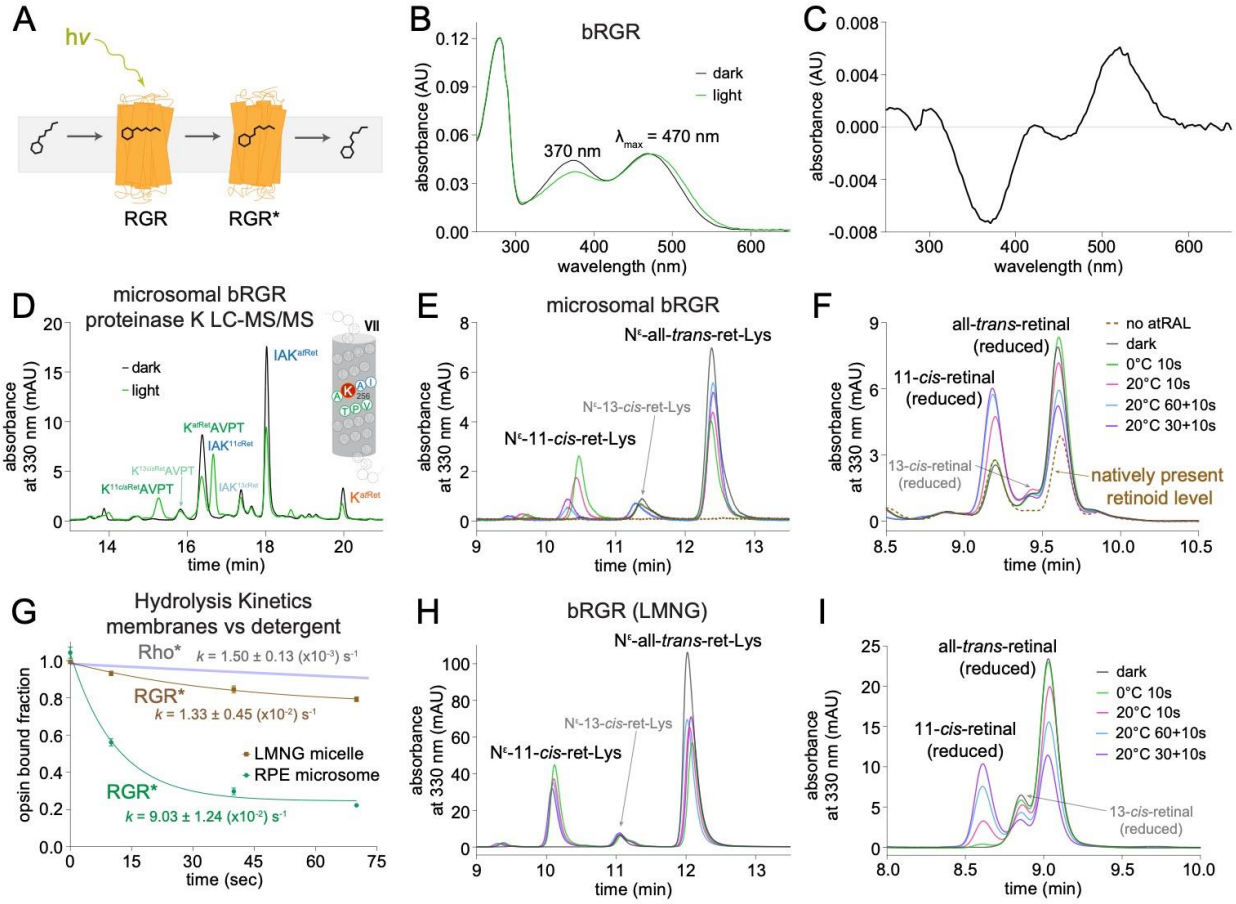

Figure 4.3 LC-MS/MS analysis of the bRGR pigment photoisomerization reaction and subsequent photoproduct hydrolysis. (A) Schematic diagram of bRGR photoconversion of all-*trans*-retinal to 11-*cis*-retinal in bRPE microsomal membranes. (B) Absorbance spectrum before and after illumination of recombinant bRGR reconstituted with all-*trans*-retinal and purified in LMNG. (C) Difference spectrum after illumination of bRGR, showing

relatively minimal changes. (D) Chromatographic separation of N$^{\varepsilon}$-retinyl-peptide products from the proteinase K digest of microsomal bRGR, before and after light exposure, with subsequent $NaBH_4$/*i*PrOH treatment. Location of chromophore-binding residue within helix VII identified as labeled N$^{\varepsilon}$-retinyl-peptide fragments detected from the proteinase K digest. Detailed LC-MS/MS analyses are shown in Figs. S12-S15. (E, H) Chromatographic detection of *trans-cis* bRGR photoisomerization as well as subsequent hydrolysis of the 11-*cis*-retinylidene adduct, with a corresponding increase in new all-*trans*-retinylidene adduct formation. (F, I) Reciprocal increase in 11-*cis*-retinal in the supernatant produced by hydrolysis and decrease in all-*trans*-retinal, with new bRGR pigment formation. (G) Hydrolysis kinetics: the hydrolysis of the 11-*cis*-retinylidene photoproduct was dramatically slower by nearly six-fold for bRGR in detergent micelles in contrast to bRGR in native RPE microsomal membranes. The hydrolysis was still faster in either case than the hydrolysis of the all-*trans* agonist from photoactivated rhodopsin, whose hydrolysis plot was adapted from Hong, *et.al.* [44].

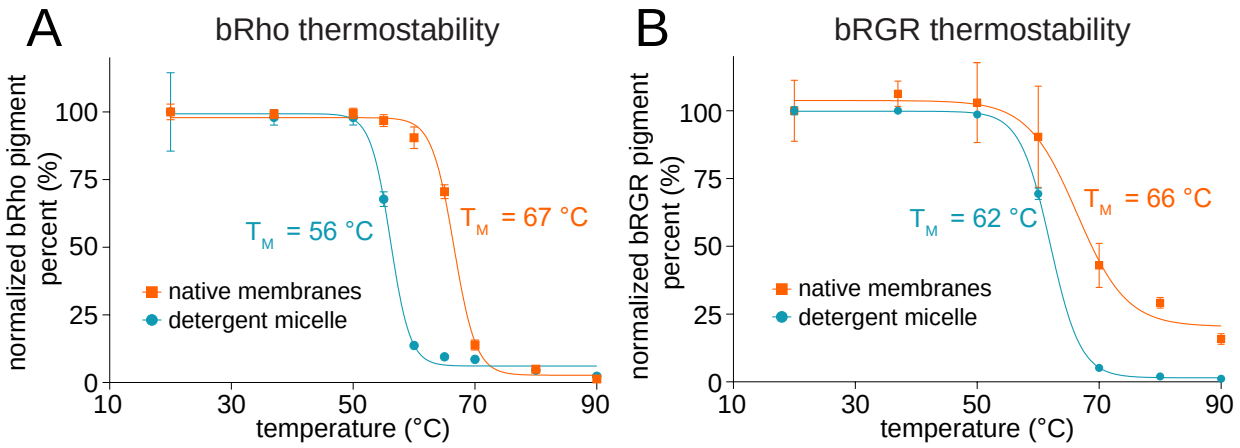

Figure 4.4 Reduction of bRho and bRGR thermostability in detergent micelles

depleted of native lipids. (A) The high thermostability of bRho in native ROS membranes is significantly diminished upon solubilization in LMNG detergent micelles and depletion of native lipids, with a decrease in T_m from 67 °C to 56 °C. (B) Similar findings were observed for bRGR in native bRPE microsomal membranes, with a high T_m = 66 °C which decreased to 62 °C for bRGR in LMNG detergent micelles depleted of lipids. For panels (A) and (B), points mean values, and error bars represent standard deviation with n = 6.

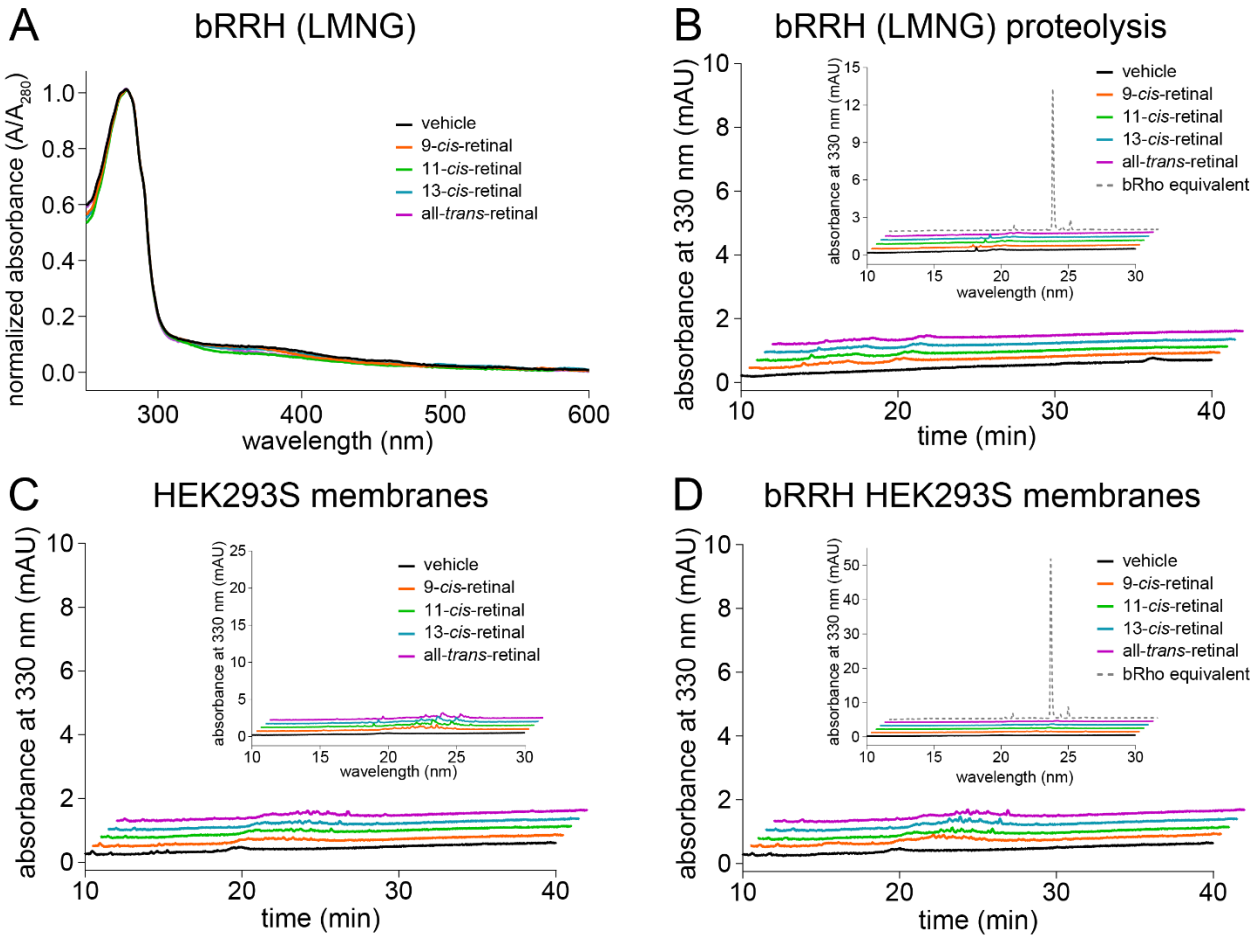

Figure 4.5 Lack of pigment formation by bRRH treated with retinal. (A) Absorbance spectra of PRH treated with different retinal isomers and subsequently purified in LMNG showed no difference from vehicle treatment, indicating lack of pigment formation with

retinal. (B) LC-MS/MS analysis of the proteinase K digest of $NaBH_4$-reduced immunopurified PRH that had been treated with retinal isomers did not detect N^{ε}-retinyl-peptides, nor did LC-MS/MS analysis of the corresponding pronase digest detect any N^{ε}-retinyl-Lys (inset). LC-MS/MS of the pronase digest of an amount of bRho equivalent to bRRH was performed to display the amount of N^{ε}-retinyl-Lys signal that would be expected if retinylidene-Schiff base adducted bRRH were present. (C) The same LC-MS/MS analyses of the proteinase K and pronase digests (inset) were done for membrane isolates of HEK293S cells treated with retinal isomers, showing no definitive N^{ε}-retinyl-peptides and N^{ε}-retinyl-Lys, respectively. (D) The same protocol was repeated with membrane isolates of HEK293S cells stably expressing bRRH, also showing lack of any definitive signals of N^{ε}-retinyl-peptides or N^{ε}-retinyl-Lys.

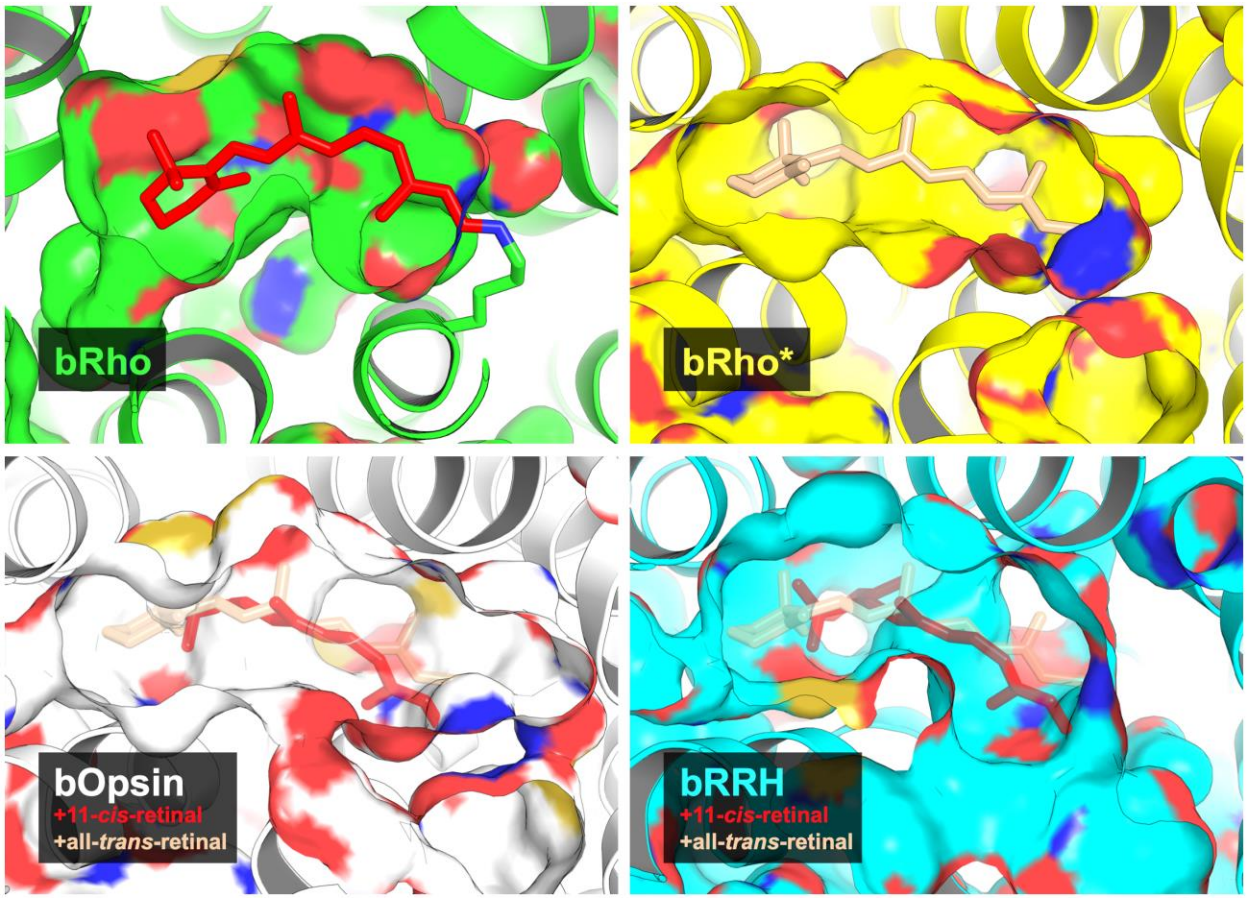

Figure 4.6 Structural analysis of the bRRH putative chromophore-binding pocket. Comparison of the ligand binding pockets in ground-state rhodopsin (bRho, top left), metarhodopsin II (bRho*, top right), apo-rhodopsin (bOpsin, bottom left) and peropsin (bRRH, bottom right). The crystal structures of bRho*, bOpsin, and the AlphaFold model of bRRH were superimposed to the crystal structure of bRho and depicted in surface representation. The models of bOpsin and bRRH include 11-*cis*-retinal from bRho and all-*trans*-retinal from bRho* (semitransparent sticks), for reference.

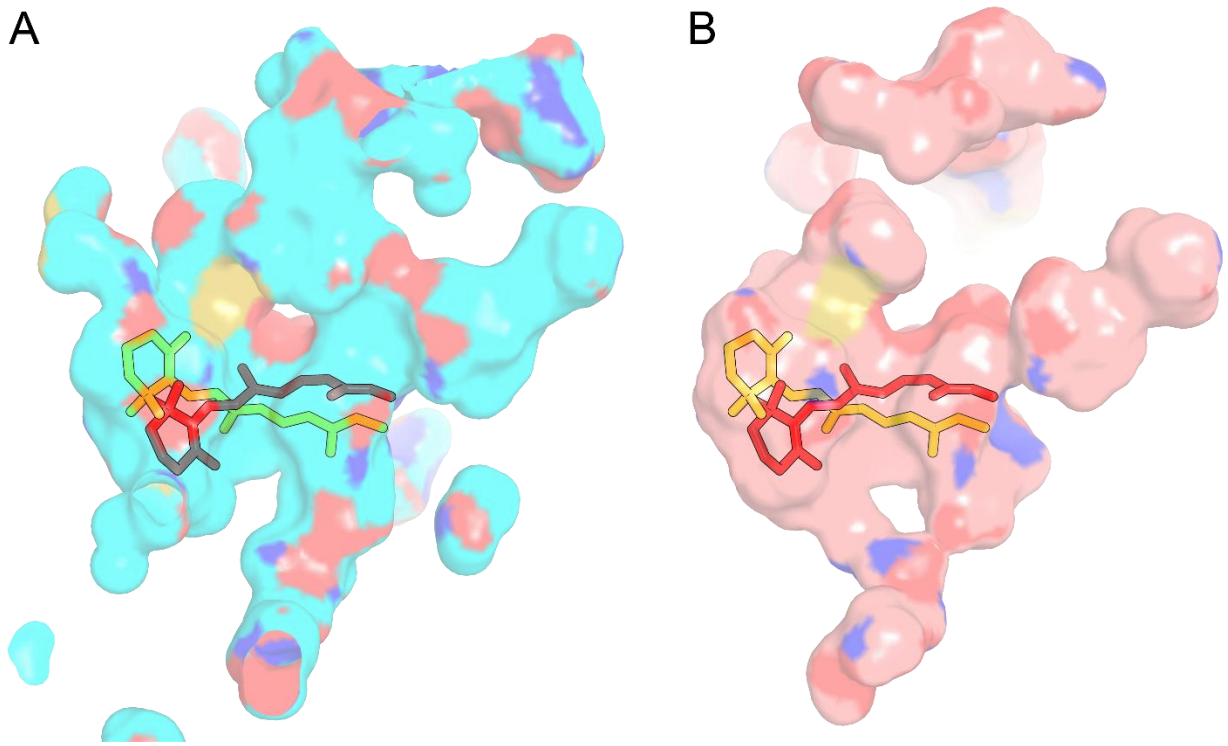

Figure 4.7 Comparison of the putative chromophore-binding pocket of vertebrate and invertebrate bRRH. AlphaFold models of bovine RRH (panel A) and *Hasarius adansoni's* RRH (panel B) are depicted in surface representation. The pocket alignment reveals that the binding pocket of bRRH is more accessible to water channels than that of HaRRH. 11-*cis*-retinal from bRho (red stick) and all-*trans*-retinal from bRho* (yellow stick) were included for reference.

CHAPTER 5

Modulating the hydrolysis of the retinylidene photoproducts of Rho and RGR

This chapter is in part derived from the manuscript published in *Journal of Biological Chemistry*:
Hong JD, Salom D, Choi EH, Tworak A, Smidak R, Gao F, Solano YJ, Zhang J, Kiser PD, Palczewski K. Retinylidene chromophore hydrolysis from mammalian visual and non-visual opsins. ***Journal of Biological Chemistry***. 2024 Jan 23:105678. doi: 10.1016/j.jbc.2024.105678. PMID: 38272218

The nanobody-mediated attenuation of Rho* Schiff base hydrolysis of its all-*trans*-retinylidene adduct was derived from contributions as co-author of manuscript published in *Nature Communications*:
Wu A*, Salom D*, **Hong JD**, Tworak A, Watanabe K, Pardon E, Steyaert J, Kandori H, Katayama K, Kiser PD, Palczewski K. Structural basis for the allosteric modulation of rhodopsin by nanobody binding to its extracellular domain. ***Nature Communications***. 2023 Aug 25;14(1):5209. doi: 10.1038/s41467-023-40911-9. PMID: 37626045

5.1 Introduction and Significance

Rhodopsin is a prototypical G-protein coupled receptor (GPCR), whose activity is triggered by light. This light sensitive property is owed to its covalently bound prosthetic ligand, namely the 11-*cis*-retinylidene chromophore, which undergoes photoisomerization to the all-*trans*-retinylidene agonist. The resultant Rho* undergoes a complex sequence of conformational changes to relax the opsin structure in response to the significant change in the rigid polyene ligand structure, accommodating the newly formed all-*trans* agonist. Rho* transitions through various short-lived intermediates before entering its MII signaling state, in the following order as shown in Figure 1.3: bathorhodopsin (λ_{max} = 543 nm), lumirhodopsin (λ_{max} = 497 nm), MI (λ_{max} = 478 nm), and MII (λ_{max} = 380 nm). MIII (λ_{max} = 465 nm) is reached via *anti-syn* isomerization of the retinylidene Schiff base. MII, the signaling state of Rho*, exists as the dominant species under physiological pH and triggers the phototransduction cascade by activation of transducin, the G-protein of rhodopsin. MII also has been shown to be the species that primarily engages in the hydrolysis of the all-*trans*-retinylidene Schiff base.[34, 35, 43, 44]

The light-triggered formation of agonist results in a series of spectrally discernable intermediates of Rho* before eventually achieving the fully activated state. Differences in the interactions between residues of the chromophore binding pocket and the polyene chain of the all-*trans*-retinylidene agonist result in differences in the absorbance properties between each Rho* intermediate. Deciphering the process of Rho activation provides a framework to understanding how GPCRs enter their signaling state upon binding agonist. This understanding began to be resolved at the atomic level with the crystal structure of ground-state rhodopsin, representing the first membrane protein and GPCR to be

structurally characterized.[31, 32] The pursuit of the structure of Rho* proved greatly challenging due to the susceptibility of the all-*trans*-retinylidene agonist to hydrolysis.[15, 33] The potential structure of the MII signaling state was determined, along with its complex with the C-terminal peptide fragment of transducin.[34, 37] Recent methodological advances have allowed for the capture of the crystal structure of a very early intermediate of Rho*. Within picoseconds after light exposure, microcrystals of Rho grown in lipidic cubic phase (LCP) were studied by X-ray diffraction for analysis and determination of the crystal structure of bathorhodopsin.[36]

Recently, camelid nanobodies were developed by the Palczewski group that stabilized early intermediates of Rho*.[195] A crystal structure between Rho* and nb2, one of several nanobodies found to bind Rho, was achieved, and was biochemically shown to be an intermediate resembling either a Lumi or MI state.[195] The MI-like state was stabilized by nb2 in detergent micelles, as demonstrated by UV-Vis spectroscopy showing an absorption maximum of around 478 nm. Using fourier transform infrared spectroscopy, nb2 was shown to stabilize the lumi-like state in native membranes. The complex between nb2 and rhodopsin showed interactions with the native glycans and residues of the N-terminus, as well as with extracellular loop2 (Figure 5.1A).[195] This binding interaction was shown to inhibit the formation of the MII signaling state of Rho* by preventing the intracellular outward movement of helices five and six, necessary across all GPCRs to bind and activate G-protein.[104, 196] The breaking of the ionic lock between Arg^{135} on helix III and Glu^{247} on helix VI also necessary for GPCR activation was also prevented by nb2.

Whether hydrolysis of the all-*trans*-retinylidene Schiff base can proceed prior to the formation of MII is largely unknown, since most studies probe hydrolysis at timescales

where MII would already have predominantly formed. With Nb2 stabilizing intermediate states prior to MII, the same hydrolysis studies with Rho presented in chapter 3 and 4 were carried out in the presence of Nb2.

The Palczewski lab also developed antibodies against bRGR, shown to target the N-terminal and C-terminal regions (Appendix B, Figure S1). These antibodies developed for structural studies of bRGR, which is thus far the only monostable mammalian opsin known to take all-*trans*-retinal as its chromophore and engage in *trans*-*cis* photochemistry. It is largely unknown if these antibodies can contribute to the stabilization of any particular intermediates of bRGR* prior to the hydrolytic release of 11-*cis*-retinal, similar to the behavior of Nb2. Therefore, hydrolysis studies were also performed for bRGR in the presence of antibodies to see whether the N- or C-terminus modulates progression through photo-intermediates and the subsequent rapid hydrolytic release of 11-*cis*-retinal.

5.2 Results

5.2.1 Nb2 binding of bRho* inhibits the Schiff base hydrolysis of its agonist.

Since the extracellular side of bRho is intralumenal in ROS, bRho was solubilized in DDM to expose the extracellular surface to Nb2 binding. Using our published LC-MS/MS based method described in chapters 3 and 4, the Schiff base hydrolysis of agonist in bRho* was assessed with or without Nb2 present. Prior to application of this hydrolysis method, the ROS solubilized in DDM and treated with Nb2 was evaluated by absorbance spectroscopy to confirm its ability to stabilize early intermediates. Without Nb2, bRho* had the absorbance spectrum characteristic of MII; however, with Nb2, the absorbance spectrum of bRho* resembled that of MI (Figure 5.2).

Nb2 does not alter the *cis*-*trans* photochemistry of bRho, given that upon light exposure, the N$^{\varepsilon}$-11-*cis*-retinyl-Lys peak decreases as the N$^{\varepsilon}$-all-*trans*-retinyl-Lys peak increased (Figure 5.3). However, in the presence of Nb2, the extent of photoisomerization is slightly suppressed, since the resultant MI could shield ground-state bRho from light, given the broad overlapping spectra of bRho (λ_{max} = 498 nm) and MI (λ_{max} = 478 nm). This inner filter effect is not as significant with MII (λ_{max} = 380 nm), since their spectra are more largely diverged. Furthermore, another photoisomerization event could occur with MI for back-isomerization or the production of 9-*cis*-retinylidene, another form of bRho pigment, known as isorhodopsin. Accordingly, the peak of N$^{\varepsilon}$-9-*cis*-retinyl-Lys is slightly increased in Nb2-bRho complexes exposed to light (Figure 5.3). After an hour post-illumination, there was a sharp decline in N$^{\varepsilon}$-all-*trans*-retinyl-Lys signal indicative of Schiff base hydrolysis in bRho*; however, this decrease was very minor for Nb2-bRho* complexes.

Therefore, the formation of isorhodopsin from photoisomerization of early bRho* intermediates directly observed for the first time by LC-MS/MS methods, confirming spectaculation of its presence and formation by earlier studies.[197, 198] Furthermore, the Schiff base hydrolysis of agonist likely does not proceed bRho* intermediates prior to MII, like Lumi or MI, which Nb2 has been shown to stabilize.

5.2.2 Nb2 stabilizes the expression of P23H-bRho and inhibits Schiff base hydrolysis of its agonist.

Rhodopsin mutations, such as P23H, lead to protein structural instability, proteasomal degradation, endoplasmic reticulum stress, and eventual photoreceptor cell death. Given the robust expression profile of rhodopsin in rods, these mutations are often

extremely deleterious to rod photoceptors and are associated with autosomal dominant retinitis pigmentosa. The ability of Nb2 to stabilize early bRho* intermediates in a structural conformation similar to ground-state bRho, preventing the transition to the MII signalling state, suggested Nb2 potential role in stabilizing the structure of ground-state bRho in mutants of bRho.

In the same co-authored study by Wu et.al., P23H-bRho expression in HEK293S cells was reduced compared to wild-type bRho expression. With co-expression of Nb2, P23H-bRho and wild-type bRho expression were each enhance by nearly 2-fold and 1.5-fold, respectively.[195] These increases in opsin expression levels by Nb2 were comparable to that by 9-*cis*-retinal, a known molecular chaperone of bRho *via* formation of isorhodopsin pigment. Interestingly, treatment by exogenous Nb2 had no effect on wild-type or P23H-bRho expression levels, suggesting the importance of Nb2 co-expression with opsins within the cell to stabilize opsin structure as it is being produced intracellularly.[195]

Given the therapeutic potential of Nb2 as a chaperone for proper expression of bRho mutants, the subsequent effect on Schiff base hydrolysis of its agonist was assessed by LC-MS/MS. Both recombinant expressed wild-type bRho and P23H-bRho were immunopurified in DDM, followed by treatment with Nb2. As anticipated, Nb2 inhibited the hydrolysis of agonist for both wild-type bRho and P23H-bRho (Figure 5.4). For either opsin in complex with Nb2, N^{ε}-9-*cis*-retinyl-Lys peak was also enhanced with light exposure, suggesting formation with isorhodopsin with either wild-type bRho and P23H-bRho (Figure 5.4B & E).

5.2.3 Modulation of the bRGR photoproduct hydrolysis by antibodies

Monoclonal bRGR antibodies were produced from hybridoma cultures generated from murine B-cells immunized with bRGR protein (**Appendix B, Figure S1**). To study their effect on hydrolysis of the 11-*cis*-retinylidene photoproduct of bRGR, two anti-N-terminal antibodies and two anti-C-terminal antibodies (**Figure 5.5A**) were incubated with bRGR in bRPE microsomes, which were solubilized in 1% w/v LMNG to allow free access of antibodies to either side of the bRGR opsin protein. At 1 min post-illumination, the extent of hydrolytic release of the 11-*cis*-retinal photoproduct was about 67% in the presence of either of the N-terminal antibodies, compared to 81% in the absence of antibodies and 79% in the presence of either of the C-terminal antibodies (**Figure 5.5B**). Notably, the addition of LMNG at 1% w/v to solubilize RPE microsomal membranes appeared to minimally affect the extent of hydrolysis, compared to native membranes alone (**Figure 5.5C**); however, the depletion of phospholipids by 1D4 immunoaffinity purification of bRGR significantly slowed the hydrolysis (**Figure 5.5C**), as described above.

5.3 Discussion

GPCRs are central to many of our physiological responses to the environment, hormones, neurotransmitters, chemokines, etc. Accordingly, they are among the most pharmacologically targeted family of proteins to date. Recent developments in biologics have introduced the use of nanobodies, which are highly specific to not only protein sequence epitopes, but also importantly, conformational epitopes. In the co-authored study by Wu and Salom et. al., a camelid nanobody (nb2) was shown to bind N-terminal residues and glycans and extracellular loop 2. Therefore, Nb2 bound allosteric to the binding site of

chromophore and served as an antagonist, preventing progression to the MII signaling state.

Nb2 served as a chaperone, stabilizing the structure of ground-state bRho, thereby enhancing the expression of the P23H mutant. The stabilization of ground-state structure also delayed the transition to the MII signaling state, since earlier intermediates like Lumi or MI are closer in structure to the ground-state conformation. Previous studies required the use of glycerol solutions of bRho as well as ultra-cold temperatures to capture these intermediates.[39, 64] The study by Wu and Salom demonstrated that Nb2 can stabilize Lumi or MI in conditions closer to physiological pH and temperature.

The apparent inhibition by Nb2 of bRho* hydrolysis of its all-*trans*-retinylidene agonist demonstrates that hydrolysis likely does not proceed via Lumi or MI intermediates, supporting the notion that hydrolysis primarily occurs through MII. By preventing the outward motion of helices V and VI necessary to achieve MII, the influx of bulk water into the chromophore binding pocket for the hydrolysis of the all-*trans*-retinylidene Schiff base is also prevented. The observation of isorhodopsin production in Nb2-bRho complexes exposed to light directly demonstrates that isorhodopsin can be formed from *trans-cis* photoisomerization of early intermediates of bRho. Both these findings were suspected but never directly shown until recently by Wu and Salom, et. al.

Aligning with these results with nb2 are the results with bRGR N-terminal antibodies, which demonstrated the importance of the N-terminus in modulating hydrolysis of photoisomerized retinylidene product of opsins, such as bRho or bRGR in our case. Antibodies targeting the extracellular N-terminus of bRGR delayed hydrolysis, while antibodies targeting the cytosolic C-terminus of bRGR had a negligible effect on hydrolysis.

Notably, the paratope of antibodies tends to target protein sequence epitopes, whereas nanobodies target sequence and conformational epitopes. Nonetheless, both nb2 and bRGR N-terminal antibodies demonstrate that N-terminus plays a key role in the eventual Schiff base hydrolysis of the retinylidene adduct of photoactivated opsins.

As done for the nb2-bRho complex, similar studies of structural characterization of bRGR seem hopeful with N-terminal antibodies especially with its effect on delaying hydrolysis, such as that the structure of bRGR* with its 11-*cis*-retinylidene adduct intact could be studied. Structural studies of bRGR could lead to breakthroughs in our understanding of the only mammalian opsin confirmed to bind all-*trans*-retinal and engage in *trans*-*cis* photochemistry to produce 11-*cis*-retinal. Although bRGR lacks to NPXXY motif for the binding and activation of G-protein, whether it engages in similar structural conformation changes with the breaking of the ionic lock between helix III and VI, as well as the outward movement of helices V and VI.

In contrast to the nb2-bRho complex study, cryo-EM appears more practical than X-ray crystallography for the structural characterization of bRGR due to at least a couple of factors: (1) low recombinant expression of bRGR in mammalian systems, such as in HEK293S cells where it localizes to the crowded space of endoplasmic reticulum membranes, and (2) significantly lower amounts of bRGR as compared to bRho from native sources, ie. bovine eyes.

Overall, the hydrolytic release of all-*trans*-retinal by bRho* or 11-*cis*-retinal by bRGR* can be attenuated by modulation of extracellular/intraluminal topological domains, namely the N-terminal chain in both cases and extracellular loop 2 for bRho*. These observations have implications to the use of allosteric nanobodies or antibodies as

antagonists that uniquely also delay the release of agonist. Nb2 as a chaperone, stabilizing P23H expression, provide promise in the use of nanobodies as small protein chaperones to stabilize mutant opsin protein expression or unstable opsin proteins, such as cone opsins.

5.4 Materials & Methods

Instrumentation

HPLC System (Agilent 1100 Series, Santa Clara, CA); 1260 Infinity HPLC System (Agilent); Dionex Ultimate 3000 UHPLC System (Thermo Fisher Scientific, Waltham, MA); LTQ XL mass spectrometer (Thermo Fisher Scientific); Cary 50 UV-Vis Spectrophotometer (Varian, Palo Alto, CA); Isotemp 3016S Water Bath (Fisher Scientific, cat no. 13-874-28); Fiber-coupled 565-nm 9.9-mW (Min) 700-mA LED (Thorlabs, Newton, NJ, cat. no. M565F3); Fiber-coupled 530-nm 6.8-mW (Min) 1000-mA LED (Thorlabs, cat. no. M530F2); Fiber-coupled 455-nm 17-mW (Min) 1000-mA LED (Thorlabs, cat.no. M455F3); Fiber Patch Cable (Thorlabs, cat. no. M92L01); Compact T-Cube 1200-mA LED Driver with Trigger Mode (Thorlabs, cat. no. LEDD1B); Power Supply Unit with 3.5-mm Jack Connector (Thorlabs, cat. no. KPS201).

Materials

Chemicals and other materials were purchased as follows: all-*trans*-retinal (Sigma-Aldrich, St. Louis, MO, cat. no. R2500), all-*trans*-retinol (Sigma-Aldrich, cat. no. R7632); bROS (InVision Bioresources, Seattle, WA, cat. no. 98740); 2-[4-(2-hydroxyethyl)piperazin-1-yl]ethanesulfonic acid (Goldbio, St. Louis, MO, cat. no. H-400-1); 1,3-bis[tris(hydroxymethyl)methylamino]propane (Sigma-Aldrich, cat. no. B6755); calcium

chloride dihydrate (Sigma-Aldrich, cat. no. 223506); n-dodecyl-β-D-maltopyranoside sol-grade (Anatrace, Maumee, OH, cat. no. D310S); lauryl maltose neopentyl glycol (Anatrace, Maumee, OH, cat. No. NG310); (3-((3-cholamidopropyl) dimethylammonio)-1-propanesulfonate) CHAPS detergent Anagrade (Anatrace, OH, cat. no. C316); pronase (Sigma-Aldrich, cat. no. PRON-RO); proteinase K solution (Viagen Biotech, cat. no. 501-PK); Amicon Ultra-0.5 Centrifugal Filter (Millipore, Burlington, MA, cat. no. UFC503096); ACN Optima LC/MS grade (Fisher Scientific, Pittsburgh, PA, cat. no. A955); methanol Optima LC/MS grade (Fisher Scientific, cat. no. A456); isopropanol Optima LC/MS grade (Fisher Scientific, cat. no. A461); FA Optima LC/MS grade (Fisher Scientific, cat. no. A117-50); methylene chloride (HPLC grade) (Fisher Scientific, cat. no. D143); hexanes (HPLC grade) (Fisher Scientific, cat. no. H302); ethyl acetate (HPLC) (Fisher Scientific, cat. no. E195); triethylamine (HPLC) (Fisher Scientific, cat. no. O4884); dimethyl sulfoxide (Sigma-Aldrich, cat. no. D2650); N,N-dimethylformamide (Fisher Scientific, cat. no. AC327171000); diethylamine (Sigma-Aldrich, cat. no. 471216); N^{α}-[(9H-fluoren-9-ylmethoxy)carbonyl]-L-Lys hydrochloride (Fisher Scientific, cat. no. F0586); 1,2-dioleoyl-sn-glycero-3-phosphoethanolamine (Avanti Polar Lipids, Alabaster, Al, cat. no. 850725P); $NaBH_4$ (Alfa Aesar, Haverhill, MA, cat. no. 88983); $NaBD_4$ (Alfa Aesar, cat. no. 35102; 85 W 2700 K Hg light bulb (Home Depot, cat. no. EDXR-40-19); BioPureSPN C18 TARGA (nestgrp, Ipswich, MA cat. no. HEM S18R); XBridge C18 (Waters, Milford, MA, 2.1 mm X 100 mm, cat. no. 186003022); Gemini Analytical C18 (Phenomenex, Torrance, CA, 250 x 4.6 mm, cat. no. 00G-4435-E0); Gemini Preparatory C18 (Phenomenex, 250 x 10 mm, cat. no. 00G-4435-N0); Luna Preparatory Silica (Phenomenex, 250 x 21.2 mm, cat. no. 00G-4091-P0-AX).

Methods

Isolation of bROS membranes. bROS membranes were prepared from fresh bovine retinas (InVision Bioresources) using sucrose gradient isolation as described previously [122], and washed with hypotonic buffer (20 mM HEPES, pH 7.4).

Purification of recombinant Rho by immunoaffinity chromatography HEK293 cells expressing WT-bOpsin and P23H-bOpsin were cultured in 1 x p150 mm culture dishes and then pelleted down for 1D4-affinity chromatography. Immunoaffinity 1D4 resin was prepared by conjugating purified, anti-Rho antibody (1D4) to CNBr-activated Sepharose 4B beads (catalog no. 17-0430-01, Cytiva, MA, USA). Pelleted cells were washed with PBS and resuspended in hypotonic buffer (10 mM Tris, pH 7.4, 1 mM $MgCl_2$) supplemented with Roche cOmplete proteinase inhibitor cocktail (catalog no. 11697498001, Roche-Sigma-Aldrich), followed by centrifugation at 10,000 × g for 10 min at 4 °C. Then, cells were homogenized by passing through a 23-gauge syringe in a hypertonic buffer (10 mM Tris, pH 7.4, 1 mM $MgCl_2$, and 1 M NaCl), followed by centrifugation. The membrane-enriched pellets were solubilized for 2 h in the cold room in an isotonic buffer (10 mM Tris, pH 7.4, 1 mM $MgCl_2$ and 0.25 M NaCl), supplemented with 10% DDM. Then, 50 µl of 1D4-resin was added to the sample, followed by 1 h incubation in the cold room. Rho-1D4-resin mixture was loaded into a centrifuge column (catalog no. 89897, Pierce-Thermo Scientific), washed in a buffer containing 10 mM HEPES, 0.25 M NaCl, and 10% DDM, and eluted with C-terminal nonapeptide (synthesized by GenScript, NJ, USA).

LC-MS/MS based retinylidene Schiff base hydrolysis assay

Briefly, immunoaffinity-purified bRho in DDM or DDM-solubilized ROS in the absence or presence of Nb2 was illuminated with 125 μW 530-nm fiber light for 10 sec; then treated with $NaBH_4$/*i*PrOH at different time points to trap any remaining internal Schiff base-adducted chromophore. Concurrently, this treatment also isolates bRho from detergents via alcohol-induced protein precipitation, and the protein pellet is washed with methanol and water, followed by a 24 h proteolytic digestion with pronase. The proteolysis products were analyzed by LC-MS/MS to capture the amount of remaining bound chromophore via detection of the amounts of N^{ε}-retinyl-lysine.[44]

Immunization protocol and hybridoma production for antibodies against bRGR. Purified bRGR was diluted to a concentration of 1.0 mg/mL in sterile PBS. Adult female C57/B6 mice (Jackson Laboratories) at 6-8 weeks of age, were injected intraperitoneally with 100 μl of PBS containing bRGR, mixed at a 1:1 (v/v) ratio with QuickAntibody Adjuvant (Beijing BIodragon Immunotechnologies). Boosters of the same volume were injected into the mice 1,4, and 5 weeks after the initial immunization. A week after the final injection, serum titers were evaluated by ELISA. Animals producing high-titer antibody were sacrificed for hybridoma production. For the development of hybridoma and monoclonal antibody production, the ClonalCell™-HY Hybridoma kit (Stem Cell Technologies) was used according to the manufacturer's instructions. Monoclonal antibodies derived from the selected hybridoma clones were evaluated using an immunoblot of lysates of HEK293S GnTI$^-$ bRGR and immunochemistry of HEK293S GnTI$^-$ bRGR.

Effect of anti-RGR antibodies on the hydrolysis of bRGR photoproduct. Each bRGR antibody was prepared at 0.5 mg/mL with 10 mM HEPES buffer, pH 7.4. One part by volume of bRPE microsomes were mixed with one part 2 % w/v LMNG, followed by two parts 0.5 mg/mL bRGR antibody or buffer (10 mM HEPES buffer, pH 7.4). The mixture was incubated for 1 hr at room temperature. Aliquots of the mixture in a 20 °C water bath were illuminated by 10 sec of 125-uW 530-nm fiber light, then left to incubate in the dark for 1 min. The mixture was immediately placed on ice and treated with $NaBH_4$/*i*PrOH to determine extent of hydrolysis, as described above.

5.5 Figures

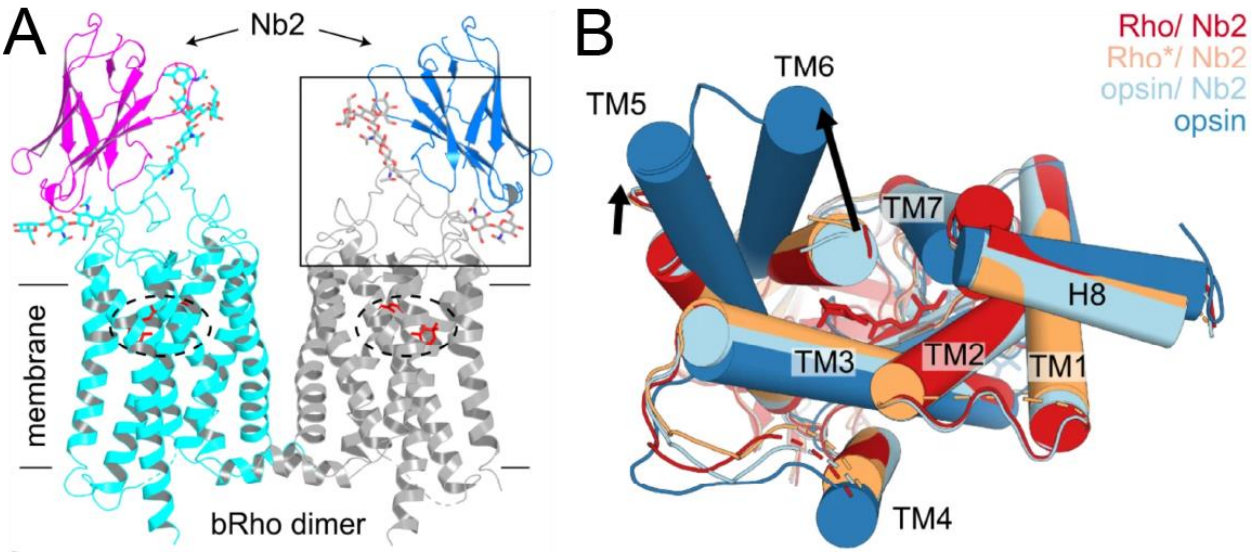

Figure 5.1 Crystal structure of Nb2 in complex with bRho and bRho*. (A) In grey and magenta is the dimer of bRho, and in magenta and blue is Nb2 bound to the extracellular side of bRho. In the dotted circle is the docked 11-*cis*-retinylidene chromophore of bRho, and in the box is Nb2 in interaction with N-terminal residues and glycans, as well as extracellular loop 2. The glycans are represented in sticks while Nb2 and bRho are represented with ribbons. (B) Superposition of the crystal structures of bRho/Nb2 (red), bRho*/Nb2 (orange), and apo-opsin/Nb2 (sky blue) complexes at 3.7 Å, 4.25 Å, and 3.7 Å resolution, respectively. The structure of apo-opsin alone (dark blue; PDB ID 5TE3) was also superimposed. Intracellular view (**e**) shows the outward movements in helices 5 and 6 (indicated by black arrows).

Figure adapted from figures 1a and 4e in Wu & Salom, et.al. 2023. [195]

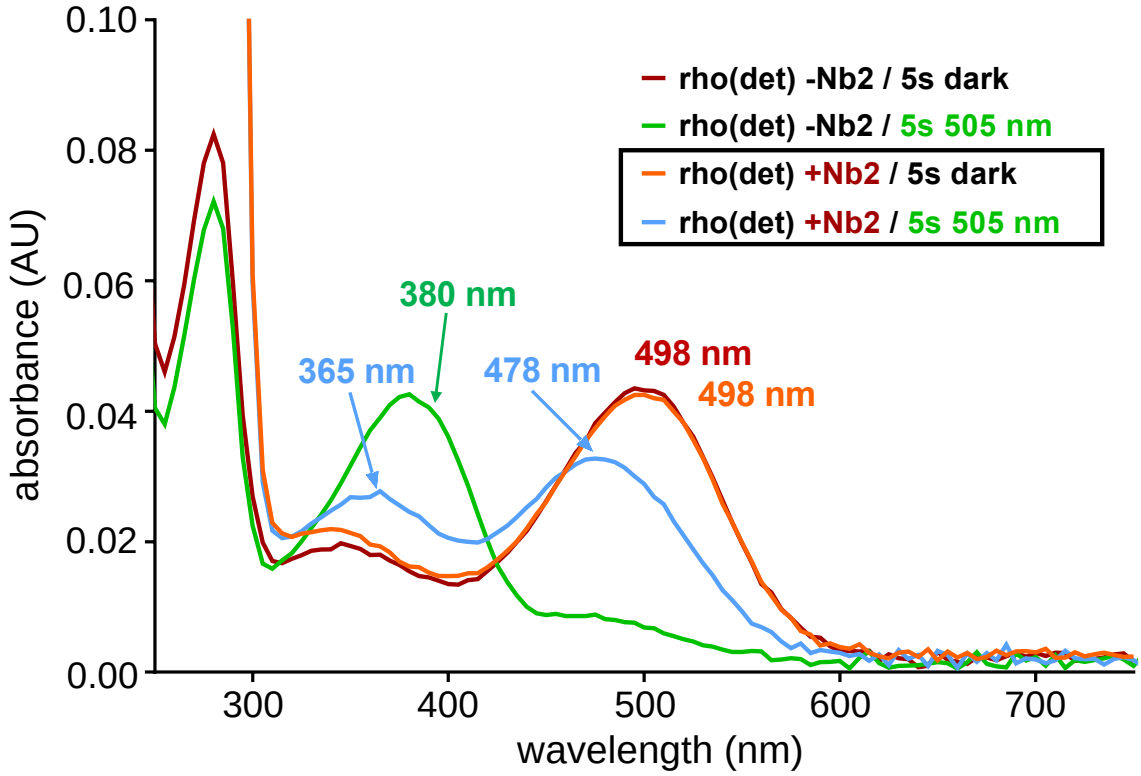

Figure 5.2 Comparison of absorbance spectrum of bRho and bRho-Nb2 complex before and after light exposure. All spectra were taken of bRho or bRho-Nb2 solubilized in DDM. Ground-state bRho with or without Nb2 in complex demonstrates the expected absorbance spectrum with a λ_{max} of 498 nm. Without Nb2, bRho* has the absorbance spectrum characteristic of MII with a λ_{max} of 380 nm. However, in the presence of Nb2, the absorbance spectrum of bRho* is shifted towards that of MI with a λ_{max} of 478 nm.

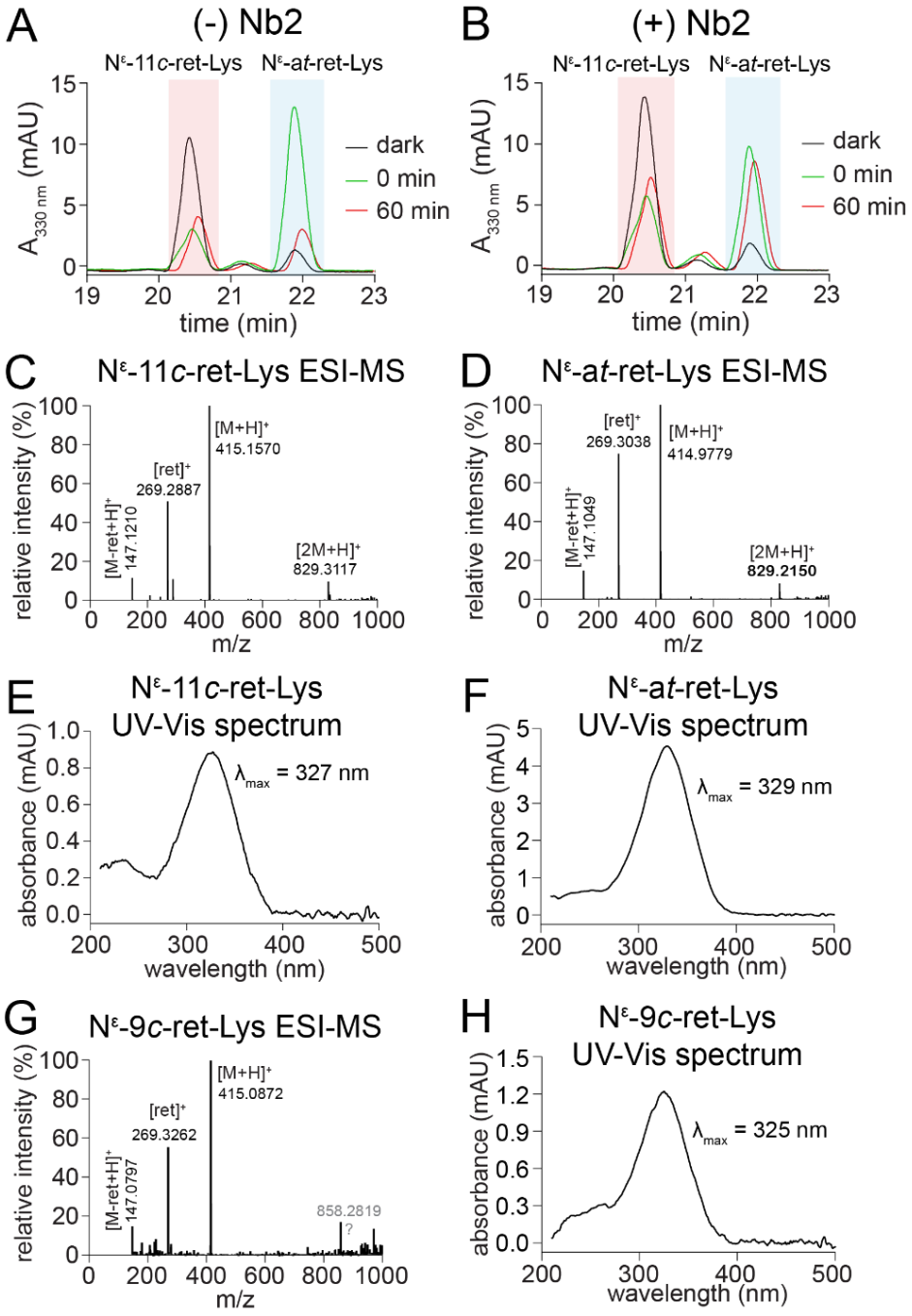

Figure 5.3 LC-MS/MS of the pronase proteolysis of the $NaBH_4$-treated bRho with or without Nb2 before and after light exposure. (A) The decrease in Nε-11-*cis*-retinyl-Lys peak and emergence of a dominant Nε-all-*trans*-retinyl-Lys peak displays the expected *cis-trans* photoisomerization. An hour after photoisomerization, the significant drop in Nε-all-

trans-retinyl-Lys signal demonstrates the bRho* hydrolysis of its all-*trans*-retinylidene agonist. (B) In the presence of Nb2, the decrease in N$^{\varepsilon}$-11-*cis*-retinyl-Lys peak and corresponding increase in N$^{\varepsilon}$-all-*trans*-retinyl-Lys peak is not nearly as dramatic as shown in panel A in the absence of Nb2. Furthermore, the drop in N$^{\varepsilon}$-all-*trans*-retinyl-Lys signal an hour after light exposure is very minor, suggesting significant inhibition of bRho* hydrolysis by Nb2. Furthermore, there is a slight increase in a peak between the 11-*cis* and all-*trans* isomer peaks after light exposure. This peak corresponds to N$^{\varepsilon}$-9-*cis*-retinyl-Lys (λ_{max} = 325 nm)[44], a byproduct of photoisomerization of early protonated all-*trans* retinylidene photointermediates.[197, 198]

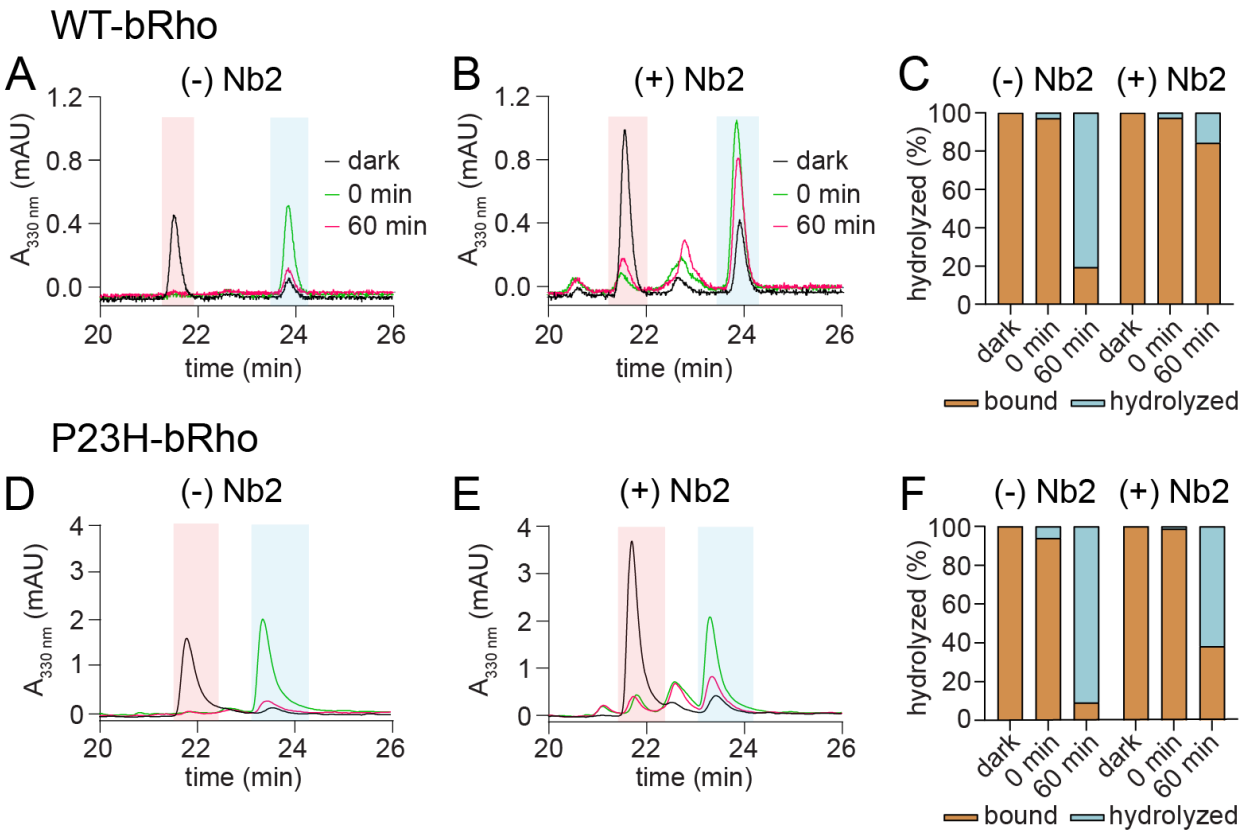

Figure 5.4 LC-MS/MS of the pronase proteolysis of the $NaBH_4$-treated wild-type or P23H-bRho with or without Nb2 before and after light exposure. (A) In the absence of Nb2, wild-type bRho exhibits the expected photochemistry and hydrolysis of its agonist. (B-C) With Nb2 present, the resultant complex has a significant reduction in the hydrolysis of the agonist. (D) In the absence of Nb2, P23H-bRho also exhibits the canonical 11-*cis* to all-*trans* photoisomerization, followed by significant hydrolysis of its agonist over the course of an hour. (E-F) With Nb2 present, the resultant complex with P23H-bRho has a significant reduction in the hydrolysis of the agonist. However, the P23H-bRho complex with Nb2 was slightly less resistant to agonist hydrolysis than wild-type bRho complex.

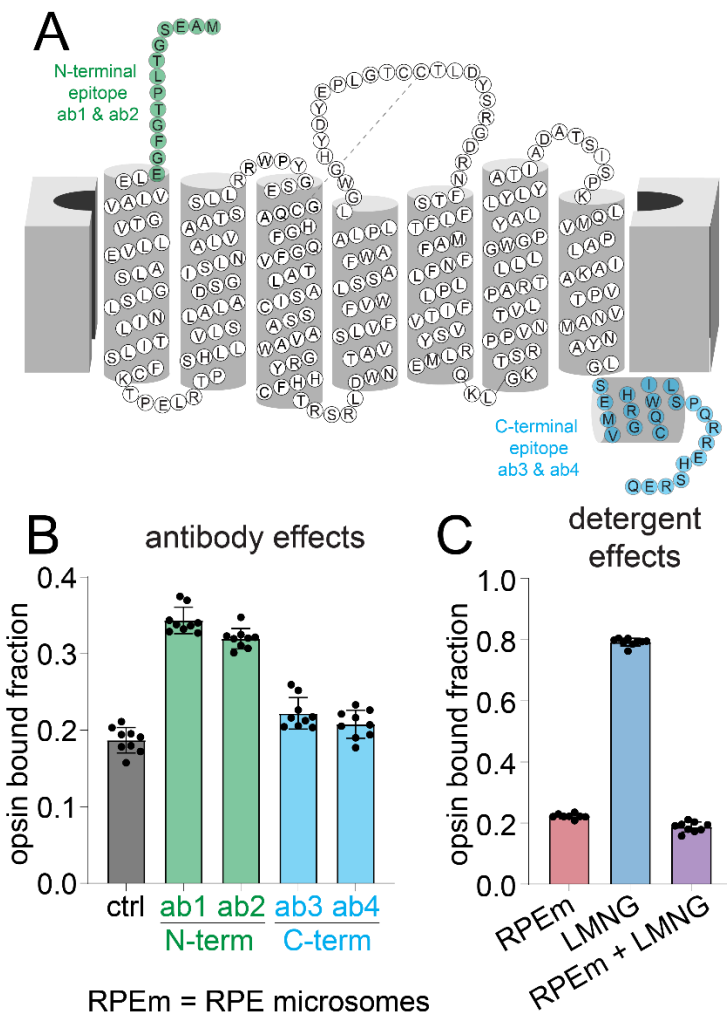

Figure 5.5 Attenuation of bRGR photoproduct hydrolysis by anti-N-terminal antibodies. (A) Epitope mapping displaying targeting of a pair of monoclonal anti-bRGR antibodies to the N-terminus (green) and another pair to the C-terminus (blue). (B) After 1 min following a 10-sec illumination with 530-nm light of bRPE microsomes solubilized in 1 % w/v LMNG, the anti-N-terminal antibodies slowed the extent of hydrolysis of the bRGR photoproduct, whereas the anti-C-terminal antibodies showed minor effect on hydrolysis. (C) The extent of hydrolysis of the 11-*cis*-retinylidene adduct was nearly unperturbed by the introduction of 1% w/v LMNG detergent to bRPE microsomes; however, the depletion of membrane lipids with immunopurification of bRGR in LMNG micelles dramatically

slowed hydrolysis. For panels (B) and (C), points represent individual replicates (n = 9), bars represent mean values, and error bars represent standard deviation.

Chapter 6

CONCLUSIONS & FUTURE DIRECTIONS

This chapter is in part derived from the manuscript published in *BioEssays*:
Hong JD, Palczewski K. A short story on how chromophore is hydrolyzed from rhodopsin for recycling. ***BioEssays***. 2023 Sep;45(9):e2300068. doi: 10.1002/bies.202300068. PMID: 37454357

6.1 Conclusions

Early descriptions of the first steps of vision were made by Müller, Böll, and Kühne, who all were part of the discovery of visual pigments and their light-induced bleaching property. Vision is sustained by maintaining levels of visual pigments in the retina, which is made possible by the opsin photocycle and visual cycle. The key step that bridges both cycles is the Schiff base hydrolysis of the all-*trans*-retinylidene agonist. Hydrolysis both supplies all-*trans*-retinal to the visual cycle to replenish 11-*cis*-retinal and frees that chromophore binding pocket for fresh 11-*cis*-retinal to regenerate rhodopsin pigment.

Prior studies of hydrolysis involved indirect measurements of bleaching rates by spectroscopic or electrophysiological measurements.[80, 162, 163] Absorbance or fluorescence spectroscopy involves solubilization of opsin proteins in detergent micelles, understood to have a deleterious effect on protein biochemistry. Our studies overcome the challenges of studying both opsin photochemistry and hydrolysis of its retinylidene adduct by leveraging the borohydride chemistry to reductively trap these adducts, allowing for analysis of their isomeric configuration as well as quantitively measure their amounts by LC-MS/MS. The preparation of borohydride in *i*PrOH allowed for immediate protein denaturation and Schiff base reduction, as well as fractionation of the protein from lipids by alcohol-induced protein precipitation and lipid solubilization. The $NaBH_4$/*i*PrOH effectively enabled opsins to be studied in any viable lipid environment, whether in detergents or in their native membrane.

Proteolysis by proteinase K of the borohydride-reduced opsin pigments and subsequent LC-MS/MS analysis of the resultant N^{ε}-retinyl-peptides can be performed to confirm the site of attachment of chromophore. LC-MS/MS analysis of the N^{ε}-retinyl-Lys

products from proteolysis by pronase demonstrated that the isomeric configuration of the retinylidene chromophore attached to the internal Lys residue can be directly determined. Accordingly, the isomeric configuration of the photoisomerized product can also be determined to demonstrate the photochemistry of opsin proteins. The subsequent decline in N^{ε}-retinyl-Lys signal at different time points following light exposure, as well as the increase in retinyl signals in the alcohol-solubilized lipid fraction demonstrate the ability to directly measure the rate of hydrolysis of photoisomerized chromophore.

This LC-MS/MS technique directly measured the hydrolysis of the all-*trans*-retinylidene agonist in bRho*, demonstrating a faster rate of reaction in ROS disc membranes than in detergent micelles. Studying hydrolysis in native membranes allowed the study of subsequent processes of N-ret-PE formation and RDH-mediated reduction of all-*trans*-retinal in the lipid fraction. Each step in the visual cycle within ROS was one order of magnitude faster than the prior. These findings have implications to how light-induced damage to the retina occurs. Intense light exposure can lead to a massive dose of all-*trans*-retinal that rapidly depletes NADPH, thereby dropping the reductive capacity of photoreceptor cells and rendering them more vulnerable to oxidative stress. Furthermore, any unreduced all-*trans*-retinal can quickly accumulate and form adducts with PE that later precipitates the production of phototoxic bisretinoids.

Our methods were than applied to other mammalian opsins involved in vision and the visual cycle, namely cone opsins, bRGR, and bRRH. The hydrolysis of photoactivated cone opsins was demonstrably much faster than that of bRho*. This faster bleaching rate of cones affirms the rapid photocycle of cone opsin, thereby a much greater demand of 11-*cis*-retinal chromophore. Our studies show that bRGR can contribute to the continuous supply

of chromophore needed to sustain photopic/color vision under bright daylight conditions. Importantly, bRGR demonstrated to be not only monostable but also very quick to hydrolyze and release 11-*cis*-retinal, especially in RPE microsomal membranes, where hydrolysis was over 6 times faster than in detergent micelles. Along with the rapid hydrolytic production of 11-*cis*-retinal, bRGR was quick to bind and form pigment with available all-*trans*-retinal. These findings show biochemical support for bRGR's role in sustaining photopic vision.

Our methods were also applicable in also showing lack of photochemical activity in the case of bRRH, an opsin in an ideal anatomical location to receive all-*trans*-retinal for photoisomerization to 11-*cis*-retinal. Our findings with bRRH demonstrates its inability to form pigment with not only all-*trans*-retinal but also any mono-*cis* isomer of retinal. Structural comparative studies display a chromophore binding pocket wide open and accessible to bulk water, suggesting a labile retinylidene Schiff base and instability with pigment formation. The role of bRRH, if any, to visual physiology remains largely unclear.

Furthermore, the allosteric modulation by nanobodies on the hydrolytic release of agonist in bRho* was directly observed by using our LC-MS/MS technique. Our findings with the nb2-bRho complex demonstrates: (1) hydrolysis likely does not proceed by intermediates prior to MII, (2) 9-*cis* configuration of isorhodopsin can be attained by photoisomerization of the early transient intermediates of bRho*, (3) extracellular/intraluminal topological domains, such as the extracellular loop 2 and N-terminal chains and glycans, modulate the hydrolysis of agonist. The allosteric modulation by N-terminal antibodies on hydrolytic release of 11-*cis*-retinal by bRGR was also observed. The findings with bRGR demonstrate the potential of targeting extracellular/intraluminal

topological domains of bRGR to better understand its unique and critical photochemistry by future structural studies.

6.2 Future Directions

Our LC-MS/MS technique demonstrated utility in the study of photochemistry and subsequent hydrolysis of chromophore for multiple opsin proteins, namely rhodopsin, cone opsins, RGR, and RRH. Given our findings, our technique can be applicable to a wide range of retinylidene opsin proteins to elucidate their photochemistry and biochemistry to better understand their role in physiology. There are nine opsin gene products encoded in the human genome, as listed in Table 6.1. Of the nine, six were studied using our technique. The remaining opsins, namely encephalopsin, melanopsin, and neuropsin, all require further investigation, especially for their reported bistability and possibly tristability in the case of melanopsin.[199-203] Other non-mammalian opsins can also be investigated, such as channelrhodopsin, essential in the field of optogenetics and as a therapeutic to restore vision *via* gene transfer to bipolar or retinal ganglion cells.[204-207]

Our study comparing hydrolysis of photoactivated cone opsins with bRho* was done with all opsins immunopurified in detergent micelles. However, a potential native source of cone opsins could be ground squirrel retinas, which exclusively possess cones expressing either M- or S-cone opsin. As such, the hydrolysis of photoactivated cone opsins can be performed on native membranes, potentially also capturing the process of N-ret-PE formation and subsequent RDH activity in cones.

Our comprehensive *in vitro* assays using LC-MS/MS to study opsins could potentially be translated *in vivo*. The method required further adjustments to allow the

reductive trapping of chromophore and isolation of a protein fraction that can be properly proteolyzed into N^{ε}-retinyl-peptides or to completion for N^{ε}-retinyl-Lys. A preliminary experiment was performed by dounce homogenization of mouse eyes in hypotonic buffer with 0.5 M $NaBH_4$. This method was adapted from the tradition retinoid analysis, which is done by dounce homogenization in 50% methanol and 50% hypotonic buffer with 100 mM NH_2OH, followed by organic-aqueous extraction of retinoids from the homogenate by addition of brine and an organic solvent, such as hexane, ethyl acetate, or ether. To the homogenate with $NaBH_4$, the unreduced $NaBH_4$ was quenched by addition of 1M HEPES pH 7.0. The homogenate was layered on top of 45% sucrose to isolate membranes containing rhodopsin by density centrifugation. The isolated membranes were washed in isotonic buffer and treated with *i*PrOH to isolate proteins from lipid membrane.

The protein fraction was then proteolyzed by pronase, then analyzed by LC-MS/MS (Figure 6.1A). The 11-*cis* to all-*trans* photochemistry was observed by analysis of mouse eyes before and after light exposure. Three camera flashes of light were insufficient to photo-isomerize most rhodopsin pigments in the eye; however, the eyes were also not dilated, which likely contributed to the insufficient extent of rhodopsin pigment photoisomerization. The hydrolysis was also halted from occurring since the experiment was performed in a cold room with the purpose of retaining as much N^{ε}-all-*trans*-retinyl-Lys as possible. Subsequent experiments should be performed with proper pupil dilation with tropicamide and phenylephrine, as well as on a 37 °C heating block for eventual experiments studying hydrolysis *in vivo*. The proteolysis by proteinase K produced N^{ε}-retinyl-peptides that confirmed that retinyl species from the pronase digest originate predominantly from rhodopsin (Figure 6.1B).

Since the current stage of the method was sufficient to detect rhodopsin and its photoisomerization, the method was tested next on RPE65$^{-/-}$ mice treated with 9-*cis*-retinyl acetate (9-*cis*-RA) to observe whether isorhodopsin can be detected. Untreated RPE65$^{-/-}$ did not possess any N$^{\varepsilon}$-retinyl-Lys signal as expected; however, upon oral gavage treatment with 9-*cis*-RA for once per day for four days in the dark, a noticeable N$^{\varepsilon}$-9-*cis*-retinyl-Lys peak was observed by LC-MS/MS (Figure 6.1C). This peak slightly decreased with 9-*cis*-RA treated mice exposed to light (one camera flash, undilated); notably, there was no increased N$^{\varepsilon}$-all-*trans*-retinyl-Lys because the mice were kept at 37 °C and eyes were collected and homogenized several minutes post-illumination. By then, most Rho* likely would have hydrolyzed its all-*trans*-retinylidene Schiff base. The treatment with 9-*cis*-RA producing isorhodopsin, detected as N$^{\varepsilon}$-9-*cis*-retinyl-Lys, was shown to be reproducible (Figure 6.1D).

To better detect hydrolysis, several more manipulations to our current method should be explored. Beyond standard anesthesia, pupil dilation, and body temperature control, the mice eyes will be immediately enucleated at various time points and flash frozen in an acetone/dry ice bath. Frozen eyes can be dounce homogenized in aqueous $NaBH_4$ buffer to reductively trap the retinylidene Schiff base, as done prior and described above. An improvement to dounce homogenization, which requires a lot of volume and could dilute our analytes, is sonication decimation, needing less than 0.5 mL to break apart tissues and cells. The buffer for the sonication decimation can include detergents to solubilize rhodopsin for separation from non-soluble choroidal material. DDM, LMNG, or CHAPS have all been excellent detergents to solubilize rhodopsin, especially DDM which firsthand had been the fastest to solubilize ROS membranes. The decimation buffer can also

include lithium dodecyl sulfate for quick denaturation of rhodopsin for faster access of $NaBH_4$ to the retinylidene Schiff base, as this property of near simultaneous denaturation and reduction was crucial to the utility of $NaBH_4$/*i*PrOH for the purposes of measuring hydrolysis.

Following decimation, the solubilized $NaBH_4$-reduced rhodopsin and retinoids can be isolated from non-soluble material by centrifugation. The $NaBH_4$-reduced rhodopsin can be isolated from $NaBH_4$-reduced retinoids and lipids/detergents by addition of *i*PrOH or EtOH to fractionate proteins from lipids *via* alcohol-induced protein precipitation. The ensuring steps of proteolysis and LC-MS/MS would be no different from what has been described by our studies. Therefore, the methods described by our studies could potentially be adapted for the investigation of hydrolysis *in vivo*. Further or different adjustments or manipulations might be required from those described here but the overall concept of leveraging rapid borohydride chemistry to trap chromophore for subsequent LC-MS/MS analysis would remain valuable to studying retinylidene Schiff base chemistry, whether hydrolysis or formation. Studying visual cycle processes, namely Rho* hydrolysis of agonist, *in vivo* would provide a much deeper understanding and accurate description of mechanisms responsible for visual physiology.

6.3 Tables and Figures

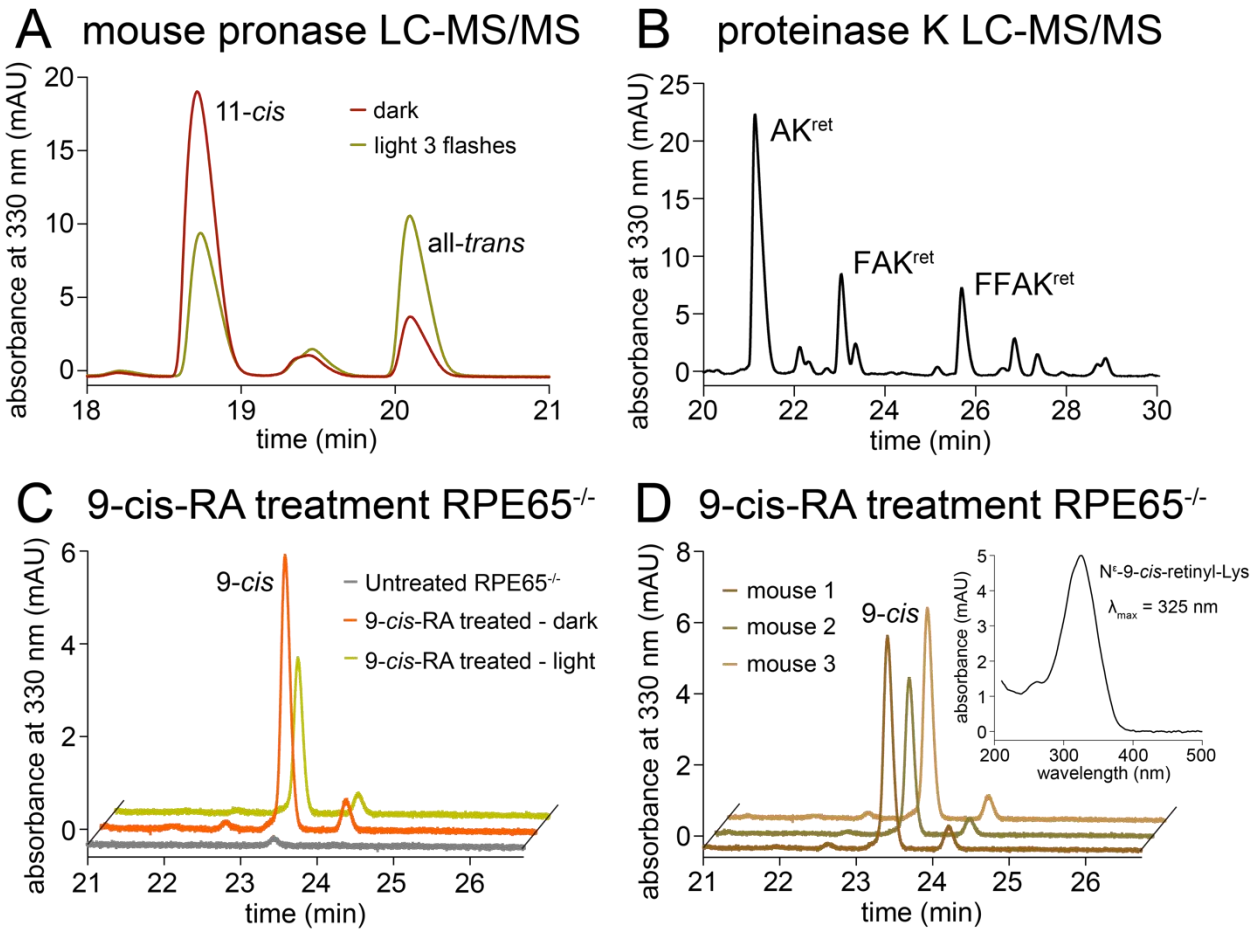

Figure 6.1 LC-MS/MS analysis of visual pigment chromophore status in mouse eyes.

(A) Pronase proteolysis of $NaBH_4$-treated rhodopsin in mouse eyes before and after light exposure. (B) Proteinase K proteolysis of $NaBH_4$-treated rhodopsin in mouse eyes validates that the retinyl signals are originating from rhodopsin. (C) 9-*cis*-RA treatment leads to isorhodopsin in RPE65$^{-/-}$ mice, as demonstrated by presence of N$^{\varepsilon}$-9-*cis*-retinyl-Lys signal that is reduced upon light exposure. (D) Reproducibility of isorhodopsin production in RPE65$^{-/-}$ mice by 9-*cis*-RA treatment. Inset of the UV-vis absorbance spectrum of the LC peak verifies its identity of N$^{\varepsilon}$-9-*cis*-retinyl-Lys with λ_{max} of 325 nm.

Table 6.1 Characteristics of opsin gene products[a].

Opsin	Gene Name	Chromophore ligand	Ground-state λ_{max} (nm)	Photoisomerized product λ_{max} (nm)	Mono-stable or Bistable	Expression Location	References
Rhodopsin	*RHO/OPN2*	11-*cis*-retinal	500	380	mono-stable	retina (PRCs)	Katayama, *et al.* 2019 [208]
Blue cone opsin	*OPN1SW*	11-*cis*-retinal	415	380	mono-stable	retina (PRCs)	Katayama, *et al.* 2019 [208]
Green cone opsin	*OPN1MW*	11-*cis*-retinal	530	380	mono-stable	retina (PRCs)	Katayama, *et al.* 2019 [208]
Red cone opsin	*OPN1LW*	11-*cis*-retinal	560	380	mono-stable	retina (PRCs)	Katayama, *et al.* 2019 [208]
Encephalopsin	*OPN3*	11-*cis*-retinal	465*	<465*	bistable	bodily; sparse in eye	Sugihara, *et al.* 2016 [201]
Melanopsin	*OPN4*	11-*cis*-retinal	470*	480*	bistable	retina (GCs)	Matsuyama, *et al.* 2012 [199]
Neuropsin	*OPN5*	11-*cis*-retinal	380	470	bistable	retina (GCs), brain, spine, testes	Kojima, *et al.* 2011 [202]
RGR	*RGR*	all-*trans*-retinal	470, 370	470, 370	mono-stable	RPE	Zhang, *et al.* 2019 [112]
Peropsin	*RRH*	all-*trans*-retinal	536**	460**	bistable	RPE	Nagata, *et al.* 2010 [170]

[a] The human genome possesses nine opsin genes, each forming pigments by Schiff base linkage to either 11-*cis*- or all-*trans*-retinal. Each opsin pigment exhibits a characteristic absorption maximum measured in the dark. Following light exposure, the photoactivated state of each opsin exhibits a new absorption maximum. Photoactivated opsins that undergo hydrolysis to release the photoisomerized retinal product are known as mono-stable or bleaching opsins, whereas those that do not undergo hydrolysis but instead produce the ground-state pigment by absorption of energy from a second photon are known as bistable opsins. Each opsin is expressed in various parts of the body, with all opsins dominantly present in the eye, except for encephalopsin.

* Measurements are from non-human vertebrate homologs: zebrafish encephalopsin and mouse melanopsin. Melanopsin reportedly exhibits tristability with an extramelanopsin state (446 nm) containing an elusive 7-*cis*-retinylidene adduct [199, 200]. In a different study involving human melanopsin, the dark-state pigment had a $\lambda_{max} \sim 470$ nm in agreement with prior studies; however, mono-stability was observed [209]. Therefore, the biochemical behavior of melanopsin remains controversial.

** Measurements are from an invertebrate peropsin homolog

Abbreviations: PRCs, photoreceptor cells; GCs, ganglion cells; RPE, retinal pigment epithelium

REFERENCES

[1] (2009) Historical Review, *Acta Ophthalmologica 13*, 13-28.
[2] Pearce, J. M. S. (2017) Samuel Thomas Soemmerring (1755-1830): The Naming of Cranial Nerves, *Eur Neurol 77*, 303-306.
[3] Stoyanov, G. S., and Matev, B. K. (2018) Samuel Thomas von Sommerring's Contributions on the Cranial Nerves and Vomeronasal Organ, *Cureus 10*, e2859.
[4] Hildebrand, R. (2005) Soemmerring's work on the nervous system: a view on brain structure and function from the late eighteenth century, *Anat Embryol (Berl) 210*, 337-342.
[5] Reese, P. D. (1986) The neglect of Purkinje's technique of ophthalmoscopy prior to Helmholtz's invention of the ophthalmoscope, *Ophthalmology 93*, 1457-1460.
[6] Mazurak, M., and Kusa, J. (2018) Jan Evangelista Purkinje: A Passion for Discovery, *Tex Heart Inst J 45*, 23-26.
[7] Werner, J. S., Gorczynska, I., and Spillmann, L. (2022) Heinrich Muller (1820-1864) and the entoptic discovery of the site in the retina where vision is initiated, *J Hist Neurosci 31*, 64-90.
[8] Kühne, F. W. (1878) *On the photochemistry of the retina and on visual purple*, Macmillan and Co., London.
[9] Falk, G., and Fatt, P. (1969) Distinctive properties of the lamellar and disk-edge structures of the rod outer segment, *J Ultrastruct Res 28*, 41-60.
[10] Rieke, F., and Baylor, D. A. (1998) Single-photon detection by rod cells of the retina, *Rev Mod Phys 70*, 1027-1036.
[11] Böll, F. (1877) On the anatomy and physiology of the retina, *Vision Res 17*, 1249-1265.
[12] Kühne, W. (1879) *Chemische vorgänge in der netzhaut*.
[13] Wald, G. (1933) Vitamin A in the retina, *Nature 132*, 316-317.
[14] Wald, G. (1935) Carotenoids and the Visual Cycle, *J Gen Physiol 19*, 351-371.
[15] Morton, R. A., and Pitt, G. A. (1955) Studies on rhodopsin. IX. pH and the hydrolysis of indicator yellow, *Biochem J 59*, 128-134.
[16] Pitt, G. A., Collins, F. D., Morton, R. A., and Stok, P. (1955) Studies on rhodopsin. VIII. Retinylidenemethylamine, an indicator yellow analogue, *Biochem J 59*, 122-128.
[17] Nakanishi, K., Balogh-Nair, V., Gawinowicz, M. A., Arnaboldi, M., Motto, M., and Honig, B. (1979) Double point charge model for visual pigments; evidence from dihydrorhodopsins, *Photochem Photobiol 29*, 657-660.
[18] Honig, B., Dinur, U., Nakanishi, K., Balogh-Nair, V., Gawinowicz, M. A., Arnaboldi, M., and Motto, M. G. (2002) An external point-charge model for wavelength regulation in visual pigments, *Journal of the American Chemical Society 101*, 7084-7086.
[19] Oroshnik, W., Brown, P. K., Hubbard, R., and Wald, G. (1956) Hindered cis isomers of vitamin A and retinene: the structure of the neo-b isomer, *Proc Natl Acad Sci U S A 42*, 578-580.
[20] Bownds, D., and Wald, G. (1965) Reaction of the rhodopsin chromophore with sodium borohydride, *Nature 205*, 254-257.
[21] Bownds, D. (1967) Site of attachment of retinal in rhodopsin, *Nature 216*, 1178-1181.
[22] Ovchinnikov, Y. A. (1982) Rhodopsin and bacteriorhodopsin: structure-function relationships, *FEBS Letters 148*, 179-191.

[23] Hargrave, P. A., McDowell, J. H., Curtis, D. R., Wang, J. K., Juszczak, E., Fong, S. L., Rao, J. K., and Argos, P. (1983) The structure of bovine rhodopsin, *Biophys Struct Mech 9*, 235-244.
[24] Nathans, J. (1990) Determinants of visual pigment absorbance: identification of the retinylidene Schiff's base counterion in bovine rhodopsin, *Biochemistry 29*, 9746-9752.
[25] Sakmar, T. P., Franke, R. R., and Khorana, H. G. (1989) Glutamic acid-113 serves as the retinylidene Schiff base counterion in bovine rhodopsin, *Proc Natl Acad Sci U S A 86*, 8309-8313.
[26] Sakmar, T. P., Franke, R. R., and Khorana, H. G. (1991) The role of the retinylidene Schiff base counterion in rhodopsin in determining wavelength absorbance and Schiff base pKa, *Proc Natl Acad Sci U S A 88*, 3079-3083.
[27] Zhukovsky, E. A., and Oprian, D. D. (1989) Effect of carboxylic acid side chains on the absorption maximum of visual pigments, *Science 246*, 928-930.
[28] Jager, F., Fahmy, K., Sakmar, T. P., and Siebert, F. (1994) Identification of glutamic acid 113 as the Schiff base proton acceptor in the metarhodopsin II photointermediate of rhodopsin, *Biochemistry 33*, 10878-10882.
[29] Ludeke, S., Beck, M., Yan, E. C., Sakmar, T. P., Siebert, F., and Vogel, R. (2005) The role of Glu181 in the photoactivation of rhodopsin, *J Mol Biol 353*, 345-356.
[30] Yan, E. C., Kazmi, M. A., Ganim, Z., Hou, J. M., Pan, D., Chang, B. S., Sakmar, T. P., and Mathies, R. A. (2003) Retinal counterion switch in the photoactivation of the G protein-coupled receptor rhodopsin, *Proc Natl Acad Sci U S A 100*, 9262-9267.
[31] Palczewski, K., Kumasaka, T., Hori, T., Behnke, C. A., Motoshima, H., Fox, B. A., Le Trong, I., Teller, D. C., Okada, T., Stenkamp, R. E., Yamamoto, M., and Miyano, M. (2000) Crystal structure of rhodopsin: a G protein-coupled receptor, *Science 289*, 739-745.
[32] Okada, T., Le Trong, I., Fox, B. A., Behnke, C. A., Stenkamp, R. E., and Palczewski, K. (2000) X-Ray diffraction analysis of three-dimensional crystals of bovine rhodopsin obtained from mixed micelles, *J Struct Biol 130*, 73-80.
[33] Blazynski, C., and Ostroy, S. E. (1984) Pathways in the hydrolysis of vertebrate rhodopsin, *Vision Res 24*, 459-470.
[34] Choe, H. W., Kim, Y. J., Park, J. H., Morizumi, T., Pai, E. F., Krauss, N., Hofmann, K. P., Scheerer, P., and Ernst, O. P. (2011) Crystal structure of metarhodopsin II, *Nature 471*, 651-655.
[35] Salom, D., Lodowski, D. T., Stenkamp, R. E., Le Trong, I., Golczak, M., Jastrzebska, B., Harris, T., Ballesteros, J. A., and Palczewski, K. (2006) Crystal structure of a photoactivated deprotonated intermediate of rhodopsin, *Proc Natl Acad Sci U S A 103*, 16123-16128.
[36] Gruhl, T., Weinert, T., Rodrigues, M. J., Milne, C. J., Ortolani, G., Nass, K., Nango, E., Sen, S., Johnson, P. J. M., Cirelli, C., Furrer, A., Mous, S., Skopintsev, P., James, D., Dworkowski, F., Bath, P., Kekilli, D., Ozerov, D., Tanaka, R., Glover, H., Bacellar, C., Brunle, S., Casadei, C. M., Diethelm, A. D., Gashi, D., Gotthard, G., Guixa-Gonzalez, R., Joti, Y., Kabanova, V., Knopp, G., Lesca, E., Ma, P., Martiel, I., Muhle, J., Owada, S., Pamula, F., Sarabi, D., Tejero, O., Tsai, C. J., Varma, N., Wach, A., Boutet, S., Tono, K., Nogly, P., Deupi, X., Iwata, S., Neutze, R., Standfuss, J., Schertler, G., and Panneels, V. (2023) Ultrafast structural changes direct the first molecular events of vision, *Nature 615*, 939-944.

[37] Standfuss, J., Edwards, P. C., D'Antona, A., Fransen, M., Xie, G., Oprian, D. D., and Schertler, G. F. (2011) The structural basis of agonist-induced activation in constitutively active rhodopsin, *Nature 471*, 656-660.
[38] Lythgoe, R. J. (1937) The absorption spectra of visual purple and of indicator yellow, *J Physiol 89*, 331-358.
[39] Wright, W. E., Brown, P. K., and Wald, G. (1973) Orientation of intermediates in the bleaching of shear-oriented rhodopsin, *J Gen Physiol 62*, 509-522.
[40] Vogel, R., Ludeke, S., Radu, I., Siebert, F., and Sheves, M. (2004) Photoreactions of metarhodopsin III, *Biochemistry 43*, 10255-10264.
[41] Bartl, F. J., and Vogel, R. (2007) Structural and functional properties of metarhodopsin III: recent spectroscopic studies on deactivation pathways of rhodopsin, *Phys Chem Chem Phys 9*, 1648-1658.
[42] Ritter, E., Elgeti, M., Hofmann, K. P., and Bartl, F. J. (2007) Deactivation and proton transfer in light-induced metarhodopsin II/metarhodopsin III conversion: a time-resolved fourier transform infrared spectroscopic study, *J Biol Chem 282*, 10720-10730.
[43] Sato, K., Morizumi, T., Yamashita, T., and Shichida, Y. (2010) Direct observation of the pH-dependent equilibrium between metarhodopsins I and II and the pH-independent interaction of metarhodopsin II with transducin C-terminal peptide, *Biochemistry 49*, 736-741.
[44] Hong, J. D., Salom, D., Kochman, M. A., Kubas, A., Kiser, P. D., and Palczewski, K. (2022) Chromophore hydrolysis and release from photoactivated rhodopsin in native membranes, *Proc Natl Acad Sci U S A 119*, e2213911119.
[45] Downer, N. W., and Englander, S. W. (1977) Hydrogen exchange study of membrane-bound rhodopsin. I. Protein structure, *J Biol Chem 252*, 8092-8100.
[46] Angel, T. E., Gupta, S., Jastrzebska, B., Palczewski, K., and Chance, M. R. (2009) Structural waters define a functional channel mediating activation of the GPCR, rhodopsin, *Proc Natl Acad Sci U S A 106*, 14367-14372.
[47] Angel, T. E., Chance, M. R., and Palczewski, K. (2009) Conserved waters mediate structural and functional activation of family A (rhodopsin-like) G protein-coupled receptors, *Proc Natl Acad Sci U S A 106*, 8555-8560.
[48] Nagata, T., Terakita, A., Kandori, H., Shichida, Y., and Maeda, A. (1998) The hydrogen-bonding network of water molecules and the peptide backbone in the region connecting Asp83, Gly120, and Glu113 in bovine rhodopsin, *Biochemistry 37*, 17216-17222.
[49] Furutani, Y., Shibata, M., and Kandori, H. (2005) Strongly hydrogen-bonded water molecules in the Schiff base region of rhodopsins, *Photochem Photobiol Sci 4*, 661-666.
[50] Andruniow, T., and Olivucci, M. (2009) How does the relocation of internal water affect resonance Raman spectra of rhodopsin? An insight from CASSCF/Amber calculations, *J Chem Theory Comput 5*, 3096-3104.
[51] Sekharan, S. (2009) Water-mediated spectral shifts in rhodopsin and bathorhodopsin, *Photochem Photobiol 85*, 517-520.
[52] Sekharan, S., Mooney, V. L., Rivalta, I., Kazmi, M. A., Neitz, M., Neitz, J., Sakmar, T. P., Yan, E. C., and Batista, V. S. (2013) Spectral tuning of ultraviolet cone pigments: an interhelical lock mechanism, *J Am Chem Soc 135*, 19064-19067.

[53] Collette, F., Renger, T., Muh, F., and Schmidt Am Busch, M. (2018) Red/Green color tuning of visual rhodopsins: electrostatic theory provides a quantitative explanation, *J Phys Chem B 122*, 4828-4837.
[54] Nikolaev, D. M., Shtyrov, A. A., Mereshchenko, A. S., Panov, M. S., Tveryanovich, Y. S., and Ryazantsev, M. N. (2020) An assessment of water placement algorithms in quantum mechanics/molecular mechanics modeling: the case of rhodopsins' first spectral absorption band maxima, *Phys Chem Chem Phys 22*, 18114-18123.
[55] Katayama, K., Furutani, Y., Imai, H., and Kandori, H. (2012) Protein-bound water molecules in primate red- and green-sensitive visual pigments, *Biochemistry 51*, 1126-1133.
[56] Buss, V., Sugihara, M., Entel, P., and Hafner, J. (2003) Thr94 and Wat2b effect protonation of the retinal chromophore in rhodopsin, *Angew Chem Int Ed Engl 42*, 3245-3247.
[57] Zhu, L., Jang, G. F., Jastrzebska, B., Filipek, S., Pearce-Kelling, S. E., Aguirre, G. D., Stenkamp, R. E., Acland, G. M., and Palczewski, K. (2004) A naturally occurring mutation of the opsin gene (T4R) in dogs affects glycosylation and stability of the G protein-coupled receptor, *J Biol Chem 279*, 53828-53839.
[58] Katayama, K., Takeyama, Y., Enomoto, A., Imai, H., and Kandori, H. (2020) Disruption of hydrogen-bond network in rhodopsin mutations cause night blindness, *J Mol Biol 432*, 5378-5389.
[59] Janz, J. M., and Farrens, D. L. (2004) Role of the retinal hydrogen bond network in rhodopsin Schiff base stability and hydrolysis, *J Biol Chem 279*, 55886-55894.
[60] Orban, T., Gupta, S., Palczewski, K., and Chance, M. R. (2010) Visualizing water molecules in transmembrane proteins using radiolytic labeling methods, *Biochemistry 49*, 827-834.
[61] Bertalan, E., Lesca, E., Schertler, G. F. X., and Bondar, A. N. (2021) C-graphs tool with graphical user interface to dissect conserved hydrogen-bond networks: applications to visual rhodopsins, *J Chem Inf Model 61*, 5692-5707.
[62] Yuan, S., Filipek, S., Palczewski, K., and Vogel, H. (2014) Activation of G-protein-coupled receptors correlates with the formation of a continuous internal water pathway, *Nat Commun 5*, 4733.
[63] Blankenship, E., Vahedi-Faridi, A., and Lodowski, D. T. (2015) The high-resolution structure of activated opsin reveals a conserved solvent network in the transmembrane region essential for activation, *Structure 23*, 2358-2364.
[64] Sandberg, M. N., Greco, J. A., Wagner, N. L., Amora, T. L., Ramos, L. A., Chen, M. H., Knox, B. E., and Birge, R. R. (2014) Low-temperature trapping of photointermediates of the rhodopsin E181Q mutant, *SOJ Biochem 1*.
[65] Maeda, A., Ohkita, Y. J., Sasaki, J., Shichida, Y., and Yoshizawa, T. (1993) Water structural changes in lumirhodopsin, metarhodopsin I, and metarhodopsin II upon photolysis of bovine rhodopsin: analysis by Fourier transform infrared spectroscopy, *Biochemistry 32*, 12033-12038.
[66] Zaitseva, E., Brown, M. F., and Vogel, R. (2010) Sequential rearrangement of interhelical networks upon rhodopsin activation in membranes: the meta II(a) conformational substate, *J Am Chem Soc 132*, 4815-4821.

[67] Chawla, U., Perera, S., Fried, S. D. E., Eitel, A. R., Mertz, B., Weerasinghe, N., Pitman, M. C., Struts, A. V., and Brown, M. F. (2021) Activation of the G-protein-coupled receptor rhodopsin by water, *Angew Chem Int Ed Engl 60*, 2288-2295.
[68] Tomobe, K., Yamamoto, E., Kholmurodov, K., and Yasuoka, K. (2017) Water permeation through the internal water pathway in activated GPCR rhodopsin, *PLoS One 12*, e0176876.
[69] Jastrzebska, B., Palczewski, K., and Golczak, M. (2011) Role of bulk water in hydrolysis of the rhodopsin chromophore, *J Biol Chem 286*, 18930-18937.
[70] Sun, X., Agren, H., and Tu, Y. (2014) Functional water molecules in rhodopsin activation, *J Phys Chem B 118*, 10863-10873.
[71] Gulati, S., Jastrzebska, B., Banerjee, S., Placeres, A. L., Miszta, P., Gao, S., Gunderson, K., Tochtrop, G. P., Filipek, S., Katayama, K., Kiser, P. D., Mogi, M., Stewart, P. L., and Palczewski, K. (2017) Photocyclic behavior of rhodopsin induced by an atypical isomerization mechanism, *Proc Natl Acad Sci U S A 114*, E2608-E2615.
[72] Lesca, E., Panneels, V., and Schertler, G. F. X. (2018) The role of water molecules in phototransduction of retinal proteins and G protein-coupled receptors, *Faraday Discuss 207*, 27-37.
[73] Bhattacharya, S., Hall, S. E., and Vaidehi, N. (2008) Agonist-induced conformational changes in bovine rhodopsin: insight into activation of G-protein-coupled receptors, *J Mol Biol 382*, 539-555.
[74] Romo, T. D., Grossfield, A., and Pitman, M. C. (2010) Concerted interconversion between ionic lock substates of the beta(2) adrenergic receptor revealed by microsecond timescale molecular dynamics, *Biophys J 98*, 76-84.
[75] Baumann, C. (1970) Flash photolysis of rhodopsin in the isolated frog retina, *Vision Res 10*, 789-798.
[76] Baumann, C., and Bender, S. (1973) Kinetics of rhodopsin bleaching in the isolated human retina, *J Physiol 235*, 761-773.
[77] Kuwayama, S., Imai, H., Morizumi, T., and Shichida, Y. (2005) Amino acid residues responsible for the meta-III decay rates in rod and cone visual pigments, *Biochemistry 44*, 2208-2215.
[78] Farrens, D. L., and Khorana, H. G. (1995) Structure and function in rhodopsin. Measurement of the rate of metarhodopsin II decay by fluorescence spectroscopy, *J Biol Chem 270*, 5073-5076.
[79] Schafer, C. T., Fay, J. F., Janz, J. M., and Farrens, D. L. (2016) Decay of an active GPCR: conformational dynamics govern agonist rebinding and persistence of an active, yet empty, receptor state, *Proc Natl Acad Sci U S A 113*, 11961-11966.
[80] Xu, J., Dodd, R. L., Makino, C. L., Simon, M. I., Baylor, D. A., and Chen, J. (1997) Prolonged photoresponses in transgenic mouse rods lacking arrestin, *Nature 389*, 505-509.
[81] Chen, C. K., Burns, M. E., Spencer, M., Niemi, G. A., Chen, J., Hurley, J. B., Baylor, D. A., and Simon, M. I. (1999) Abnormal photoresponses and light-induced apoptosis in rods lacking rhodopsin kinase, *Proc Natl Acad Sci U S A 96*, 3718-3722.
[82] Anderson, R. E., and Maude, M. B. (1970) Phospholipids of bovine outer segments, *Biochemistry 9*, 3624-3628.
[83] Park, J. H., Morizumi, T., Li, Y., Hong, J. E., Pai, E. F., Hofmann, K. P., Choe, H. W., and Ernst, O. P. (2013) Opsin, a structural model for olfactory receptors?, *Angew Chem Int Ed Engl 52*, 11021-11024.

[84] Chen, S., Getter, T., Salom, D., Wu, D., Quetschlich, D., Chorev, D. S., Palczewski, K., and Robinson, C. V. (2022) Capturing a rhodopsin receptor signalling cascade across a native membrane, *Nature 604*, 384-390.
[85] Schadel, S. A., Heck, M., Maretzki, D., Filipek, S., Teller, D. C., Palczewski, K., and Hofmann, K. P. (2003) Ligand channeling within a G-protein-coupled receptor. The entry and exit of retinals in native opsin, *J Biol Chem 278*, 24896-24903.
[86] Wald, G., and Hubbard, R. (1949) The reduction of retinene1 to vitamina A1 in vitro, *J Gen Physiol 32*, 367-389.
[87] v. Euler, H., Karrer, P., Klussmann, E., and Morf, R. (2004) Spektrometrische Messungen an Carotinoiden, *Helvetica Chimica Acta 15*, 502-507.
[88] Wald, G. (1968) Molecular basis of visual excitation, *Science 162*, 230-239.
[89] Berman, E. R., Segal, N., and Feeney, L. (1979) Subcellular distribution of free and esterified forms of vitamin A in the pigment epithelium of the retina and in liver, *Biochim Biophys Acta 572*, 167-177.
[90] Berman, E. R., Segal, N., Schneider, A., and Feeney, L. (1980) An hypothesis for a vitamin A cycle in the pigment epithelium of bovine retina, *Neurochem Int 1C*, 113-122.
[91] Berman, E. R., Horowitz, J., Segal, N., Fisher, S., and Feeney-Burns, L. (1980) Enzymatic esterification of vitamin A in the pigment epithelium of bovine retina, *Biochim Biophys Acta 630*, 36-46.
[92] Baker, B. N., Moriya, M., Maude, M. B., Anderson, R. E., and Williams, T. P. (1986) Oil droplets of the retinal epithelium of the rat, *Exp Eye Res 42*, 547-557.
[93] Trehan, A., Canada, F. J., and Rando, R. R. (1990) Inhibitors of retinyl ester formation also prevent the biosynthesis of 11-cis-retinol, *Biochemistry 29*, 309-312.
[94] Bernstein, P. S., Law, W. C., and Rando, R. R. (1987) Biochemical characterization of the retinoid isomerase system of the eye, *J Biol Chem 262*, 16848-16857.
[95] Barry, R. J., Canada, F. J., and Rando, R. R. (1989) Solubilization and partial purification of retinyl ester synthetase and retinoid isomerase from bovine ocular pigment epithelium, *J Biol Chem 264*, 9231-9238.
[96] Redmond, T. M., Yu, S., Lee, E., Bok, D., Hamasaki, D., Chen, N., Goletz, P., Ma, J. X., Crouch, R. K., and Pfeifer, K. (1998) Rpe65 is necessary for production of 11-cis-vitamin A in the retinal visual cycle, *Nat Genet 20*, 344-351.
[97] Marlhens, F., Bareil, C., Griffoin, J. M., Zrenner, E., Amalric, P., Eliaou, C., Liu, S. Y., Harris, E., Redmond, T. M., Arnaud, B., Claustres, M., and Hamel, C. P. (1997) Mutations in RPE65 cause Leber's congenital amaurosis, *Nat Genet 17*, 139-141.
[98] Hecht, S. (1920) Human Retinal Adaptation, *Proc Natl Acad Sci U S A 6*, 112-115.
[99] Hecht, S., Haig, C., and Chase, A. M. (1937) The influence of light adaptation on subsequent dark adaptation of the eye, *J Gen Physiol 20*, 831-850.
[100] Shen, D., Jiang, M., Hao, W., Tao, L., Salazar, M., and Fong, H. K. (1994) A human opsin-related gene that encodes a retinaldehyde-binding protein, *Biochemistry 33*, 13117-13125.
[101] Hao, W., and Fong, H. K. (1999) The endogenous chromophore of retinal G protein-coupled receptor opsin from the pigment epithelium, *J Biol Chem 274*, 6085-6090.
[102] Stenkamp, R. E., Filipek, S., Driessen, C. A., Teller, D. C., and Palczewski, K. (2002) Crystal structure of rhodopsin: a template for cone visual pigments and other G protein-coupled receptors, *Biochim Biophys Acta 1565*, 168-182.

[103] Nakamichi, H., and Okada, T. (2006) Crystallographic analysis of primary visual photochemistry, *Angew Chem Int Ed Engl 45*, 4270-4273.
[104] Nakamichi, H., and Okada, T. (2006) Local peptide movement in the photoreaction intermediate of rhodopsin, *Proc Natl Acad Sci U S A 103*, 12729-12734.
[105] Park, J. H., Scheerer, P., Hofmann, K. P., Choe, H. W., and Ernst, O. P. (2008) Crystal structure of the ligand-free G-protein-coupled receptor opsin, *Nature 454*, 183-187.
[106] Okada, T., Fujiyoshi, Y., Silow, M., Navarro, J., Landau, E. M., and Shichida, Y. (2002) Functional role of internal water molecules in rhodopsin revealed by X-ray crystallography, *Proc Natl Acad Sci U S A 99*, 5982-5987.
[107] Palczewski, K. (2006) G protein-coupled receptor rhodopsin, *Annu Rev Biochem 75*, 743-767.
[108] Periole, X., Ceruso, M. A., and Mehler, E. L. (2004) Acid-base equilibria in rhodopsin: dependence of the protonation state of glu134 on its environment, *Biochemistry 43*, 6858-6864.
[109] Frahmcke, J. S., Wanko, M., Phatak, P., Mroginski, M. A., and Elstner, M. (2010) The protonation state of Glu181 in rhodopsin revisited: interpretation of experimental data on the basis of QM/MM calculations, *J Phys Chem B 114*, 11338-11352.
[110] Sandberg, M. N., Amora, T. L., Ramos, L. S., Chen, M. H., Knox, B. E., and Birge, R. R. (2011) Glutamic acid 181 is negatively charged in the bathorhodopsin photointermediate of visual rhodopsin, *J Am Chem Soc 133*, 2808-2811.
[111] Yan, E. C., Kazmi, M. A., De, S., Chang, B. S., Seibert, C., Marin, E. P., Mathies, R. A., and Sakmar, T. P. (2002) Function of extracellular loop 2 in rhodopsin: glutamic acid 181 modulates stability and absorption wavelength of metarhodopsin II, *Biochemistry 41*, 3620-3627.
[112] Zhang, J., Choi, E. H., Tworak, A., Salom, D., Leinonen, H., Sander, C. L., Hoang, T. V., Handa, J. T., Blackshaw, S., Palczewska, G., Kiser, P. D., and Palczewski, K. (2019) Photic generation of 11-cis-retinal in bovine retinal pigment epithelium, *J Biol Chem 294*, 19137-19154.
[113] Robinson, P. R., Buczylko, J., Ohguro, H., and Palczewski, K. (1994) Opsins with mutations at the site of chromophore attachment constitutively activate transducin but are not phosphorylated by rhodopsin kinase, *Proc Natl Acad Sci U S A 91*, 5411-5415.
[114] Futterman, S., and Rollins, M. H. (1973) The catalytic isomerization of all-trans-retinal to 9-cis-retinal and 13-cis-retinal, *J Biol Chem 248*, 7773-7779.
[115] Brown, H. C., Mead, E. J., and Rao, B. C. S. (1955) A Study of Solvents for Sodium Borohydride and the Effect of Solvent and the Metal Ion on Borohydride Reductions1, *Journal of the American Chemical Society 77*, 6209-6213.
[116] Brown, H. C., and Ichikawa, K. (1961) The Influence of Solvent and Metal Ion on the Rate of Reaction of Alkali Metal Borohydrides with Acetone1, *Journal of the American Chemical Society 83*, 4372-4374.
[117] Van Breemen, R. B., and Huang, C. R. (1996) High-performance liquid chromatography-electrospray mass spectrometry of retinoids, *FASEB J 10*, 1098-1101.
[118] van Breemen, R. B., Nikolic, D., Xu, X., Xiong, Y., van Lieshout, M., West, C. E., and Schilling, A. B. (1998) Development of a method for quantitation of retinol and retinyl palmitate in human serum using high-performance liquid chromatography-

atmospheric pressure chemical ionization-mass spectrometry, *J Chromatogr A 794*, 245-251.
[119] Wingerath, T., Kirsch, D., Spengler, B., Kaufmann, R., and Stahl, W. (1997) High-performance liquid chromatography and laser desorption/ionization mass spectrometry of retinyl esters, *Anal Chem 69*, 3855-3860.
[120] Rocchi, S., Caretti, F., Gentili, A., Curini, R., Perret, D., and Perez-Fernandez, V. (2016) Quantitative profiling of retinyl esters in milk from different ruminant species by using high performance liquid chromatography-diode array detection-tandem mass spectrometry, *Food Chem 211*, 455-464.
[121] Kahremany, S., Sander, C. L., Tochtrop, G. P., Kubas, A., and Palczewski, K. (2019) Z-isomerization of retinoids through combination of monochromatic photoisomerization and metal catalysis, *Org Biomol Chem 17*, 8125-8139.
[122] Papermaster, D. S. (1982) Preparation of retinal rod outer segments, *Methods Enzymol 81*, 48-52.
[123] McCaffery, P., Evans, J., Koul, O., Volpert, A., Reid, K., and Ullman, M. D. (2002) Retinoid quantification by HPLC/MS(n), *J Lipid Res 43*, 1143-1149.
[124] Khaksari, M., Mazzoleni, L. R., Ruan, C., Kennedy, R. T., and Minerick, A. R. (2017) Data representing two separate LC-MS methods for detection and quantification of water-soluble and fat-soluble vitamins in tears and blood serum, *Data Brief 11*, 316-330.
[125] Mitchell, D. C., Straume, M., and Litman, B. J. (1992) Role of sn-1-saturated,sn-2-polyunsaturated phospholipids in control of membrane receptor conformational equilibrium: effects of cholesterol and acyl chain unsaturation on the metarhodopsin I in equilibrium with metarhodopsin II equilibrium, *Biochemistry 31*, 662-670.
[126] Harayama, T., and Shimizu, T. (2020) Roles of polyunsaturated fatty acids, from mediators to membranes, *J Lipid Res 61*, 1150-1160.
[127] Baccouch, R., Shi, Y., Vernay, E., Mathelie-Guinlet, M., Taib-Maamar, N., Villette, S., Feuillie, C., Rascol, E., Nuss, P., Lecomte, S., Molinari, M., Staneva, G., and Alves, I. D. (2023) The impact of lipid polyunsaturation on the physical and mechanical properties of lipid membranes, *Biochim Biophys Acta Biomembr 1865*, 184084.
[128] Beharry, S., Zhong, M., and Molday, R. S. (2004) N-retinylidene-phosphatidylethanolamine is the preferred retinoid substrate for the photoreceptor-specific ABC transporter ABCA4 (ABCR), *J Biol Chem 279*, 53972-53979.
[129] Boyer, N. P., Higbee, D., Currin, M. B., Blakeley, L. R., Chen, C., Ablonczy, Z., Crouch, R. K., and Koutalos, Y. (2012) Lipofuscin and N-retinylidene-N-retinylethanolamine (A2E) accumulate in retinal pigment epithelium in absence of light exposure: their origin is 11-cis-retinal, *J Biol Chem 287*, 22276-22286.
[130] Quazi, F., Lenevich, S., and Molday, R. S. (2012) ABCA4 is an N-retinylidene-phosphatidylethanolamine and phosphatidylethanolamine importer, *Nat Commun 3*, 925.
[131] Xu, T., Molday, L., and Molday, R. (2023) Retinal-phospholipid Schiff-base conjugates and their interaction with ABCA4, the ABC transporter associated with Stargardt disease, *J Biol Chem*, 104614.

[132] Quazi, F., and Molday, R. S. (2014) ATP-binding cassette transporter ABCA4 and chemical isomerization protect photoreceptor cells from the toxic accumulation of excess 11-cis-retinal, *Proc Natl Acad Sci U S A 111*, 5024-5029.
[133] Sparrow, J. R., Wu, Y., Kim, C. Y., and Zhou, J. (2010) Phospholipid meets all-trans-retinal: the making of RPE bisretinoids, *J Lipid Res 51*, 247-261.
[134] Liu, J., Itagaki, Y., Ben-Shabat, S., Nakanishi, K., and Sparrow, J. R. (2000) The biosynthesis of A2E, a fluorophore of aging retina, involves the formation of the precursor, A2-PE, in the photoreceptor outer segment membrane, *J Biol Chem 275*, 29354-29360.
[135] Fishkin, N. E., Sparrow, J. R., Allikmets, R., and Nakanishi, K. (2005) Isolation and characterization of a retinal pigment epithelial cell fluorophore: An all-trans-retinal dimer conjugate.
[136] Sparrow, J. R., Vollmer-Snarr, H. R., Zhou, J., Jang, Y. P., Jockusch, S., Itagaki, Y., and Nakanishi, K. (2003) A2E-epoxides damage DNA in retinal pigment epithelial cells. Vitamin E and other antioxidants inhibit A2E-epoxide formation, *J Biol Chem 278*, 18207-18213.
[137] Zhou, J., Jang, Y. P., Kim, S. R., and Sparrow, J. R. (2006) Complement activation by photooxidation products of A2E, a lipofuscin constituent of the retinal pigment epithelium, *Proc Natl Acad Sci U S A 103*, 16182-16187.
[138] Wu, Y., Yanase, E., Feng, X., Siegel, M. M., and Sparrow, J. R. (2010) Structural characterization of bisretinoid A2E photocleavage products and implications for age-related macular degeneration, *Proc Natl Acad Sci U S A 107*, 7275-7280.
[139] Jin, K. H., and Sparrow, J. R. (2021) Bisretinoid phospholipid and vitamin A aldehyde: shining a light, *J Lipid Res 0*, 100042.
[140] Parish, C. A., Hashimoto, M., Nakanishi, K., Dillon, J., and Sparrow, J. (1998) Isolation and one-step preparation of A2E and iso-A2E, fluorophores from human retinal pigment epithelium, *95*, 14609-14613.
[141] Sparrow, J. R., Gregory-Roberts, E., Yamamoto, K., Blonska, A., Ghosh, S. K., Ueda, K., and Zhou, J. (2012) The bisretinoids of retinal pigment epithelium, *Prog Retin Eye Res 31*, 121-135.
[142] Jin, Q. X., Dong, X. R., Chen, J. M., Yao, K., and Wu, Y. L. (2014) Effects of organic solvents on two retinal pigment epithelial lipofuscin fluorophores, A2E and all-trans-retinal dimer, *J Zhejiang Univ Sci B 15*, 661-669.
[143] Kiser, P. D., and Palczewski, K. (2021) Pathways and disease-causing alterations in visual chromophore production for vertebrate vision, *J Biol Chem 296*, 100072.
[144] Christie, W. W., and Han, X. (2012) Lipids: their structures and occurrence, In *Lipid Analysis*, pp 3-19.
[145] Matthews, R. G., Hubbard, R., Brown, P. K., and Wald, G. (1963) Tautomeric Forms of Metarhodopsin, *J Gen Physiol 47*, 215-240.
[146] Martinez-Mayorga, K., Pitman, M. C., Grossfield, A., Feller, S. E., and Brown, M. F. (2006) Retinal counterion switch mechanism in vision evaluated by molecular simulations, *J Am Chem Soc 128*, 16502-16503.
[147] Cooper, A. (1981) Rhodopsin photoenergetics: lumirhodopsin and the complete energy profile, *FEBS Lett 123*, 324-326.

[148] Zhao, J., Ueda, K., Riera, M., Kim, H. J., and Sparrow, J. R. (2018) Bisretinoids mediate light sensitivity resulting in photoreceptor cell degeneration in mice lacking the receptor tyrosine kinase Mer, *J Biol Chem 293*, 19400-19410.
[149] Maeda, A., Golczak, M., Maeda, T., and Palczewski, K. (2009) Limited roles of Rdh8, Rdh12, and Abca4 in all-trans-retinal clearance in mouse retina, *Invest Ophthalmol Vis Sci 50*, 5435-5443.
[150] Boyer, N. P., Thompson, D. A., and Koutalos, Y. (2021) Relative Contributions of All-Trans and 11-Cis Retinal to Formation of Lipofuscin and A2E Accumulating in Mouse Retinal Pigment Epithelium, *Invest Ophthalmol Vis Sci 62*, 1.
[151] Kaylor, J. J., Xu, T., Ingram, N. T., Tsan, A., Hakobyan, H., Fain, G. L., and Travis, G. H. (2017) Blue light regenerates functional visual pigments in mammals through a retinyl-phospholipid intermediate, *Nat Commun 8*, 16.
[152] Maeda, A., Maeda, T., Golczak, M., Chou, S., Desai, A., Hoppel, C. L., Matsuyama, S., and Palczewski, K. (2009) Involvement of all-trans-retinal in acute light-induced retinopathy of mice, *J Biol Chem 284*, 15173-15183.
[153] Salom, D., Le Trong, I., Pohl, E., Ballesteros, J. A., Stenkamp, R. E., Palczewski, K., and Lodowski, D. T. (2006) Improvements in G protein-coupled receptor purification yield light stable rhodopsin crystals, *J Struct Biol 156*, 497-504.
[154] Furness, J. W., Kaplan, A. D., Ning, J., Perdew, J. P., and Sun, J. (2020) Accurate and Numerically Efficient r(2)SCAN Meta-Generalized Gradient Approximation, *J Phys Chem Lett 11*, 8208-8215.
[155] Weigend, F., and Ahlrichs, R. (2005) Balanced basis sets of split valence, triple zeta valence and quadruple zeta valence quality for H to Rn: Design and assessment of accuracy, *Phys Chem Chem Phys 7*, 3297-3305.
[156] Bannwarth, C., Ehlert, S., and Grimme, S. (2019) GFN2-xTB-An Accurate and Broadly Parametrized Self-Consistent Tight-Binding Quantum Chemical Method with Multipole Electrostatics and Density-Dependent Dispersion Contributions, *J Chem Theory Comput 15*, 1652-1671.
[157] Ehlert, S., Stahn, M., Spicher, S., and Grimme, S. (2021) Robust and Efficient Implicit Solvation Model for Fast Semiempirical Methods, *J Chem Theory Comput 17*, 4250-4261.
[158] Neese, F., Wennmohs, F., Becker, U., and Riplinger, C. (2020) The ORCA quantum chemistry program package, *J Chem Phys 152*, 224108.
[159] Bannwarth, C., Caldeweyher, E., Ehlert, S., Hansen, A., Pracht, P., Seibert, J., Spicher, S., and Grimme, S. (2020) Extended tight-binding quantum chemistry methods, *WIREs Computational Molecular Science 11*.
[160] Emeis, D., Kuhn, H., Reichert, J., and Hofmann, K. P. (1982) Complex formation between metarhodopsin II and GTP-binding protein in bovine photoreceptor membranes leads to a shift of the photoproduct equilibrium, *FEBS Lett 143*, 29-34.
[161] Hong, J. D., and Palczewski, K. (2023) A short story on how chromophore is hydrolyzed from rhodopsin for recycling, *Bioessays*, e2300068.
[162] Chen, M. H., Kuemmel, C., Birge, R. R., and Knox, B. E. (2012) Rapid release of retinal from a cone visual pigment following photoactivation, *Biochemistry 51*, 4117-4125.
[163] Shi, G., Yau, K. W., Chen, J., and Kefalov, V. J. (2007) Signaling properties of a short-wave cone visual pigment and its role in phototransduction, *J Neurosci 27*, 10084-10093.

[164] Mandelbaum, J. (1941) Dark adaptation - some physiologic and clinical considerations, *Arch Ophthalmol-Chic 26*, 203-239.
[165] Lamb, T. D. (1981) The involvement of rod photoreceptors in dark adaptation, *Vision Res 21*, 1773-1782.
[166] Lamb, T. D., and Pugh, E. N., Jr. (2006) Phototransduction, dark adaptation, and rhodopsin regeneration the proctor lecture, *Invest Ophthalmol Vis Sci 47*, 5137-5152.
[167] Morimoto, N., Nagata, T., and Inoue, K. (2023) Reversible Photoreaction of a Retinal Photoisomerase, Retinal G-Protein-Coupled Receptor RGR, *Biochemistry 62*, 1429-1432.
[168] Sun, H., Gilbert, D. J., Copeland, N. G., Jenkins, N. A., and Nathans, J. (1997) Peropsin, a novel visual pigment-like protein located in the apical microvilli of the retinal pigment epithelium, *Proc Natl Acad Sci U S A 94*, 9893-9898.
[169] Nagata, T., Koyanagi, M., Lucas, R., and Terakita, A. (2018) An all-trans-retinal-binding opsin peropsin as a potential dark-active and light-inactivated G protein-coupled receptor, *Sci Rep 8*, 3535.
[170] Nagata, T., Koyanagi, M., Tsukamoto, H., and Terakita, A. (2010) Identification and characterization of a protostome homologue of peropsin from a jumping spider, *J Comp Physiol A Neuroethol Sens Neural Behav Physiol 196*, 51-59.
[171] Tworak, A., Kolesnikov, A. V., Hong, J. D., Choi, E. H., Luu, J. C., Palczewska, G., Dong, Z., Lewandowski, D., Brooks, M. J., Campello, L., Swaroop, A., Kiser, P. D., Kefalov, V. J., and Palczewski, K. (2023) Rapid RGR-dependent visual pigment recycling is mediated by the RPE and specialized Muller glia, *Cell Rep 42*, 112982.
[172] Hubbard, R. (1958) The thermal stability of rhodopsin and opsin, *J Gen Physiol 42*, 259-280.
[173] Guo, Y., Sekharan, S., Liu, J., Batista, V. S., Tully, J. C., and Yan, E. C. (2014) Unusual kinetics of thermal decay of dim-light photoreceptors in vertebrate vision, *Proc Natl Acad Sci U S A 111*, 10438-10443.
[174] Liu, J., Liu, M. Y., Nguyen, J. B., Bhagat, A., Mooney, V., and Yan, E. C. (2009) Thermal decay of rhodopsin: role of hydrogen bonds in thermal isomerization of 11-cis retinal in the binding site and hydrolysis of protonated Schiff base, *J Am Chem Soc 131*, 8750-8751.
[175] Kiser, P. D., Kolesnikov, A. V., Kiser, J. Z., Dong, Z., Chaurasia, B., Wang, L., Summers, S. A., Hoang, T., Blackshaw, S., Peachey, N. S., Kefalov, V. J., and Palczewski, K. (2019) Conditional deletion of Des1 in the mouse retina does not impair the visual cycle in cones, *FASEB J 33*, 5782-5792.
[176] Hoang, T., Wang, J., Boyd, P., Wang, F., Santiago, C., Jiang, L., Yoo, S., Lahne, M., Todd, L. J., Jia, M., Saez, C., Keuthan, C., Palazzo, I., Squires, N., Campbell, W. A., Rajaii, F., Parayil, T., Trinh, V., Kim, D. W., Wang, G., Campbell, L. J., Ash, J., Fischer, A. J., Hyde, D. R., Qian, J., and Blackshaw, S. (2020) Gene regulatory networks controlling vertebrate retinal regeneration, *Science 370*.
[177] Lu, Y., Shiau, F., Yi, W., Lu, S., Wu, Q., Pearson, J. D., Kallman, A., Zhong, S., Hoang, T., Zuo, Z., Zhao, F., Zhang, M., Tsai, N., Zhuo, Y., He, S., Zhang, J., Stein-O'Brien, G. L., Sherman, T. D., Duan, X., Fertig, E. J., Goff, L. A., Zack, D. J., Handa, J. T., Xue, T., Bremner, R., Blackshaw, S., Wang, X., and Clark, B. S. (2020) Single-Cell Analysis of

Human Retina Identifies Evolutionarily Conserved and Species-Specific Mechanisms Controlling Development, *Dev Cell 53*, 473-491 e479.
[178] Tarttelin, E. E., Bellingham, J., Bibb, L. C., Foster, R. G., Hankins, M. W., Gregory-Evans, K., Gregory-Evans, C. Y., Wells, D. J., and Lucas, R. J. (2003) Expression of opsin genes early in ocular development of humans and mice, *Exp Eye Res 76*, 393-396.
[179] Owen, T. S., Salom, D., Sun, W., and Palczewski, K. (2018) Increasing the stability of recombinant human green cone pigment, *Biochemistry 57*, 1022-1030.
[180] Salom, D., Jin, H., Gerken, T. A., Yu, C., Huang, L., and Palczewski, K. (2019) Human red and green cone opsins are O-glycosylated at an N-terminal Ser/Thr-rich domain conserved in vertebrates, *J Biol Chem 294*, 8123-8133.
[181] Shichida, Y., Imai, H., Imamoto, Y., Fukada, Y., and Yoshizawa, T. (1994) Is chicken green-sensitive cone visual pigment a rhodopsin-like pigment? A comparative study of the molecular properties between chicken green and rhodopsin, *Biochemistry 33*, 9040-9044.
[182] Wang, J. S., and Kefalov, V. J. (2011) The cone-specific visual cycle, *Prog Retin Eye Res 30*, 115-128.
[183] Weale, R. A. (1961) Limits of human vision, *Nature 191*, 471-473.
[184] Schnapf, J. L., Nunn, B. J., Meister, M., and Baylor, D. A. (1990) Visual transduction in cones of the monkey Macaca fascicularis, *J Physiol 427*, 681-713.
[185] Cook, J. D., Ng, S. Y., Lloyd, M., Eddington, S., Sun, H., Nathans, J., Bok, D., Radu, R. A., and Travis, G. H. (2017) Peropsin modulates transit of vitamin A from retina to retinal pigment epithelium, *J Biol Chem 292*, 21407-21416.
[186] Alexander, N. S., Katayama, K., Sun, W., Salom, D., Gulati, S., Zhang, J., Mogi, M., Palczewski, K., and Jastrzebska, B. (2017) Complex binding pathways determine the regeneration of mammalian green cone opsin with a locked retinal analogue, *J Biol Chem 292*, 10983-10997.
[187] Choi, E. H., Suh, S., Sander, C. L., Hernandez, C. J. O., Bulman, E. R., Khadka, N., Dong, Z., Shi, W., Palczewski, K., and Kiser, P. D. (2018) Insights into the pathogenesis of dominant retinitis pigmentosa associated with a D477G mutation in RPE65, *Hum Mol Genet 27*, 2225-2243.
[188] Kitamura, T., Koshino, Y., Shibata, F., Oki, T., Nakajima, H., Nosaka, T., and Kumagai, H. (2003) Retrovirus-mediated gene transfer and expression cloning: powerful tools in functional genomics, *Exp Hematol 31*, 1007-1014.
[189] Chelstowska, S., Widjaja-Adhi, M. A. K., Silvaroli, J. A., and Golczak, M. (2017) Impact of LCA-Associated E14L LRAT Mutation on Protein Stability and Retinoid Homeostasis, *Biochemistry 56*, 4489-4499.
[190] Hofmann, L., Alexander, N. S., Sun, W., Zhang, J., Orban, T., and Palczewski, K. (2017) Hydrogen/Deuterium Exchange Mass Spectrometry of Human Green Opsin Reveals a Conserved Pro-Pro Motif in Extracellular Loop 2 of Monostable Visual G Protein-Coupled Receptors, *Biochemistry 56*, 2338-2348.
[191] Molday, L. L., and Molday, R. S. (2014) 1D4: a versatile epitope tag for the purification and characterization of expressed membrane and soluble proteins, *Methods Mol Biol 1177*, 1-15.
[192] Saari, J. C., and Bredberg, D. L. (1990) Acyl-CoA:retinol acyltransferase and lecithin:retinol acyltransferase activities of bovine retinal pigment epithelial microsomes, *Methods Enzymol 190*, 156-163.

[193] Varadi, M., Anyango, S., Deshpande, M., Nair, S., Natassia, C., Yordanova, G., Yuan, D., Stroe, O., Wood, G., Laydon, A., Zidek, A., Green, T., Tunyasuvunakool, K., Petersen, S., Jumper, J., Clancy, E., Green, R., Vora, A., Lutfi, M., Figurnov, M., Cowie, A., Hobbs, N., Kohli, P., Kleywegt, G., Birney, E., Hassabis, D., and Velankar, S. (2022) AlphaFold Protein Structure Database: massively expanding the structural coverage of protein-sequence space with high-accuracy models, *Nucleic Acids Res 50*, D439-D444.
[194] Jumper, J., Evans, R., Pritzel, A., Green, T., Figurnov, M., Ronneberger, O., Tunyasuvunakool, K., Bates, R., Zidek, A., Potapenko, A., Bridgland, A., Meyer, C., Kohl, S. A. A., Ballard, A. J., Cowie, A., Romera-Paredes, B., Nikolov, S., Jain, R., Adler, J., Back, T., Petersen, S., Reiman, D., Clancy, E., Zielinski, M., Steinegger, M., Pacholska, M., Berghammer, T., Bodenstein, S., Silver, D., Vinyals, O., Senior, A. W., Kavukcuoglu, K., Kohli, P., and Hassabis, D. (2021) Highly accurate protein structure prediction with AlphaFold, *Nature 596*, 583-589.
[195] Wu, A., Salom, D., Hong, J. D., Tworak, A., Watanabe, K., Pardon, E., Steyaert, J., Kandori, H., Katayama, K., Kiser, P. D., and Palczewski, K. (2023) Structural basis for the allosteric modulation of rhodopsin by nanobody binding to its extracellular domain, *Nat Commun 14*, 5209.
[196] Ahuja, S., Hornak, V., Yan, E. C., Syrett, N., Goncalves, J. A., Hirshfeld, A., Ziliox, M., Sakmar, T. P., Sheves, M., Reeves, P. J., Smith, S. O., and Eilers, M. (2009) Helix movement is coupled to displacement of the second extracellular loop in rhodopsin activation, *Nat Struct Mol Biol 16*, 168-175.
[197] Reuter, T. (1964) Formation of Isorhodopsin in the Frog's Eye during Continuous Illumination, *Nature 204*, 784-785.
[198] Catt, M., Ernst, W., and Kemp, C. M. (1983) The products of photoreversing rhodopsin bleaching by microsecond flashes in the isolated vertebrate retina, *Vision Res 23*, 971-982.
[199] Matsuyama, T., Yamashita, T., Imamoto, Y., and Shichida, Y. (2012) Photochemical properties of mammalian melanopsin, *Biochemistry 51*, 5454-5462.
[200] Emanuel, A. J., and Do, M. T. (2015) Melanopsin tristability for sustained and broadband phototransduction, *Neuron 85*, 1043-1055.
[201] Sugihara, T., Nagata, T., Mason, B., Koyanagi, M., and Terakita, A. (2016) Absorption characteristics of vertebrate non-visual opsin, Opn3, *PLoS One 11*, e0161215.
[202] Kojima, D., Mori, S., Torii, M., Wada, A., Morishita, R., and Fukada, Y. (2011) UV-sensitive photoreceptor protein OPN5 in humans and mice, *PLoS One 6*, e26388.
[203] Kojima, K., Yamashita, T., Imamoto, Y., Kusakabe, T. G., Tsuda, M., and Shichida, Y. (2017) Evolutionary steps involving counterion displacement in a tunicate opsin, *Proc Natl Acad Sci U S A 114*, 6028-6033.
[204] Bi, A., Cui, J., Ma, Y. P., Olshevskaya, E., Pu, M., Dizhoor, A. M., and Pan, Z. H. (2006) Ectopic expression of a microbial-type rhodopsin restores visual responses in mice with photoreceptor degeneration, *Neuron 50*, 23-33.
[205] Lagali, P. S., Balya, D., Awatramani, G. B., Munch, T. A., Kim, D. S., Busskamp, V., Cepko, C. L., and Roska, B. (2008) Light-activated channels targeted to ON bipolar cells restore visual function in retinal degeneration, *Nat Neurosci 11*, 667-675.
[206] Doroudchi, M. M., Greenberg, K. P., Liu, J., Silka, K. A., Boyden, E. S., Lockridge, J. A., Arman, A. C., Janani, R., Boye, S. E., Boye, S. L., Gordon, G. M., Matteo, B. C., Sampath, A. P., Hauswirth, W. W., and Horsager, A. (2011) Virally delivered channelrhodopsin-

2 safely and effectively restores visual function in multiple mouse models of blindness, *Mol Ther 19*, 1220-1229.
[207] Tomita, H., Sugano, E., Yawo, H., Ishizuka, T., Isago, H., Narikawa, S., Kugler, S., and Tamai, M. (2007) Restoration of visual response in aged dystrophic RCS rats using AAV-mediated channelopsin-2 gene transfer, *Invest Ophthalmol Vis Sci 48*, 3821-3826.
[208] Katayama, K., Gulati, S., Ortega, J. T., Alexander, N. S., Sun, W., Shenouda, M. M., Palczewski, K., and Jastrzebska, B. (2019) Specificity of the chromophore-binding site in human cone opsins, *J Biol Chem 294*, 6082-6093.
[209] Tsukamoto, H., Kubo, Y., Farrens, D. L., Koyanagi, M., Terakita, A., and Furutani, Y. (2015) Retinal Attachment Instability Is Diversified among Mammalian Melanopsins, *J Biol Chem 290*, 27176-27187.

APPENDIX A

Supplementary Figures – Chapter 4

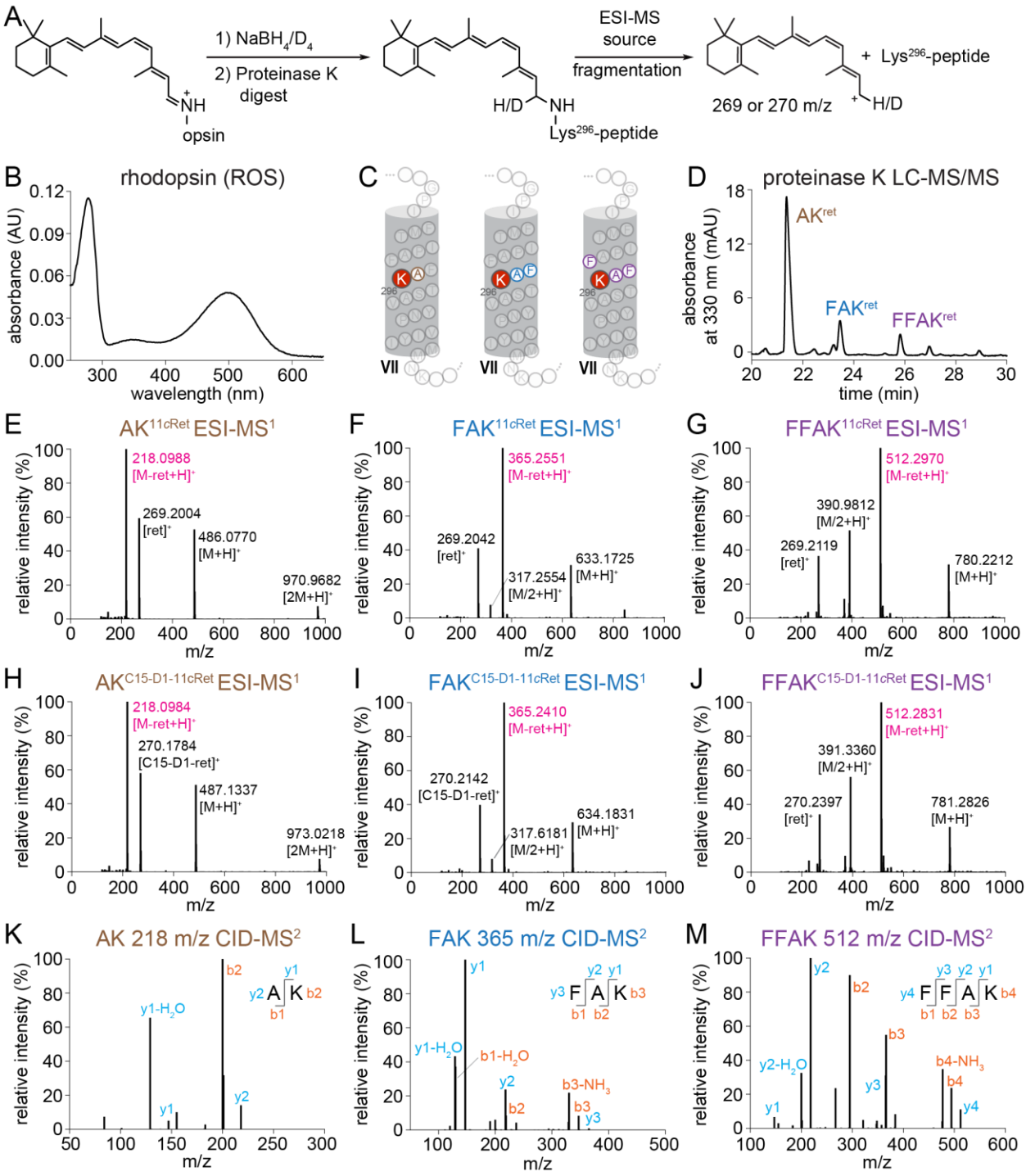

Figure S1. LC-MS/MS analysis of proteinase K digests of bRho from bROS membranes. (A) Schematic diagram of sample preparation and MS workflow. (B) UV-Vis spectrum of bRho in bROS solubilized in LMNG. (C) Location of chromophore-binding residue within helix VII of bRho, with labeled N^{ε}-retinyl-peptide fragments detected from the proteinase K digest. (D) Chromatographic separation of N^{ε}-retinyl-peptides from proteinase K digestion of bRho from bROS membranes, treated with $NaBH_4$ or $NaBD_4$ in *i*PrOH. (E-J) ESI-MS^1 spectra showing the characteristic cleavage of the retinyl cation from precursor retinyl-peptide analyte, producing a product peptide peak. (K-M) MS^2 spectra of CID fragmentation of product peptide ion for sequence determination.

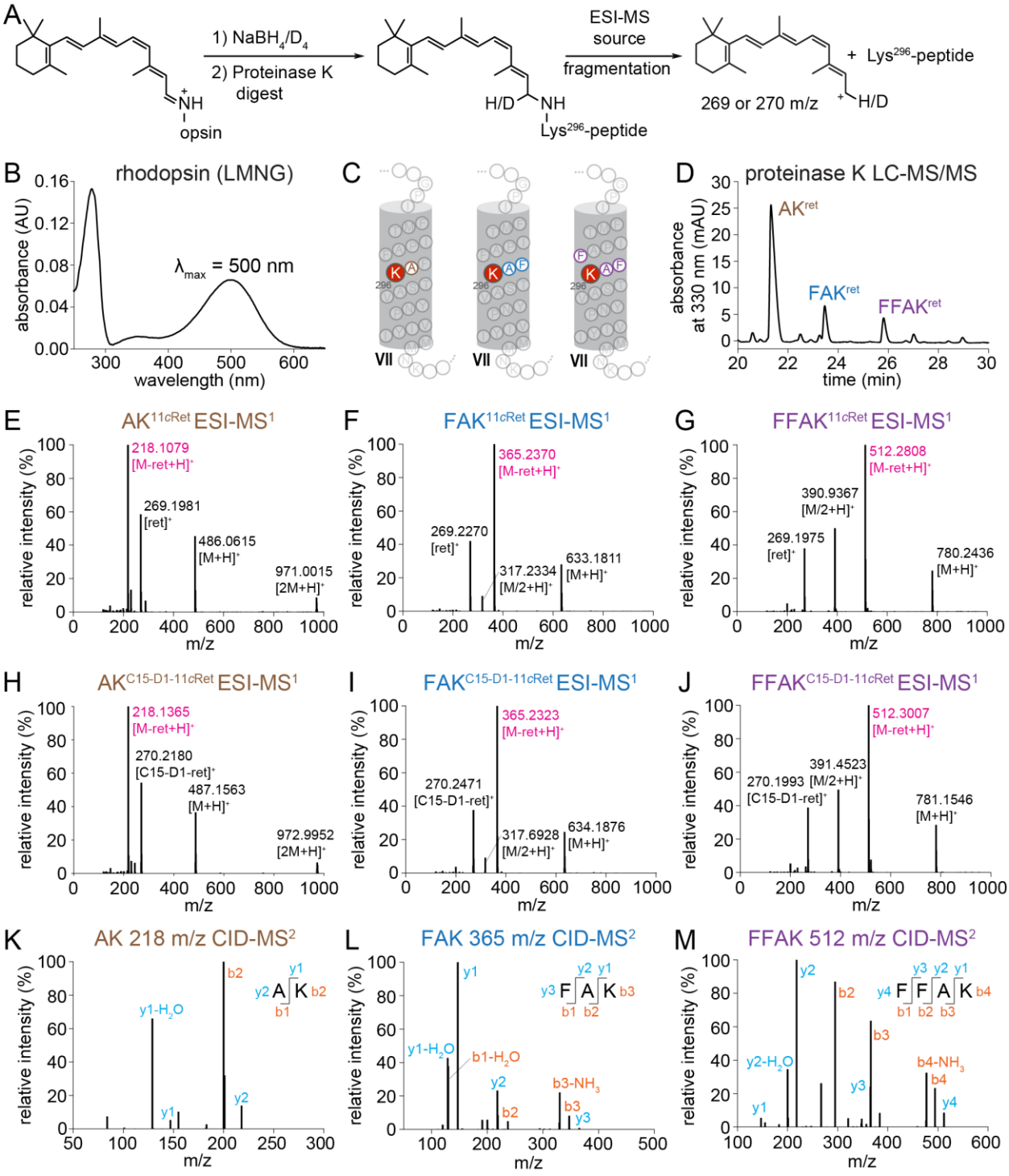

Figure S2. LC-MS/MS analysis of proteinase K digests of bRho purified in LMNG detergent micelles. (A) Schematic diagram of sample preparation and MS workflow. (B) UV-Vis spectrum of purified bRho in LMNG. (C) Location of chromophore-binding residue

within helix VII of bRho, with labeled N^{ε}-retinyl-peptide fragments detected from the proteinase K digest. (D) Chromatographic separation of N^{ε}-retinyl-peptides from proteinase K digestion of purified bRho, treated with $NaBH_4$ or $NaBD_4$ in *i*PrOH. (E-J) ESI-MS^1 spectra showing the characteristic cleavage of the retinyl cation from precursor retinyl-peptide analyte, producing a product peptide peak. (K-M) MS^2 spectra of CID fragmentation of product peptide ion for sequence determination.

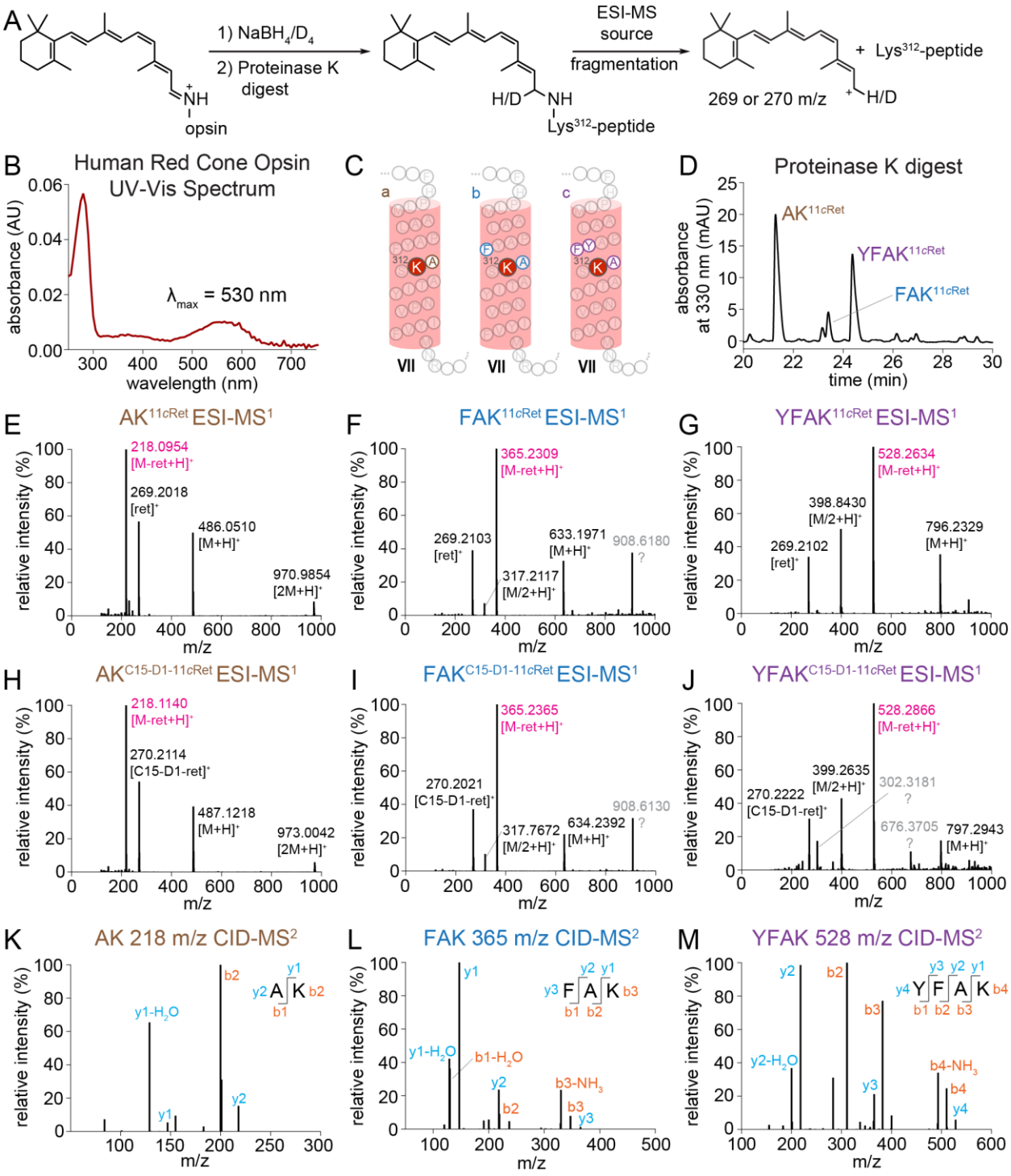

Figure S3. LC-MS/MS analysis of proteinase K digests of red cone opsin purified in LMNG detergent micelles. (A) Schematic diagram of sample preparation and MS workflow. (B) UV-Vis spectrum of purified red-cone opsin in LMNG. (C) Location of

chromophore-binding residue within helix VII of red-cone opsin, with labeled N^{ε}-retinyl-peptide fragments detected from the proteinase K digest. (D) Chromatographic separation of N^{ε}-retinyl-peptides from proteinase K digestion of purified red-cone opsin, treated with $NaBH_4$ or $NaBD_4$ in *i*PrOH. (E-J) ESI-MS^1 spectra showing characteristic cleavage of the retinyl cation from precursor retinyl-peptide analyte, producing a product peptide peak. (K-M) MS^2 spectra of CID fragmentation of product peptide ion for sequence determination.

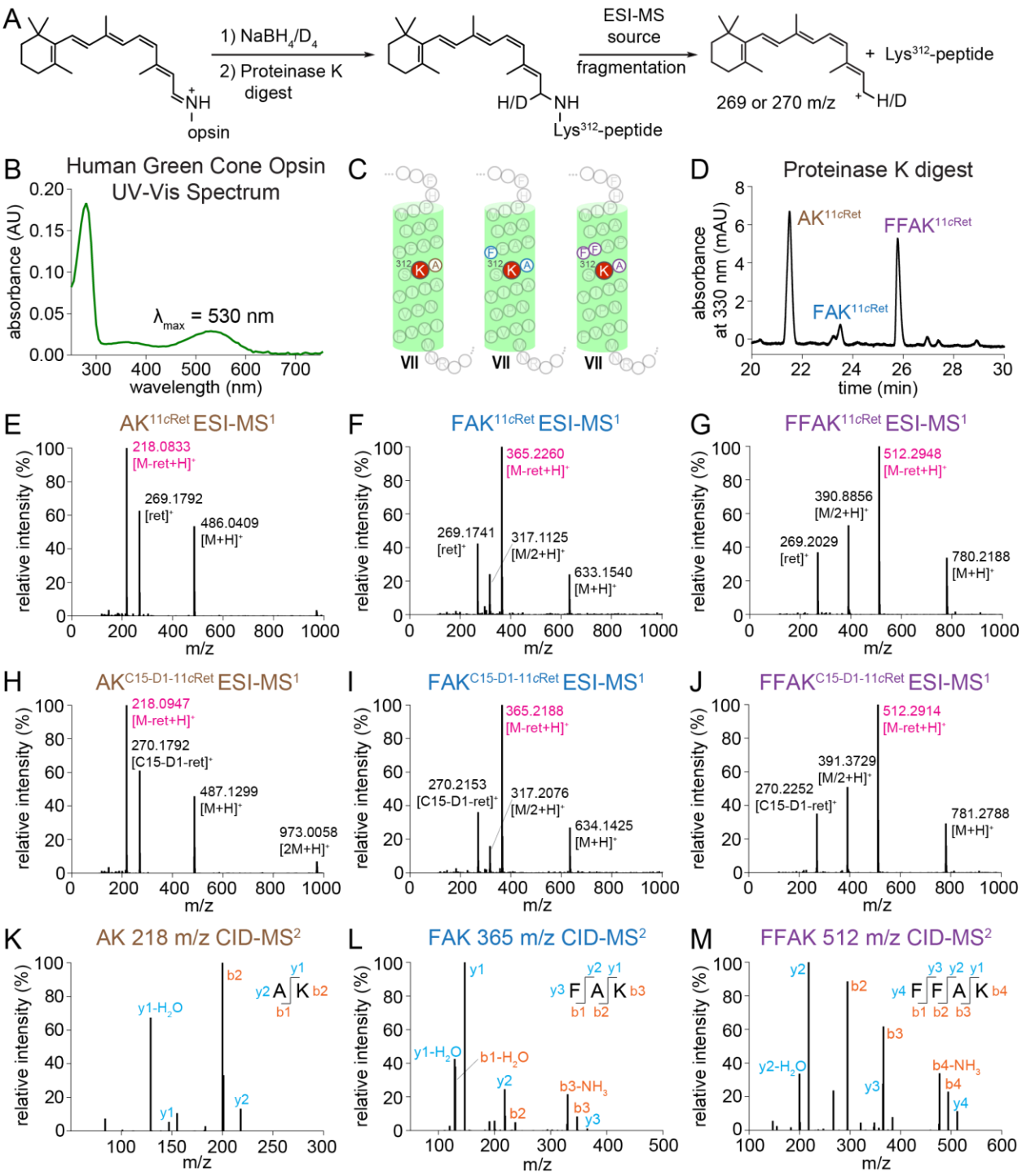

Figure S4. LC-MS/MS analysis of proteinase K digests of green-cone opsin purified in LMNG-detergent micelles. (A) Schematic diagram of sample preparation and MS workflow. (B) UV-Vis spectrum of purified green-cone opsin in LMNG. (C) Location of

chromophore-binding residue within helix VII of green-cone opsin, with labeled N^{ε}-retinyl-peptide fragments detected from the proteinase K digest. (D) Chromatographic separation of N^{ε}-retinyl-peptides from proteinase K digestion of purified green-cone opsin, treated with $NaBH_4$ or $NaBD_4$ in *i*PrOH. (E-J) ESI-MS^1 spectra showing characteristic cleavage of the retinyl cation from precursor retinyl-peptide analyte, producing a product peptide peak. (K-M) MS^2 spectra of CID fragmentation of product peptide ion for sequence determination.

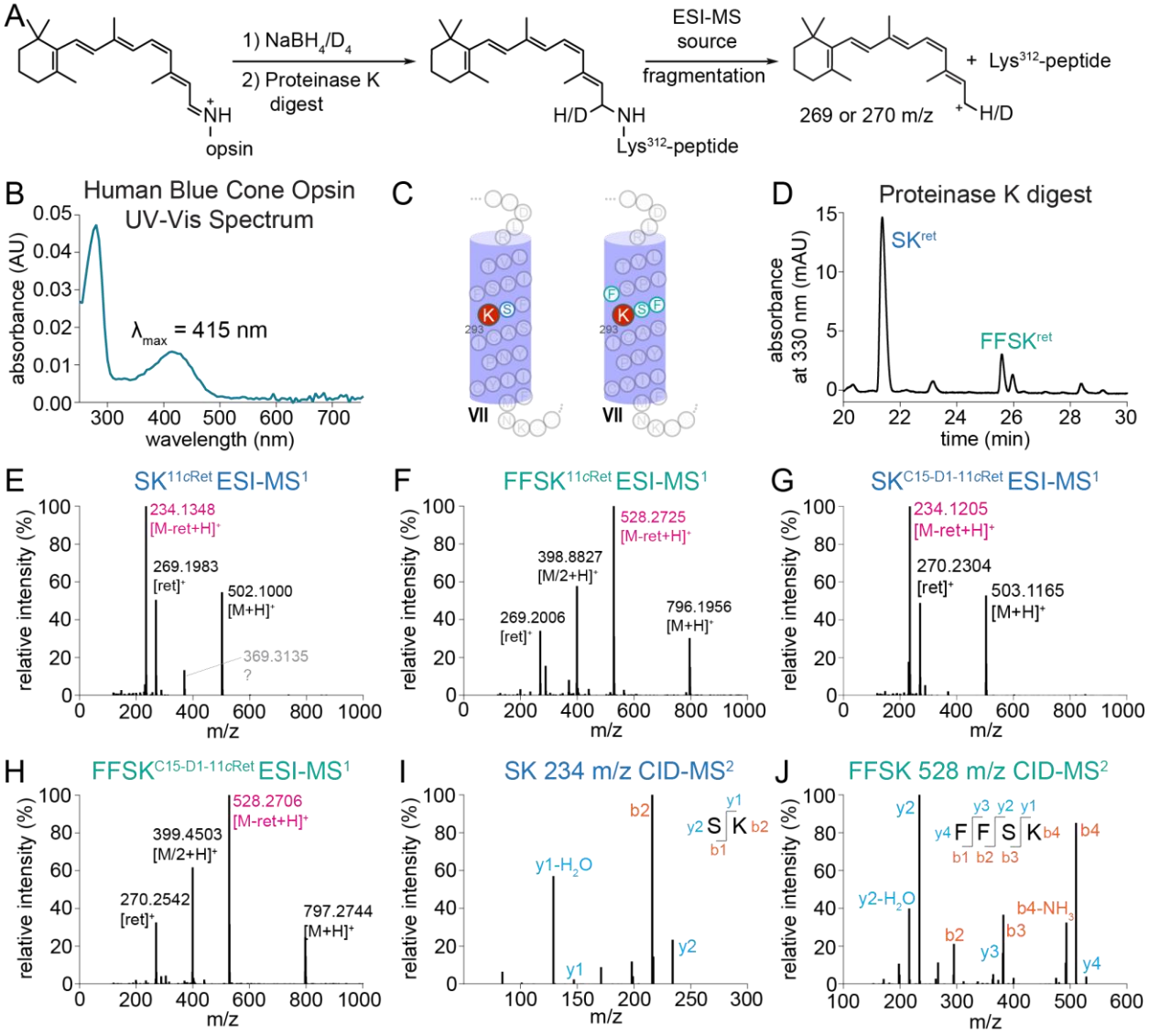

Figure S5. LC-MS/MS analysis of proteinase K digests of blue cone opsin purified in LMNG detergent micelles. (A) Schematic diagram of sample preparation and MS workflow. (B) UV-Vis spectrum of purified blue-cone opsin in LMNG. (C) Location of chromophore-binding residue within helix VII of blue-cone opsin, with labeled N$^{\varepsilon}$-retinyl-peptide fragments detected from the proteinase K digest. (D) Chromatographic separation of N$^{\varepsilon}$-retinyl-peptides from proteinase K digestion of purified blue-cone opsin, treated with $NaBH_4$ or $NaBD_4$ in *i*PrOH. (E-H) ESI-MS^1 spectra showing characteristic cleavage of the

retinyl cation from precursor retinyl-peptide analytes, producing product peptide peaks. (I, J) MS^2 spectra of CID fragmentation of product peptide ions for sequence determination.

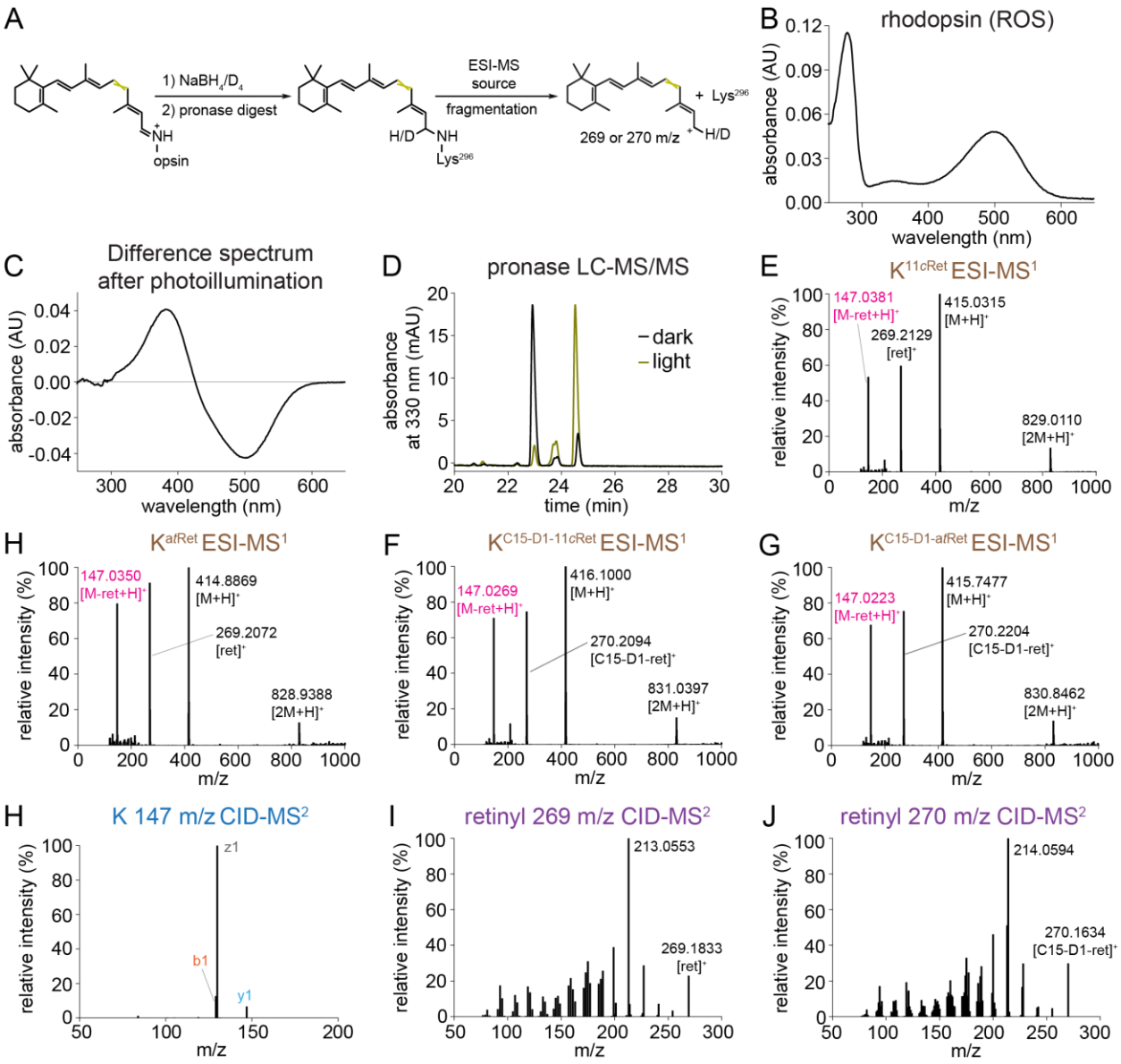

Figure S6. LC-MS/MS analysis of pronase digest of bRho from bROS membranes. (A) Schematic diagram of sample preparation and MS workflow. (B) UV-Vis spectrum of bRho in bROS membranes solubilized in LMNG. (C) Difference absorbance spectrum after illumination (subtracting the ground-state spectrum) of bROS membranes with 505-nm

fiber light at 125 μW for 10 sec at 4 °C. (D) Chromatographic separation of N^{ε}-retinyl-Lys peaks from pronase digest of ground-state and photoactivated bRho treated with $NaBH_4$ or $NaBD_4$ in *i*PrOH. (E-H) ESI-MS^1 spectra showing characteristic cleavage of retinyl cation from precursor N^{ε}-retinyl-Lys analyte, producing a product Lys ion. (I) CID-MS^2 spectrum of the product Lys ion exhibiting the characteristic fragmentation pattern of Lys. (J, K) CID-MS^2 spectrum of retinyl cation displaying complex fragmentation patterns with a characteristic dominant 213 m/z signal from $NaBH_4$-reduced bRho and 214 m/z signal for $NaBD_4$-reduced bRho [123, 124].

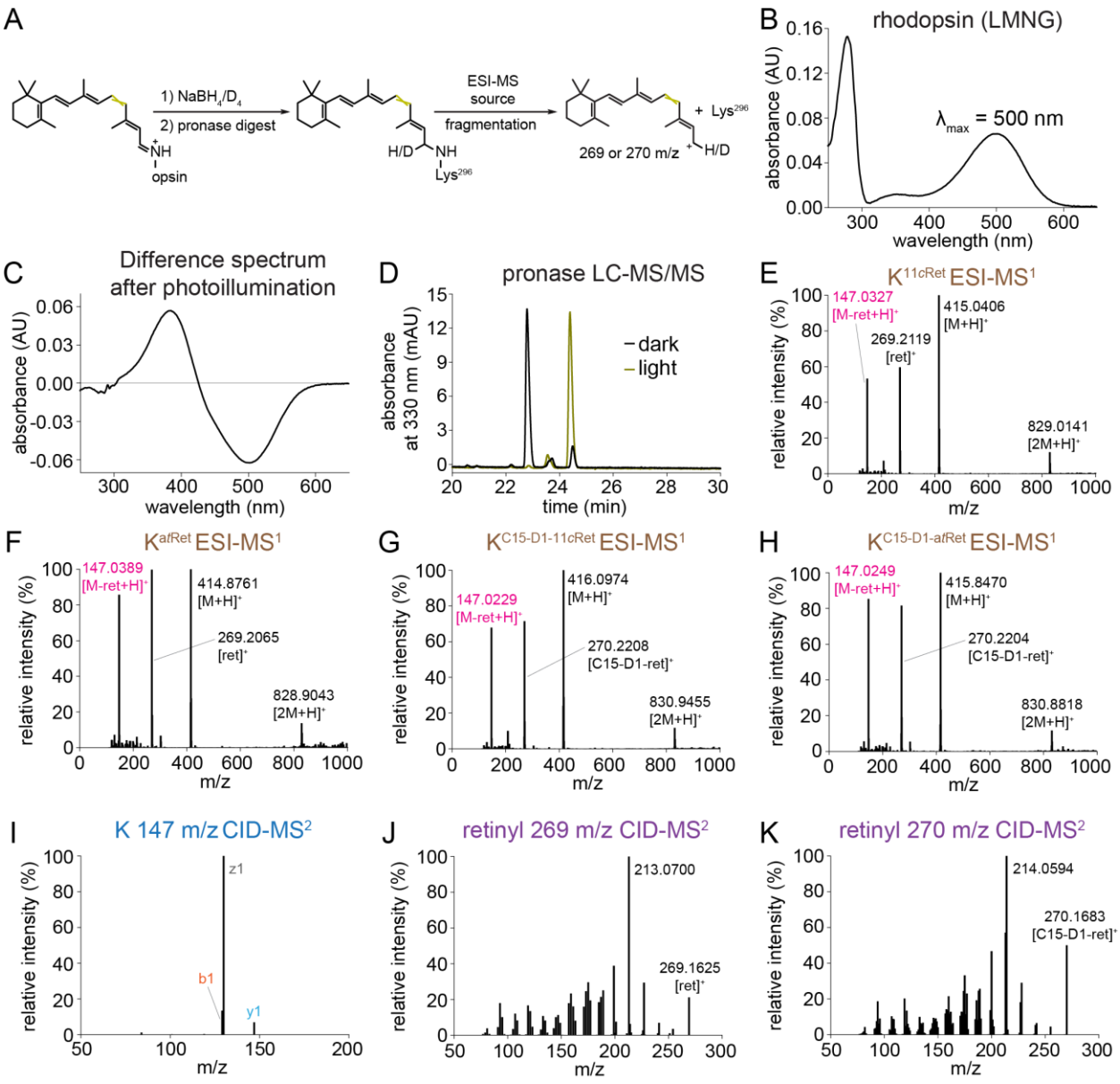

Figure S7. LC-MS/MS analysis of pronase digest of bRho purified in LMNG detergent.

(A) Schematic diagram of sample preparation and MS workflow. (B) UV-Vis spectrum of purified bRho in LMNG. (C) Difference absorbance spectrum after illumination (post-illumination *minus* pre-illumination spectrum) of bRho with 505-nm fiber light at 125 µW for 10 sec at 4 °C. (D) Chromatographic separation of N$^{\varepsilon}$-retinyl-Lys peaks from pronase digest of ground-state and photoactivated bRho, treated with $NaBH_4$ or $NaBD_4$ in *i*PrOH. (E-

H) ESI-MS^1 spectra showing characteristic cleavage of the retinyl cation from precursor N^{ε}-retinyl-Lys analytes, producing a product Lys ion. (I) CID-MS^2 spectrum of the product Lys ion exhibiting the characteristic fragmentation pattern of Lys. (J, K) CID-MS^2 spectrum of retinyl cation demonstrating complex fragmentation pattern with characteristic dominant 213 m/z signal for $NaBH_4$-reduced bRho and 214 m/z signal for $NaBD_4$-reduced bRho [123, 124].

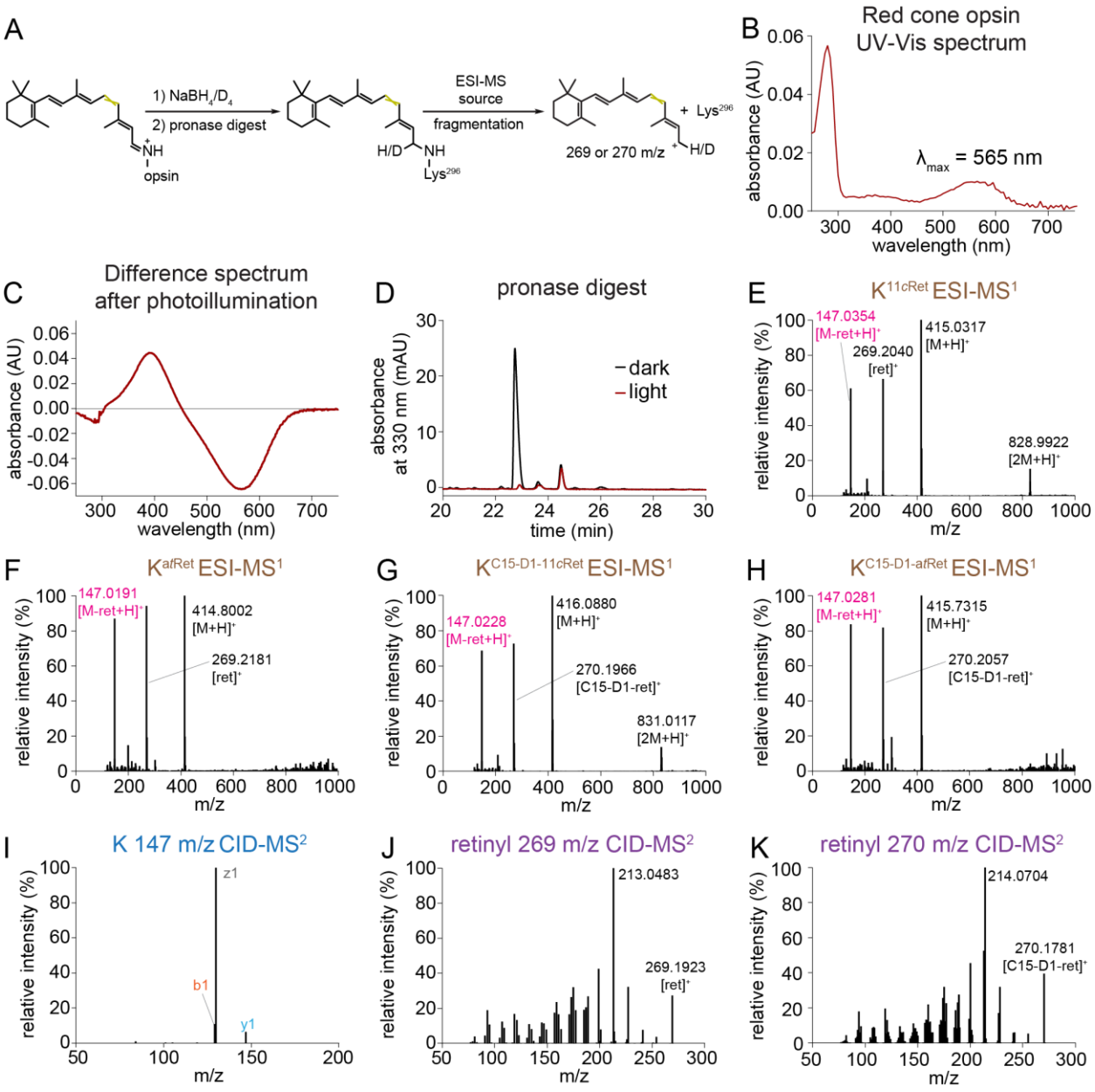

Figure S8. LC-MS/MS analysis of pronase digest of red cone opsin purified in LMNG detergent. (A) Schematic diagram of sample preparation and MS workflow. (B) UV-Vis spectrum of purified Red in LMNG. (C) Difference absorbance spectrum after illumination (subtracting the ground-state spectrum) of red cone opsin with 565-nm fiber light at 125 μW for 10 sec at 4 °C. (D) Chromatographic separation of N^{ε}-retinyl-Lys peaks from pronase digest of ground-state and photoactivated red cone opsin, treated with $NaBH_4$ or

$NaBD_4$ in *i*PrOH. (E-H) ESI-MS^1 spectra showing characteristic cleavage of retinyl cation from precursor N^{ε}-retinyl-Lys analyte, producing a product Lys ion. (I) CID-MS^2 spectrum of the product Lys ion exhibiting the characteristic fragmentation pattern of Lys. (J, K) CID-MS^2 spectrum of retinyl cation demonstrating complex fragmentation pattern with characteristic dominant 213 m/z signal for $NaBH_4$-reduced red-cone opsin and 214 m/z signal for $NaBD_4$-reduced red-cone opsin [123, 124].

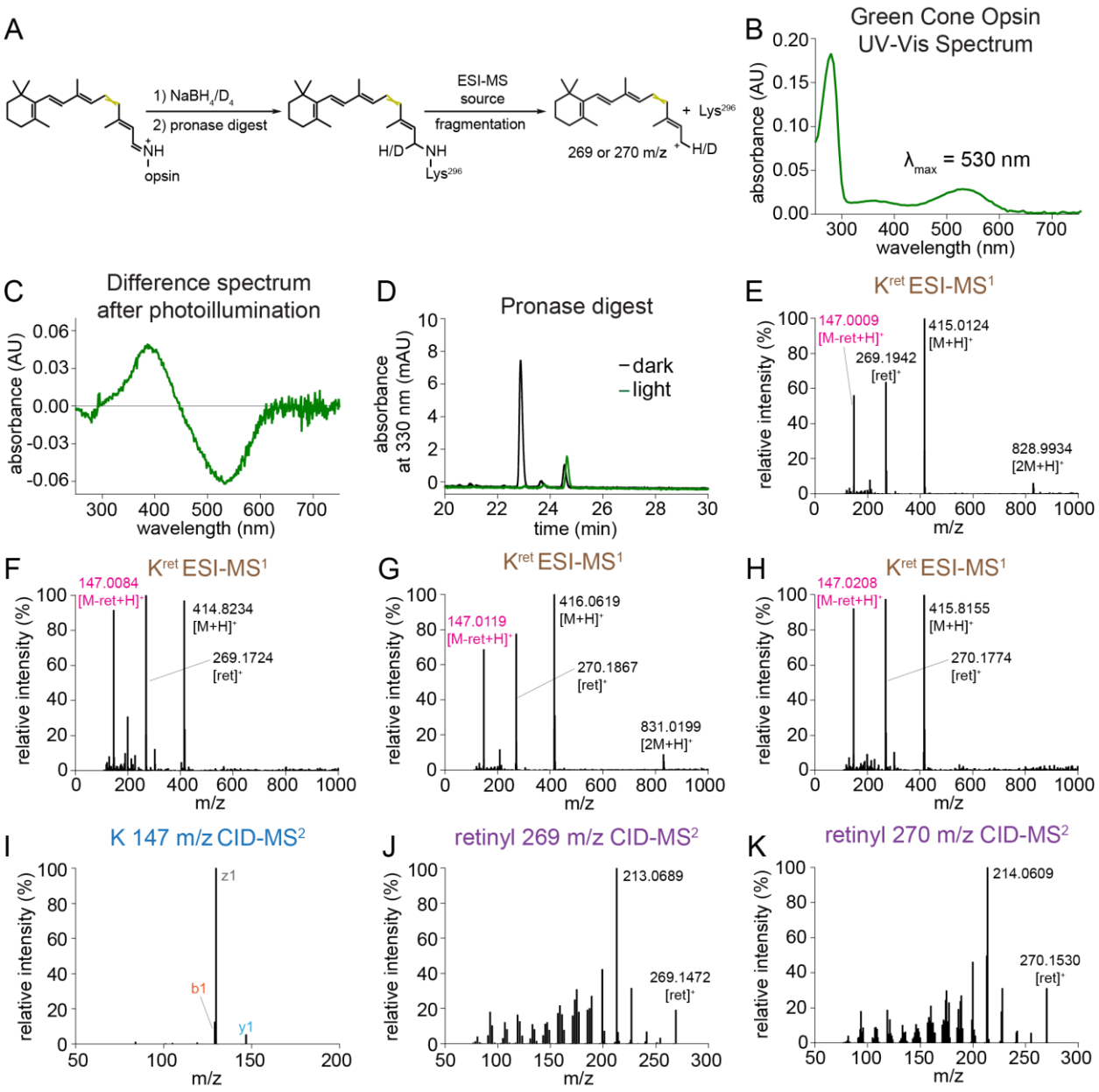

Figure S9. LC-MS/MS analysis of pronase digest of green cone opsin purified in LMNG detergent. (A) Schematic diagram of sample preparation and MS workflow. (B) UV-Vis spectrum of purified Green in LMNG. (C) Difference absorbance spectrum after illumination (post-illumination *minus* pre-illumination spectrum) of green cone opsin with 530-nm fiber light at 125 µW for 10 sec at 4 °C. (D) Chromatographic separation of N$^{\varepsilon}$-retinyl-Lys peaks from pronase digest of ground-state and photoactivated green cone opsin, treated with

$NaBH_4$ or $NaBD_4$ in *i*PrOH. (E, H) ESI-MS^1 spectrum showing characteristic cleavage of retinyl cation from precursor N^{ε}-retinyl-Lys analyte, producing a product Lys ion. (F, I) CID-MS^2 spectrum of the product Lys ion exhibiting the characteristic fragmentation pattern of Lys. (G, J) CID-MS^2 spectrum of the retinyl cation demonstrating complex fragmentation pattern with characteristic dominant 213 m/z signal for $NaBH_4$-reduced green-cone opsin and 214 m/z signal for $NaBD_4$-reduced green-cone opsin [123, 124].

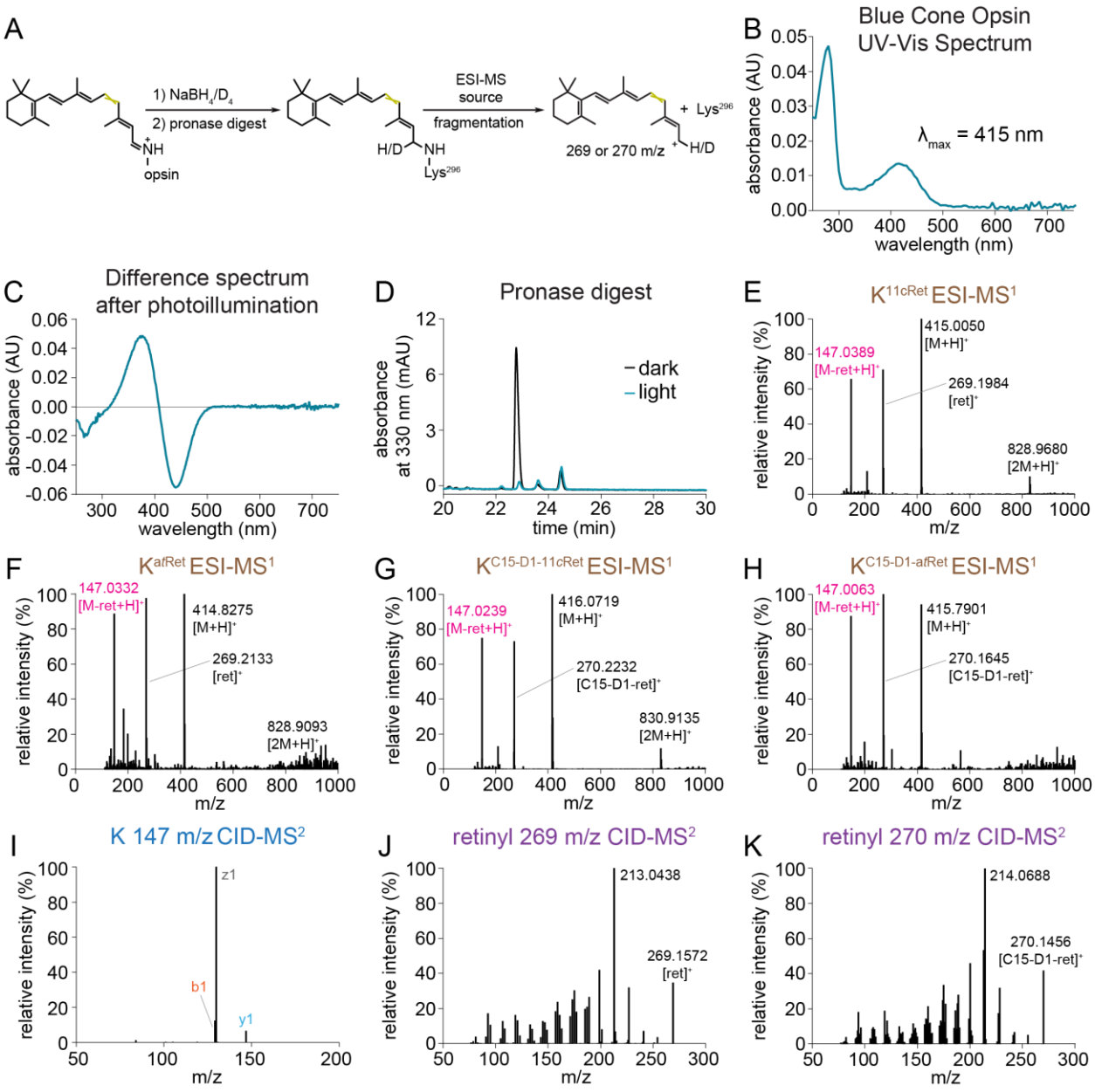

Figure S10. LC-MS/MS analysis of pronase digests of blue-cone opsin, purified in LMNG detergent (A) Schematic diagram of sample preparation and MS workflow. (B) UV-Vis spectrum of purified Blue in LMNG. (C) Difference absorbance spectrum after illumination (post-illumination *minus* pre-illumination spectrum) of blue cone opsin with 455-nm fiber light at 125 µW for 10 sec at 4 °C. (D) Chromatographic separation of N^{ε}-retinyl-Lys peaks from pronase digest of ground-state and photoactivated blue cone opsin,

treated with $NaBH_4$ or $NaBD_4$ in *i*PrOH. (E-H) ESI-MS^1 spectra showing characteristic cleavage of the retinyl cation from precursor N^{ε}-retinyl-Lys analytes, producing a product Lys ion. (I) CID-MS^2 spectrum of the product Lys ion, exhibiting the characteristic fragmentation pattern of Lys. (J, K) CID-MS^2 spectra of the respective retinyl cations, displaying complex fragmentation patterns with a characteristic dominant 213 m/z signal for $NaBH_4$-reduced blue-cone opsin, and a 214 m/z signal for $NaBD_4$-reduced blue-cone opsin [123, 124].

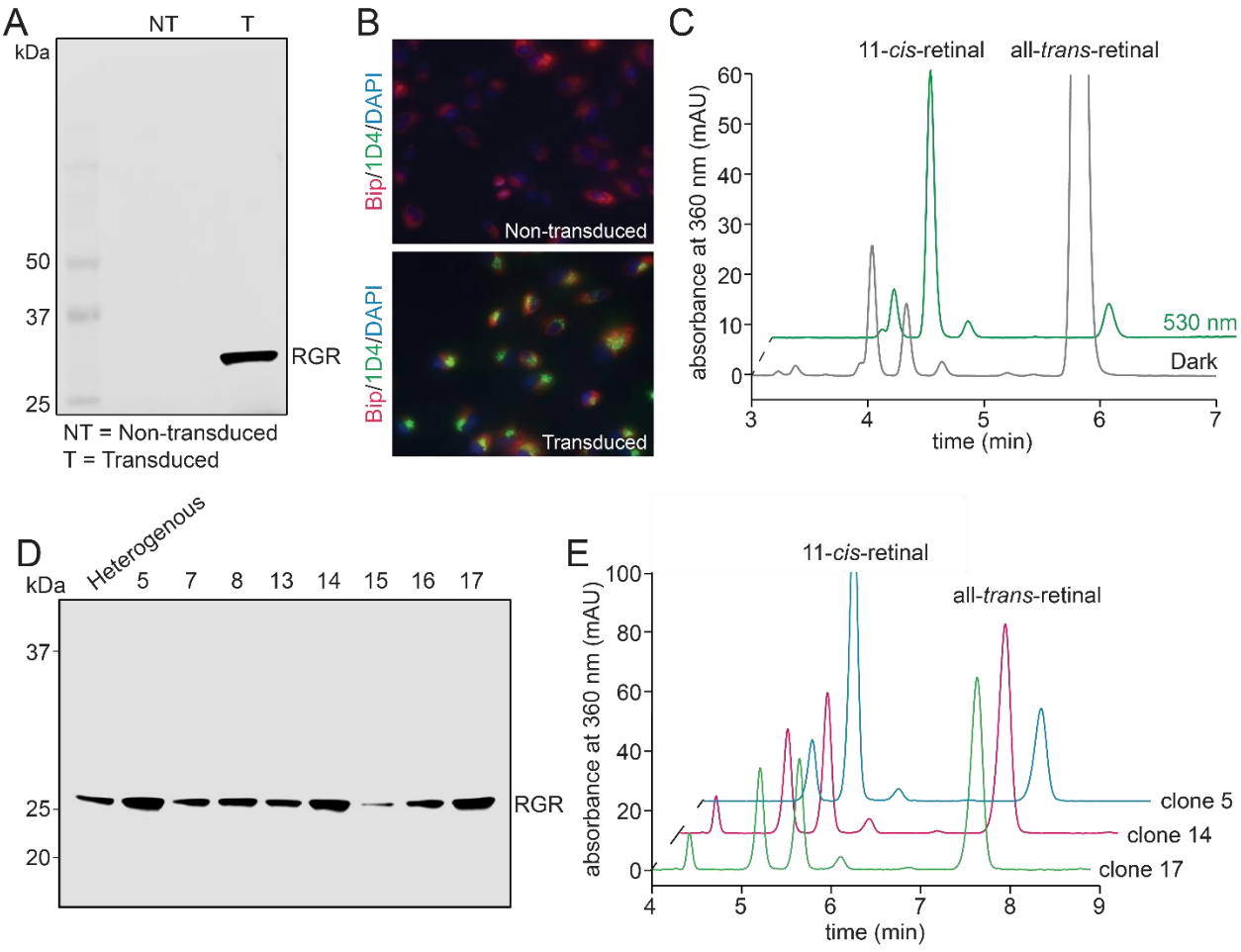

Figure S11. Generation of the bRGR HEK293 cell line. (A) Immunoblot of HEK293S and HEK293S-bRGR cells. (B) Subcellular localization of bRGR. The merged images show the

colocalization of bRGR with the endoplasmic reticulum marker, BiP. (C) HPLC analysis of retinoids extracted from HEK293S-bRGR cells after addition of all-*trans*-retinal and either dark incubation or exposure to 530 nm light. (D) Immunoblot comparing relative expression of bRGR in various clones of HEK293T-bRGR monoclonal cells. (E) HPLC analysis of retinoids extracted from HEK293S-bRGR monoclonal cells to compare photoisomerization activities.

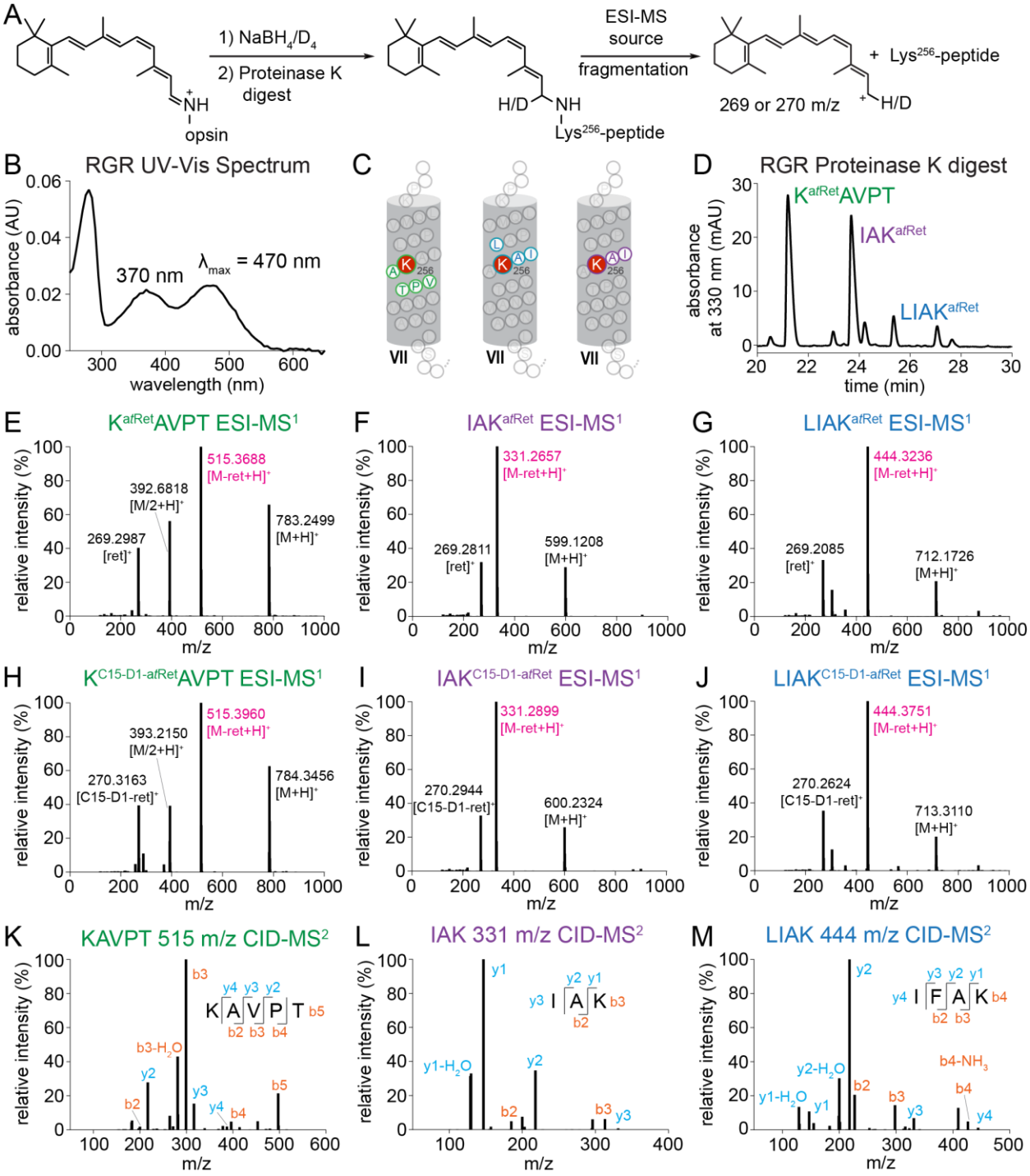

Figure S12. LC-MS/MS analysis of proteinase K digests of bRGR purified in LMNG detergent micelles. (A) Schematic diagram of sample preparation and MS workflow. (B) UV-Vis spectrum of recombinant bRGR reconstituted with all-*trans*-retinal and purified in

LMNG. (C) Location of chromophore-binding residue within helix VII of bRGR, with labeled N^{ε}-retinyl-peptide fragments detected from the proteinase K digest. (D) Chromatographic separation of N^{ε}-retinyl-peptides from proteinase K digestion of purified bRGR, treated with $NaBH_4$ or $NaBD_4$ in *i*PrOH. (E-J) ESI-MS^1 spectra showing characteristic cleavage of the retinyl cation from precursor retinyl-peptide analytes, producing product peptide peaks. (K-M) MS^2 spectra of CID fragmentation of product peptide ion for sequence determination.

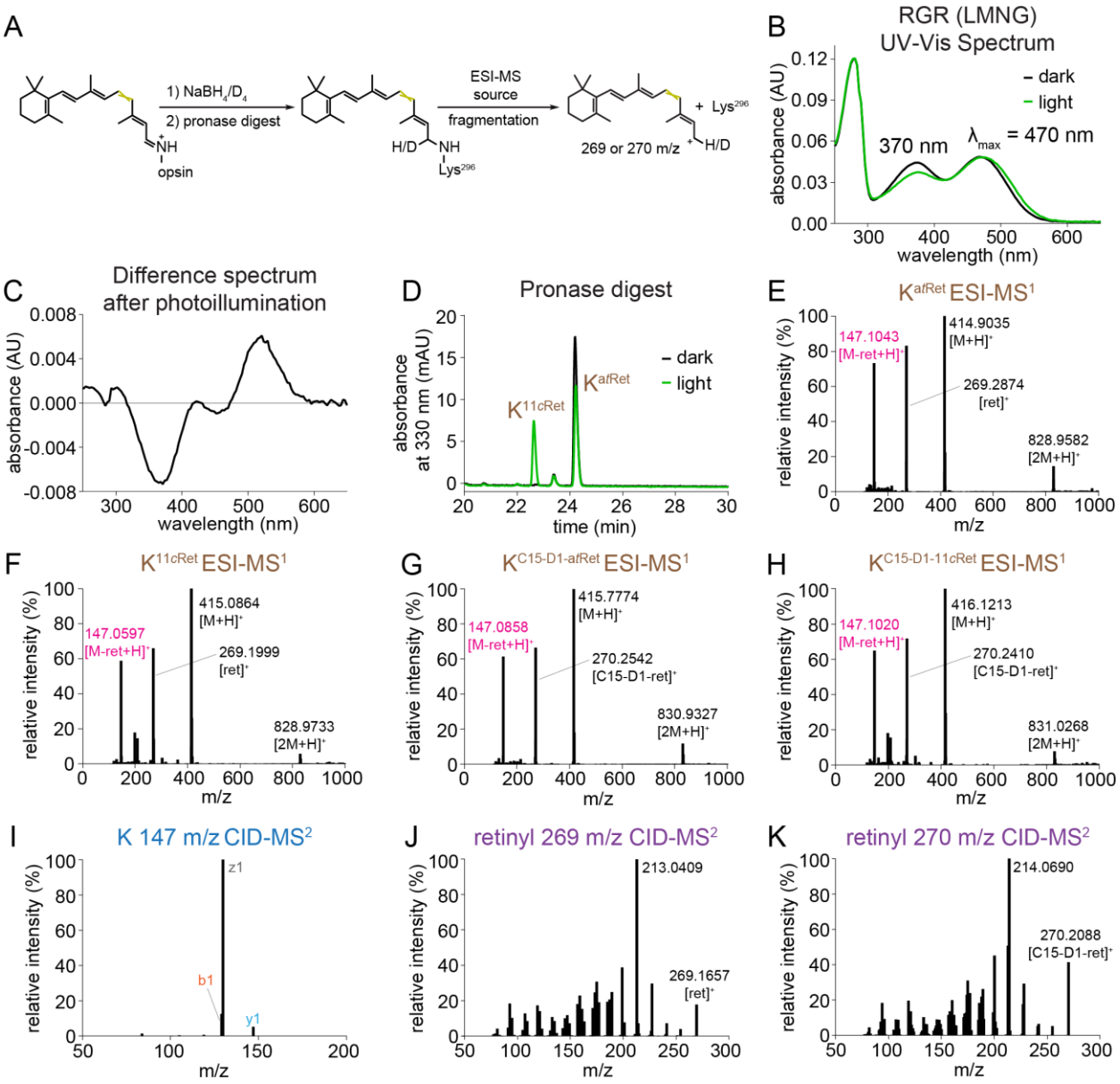

Figure S13. LC-MS/MS analysis of pronase digests of bRGR purified in LMNG detergent. (A) Schematic diagram of sample preparation and MS workflow. (B) UV-Vis spectrum of recombinant bRGR reconstituted with all-*trans*-retinal and purified in LMNG. (C) Difference absorbance spectrum after illumination (post-illumination *minus* pre-illumination spectrum) of bRGR with 530-nm fiber light at 125 μW for 10 sec at 4 °C. (D) Chromatographic separation of N$^{\varepsilon}$-retinyl-Lys peaks from pronase digest of bRGR before

and after illumination, treated with $NaBH_4$ or $NaBD_4$ in *i*PrOH. (E-H) ESI-MS^1 spectra showing the characteristic cleavage of the retinyl cation from precursor N^{ε}-retinyl-Lys analytes, producing a product Lys ion. (I) CID-MS^2 spectrum of the product Lys ion, exhibiting the characteristic fragmentation pattern of Lys. (J, K) CID-MS^2 spectra of the respective retinyl cations, displaying complex fragmentation patterns with a characteristic dominant 213 m/z signal for $NaBH_4$-reduced bRGR, and a 214 m/z signal for $NaBD_4$-reduced bRGR [123, 124].

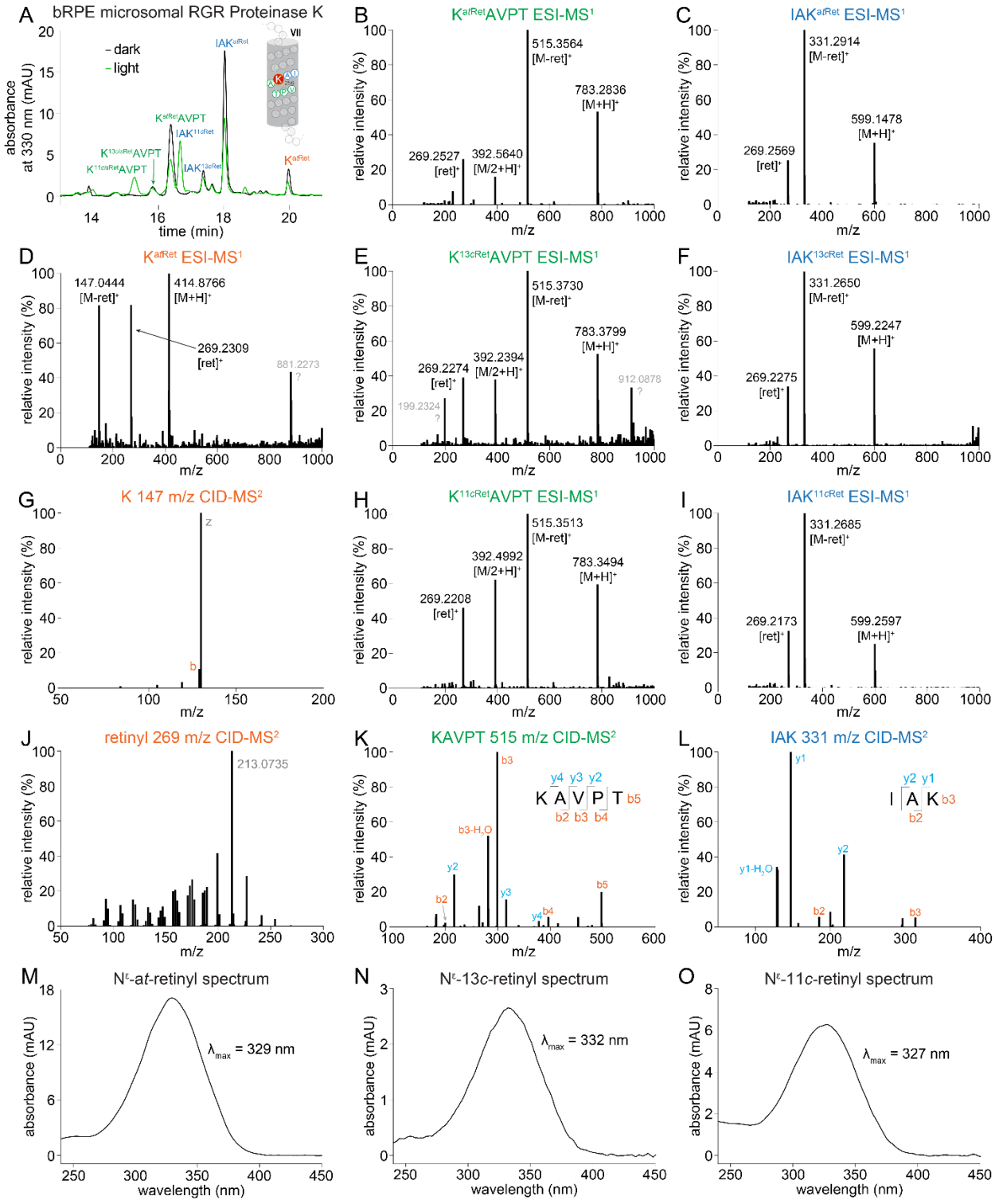

Figure S14. LC-MS/MS analysis of proteinase K digests of bRGR from bRPE microsomes. (A) Chromatographic separation of Nε-retinyl-peptides from proteinase K

digestion of purified bRGR, treated with $NaBH_4$ or $NaBD_4$ in *i*PrOH. (B-F, H-I) ESI-MS^1 spectra showing characteristic cleavage of retinyl cation from precursor retinyl-peptide analyte, producing product peptide peaks. (G, K-L) MS^2 spectra of CID fragmentation of product peptide ion for sequence determination. (J) CID-MS^2 spectrum of retinyl cation demonstrating a complex fragmentation pattern with a characteristic dominant 213 m/z signal for $NaBH_4$-reduced bRGR, and a 214 m/z signal for $NaBD_4$-reduced bRGR [123, 124]. (M-O) UV-Vis absorption spectra collected during chromatography showing the characteristic spectrum for each retinyl-peptide isomer.

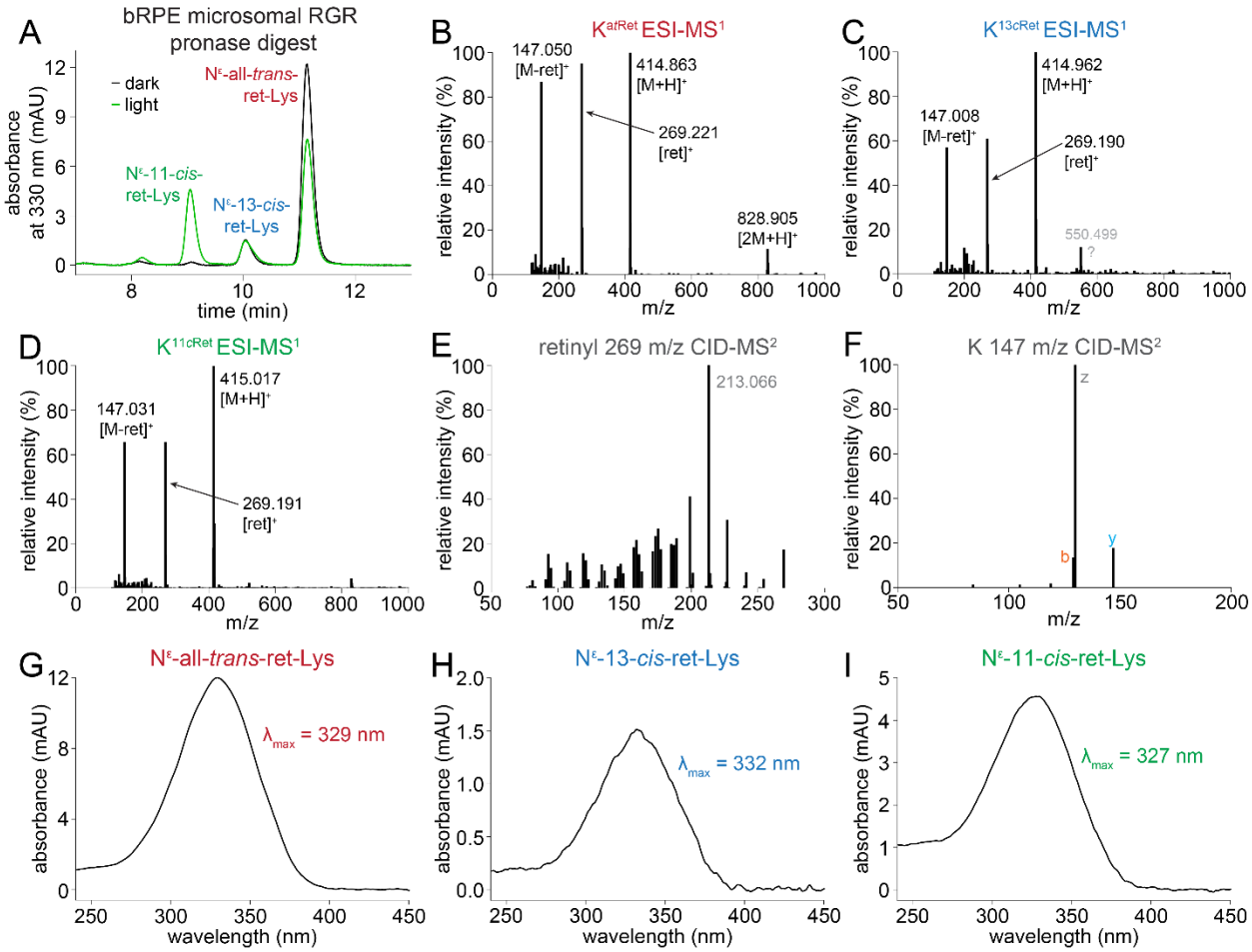

Figure S15. LC-MS/MS analysis of the pronase digest of bRGR from bRPE microsomes. (A) Chromatographic separation of Nε-retinyl-Lys peaks from pronase digest of bRGR before and after illumination, treated with $NaBH_4$ or $NaBD_4$ in *i*PrOH. (B-D) ESI-MS^1 spectra showing characteristic cleavage of the retinyl cation from precursor Nε-retinyl-Lys analyte, producing a product Lys ion. (E) CID-MS^2 spectrum of the retinyl cation demonstrating complex fragmentation pattern with characteristic dominant 213 m/z signal for $NaBH_4$-reduced bRGR, and a 214 m/z signal for $NaBD_4$-reduced bRGR [123, 124]. (F) CID-MS^2 spectrum of the product Lys ion exhibiting the characteristic fragmentation pattern of Lys. (G-I) UV-Vis absorption spectra collected during chromatography, showing the characteristic spectrum for each retinyl-peptide isomer.

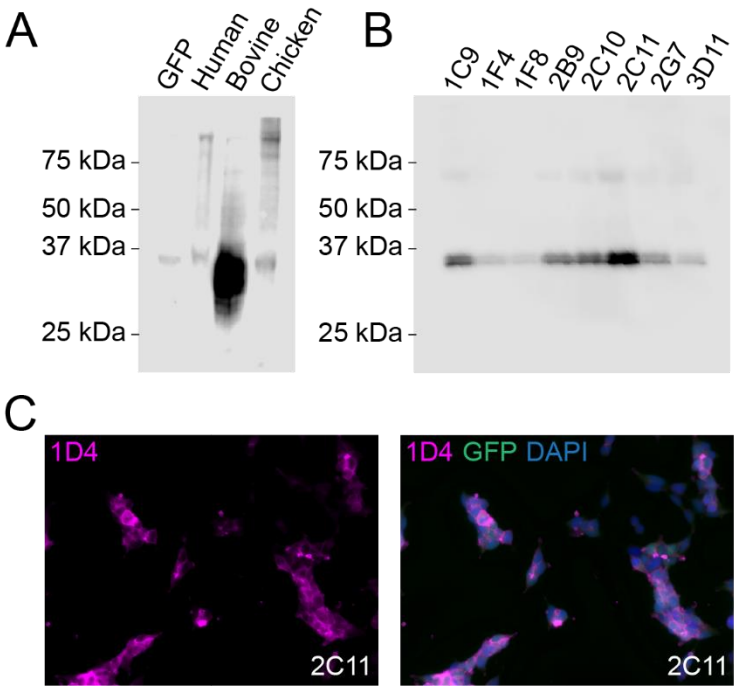

Figure S16. Generation of HEK293 cell line stably expressing bRRH. (A) Comparison by anti-1D4 western blot analysis of different species of bRRH, each with a C-terminal 1D4 tag transiently expressed in HEK293S cells. (B) Clonal selection of HEK293S cells stably expressing bRRH. (C) Immunostaining of HEK293S-bRRH cells against 1D4 tag and counterstained with DAPI. GFP is cotranslationally expressed.

APPENDIX B

Supplementary Figures – Chapter 5

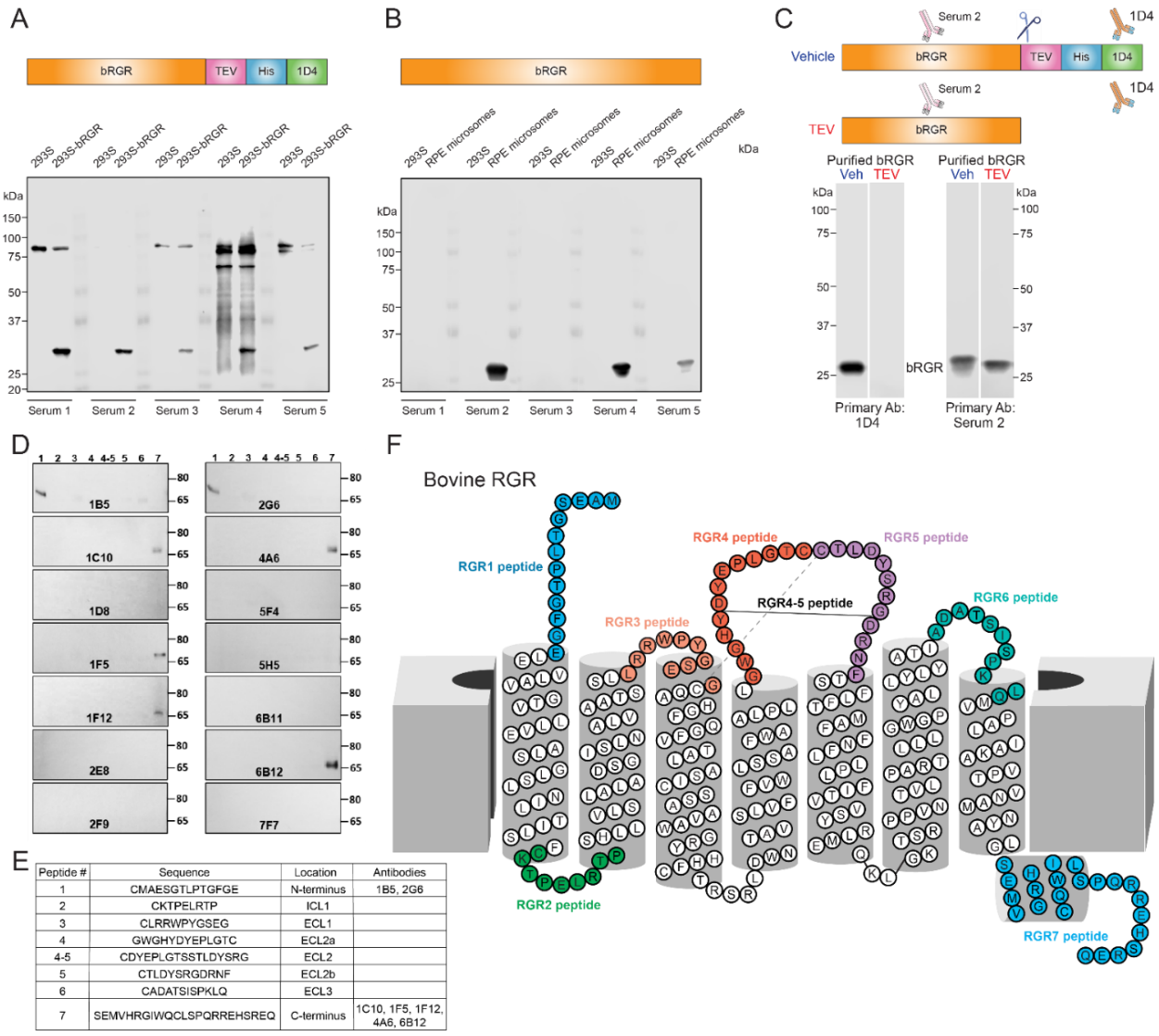

Peptide #	Sequence	Location	Antibodies
1	CMAESGTLPTGFGE	N-terminus	1B5, 2G6
2	CKTPELRTP	ICL1	
3	CLRRWPYGSEG	ECL1	
4	GWGHYDYEPLGTC	ECL2a	
4-5	CDYEPLGTSSTLDYSRG	ECL2	
5	CTLDYSRGDRNF	ECL2b	
6	CADATSISPKLQ	ECL3	
7	SEMVHRGIWQCLSPQRREHSREQ	C-terminus	1C10, 1F5, 1F12, 4A6, 6B12

Figure S1. Production of bRGR monoclonal antibodies. (A) Evaluation of sera from mice immunized with bRGR to assess antibody production against bRGR-TEV-His-1D4. Immunoblot analysis was performed using lysates from HEK293S and HEK293-bRGR cells. (B) Evaluation of sera from mice injected with bRGR to assess antibody production against

bRGR. Immunoblot analysis was performed using lysates from HEK293S microsomes and bovine RPE microsomes. (C) Analysis of serum2 against purified bRGR-TEV-His-1D4 and purified bRGR following TEV cleavage to ensure antibody reactivity against bRGR. Serum 2 detected purified bRGR following TEV cleavage but the 1D4 antibody did not. (D) Screening of monoclonal hybridomas from the mouse that produced serum 2. Immunoblot analysis was performed using bovine RPE microsomes. (E) Peptides used to identify the epitope of antibodies produced by the selected monoclonal hybridoma. (F) Putative two-dimensional model of bRGR showing peptide sequences used for epitope mapping.